Jagiellonian University

Faculty of Physcis, Astronomy and Applied Computer Sciences

Karol Piotr Capała

Anomalous Stochastic Dynamics in the Underdamped Regime

Thesis for the degree of Doctor of Philosophy in Physics

Supervisor:
Prof. dr hab. Bartłomiej Dybiec

Kraków 2022

Wydział Fizyki, Astronomii i Informatyki Stosowanej
Uniwersytet Jagielloński

Oświadczenie

Ja niżej podpisany Karol Capała (nr indeksu: **1100288**) doktorant Wydziału Fizyki, Astronomii i Informatyki Stosowanej Uniwersytetu Jagiellońskiego oświadczam, że przedłożona przeze mnie rozprawa doktorska pt. „ Anomalous Stochastic Dynamics in the Underdamped Regime" jest oryginalna i przedstawia wyniki badań wykonanych przeze mnie osobiście, pod kierunkiem prof. dr hab. Bartłomieja Dybca. Pracę napisałem samodzielnie.

Oświadczam, że moja rozprawa doktorska została opracowana zgodnie z Ustawą o prawie autorskim i prawach pokrewnych z dnia 4 lutego 1994 r. (Dziennik Ustaw 1994 nr 24 poz. 83 wraz z późniejszymi zmianami).

Jestem świadom, że niezgodność niniejszego oświadczenia z prawdą ujawniona w dowolnym czasie, niezależnie od skutków prawnych wynikających z ww. ustawy, może spowodować unieważnienie stopnia nabytego na podstawie tej rozprawy.

Kraków, dnia ....

Contents

Abstract

Random processes or their fingerprints are ubiquitous in nature. Many systems are either too complex to be described deterministically or exhibit inherent randomness. These systems can be described in the language of stochastic processes, using stochastic force (noise).

This thesis discusses representative phenomena induced by Lévy noise with special attention to stationary states in single-well potentials and escape problems. Selected systems are analyzed mainly using numerical simulations of the Langevin equation. However, analytical results are also provided if possible.

Stationary states in single-well potentials have been studied in overdamped and full dynamic regimes. For the overdamped case, numerical evidence for existence of the non-equilibrium stationary states of modality higher than two are presented along with phenomenological arguments when their emergence is possible. For the underdamped case, stationary states in quartic potential are studied both for linear and nonlinear friction. Conditions assuring the emergence of bimodality in both cases are presented and discussed.

The second part of the thesis focuses on two archetypal escape processes. For the inertial motion in the finite interval analysis of mean first passage time and escape characteristics are presented. We showed that the qualitative behavior of mean first passage time is similar for all values of the stability index. Finally, forward and backward transition rates for a double-well potential system are analyzed. For the overdamped limit, deviations from weak noise approximation are discussed. For the full dynamic, an approximated analytical formula is presented, showing that the ratio of forward and backward transition rates depends on both potential barrier height and width. The approximation is compared with numerical simulations.

Streszczenie

Procesy stochastyczne lub ich ślady są widoczne w otaczającym nas świecie. Wiele układów jest albo zbyt złożonych, aby można je było opisać deterministycznie, albo wykazuje wbudowaną losowość. Układy te można opisać językiem procesów stochastycznych, używając siły losowej (szumu).

Niniejsza praca omawia typowe zjawiska indukowane przez szum Lévy'ego, ze szczególnym uwzględnieniem stanów stacjonarnych w potencjałach jednodołkowych i zagadnień pierwszej ucieczki. Wybrane układy analizowane są głównie za pomocą symulacji numerycznych równania Langevina. Jednakże w miarę możliwości przedstawione są również wyniki analityczne.

Stany stacjonarne w potencjałach jednodołkowych badane były w reżimie przetłumionym i w obszarze pełnej dynamiki. W przypadku przetłumionym przedstawiono numeryczne dowody na istnienie nierównowagowych stacjonarnych stanów o modalności wyższej niż dwa, wraz z argumentami fenomenologicznymi, kiedy ich pojawienie się jest możliwe. Stany stacjonarne w przypadku nieprzetłumionym w potencjale czwartego stopnia są badane zarówno w obszarze tarcia liniowego, jak i nieliniowego. Ponadto przedstawiono i omówiono warunki zapewniające pojawienie się bimodalności w obu przypadkach.

Druga część pracy skupia się na dwóch archetypicznych procesach ucieczki. Dla inercjalnego ruchu w skończonym przedziale przedstawiono analizę średniego pierwszego czasu wyjścia i charakterystyki ucieczki. Pokazano, że jakościowe zachowanie średniego pierwszego czasu wyjścia jest podobne dla wszystkich wartości wykładnika stabilności. W końcu, analizowana jest szybkości przejścia między stanami dla ruchu w potencjałem dwudołkowym. W granicy ruchu przetłumionego omówiono odchylenia od przybliżenia słabego szumu. Dla pełnej dynamiki przedstawiono przybliżony wzór analityczny, pokazujący, że stosunek szybkości przejścia zależy zarówno od wysokości bariery potencjału, jak i jego szerokości. Przybliżenie jest porównywane z symulacjami numerycznymi.

List of Abbreviations

FPT	first passage time
GWN	Gaussian white noise
LHP	last hitting point
MFPT	mean first passage time
RAP	randomly accelerated process
FFPS	fractional Fokker-Planck-Smoluchowski (equation)

Foreword

This doctoral dissertation is based on the series of articles on properties of stationary states and escape problems, published in the reputable, international, peer-reviewed scientific journals during the period 2019-2021. It includes a Guidebook, in which the author presents the background and motivation for this work and briefly summarizes the results, as well as the following original articles which are referred in the Guidebook by A.1 through A.6.

A.1 K. Capała, B. Dybiec, *Multimodal Stationary states in symmetric single-well potentials driven by Cauchy noise*, J. Stat. Mech., 033206 (2019).
DOI: 10.1088/1742-5468/ab054c also arXiv:1811.06265.

A.2 K. Capała, B. Dybiec, *Stationary states for underdamped anharmonic oscillators driven by Cauchy noise*, Chaos **29**, 093113 (2019).
DOI: 10.1063/1.5111637 also arXiv:1905.12078.

A.3 K. Capała, B. Dybiec, E. Gudowska-Nowak, *Nonlinear friction in underdamped anharmonic stochastic oscillators*, Chaos **30**, 073140 (2020).
DOI: 10.1063/5.0007581 also arXiv:2003.05918.

A.4 K. Capała, B. Dybiec, *Inertial Lévy flights in bounded domains*, Chaos **31**, 083120 (2021).
DOI: 10.1063/5.0054634 also arXiv:2104.10185.

A.5 K. Capała, B. Dybiec, E. Gudowska-Nowak, *Peculiarities of escape kinetics in the presence of athermal noises*, Chaos **30**, 013127 (2020).
DOI: 10.1063/1.5126263 also arXiv:1909.00196.

A.6 K. Capała, B. Dybiec, *Underdamped, anomalous kinetics in double-well potentials*, Phys. Rev. E **102**, 052123 (2020).
DOI: 10.1103/PhysRevE.102.052123 also arXiv:2006.12249.

Due to possible copyright restrictions, instead of Publishers' versions, preprints of the articles are attached. Published versions are available at the respective DOI links provided in the references.

In addition to the publications listed, the author significantly contributed to another eight scientific papers published in peer reviewed journals. This research was supported by the National Science Center (Poland) grant 2018/31/N/ST2/00598.

Acknowledgements

I would like to express my gratitude to my supervisor prof. Bartłomiej Dybiec for his help and guidance. I am really grateful for such an amazing mentor. I want also thank prof. Ewa Gudowska-Nowak for sharing her knowledge during collaborative projects, dr Wojciech Tomczyk for his support and advices, and dr Maciej Majka for numerous discussions. I am grateful to all members of Statistical Physics Department for always being supportive and open to conversation. Finally, I want to thank my family and everyone who supported me on this journey.

Chapter 1

Introduction

Random processes or their fingerprints are ubiquitous in nature. They can be used to describe or approximate movement of people [1, 2], searching (foraging) strategies of animals [3, 4], chemical reactions [5, 6], climate changes [7], diffusion in turbulent media [8, 9] and many processes in body cells [10–12], just to name few. The above systems are related through the presence of interactions that are too complex to describe deterministically or they are simply random. Therefore, such interactions can be efficiently approximated by noise. A very simple yet useful type of noise is Gaussian white noise (GWN), $\eta(t)$. Its statistical properties are determined by a normal distribution with zero mean value, i.e., $\langle \eta(t) \rangle = 0$. Moreover, GWN is uncorrelated, i.e. $\langle \eta(t)\eta(s) \rangle = \sigma\delta(t-s)$, where σ is a standard deviation of normal distribution and represents the noise intensity. GWN is widely used to describe equilibrium systems. However, many systems exhibit non-equilibrium behavior and they cannot be described by GWN. Therefore generalization of GWN is required for their analysis. One of possible options is (white) Lévy noise. The α-stable (Lévy) type noise is a formal time derivative of the Lévy process, whose increments are independent and identically distributed according to the α-stable density [13, 14]. The α-stable density $p(x)$ is defined by the characteristic function ($\phi(k) = \langle e^{ikx} \rangle$)

$$\phi(k) = \begin{cases} \exp\left[ik\mu - \sigma^\alpha |k|^\alpha \left(1 - i\beta \mathrm{sgn}(k) \tan\frac{\pi\alpha}{2}\right)\right] & \text{for} \quad \alpha \in (0,1) \cup (1,2] \\ \exp\left[ik\mu - \sigma|k| \left(1 - i\beta\frac{2}{\pi}\mathrm{sgn}(k) \ln|k|\right)\right] & \text{for} \quad \alpha = 1 \end{cases} . \tag{1.1}$$

In Eq. (1.1), $\alpha \in (0, 2]$ stands for stability index, while β ($\beta \in [-1, 1]$) is the skewness parameter. Finally, σ and μ are scale and location parameters respectively. In the further discussion we will limit ourselves to symmetric distributions without drift, i.e., $\beta = 0$ and $\mu = 0$. In this case Eq. (1.1) simplifies to

$$\phi(k) = \exp\left[-\sigma^\alpha |k|^\alpha\right]. \tag{1.2}$$

For $\alpha < 2$, α-stable distributions have asymptotic behavior of the power law type, i.e., $P(x) \sim |x|^{-(\alpha+1)}$. Therefore, only fractional moments of order ν smaller than α are finite ($\nu < \alpha$), i.e., $\langle |x|^\nu \rangle < \infty$. In general, inverting the Fourier transform of a characteristic function given by

Eq. (1.2) is a challenging task [15, 16]. Simple analytical formulae for α-stable distributions are known only for few cases. For example, for $\alpha = 1$ we obtain a Cauchy distribution and for $\alpha = 2$ – a normal density. The inclusion of the Gaussian noise as a special case is one reason to consider Lévy flights as an extension of the stochastic system to non-equilibrium regimes. However, and more importantly the α-stable distributions, used to describe Lévy flights, possess nice mathematical properties and they share many arithmetic features with the normal distribution. The most important are self-similarity and (generalized) central limit theorem.

To describe evolution of the system we need an equation of motion of the particle under action of deterministic and stochastic forces. For the random walk, it takes the form of the Langevin equation, which is the stochastic analog of the Newton's Second Law [17]

$$\frac{d^2x(t)}{dt^2} = -\gamma\frac{dx(t)}{dt} - V'(x) + \zeta(t), \tag{1.3}$$

where γ is a friction coefficient and $V(x)$ is a deterministic potential. In general the potential can also be a function of time, i.e., $V(x,t)$, however in the following thesis we will limit ourselves to a time independent case. Term $\zeta(t)$ in the equation (1.3) describes the stochastic driving. In our considerations $\zeta(t)$ is a symmetric Lévy noise, discussed in more detail in the previous paragraph. The process described by Eq. (1.3) is called underdamped. On the other hand, usually, an overdamped limit of Eq. (1.3) is considered, for which the friction coefficient $\gamma \gg 1$. For the overdamped regime the Langevin equation (1.3) simplifies to the typical form [17]

$$\frac{dx(t)}{dt} = -V'(x) + \zeta(t). \tag{1.4}$$

Complementary to the underdamped Langevin equation (1.3) the evolution of the probability $P(x,v,t)$ density is described by the fractional Fokker-Planck-Smoluchowski equation [14, 18, 19]

$$\frac{\partial P(x,v,t)}{\partial t} = \left(-v\frac{\partial}{\partial x} + \frac{\partial}{\partial v}\left(\gamma v - V'(x)\right) + \sigma^\alpha \frac{\partial^\alpha}{\partial |v|^\alpha}\right) P(x,v,t), \tag{1.5}$$

where the Riesz-Weil fractional derivative [18,20] is defined via the Fourier transform $\mathcal{F}_k\left(\frac{\partial^\alpha f(x)}{\partial |x|^\alpha}\right) = -|k|^\alpha \mathcal{F}_k(f(x))$. For the overdamped case the fractional Fokker-Planck-Smoluchowski equation has form [18, 21]

$$\frac{\partial P(x,t)}{\partial t} = \left(-\frac{\partial}{\partial x}V'(x) + \sigma^\alpha \frac{\partial^\alpha}{\partial |x|^\alpha}\right) P(x,t), \tag{1.6}$$

where analogously like in Eq. (1.5), the fractional derivative is defined by Fourier transform.

Usually solving Langevin (Eq (1.3)) or fractional Fokker-Planck-Smoluchowski (Eq (1.5)) equation is very difficult and, except in special cases, it is impossible to get a general analytical formula. Therefore, many problems require a numerical approach. On the one hand, the development of numerical methods for fractional partial differential equations has enabled construction of the numerical solution of the fractional Fokker-Planck-Smoluchowski equation [22, 23]. On the other hand, the Euler-Maruyama scheme [13, 24] allows to generate trajectories from the Langevin equation, from which, inter alia, $P(x,t)$ or $P(x,v,t)$ can be extracted. Here, the implementation of the latter method will be presented. Let us start by rewriting the Eq. (1.3) in the discretized form

$$\begin{cases} v_{i+1} = v_i - (\gamma v_i + V'(x_i))\Delta t + \sigma\,(\Delta t)^{1/\alpha}\,\zeta_i \\ x_{i+1} = x_i + v_i \Delta t \end{cases}, \tag{1.7}$$

where ζ_i is the sequence of independent and identically distributed α-stable random variables with the unit width ($\sigma = 1$) and Δt is the integration times step. Random variables following α-stable densities can be generated using the Chambers-Mallows-Stuck method [13, 24–27]. The first equation of (1.7) describes the azevolution of velocity and contains the stochastic part.Therefore, it should be approximated using the Euler-Maruyama scheme [13, 24]. To generate a full trajectory, the second (spatial) part of Eq (1.7)) is constructed trajectory-wise. The trajectory generation procedure can be repeated many times. From the set of generated trajectories, required quantities such as probability density, median energy or distribution of first exit times, to name a few, can be obtained. Since the Langevin dynamics allows the analysis of many quantities characterizing stochastic systems, their detailed discussion is addressed in the chapters dedicated to the individual issues.

A key element for applying the Euler-Maruyama scheme to approximate Lévy processes is the ability to generate random numbers ζ_i from the α-stable distribution. Let V and W be two independent random variables. V is generated from uniform distribution on the interval $(-\pi/2, \pi/2)$, while W is distributed according to exponential distribution with a unit mean [13, 24, 26, 27]. For $\alpha \neq 1$ the formula reads

$$\zeta = D_{\alpha,\beta,\sigma} \frac{\sin(\alpha V + \alpha C_{\alpha,\beta})}{\cos^{1/\alpha} V} \left(\frac{\cos((1-\alpha)V - \alpha C_{\alpha,\beta})}{W} \right)^{\frac{1-\alpha}{\alpha}}, \tag{1.8}$$

where

$$C_{\alpha,\beta} = \frac{\arctan\left(\beta \tan \frac{\pi\alpha}{2}\right)}{\alpha} \tag{1.9}$$

and

$$D_{\alpha,\beta,\sigma} = \sigma \left[\cos\left(\arctan\left(\beta \tan \frac{\pi\alpha}{2} \right) \right) \right]^{-1/\alpha}. \tag{1.10}$$

The case of $\alpha = 1$ needs to be considered separately. Random numbers generated from the α-stable distribution with $\alpha = 1$ and any $\beta \in [-1, 1]$ can be obtained form

$$\zeta = \frac{2\sigma}{\pi} \left[\left(\frac{\pi}{2} + \beta V \right) \tan V - \beta \ln \left(\frac{\pi W \cos V}{\pi + 2\beta V} \right) \right]. \tag{1.11}$$

Chapter 2

Stationary States

For the noise perturbed systems one, one may wonder about their long-time properties. For instance, for the particle which moves in the certain potential $V(x)$, it i possible to verify existence of stationary states and their properties. If the stationary state exists, the probability density is time independent, and therefore the left-hand side of the FFPS equation vanishes, i.e.,

$$\frac{\partial P(x,v,t)}{\partial t} \equiv 0. \tag{2.1}$$

Consequently, in this chapter we will use simplified notation for probability densities in stationary states $P(x) \equiv P(x, t \to \infty)$ for the overdamped case and $P(x,v) \equiv P(x,v,t \to \infty)$ for the underdamped case.

Stationary states for the additive GWN in the potential $V(x)$ are given by the Boltzmann-Gibbs distribution [28]

$$P(x,v) = \mathcal{Z} \exp\left(-\frac{E}{\sigma}\right) = \mathcal{Z} \exp\left(-\frac{\frac{v^2}{2} + V(x)}{\sigma^2}\right), \tag{2.2}$$

as long as $V(x) \to \infty$ when $|x| \to \infty$. In the Eq. (2.2), $\mathcal{Z}$ is a normalization factor. Therefore, stationary states are known as long as one is able to calculate $\mathcal{Z}$. For the non-Gaussian, α-stable noises, the problem of the stationary state is more difficult to solve. First, in order to assure the existence of stationary states, it is not sufficient to assume $V(x) \to \infty$ for $|x| \to \infty$ [29]. The condition necessary for the existence of stationary states under the influence of Lévy noise has been extensively studied in the overdamped regime for the power-law potentials [29]

$$V(x) \propto |x|^c. \tag{2.3}$$

It has been demonstrated that the stationary state exists only for $c > 2 - \alpha$. Even if a stationary state exists, the analytical form of its distribution may be challenging to obtain. Therefore, analytical formulae for stationary states are known only for few potentials. The simplest examples are overdamped motion in an infinite rectangular potential well [30] and the harmonic oscillator in the regime of overdamped and full dynamics [31, 32].

In the overdamped regime, there is another important potential for which stationary state is known. It is quartic potential with the Cauchy driving, i.e., $V(x) = x^4/4$ and α-stable noise with $\alpha = 1$. In this case the stationary probability density reads [33–37]

$$P_{\alpha=1}(x) = \frac{1}{\pi\sigma^{\frac{1}{3}}\left[\left(x\sigma^{-\frac{1}{3}}\right)^4 - \left(x\sigma^{-\frac{1}{3}}\right)^2 + 1\right]}. \tag{2.4}$$

The probability density given by Eq. (2.4) exhibits an unexpected property. Although the quartic potential has only one minimum, the solution (2.4) has two spatially separated maxima located at $\pm\sigma^{\frac{1}{3}}/\sqrt{2}$. This behavior is in contradiction to the intuition which one may have based on GWN, since the density (2.2) has the same number of maxima as $V(x)$ minima. Moreover, bimodality is observed in the overdamped regime for any $\alpha < 2$ and in any potential of the x^n/n type [33–38] or even for

$$V(x) = \frac{x^4}{4} + a\frac{x^2}{2} \tag{2.5}$$

with $a > 0$ if $a < a_c = 0.794$ [34].

These results rise an important question whether it is possible to obtain states of higher modality than 2 in a single-well potential. In [A.1] we explored this possibility. As a starting point we have used the observation made in [33] that for a quartic potential the locations of the modal values in the steady state coincide with the location of the curvature maxima, where the curvature $\kappa(x)$ of the potential $V(x)$ is defined as

$$\kappa(x) = \frac{V''(x)}{[1 + V'(x)^2]^{3/2}}. \tag{2.6}$$

We assumed that the number of modes in the stationary state is not larger than the number of maxima of the potential curvature. In addition, the curvature maxima determines the likely position of the modal values. Unfortunately, the number of curvature maxima itself is not sufficient to assure the multimodal state. They need to be adequately spatially separated. Otherwise, modes of a stationary state can interfere, resulting in a smaller number of peaks in the stationary state than the number of maxima in the potential curvature. Therefore, the condition on the number of maxima of the potential curvature needs to be accompanied by additional numerical tests.

Using this assumption, we constructed a few fine-tuned, single-well potentials discussed below, for which stationary state has modality higher than two. We started with the potential

$$V(x) = x^2 - ax^4 + x^6, \tag{2.7}$$

where $a < \sqrt{3}$. The upper limit on a ensures a single-well potential. However, even for $a < \sqrt{3} \approx 1.73$, produced states demonstrate predicted trimodality. An example of such behavior is shown in the Fig. 2.1, where for $a = 19/11$ three modes are well-visible. Trimodality can be observed as long as $a > a_c$. For $a < a_c$, the stationary state is unimodal since the outer peaks have merged with the central one. From the numerical simulations, it can be estimated that $a_c \in (1.17, 1.2]$.

Unfortunately, due to inherent uncertainties of our methodology, it is difficult to provide a better estimation.

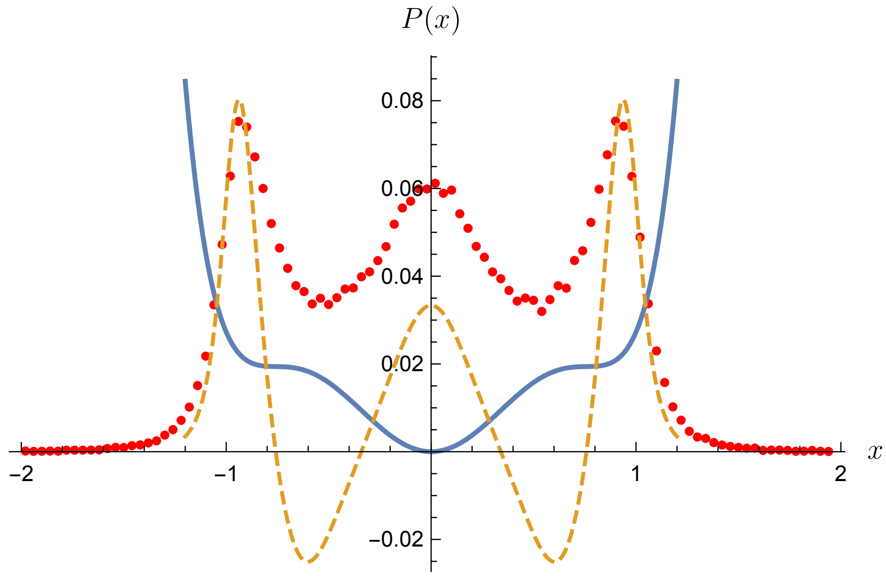

Figure 2.1: The stationary state for the potential given by Eq. (2.7) with $a = 19/11$, i.e., $V(x) = x^2 - 19/11x^4 + x^6$, subject to the Cauchy driving (α-stable noise with $\alpha = 1$) and $\sigma = 1$ (dots) along with the potential profile $V(x)$ (blue solid line) and the potential curvature $\kappa(x)$ (orange dashed line), see Eq. (2.6).

Analogously, using the maximal curvature argument, it is possible to produce potentials leading to a higher modality. An example of the potential generating four modes is

$$V(x) = \frac{7}{6}x^4 - 2x^6 + x^8. \tag{2.8}$$

The stationary state for the potential (2.8) is shown in Fig. 2.2. The stationary distribution consists of two distinct outer peaks and two smaller inner peaks. Since it behaves like x^4 for $x \to 0$, the stationary state has a minimum at $x = 0$, see Eq. (2.4). [A.1] also shows also two examples of fine-tuned, polynomial potentials of the 10th order, generating five-modal stationary states. Unfortunately, modality higher than five requires very steep potentials, which pose a problem for numerical simulations. To circumvent this problem, we implemented ‘glued’ potentials composed of pieces of the quartic potential. For such a potential one may an generate arbitrary high modality.

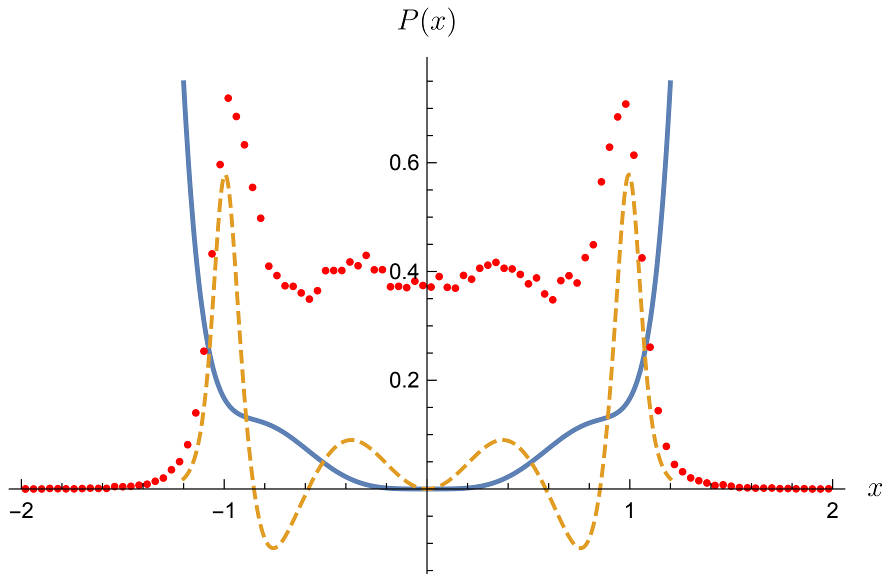

Figure 2.2: The same as in Fig. 2.1 for the potential given by Eq. (2.8), i.e.,$V(x) = \frac{7}{6}x^4 - 2x^6 + x^8$.

For example,

$$V(x) = \begin{cases} \frac{1}{4}(x+3)^4 + \frac{3}{4} & \text{for} \quad x < -3 \\ \frac{1}{4}(x+2)^4 + \frac{1}{2} & \text{for} \quad -3 \leqslant x < -2 \\ \frac{1}{4}(x+1)^4 + \frac{1}{4} & \text{for} \quad -2 \leqslant x < -1 \\ \frac{x^4}{4} & \text{for} \quad |x| \leqslant 1 \\ \frac{1}{4}(x-1)^4 + \frac{1}{4} & \text{for} \quad 1 < x \leqslant 2 \\ \frac{1}{4}(x-2)^4 + \frac{1}{2} & \text{for} \quad 2 < x \leqslant 3 \\ \frac{1}{4}(x-3)^4 + \frac{3}{4} & \text{for} \quad x > 3 \end{cases} \tag{2.9}$$

results in the emergence of an eight-modal stationary state, see Fig. 2.3. Due to its segmented nature, stationary density in the potential given by Eq. (2.9) can be understood as a composition of behaviors for the quartic potential in each part individually. It is also important that the time of deterministic sliding from the distant segment to the one closer to the origin is infinite. However, in such a 'glued' potential, the curvature argument holds. More examples of stationary states obtained using 'glued' potentials, together with a broader discussion, can be found in [A.1].

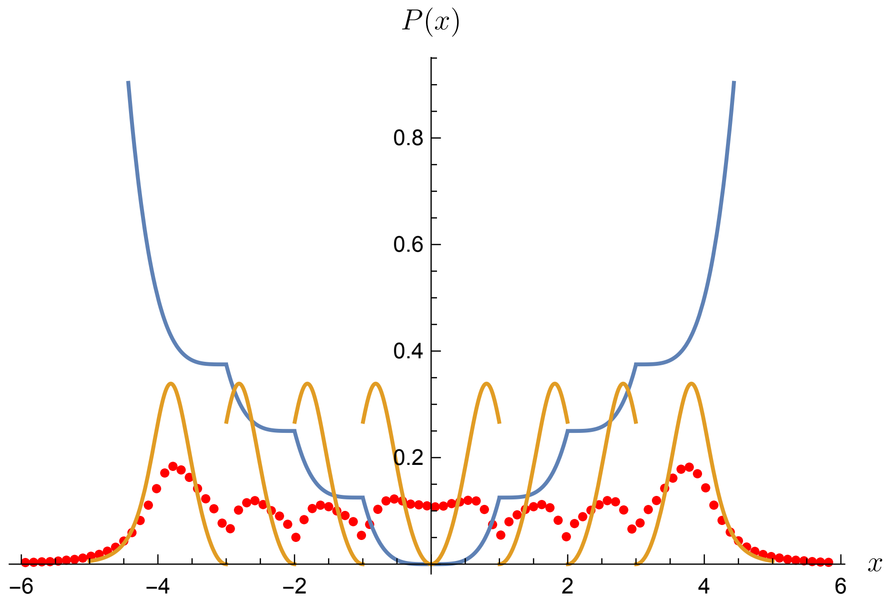

Figure 2.3: The same as in Fig. 2.1 for the potential given by Eq. (2.9).

2.1 Linear Friction

The multimodality of the stationary states in the system driven by α-stable noise were intensively investigated in the overdamped regime. However, this topic was not explored in the underdamped case. This issue was addressed in [A.2], where we considered the underdamped Langevin equation (1.3) with the potential given by Eq. (2.5) and the Cauchy noise ($\alpha = 1$). Stationary states were estimated from numerical simulations of the Langevin equation using the schema given by Eq. (1.7).

Indeed, also the underdamped process can produce bimodal stationary states in the single-well potential. Fig. 2.4 shows plots of stationary states together with velocity and position marginal distributions for $V(x)$ given by Eq. (2.5) $a = 0$ and $\gamma = 1$ (left column) or $\gamma = 6$ (right column). Parameters are chosen in such a way to present two distinct regimes observed in the system. On the one hand, $\gamma = 1$ corresponds to a weak damping limit, for which stationary states are unimodal. On the other hand, $\gamma = 6$, displays bimodality, characteristic for large damping. It is worth noting that γ does not need to be very large for the emergence of bimodality. Transition between unimodal and bimodal regimes is very smooth. With decreasing γ outer peaks are getting smaller and finally disappear. The decrease in γ is not the only protocol of moving the system from bimodal to unimodal stationary states. Also, the increasing value of a may lead to transition to unimodal state. This behavior is analogous to the overdamped case, where a critical parameter a_c separating two regimes was also observed. Since the modality of the stationary state depends on two parameters it is convenient to present the results in the form of a phase diagram, see Fig. 2.5. Blue corresponds to the bimodal stationary state, while the white area represents parameters resulting in the unimodal stationary state. Using the diagram, see Fig. 2.5, one can easily identify the two modality transition scenarios described earlier.

The analysis of full probability densities allowed for a qualitative investigation of the system's behavior. However, quantitative analysis is easier to perform in one dimension. Therefore, the study of stationary states was complemented by examination of position and velocity marginal distributions. Position marginal distribution for $a = 0$ may be compared with the analytical solution given by Eq (2.4), since for large γ, results for the overdamped limit should be restored. Indeed, even for finite, although large, γ position marginal distribution follows the curve given by an overdamped solution very well. Moreover, bimodality is recorded for relatively small γ, i.e., $\gamma > 1.5$, although the effect is weaker. Finding the right estimate for a velocity marginal distribution is not as obvious. The limiting case for which the velocity distribution would be known is the motion in the absence of the deterministic potential $V(x)$. In this case, the velocity marginal distribution has the non-trivial long-time solution, despite lack of full stationary state

$$P(v) = \frac{1}{\pi}\frac{\tilde{\sigma}}{\tilde{\sigma}^2 + v^2}, \tag{2.10}$$

where

$$\tilde{\sigma} = \sigma/\gamma. \tag{2.11}$$

More precisely, due to linear friction, velocity attains the stationary density which is of (rescaled) Cauchy type. Analogous reasoning can be carried out for any α, showing that for linear friction $P(v)$ is given by the α-stable distribution with the same stability index α as the noise. At the same time, due to absence of the deterministic force the particle cannot be confined. The application of the (deterministic) force-free approximation for motion in a quartic potential is not ideal due to presence of the deterministic force. Yet, comparison between force-free solution and simulations for the quartic potential shows some similarity between the actual velocity marginal distribution and the properly rescaled Cauchy distribution (2.10). This similarity is well visible in the power-law tails of the distribution, while some disagreement appears in the central part.

Finally, the analysis of the velocity marginal distribution is important in understanding the mechanism of emergence of bimodal states in underdamped systems. This mechanism is described in detail in sections II and III of [A.2]. In short, it is based on the fact that particles with high velocity penetrate the outer part of the potential ($|x| \gg 1$), but for a sufficiently high damping factor γ they lose their velocity quickly and are unable to return efficiently to the origin. This is manifested in the heavy tails and the narrow central part of the velocity marginal distribution.

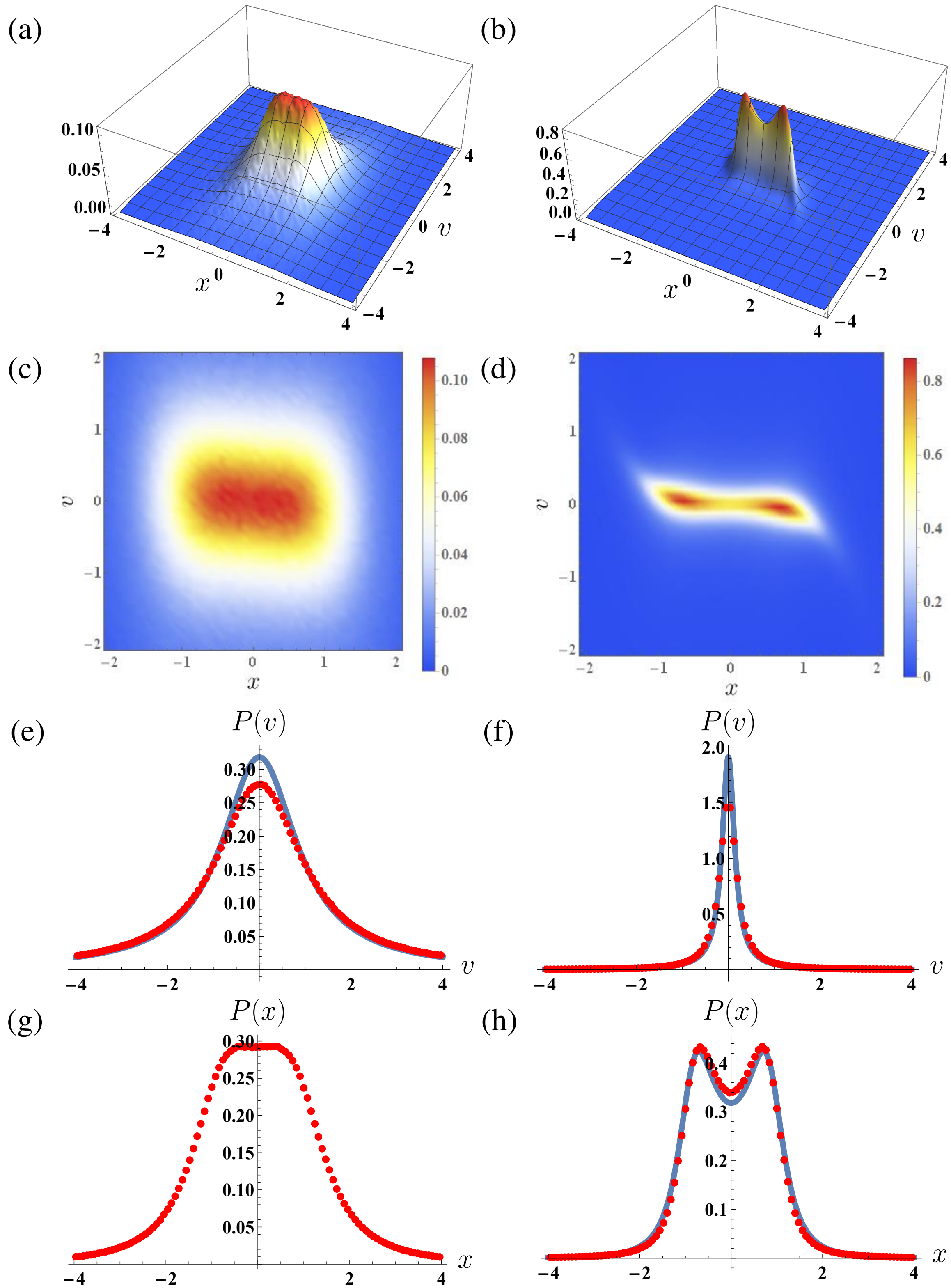

Figure 2.4: Panels (a) – (d) depict the stationary probability densities $P(x, v)$ as 3D-plot and the heat map. Panels (e) – (f) show the velocity marginal densities $P(v)$ (points) with the asymptotic density (2.10) (solid line) while panels (g) – (h) present the position marginal distributions $P(x)$ (points) with the asymptotic density (2.4). The damping parameter γ is set to $\gamma = 1$ (left column) and $\gamma = 6$ (right column).

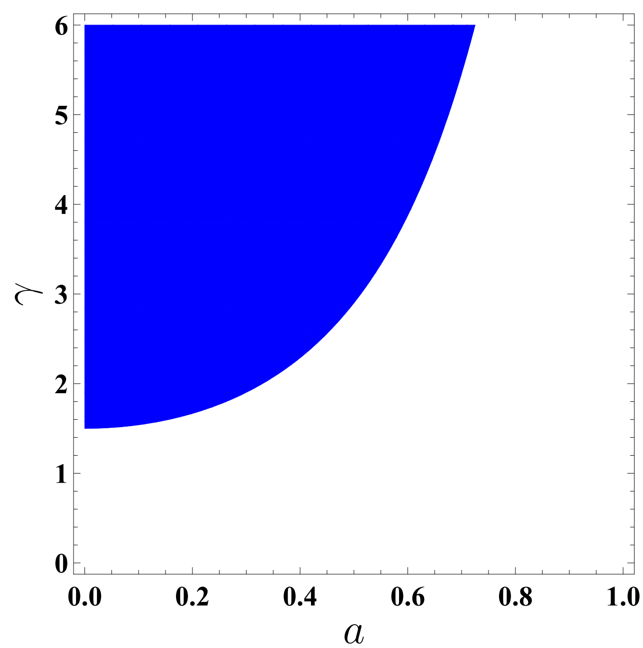

Figure 2.5: The phase diagram bimodal–unimodal stationary states for underdamped motion in potential given by Eq. (2.5), i.e., $V(x) = x^4/4 + ax^2/2$. The blue region represents values of parameters a and γ for which the full stationary state is bimodal.

2.2 Nonlinear Friction

Up to now we have considered linear friction as it is widely used and leads to simple intuitive overdamped limit. However other forms of damping are also studied in the literature [39]. Therefore, in [A.3], the model considered in Sec. 2.1 was reformulated for the nonlinear friction. For this purpose, we substituted the linear friction term $-\gamma v$ with a more general velocity-dependent term $T(v)$, i.e.

$$\begin{cases} \dot{x}(t) &= v(t) \\ \dot{v}(t) &= T(v) - V'(x) + \zeta(t) \end{cases}. \tag{2.12}$$

If we consider the deterministic force-free case, i.e. $V(x) \equiv 0$, the velocity part of the Eq. (2.12) reduces to

$$\dot{v}(t) = T(v) + \zeta(t). \tag{2.13}$$

One can easily see that in Eq. (2.13) $T(v)$ plays the similar role to the deterministic force $-V'(x)$ in the overdamped regime, see Eq. (1.4). Therefore, the generalized v-potential can be used to relate overdamped solutions to the velocity marginal distribution $P(v)$. It is important to emphasize that, despite its similarity to the external force in the overdamped limit, the velocity dependent friction $T(v)$ is always dissipative, i.e., $T(v)v < 0$ – the 'friction force' $T(v)$ is opposite to velocity. Moreover, similarly to the Sec. 2.1 we focus on $\zeta(t)$ being the Cauchy noise ($\alpha = 1$).

One of the simplest yet frequently used [39] form of $T(v)$ is

$$T(v) = -\gamma \mathrm{sgn}(v)|v|^{\kappa-1} \quad (\kappa > 1), \tag{2.14}$$

which corresponds in the overdamped case to the $|x|^\kappa/\kappa$ potential well and for $\kappa = 2$ reduces to the previously considered linear friction. From studies of the overdamped motion, it is known that for $\kappa < 2 - \alpha$, there is no stationary velocity distribution [29]. Therefore, in further studies, we will focus on $\kappa > 2$, and especially $\kappa = 4$, for which the analytical result of Eq (2.4) can be used.

Let us start with $\kappa = 4$ and the quartic potential $V(x) = x^4/4$. From the analogy to the overdamped case, one may expect bimodality in the velocity marginal distribution. As one can see in the Fig. 2.6, indeed, this is the case. With the increasing γ, the velocity marginal distribution better resembles the shape given by Eq. (2.4) with the scale parameter σ rescaled as in Eq. (2.11). One may also wonder if there is multimodality in the spatial part, which is determined by the velocity distribution and the quartic potential $V(x)$. However, even for very large sigma, there is no spatial multimodality, i.e., the position marginal distribution is unimodal. This behavior is also visible in the full stationary density. Modal values of the full stationary states are separated only along the velocity.

The modality is not the only phenomenon that may be analyzed by the analogy to the overdamped motion. The solution (2.4) exhibits the power-law behavior of the x^{-4} type. Therefore, all moments of the order lower than 4^{th} exist. The same asymptotics is observed in the marginal velocity distribution for the nonlinear friction with $\kappa = 4$. This leads to the finite mean value of the kinetic energy since the kinetic energy is proportional to $\langle v^2 \rangle$. Moreover, the rapid decay of position marginal distribution suggests that the mean value of potential energy $\langle V(x) \rangle$ is finite as well. Unfortunately, due to numerical instability produced by rare events when particle penetrates distant points i.e. $|x| \gg 0$, in the [A.3] we relied on robust measures i.e., medians of energies. Both medians of potential and kinetic energy are exponentially decreasing functions of γ. However, the median of the potential energy decays faster, and it is an order of magnitude smaller than the median of kinetic energy.

We explore simultaneous action of linear and nonlinear friction. To reach this aim we have used

$$T(v) = -\gamma(v^3 + av), \tag{2.15}$$

where a controls the relative strength of the linear part. The aforementioned form of friction $T(v)$, given by Eq. (2.15), resembles the deterministic force $-V'(x)$ with $V(x)$ given by Eq. (2.5). Therefore, one may expect a transition between bimodality and unimodality in velocities. Similarly to the overdamped motion, such a transition has been recorded, indicating that a plays a role of the control parameter determining the modality of the velocity marginal distribution. Nevertheless, even for a corresponding to unimodal velocity marginal distribution and large γ, there is no spatial bimodality in the full stationary state. This can be easily explained in the context of the mechanism of linear friction described in the last paragraph of the Sec. 2.1. In order to induce multimodality for the linear friction, large velocities are important as they allow penetration of outer parts of the potential, i.e., $|x| \gg 1$. For the nonlinear damping given by Eq. (2.15), the quartic part efficiently eliminates large velocities and therefore removes a crucial mechanism responsible for emergence of multimodality.

Finally, we have examined motion of a stochastic particle under action of the Cauchy noise with the friction term given by a polynomial steeper than cubic

$$T(v) = -\gamma \left(6v^5 - \frac{76}{11} v^3 + 2v \right). \tag{2.16}$$

One can easily see that despite its complex form this damping force is dissipative. Moreover, friction given by Eq. (2.16) resembles the deterministic force $-V'(x)$ with $V(x)$ given by Eq. (2.7) with $a = 19/11$. In the overdamped case this potential leads to the trimodal stationary state. Therefore, in the underdamped motion with friction given by Eq. (2.16), a pronounced trimodality can be observed in the velocity marginal distribution $P(v)$, see Fig. 2.7. This rich behavior is reflected in the full stationary density, where one can observe three peaks separated in the velocity direction. The two outer peaks ($|v| \gg 0$) behave similarly to the friction given by Eq. (2.15). Despite separation in the velocity direction, they are located at $x = 0$, and therefore there is no spatial multimodality for $v \neq 0$. On the other hand, the central mode of the velocity marginal distribution corresponds to particles which, due to small velocity, behave similarly to the process

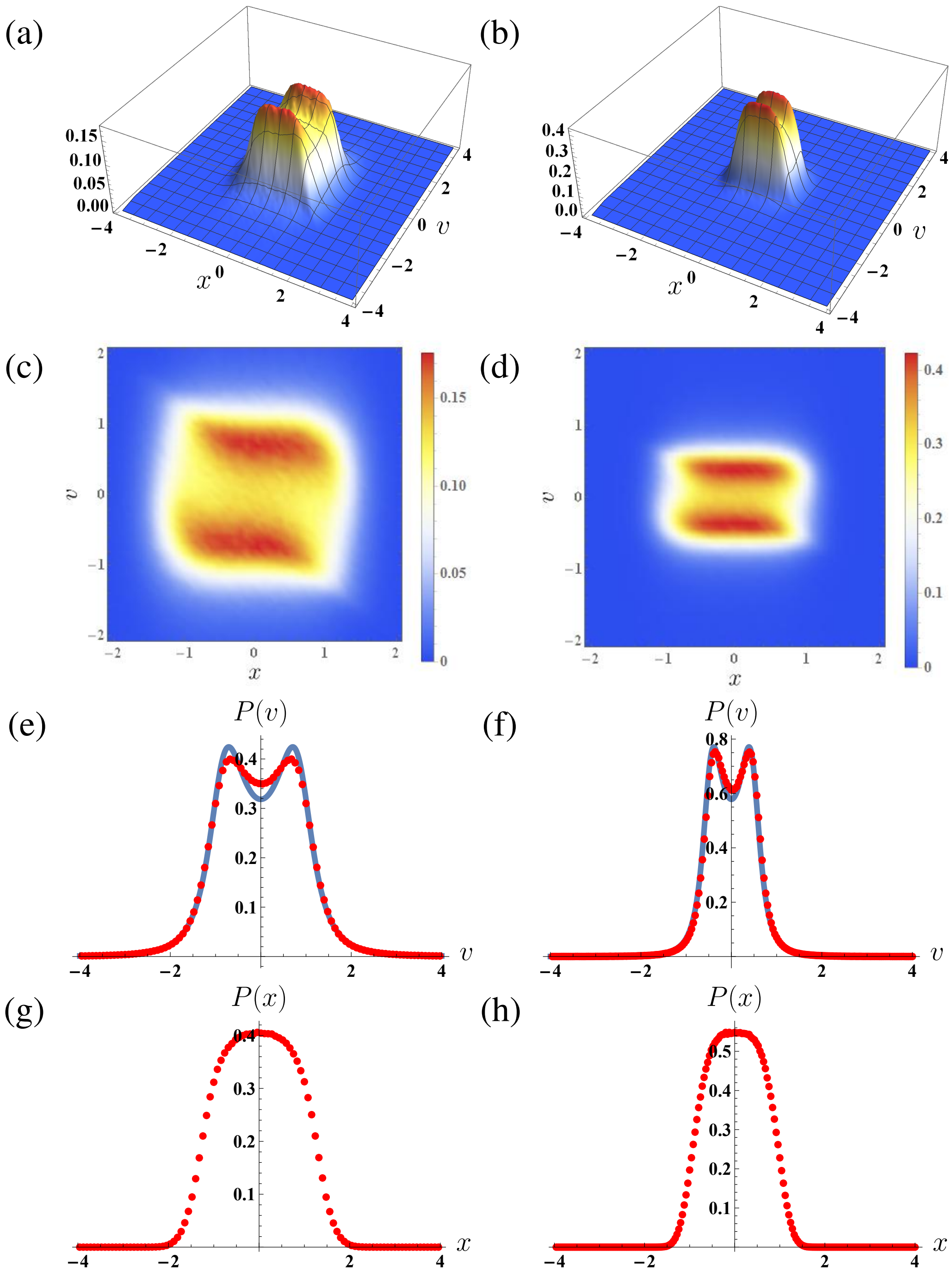

Figure 2.6: Panels (a) – (d) show the stationary probability densities $P(x, v)$ for the nonlinear friction $T(v) = -\gamma v^3$ as 3D-plots and the heat maps. Additionally, the velocity marginal densities $P(v)$ (points) with the asymptotic density (2.4) (solid line) is depicted in the panels (e) – (f), while the position marginal distributions $P(x)$ (points) is shown in the panels (g) – (h). The damping parameter γ is set to $\gamma = 1$ (left column) and $\gamma = 6$ (right column).

with linear friction. Therefore, for $v \approx 0$, the full probability density $P(x, v)$ has two maxima, as $P(x = 0, v = 0)$ is a saddle point. Thus, stationary density $P(x, v)$ has four modal values, separated both spatially and in the velocity direction. At the same time, the position marginal distribution $P(x)$ remains unimodal.

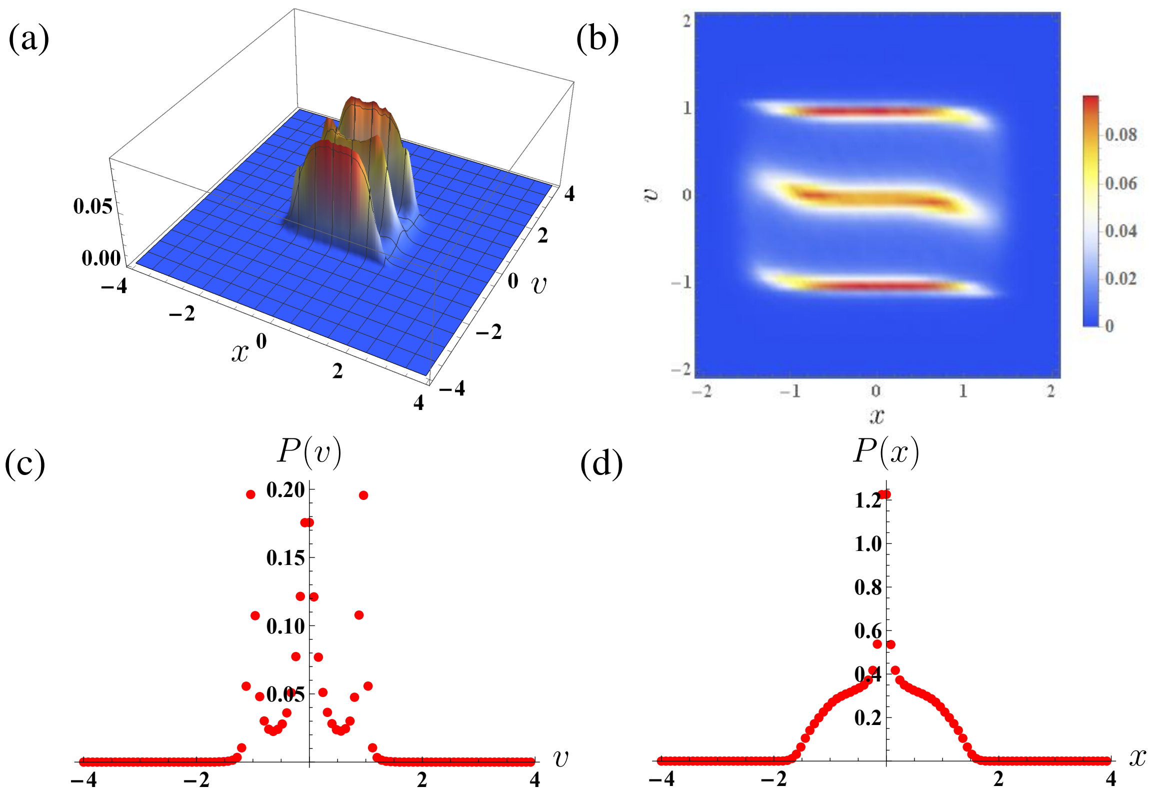

Figure 2.7: The stationary density $P(x, v)$ as 3D-plots (a) and the heat maps (b) together with velocity $P(v)$ (c) and position $P(x)$ (d) marginal densities for $T(v)$ given by Eq. (2.16) with $\gamma = 4$.

Chapter 3

Escape Kinetics

Various types of escape problems are widely studied within the theory of stochastic processes. They are considered in systems where the domain of motion is somehow restricted, and a particle is able to leave it. Therefore, the process in such a system is studied as long as the particle stays within the given domain. Shape and properties of the domain depend on a particular problem. However, there are common quantities which can be used to describe escape dynamics. One of them is the distribution of first passage times (FPT) τ, which is the distribution of times when the particle escapes from the given domain for the first time. From the distribution or large sample of first passage times it is possible to calculate various characteristics of the escape process. In general, distribution of FPT could be of the heavy tailed type and therefore it may not have any moments, particularly the first one. The simplest example of a system in which all moments of the FPT distribution diverge is the escape of the Brownian particle from the semi-axis in the absence of external forces [40, 41]. However, for the system perturbed by GWN or Lévy noise, if the domain of motion is finite or the potential prevents the particle from penetrating the space away from the boundary, typically the mean value exists. In these cases, the escape problem can be conveniently described by a single characteristic – the mean first passage time (MFPT), which is formally defined as

$$\mathcal{T} = \langle \tau \rangle = \langle \min\{t : x(0) = x_0 \ \wedge \ x(t) \notin \Sigma\} \rangle, \tag{3.1}$$

where Σ stands for the domain of motion and $x_0 \in \Sigma$ is the initial position.

If the MFPT is not sufficient to characterize the escape problem, other quantities can be used. For a discontinuous process, the particle can leave the domain of motion without visiting the vicinity of the boundary. Therefore, it is useful to pose a question about distribution of the so called last hitting points (LHP). LHP is the last point visited by a particle before leaving the domain of motion. Examination of the LHP distribution can provide deeper insight into a system's dynamics. In particular, it can be used for the overdamped Lévy flights to assess the role played by single jump escapes. The LHP distribution for the escape from the finite interval restricted by two absorbing boundaries ($\Sigma = [-1, 1]$) is depicted in the Fig. 3.1. As α decreases, the peaks located at the boundaries weaken, while the central peak becomes more pronounced. This is due to the increasing importance of the single jump escapes for small α. However, LHP also has its own limitations. They are especially well visible for the continuous trajectories, for which last visited points are located on boundaries. Therefore, for the escape from the bounded domain, the distribution of LHP is just a sum of the Dirac deltas centered on the boundaries with coefficients equal to the probabilities of escaping through a particular boundary. These coefficients define the so called splitting probability. For the fully symmetric problem on the finite interval, the splitting probability is equal to 0.5 since probabilities of escaping through both ends are the same. Therefore, deviations from 0.5 indicate asymmetries in the system dynamics.

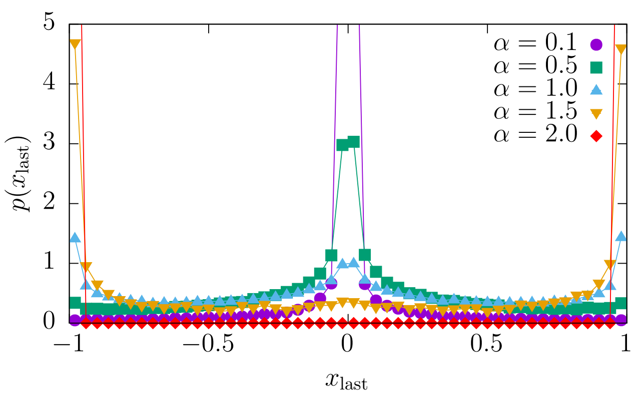

Figure 3.1: The last hitting point density $P(x_{\mathrm{last}})$ for the escape from the finite interval $[-1, 1]$ for $\sigma = 0.1$.

Underdamped Lévy flights, which are the main topic of this thesis, are continuous in the position $x(t)$, therefore LHP distribution is not very insightful in their description. Analysis of the full dynamic allows us to study properties of one more variable during escape – velocity. The distribution of escape velocities may display complex and unexpected behavior. This issue is covered in the next section (3.1) and [A.4].

3.1 Underdamped Escape from the Finite Interval

One of the basic examples of systems in which the escape dynamics is analyzed is the escape of the free particle from the finite interval restricted by two absorbing boundaries. Due to the system symmetries, the domain of motion Σ can be chosen in numerous ways. In [A.4] we choose $\Sigma = [-l, l]$. Due to the final size of the domain of motion and assumed driving type, the MFPT is finite, and therefore it is one of the main quantities describing the system. The analytical formula for the MFPT for any α is known in the overdamped limit [42–46], and it reads

$$\mathcal{T}(x) = \frac{(l^2 - x_0^2)^{\alpha/2}}{\Gamma(1+\alpha)\sigma^\alpha}, \tag{3.2}$$

where x_0 is the initial position.

The escape from the finite interval restricted by two absorbing boundaries can be extended to the regime of full dynamics. The underdamped random walk in the finite interval is described by four parameters – the interval half-width l, the friction coefficient γ, the noise intensity σ and the stability index α. However, the number of parameters can be significantly reduced in dimensionless units

$$\left\{ \begin{array}{lcl} \tilde{x} & = & x/l \\ \tilde{t} & = & \gamma t \end{array} \right. . \tag{3.3}$$

As one can see, the only free parameter, because α is fixed, is the dimensionless noise intensity $\tilde{\sigma}$, which is expressed by dimensional variables as

$$\tilde{\sigma} = \frac{\sigma}{l\gamma^{(1+\alpha)/\alpha}}.$$

Unfortunately, these variables cannot be applied in the undamped limit, i.e., for $\gamma = 0$. In this case another set of dimensionless variables is used

$$\left\{ \begin{array}{lcl} \tilde{x} & = & x/l \\ \tilde{t} & = & t/\left[\frac{l}{\sigma}\right]^{\frac{\alpha}{1+\alpha}} \end{array} \right. . \tag{3.4}$$

Consequently, for the undamped escape problem there are no free parameters for fixed α. In the mathematical literature, undamped process, or so called randomly accelerated process (RAP) [47, 48], for arbitrary α is often called integrated Lévy process, while the case with $\alpha = 2$ has many names – integrated Brownian motion [49, 50] or integrated Wiener process. Only for the RAP with Gaussian driving, analytical solution for the MFPT is known [48–50]. Since the general formula for any v_0 is very complicated, here, we will present only $v_0 = 0$ case. After transformation of the original $[0, l]$ setup considered in [49, 50] to the $[-l, l]$ and passing to the dimensionless variables, see [A.4], the formula for the MFPT with $v_0 = 0$ reads

$$\begin{aligned} \mathcal{T}(x, 0) &= \frac{2}{3^{1/6}\Gamma(7/3)} \left[\frac{1+x}{2}\right]^{1/6} \left[\frac{1-x}{2}\right]^{1/6} \\ &\times \left\{ {}_2F\left(1, -\frac{1}{3}; \frac{7}{6}; \frac{1+x}{2}\right) + {}_2F\left(1, -\frac{1}{3}; \frac{7}{6}; \frac{1-x}{2}\right) \right\}, \end{aligned} \tag{3.5}$$

where ${}_2F\left(a, b; c; x\right)$ is the Gauss hypergeometric function [51].

[A.4] extends the analysis of the underdamped escape from the finite interval to the Lévy driving. Qualitatively, MFPTs behave very similarly for every value of the stability index α. However, the relations between MFPTs for different values of the stability index α depend on the specific value of the (dimensionless) parameter σ. Fig. 3.2 shows MFPT for different values of the stability index α and $\sigma = 1$. Solid line represents analytical solution for the Gaussian driven RAP with $v_0 = 0$, see Eq. (3.5). Based on the examination of Fig. 3.2, one may expect that decreasing α lowers the MFPT, but it is not always the case. Order of MFPT surfaces depends on the initial position and the (dimensionless) noise intensity σ. For example, for $\sigma = 4$ with $v_0 = 0$ order of MFPTs as function of α is reversed in comparison to $\sigma = 1$ case. This difference decreases as the initial velocity increases, and the order of the curves is eventually reversed.

MFPT is not the only quantity describing escape dynamics. For the underdamped motion, as was mentioned at the beginning of this chapter, one may also ask questions about escape velocity and escape energy. To conveniently describe these quantities with one number, their medians were analyzed in [A.4]. For the velocity, we also used the ratio of interquantile widths

$$\mathcal{R} = \frac{v_{0.5} - v_{0.1}}{v_{0.9} - v_{0.5}}, \tag{3.6}$$

where $v_{\dots}$ indicates quantiles of a given order q ($0 < q < 1$) of the exit velocity, e.g., $v_q(t)$ is defined by

$$q = \int_{-\infty}^{v_q(t)} p(v;t)dv. \tag{3.7}$$

In the above equation, $p(v;t)$ stands for the exit velocity distribution. The ratio defined by Eq. (3.6) measures the fraction of widths of intervals containing 40% of the exit velocities above ($v_{0.9} - v_{0.5}$) and below ($v_{0.5} - v_{0.1}$) the median ($v_{0.5}$). Therefore, the closer $\mathcal{R}$ is to unity, the more symmetrical the distribution is. The median of escape velocity does not display any significant dependence on the value of the stability index α. Contrary to the median, the symmetry of the escape velocity distribution may significantly change with α. To be more precise, for the small value of stability index α, e.g., for $\alpha = 0.5$, the distribution of the exit velocity is almost symmetric, i.e., $\mathcal{R} \approx 1$. With the increasing α, asymmetry increases, as it is easier to escape through the nearest boundary. However, symmetry can be reintroduced to the escape velocity distribution twofold. On the one hand, $\mathcal{R} = 1$ for every value of stability index α when initial conditions are set to $v_0 = 0$ and $x_0 = 0$, due to the system's symmetry. On the other hand, the escape velocity distribution is more symmetric for large $|v_0|$, as it becomes narrower due to the short time before escape, see MFPT Fig. 3.2. Finally, the median of escape energy for small values of initial conditions x_0 and v_0 is very sensitive to α and rapidly decreases with the increasing value of the stability index. However, for large value of v_0, median is almost insensitive to α and increases to infinity with increasing $|v_0|$. Between these two regions one may find minimal value of median of escape energy usually for $v_0 \neq 0$, see Fig. 3.3.

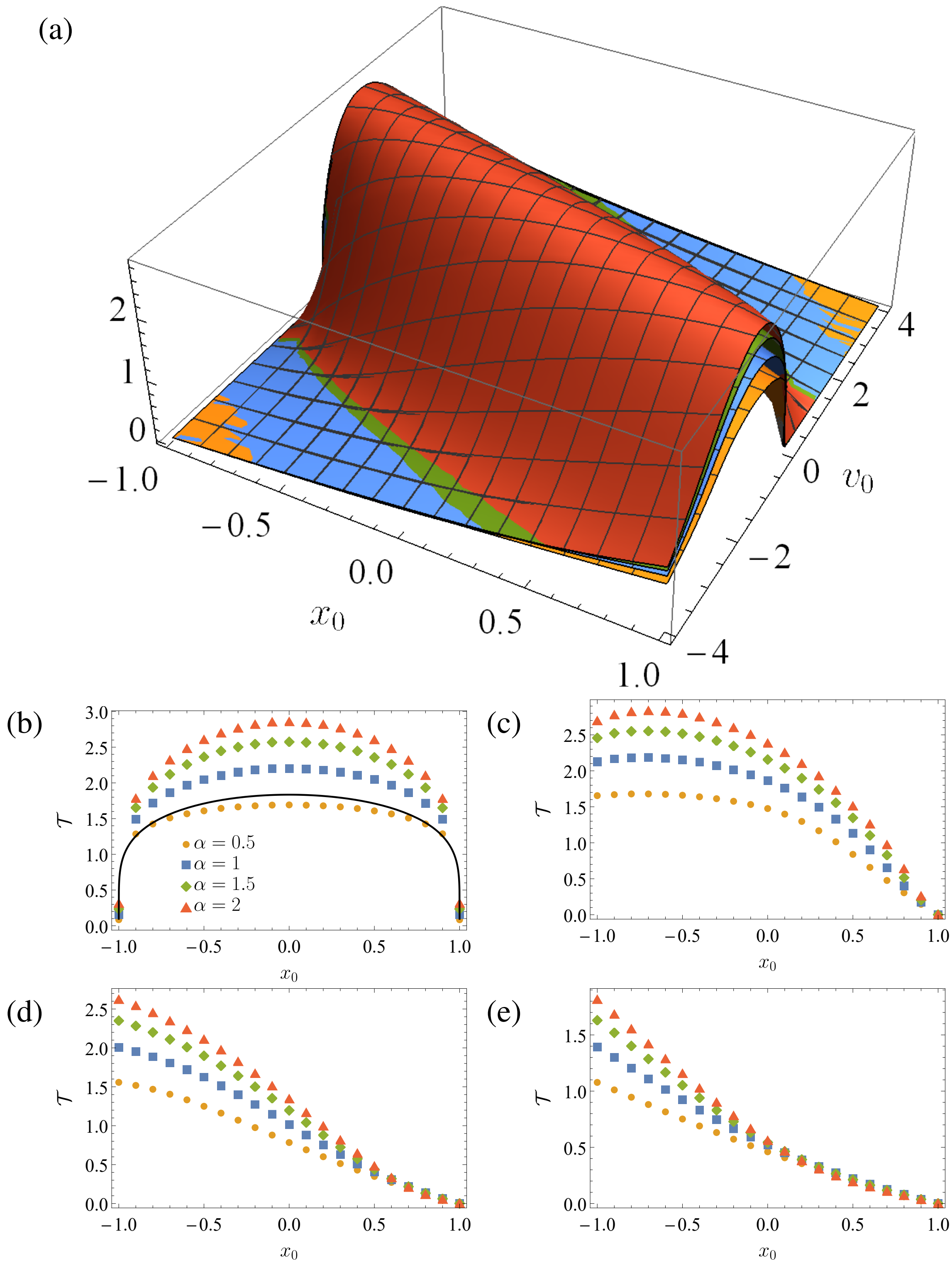

Figure 3.2: The MFPT $\mathcal{T}(x_0, v_0)$ as a function of the initial condition (x_0, v_0) for various values of the stability index α ($\alpha \in \{0.5, 1, 1.5, 2\}$) from the lowest to highest MFPT respectively. Bottom part shows cross-sections for $v_0 = 0$ (b), $v_0 = 1$ (c), $v_0 = 2$ (d) and $v_0 = 3$ (e). The scale parameter σ is set to $\sigma = 1$.

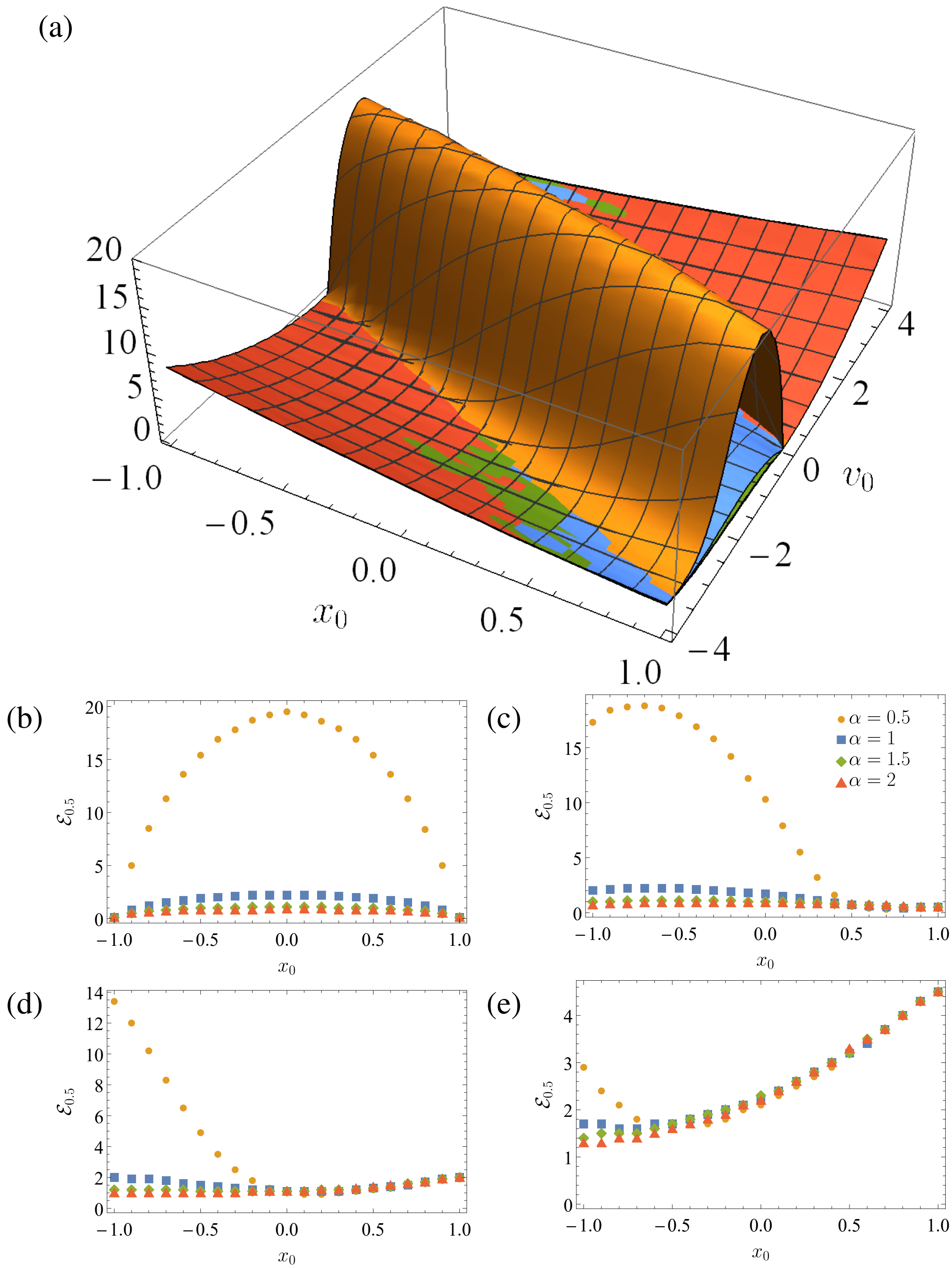

Figure 3.3: Median of exit energy $\mathcal{E}_{0.5}$ as a function of the initial condition (x_0, v_0) for various values of the stability index α ($\alpha \in \{0.5, 1, 1.5, 2\}$ (orange, blue, green, red)). Bottom part shows cross-sections for $v_0 = 0$ (b), $v_0 = 1$ (c), $v_0 = 2$ (d) and $v_0 = 3$ (e). The scale parameter σ is set to $\sigma = 1$.

3.2 Anomalous Diffusion in a Double-well Potential

One of the fundamental escape problems is the transition over the potential barrier. It can be examined for example in a double-well potential, see Fig. 3.5. The escape can be described using MFPTs $\mathcal{T}_{ij}$ or transition rates k_{ij}, where $i, j = 1, 2$ are indexes of initial and final minimum respectively. To be more precise, for instance, k_{12} describes the transition rate from, e.g., left minimum to the right minimum and vice versa for k_{21} – from right to left. Consequently, k_{12} and k_{21} represent forward and backward transition rates, see Fig. 3.5. For weak enough noise (small σ), the transition rates and MFPTs can be connected by simple relation [6]

$$k_{ij} = \frac{1}{\mathcal{T}_{ij}}. \tag{3.8}$$

Finally, one can calculate the ratio of transition rates

$$\kappa = \frac{k_{12}}{k_{21}} = \frac{\mathcal{T}_{21}}{\mathcal{T}_{12}}. \tag{3.9}$$

For the Gaussian white noise in the overdamped limit, analytical formula for the ratio of transition rates is known [52]

$$\kappa \propto \exp\left(-\frac{E_2 - E_1}{\sigma^2}\right). \tag{3.10}$$

Please note that even though forward and backward transition rates depend on the barrier height, the ratio of transition rates does not depend on the barrier height [6]. Moreover, this model is used as a stochastic model of chemical reactions as Eq. (3.10) corresponds to Arrhenious formula [53]. In this interpretation, the transition rate becomes a reaction rate.

The GWN driving is not the only case where analytical results are known. In the weak noise limit, Lévy noise can be decomposed using the Wiener process (central part of the jump length distribution) and compound Poisson process (long jumps controlled by the tails of the jump length distribution) [54, 55]. Importantly in the $\sigma \to 0$ limit, the transition over the potential barrier is possible only due to a single extreme kick [54–56]. Using the power-law asymptotics of α-stable density, the probability of a random jump larger than x_0 is given by

$$P(x > x_0) \sim x_0^{-\alpha}. \tag{3.11}$$

Therefore, for the overdamped Lévy flights in the weak noise regime, the analytical formula for the ratio of transition rates can be derived [54–56]

$$\kappa = \frac{k_{12}}{k_{21}} = \left(\frac{l_2}{l_1}\right)^{\alpha}. \tag{3.12}$$

Our main goal in [A.5] was to verify how weak noise behavior predicted by Eq. (3.12) changes when small kicks cannot be neglected. The role played by small kicks can be controlled in two main ways. More straightforward method requires increasing σ. The other way requires simultaneous action of (additive) Lévy ($\zeta(t)$) and Gaussian ($\eta(t)$) noise. The corresponding Langevin equation takes the form

$$\frac{dx(t)}{dt} = -V'(x) + \sigma\zeta(t) + \eta(t). \tag{3.13}$$

Please note that the GWN intensity is set to unity while Lévy noise intensity σ is written explicitly for clarity. In this setup the GWN can be interpreted as thermal (internal) noise while the Lévy part describes external (athermal) noise. In our analysis we have used

$$V(x) = 128x^4 - 64x^2 + ax, \tag{3.14}$$

where a controls the potential asymmetry, depths of minima and their location. The coefficients of the polynomial, see Eq. (3.14), have been chosen to ensure that recrossing events are rare. In order to eliminate recrossing events, the potential wells have to be deep enough and the barrier region sufficiently narrow [57]. In such a case, a particle spends the majority of time in the vicinity of potential wells. Consequently, the motion in a double-well potential can be approximated as a two states process. For the two-state process probability of being to the left from the potential barrier P_1 and to the right P_2 satisfy the following condition

$$\frac{k_{12}}{k_{21}} = \frac{P_2}{P_1}, \tag{3.15}$$

which implies from the master equation [58]. Therefore, the comparison between $\kappa = k_{12}/k_{21}$ and $\mathcal{P} = P_2/P_1$ can be used to verify if states are properly separated.

Fig. 3.4 shows ratio of transition rates κ for combined Gaussian and Lévy drivings with the Lévy noise intensity $\sigma = 1$ and $\sigma = 10$ as a function of stability index α. The parameter a in the potential (3.14) is set to $a = 10$. Points correspond to the numerical results while the blue solid line represents weak noise approximation given Eq (3.12). In both cases discrepancy between formula (3.12) and numerical results is significant. Moreover, for $\sigma = 10$ and $\alpha > 1$ weak noise approximation breaks even in absence of GWN, see [A.5], as central part of the Lévy distribution is too wide to consider single jump escape as the main protocol of transition between potential wells. The problem of weak noise approximation in the overdamped motion has been further analyzed in [59].

The similar approach to the one used to derive Eq. (3.12) was applied in the [A.6] to construct the approximated formula for the underdamped process. Contrary to the overdamped case, now instead of long stochastic jump, we are looking for a single noise ‘kick’ giving rise to the velocity necessary to escape from the potential well, see Fig. 3.6. To escape from the ith minimum a particle without the initial velocity needs to harvest energy necessary to surmount the potential barrier, see Fig. 3.6. In the absence of friction, the adequate formula reads

$$\frac{mv^2}{2} \geqslant E_b - E_i = \Delta E_i. \tag{3.16}$$

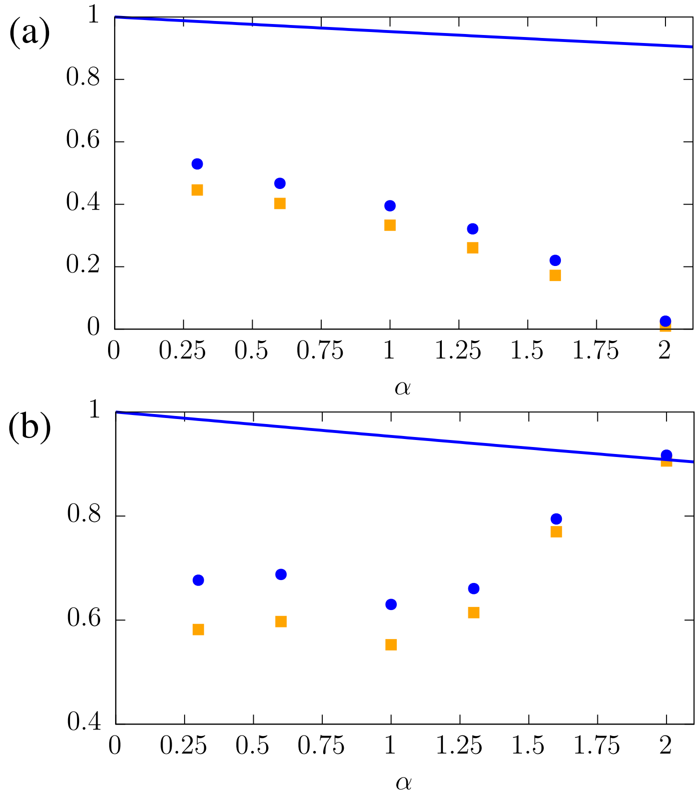

Figure 3.4: Symbols represent the ratios $\mathcal{P}$ of occupation probabilities (■) and κ of transition rates (•) for the double-well potential (3.14) with $a = 10$, i.e., $V(x) = 128x^4 - 64x^2 + 10x$. Solid blue lines show the theoretical 'width ratio' scaling (see Eq. (3.12)). Subsequent panels correspond to various values of the σ parameter scaling the strength of Lévy noise: $\sigma = 1$ (top panel – (a)) and $\sigma = 10$ (bottom panel – (b)).

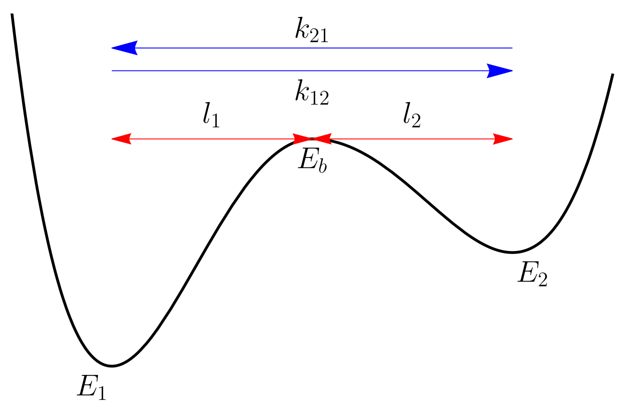

Figure 3.5: Schematic sketch of the potential given by Eq. (3.21), used in numerical studies of noise induced escape kinetics for underdamped process.

During the motion the energy is dissipated by friction, and therefore, the minimal initial velocity

v_0 needs to be larger

$$v_0 = v + \frac{\gamma}{m}\int_{t_0}^{t_0+\delta t} v(t)dt, \tag{3.17}$$

where δt ($\delta t \gg 0$) is the time necessary to reach the top of the potential barrier. Assuming that initially a particle is located in the vicinity of the potential well, the integration over time gives the distance between the initial position x_i and the potential barrier x_b, i.e., l_i. Consequently, the initial velocity reads

$$v_0 = v + \frac{\gamma}{m} l_i. \tag{3.18}$$

Combining Eqs. (3.16) and (3.18), we get the following estimate for the minimal initial velocity v_0

$$v_0 = \sqrt{\frac{2\Delta E_i}{m}} + \frac{\gamma}{m} l_i. \tag{3.19}$$

Fig. 3.6 shows exemplary trajectories underlying the escape events.

If the particle starts in the ith minimum, i.e., $x(t_0) = x_i$, the probability of velocity change larger than v_0 is equal to the transition rate k_{ij}, as v_0 is the minimal velocity required for the transition over potential barrier from the ith minimum. Therefore, similarly to the overdamped case, the ratio κ for the underdamped process reads

$$\kappa = \frac{k_{12}}{k_{21}} = \left(\frac{\sqrt{2\Delta E_2} + \gamma\sqrt{m} l_2}{\sqrt{2\Delta E_1} + \gamma\sqrt{m} l_1}\right)^{\alpha}. \tag{3.20}$$

From Eq. (3.20), it implies that the ratio of transition rates κ depends not only on the energy of the states, like for the overdamped escape induced by the action of GWN or on the barrier width like for the overdamped Lévy process but on all parameters describing the system. Moreover, in the strong friction limit, i.e., $\gamma \to \infty$, Eq. (3.20) reduces to the overdamped formula (3.12).

To verify the quality of the approximation given by Eq. (3.20), numerical simulations of Langevin equation were conducted. For this purpose, a fine-tailored potential was used

$$V(x) = \begin{cases} 4h_1\left[\frac{x^4}{4l_1^4} - \frac{x^2}{2l_1^2}\right] & x < 0 \\ \\ 4h_2\left[\frac{x^4}{4l_2^4} - \frac{x^2}{2l_2^2}\right] & x \geqslant 0 \end{cases}. \tag{3.21}$$

Potential given by Eq. (3.21) allows easy control of its depths and distances between minima and the maximum. Parameters h_1 and h_2 control depths of the left and right minimum respectively, while l_1 and l_2 represent distances between the potential maximum and the corresponding minimum. The top of the potential barrier is located at $x_b = 0$. The potential given by Eq. (3.21) is schematically depicted in Fig. 3.5.

Fig. 3.7 shows the ratio of transition rates for different values of left and right potential well depths h_1 and h_2. Remaining parameters were set to $l_1 = 1$, $l_2 = 1$, $\gamma = 1$ and $\sigma = 0.2$. It is clearly visible that despite many assumptions in the derivation, the formula given by Eq (3.20) (solid lines)

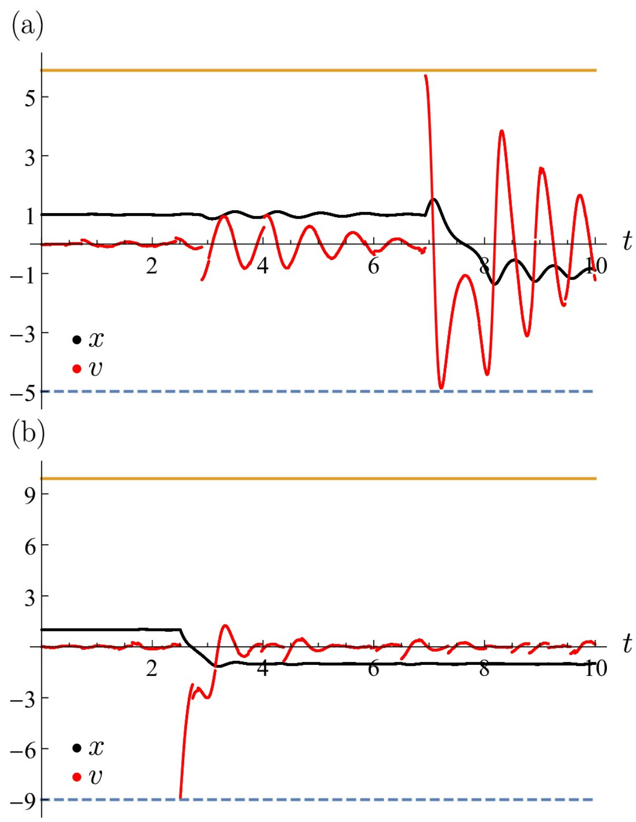

Figure 3.6: Sample trajectories of the particle moving in the potential (3.21) with $l_1 = l_2 = 1$, $h_1 = 12$ and $h_2 = 8$. The stability index α is equal to $\alpha = 1$ and the damping coefficient γ is set to $\gamma = 1$ (top panel — (a)) and $\gamma = 5$ (bottom panel — (b)). Horizontal lines show minimal velocities for forward (solid orange) and backward (dashed blue) transitions which are given by Eq. (3.19).

approximates results obtained from numerical simulations (points) fairly accurately. However, the weak noise approximation breaks down for much smaller σ than in the overdamped case, see [A.5]. Examination of κ for varying friction strength γ and widths l_1, l_2 also shows agreement between approximation (3.20) and simulation results, see [A.6]. Moreover, even if results differ from the formula (3.20) for given set of parameters, they still qualitatively follow the predicted scaling.

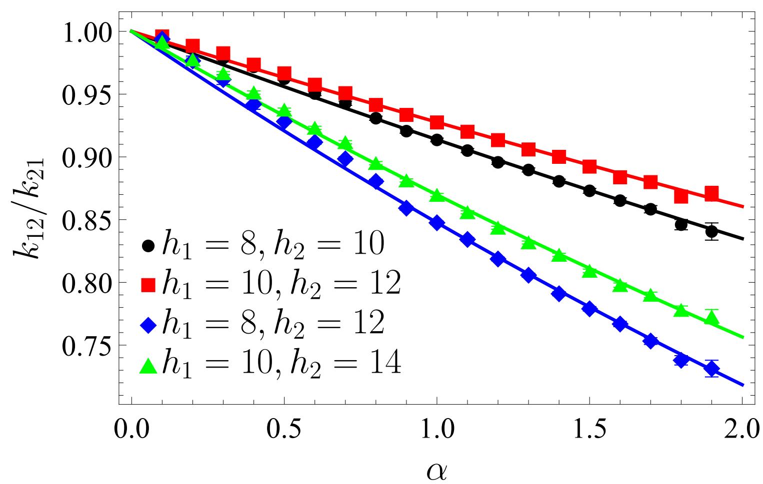

Figure 3.7: The ratio $\kappa(\alpha)$ of transition rates from minima of the potential (3.21) to the barrier top as a function of the stability index α. Various points correspond to numerical results for different depths of potential wells, i.e., different values of h_1 and h_2, while lines plot the scaling given by Eq. (3.20). Simulation parameters $l_1 = 1$, and $l_2 = 1$, $\gamma = 1$ and $\sigma = 0.2$.

Chapter 4

Concluding Remarks

The main motif of this thesis was to examine unusual phenomena induced by the Lévy noise with the special emphasis on the stationary states in single-well potentials and escape problems.

One of the counter intuitive phenomena is that the overdamped Lévy flights in single-well potentials might produce bimodal stationary states. In the chapter 2, we extended the phenomenological argument linking the number and position of modal values with the curvature maxima of the potential under consideration. The number of modal values of a stationary state in a given potential cannot be larger than the number of maxima of this potential curvature, but, it might be smaller. Using this hypothesis, we constructed a few fine-tuned, single-well potentials for which non-equilibrium stationary states have modality larger than two. Moreover, we analyzed how the aforementioned overdamped phenomena of multimodality translates to the full (underdamped) dynamics regime, with special attention to the quartic potential. We have demonstrated that for small linear friction bimodality in the quartic potential is not observed. However, it can be restored for finite and not very large friction. Contrary to the linear friction, superlinear friction cannot produce spatially bimodal stationary states. Bimodality in the velocities can be observed as long as the linear addition is not too large. This phenomenon was explained by the analogy to the overdamped regime.

Regarding escape problems, we considered two archetypal models – the escape from a finite interval and diffusion in a double-well potential. Detailed examination of the underdamped escape process driven by Lévy noise indicates that the mean first passage time displays limited sensitivity to the exact value of the stability index α. Therefore, despite very different velocity distributions, the qualitative system properties are very close to the properties of the randomly accelerated process. Nevertheless, the increase in the scale parameter (the only significant parameter besides the stability index α) can differentiate results corresponding to various values of α. On the one hand, for the Lévy-driven inertial process, medians of the escape velocity are weakly sensitive to the stability index α. On the other hand, analysis of the asymmetry of the escape velocity distributions shows a high level of responsivity to the stability index. In contrast to velocities, the studies of the medians of escape energies display significant sensitivity to the value of the stability index α, especially for small initial velocities. Finally, the median of the escape energy can decrease with the increasing value of the initial velocity.

We have also studied escape kinetics in a double-well potential, in the weak noise limit. The ratio of forward and backward transition rates between two states for the Lévy driven overdamped kinetics in a double-well potential depends only on the potential barrier width. In the [A.5] we examined possible protocols of breaking these properties in the overdamped system. We have numerically shown that both increase of noise intensity σ and addition of the GWN term leads to the violation of the 'width' formula. Also, for an underdamped process, the ratio of transition rates does not only depend on potential barrier width but also on its height. We derived an approximate formula describing the observed behavior of the ratio of transition rates for the weak noise (small σ). Comparison with numerical simulations shows that despite its limitations, the obtained formula can well approximate behavior for a wide range of parameters and give insight into the system dynamics.

Phenomena described by stochastic processes are ubiquitous in nature. They often cannot be described using equilibrium noise. Therefore, it is important to better understand non-equilibrium noises. The non-equilibrium Lévy processes were intensively studied in the overdamped regime. Here, we extended studies on the stationary states in single-well potentials and escape problems in the presence of Lévy noise to the full dynamics regime. Exploration of the Lévy processes in the underdamped regime may extend our knowledge about phenomena described by heavy-tailed noise, like searching strategies or stochastic optimization. Further studies should address simultaneous action of Lévy driving and stochastic resetting with the emphasis on underdamped regime.

Bibliography

[1] M. C. González, C. A. Hidalgo, and A. L. Barabási, Nature (London) **453**, 779 (2008).

[2] I. Rhee, M. Shin, S. Hong, K. Lee, and S. Chong, INFOCOM 2008. The 27th Conference on Computer Communications. IEEE 924 (2008).

[3] G. M. Viswanathan, V. Afanasyev, S. V. Buldyrev, E. J. Murphy, P. A. Prince, and H. E. Stanley, Nature (London) **381**, 413 (1996).

[4] D. W. Sims, E. J. Southall, N. E. Humphries, G. C. Hays, C. J. A. Bradshaw, J. W. Pitchford, A. James, M. Z. Ahmed, A. S. Brierley, M. A. Hindell, D. Morritt, M. K. Musyl, D. Righton, E. L. C. Shepard, V. J. Wearmouth, R. P. Wilson, M. J. Witt, and J. D. Metcalfe, Nature (London) **451**, 1098 (2008).

[5] C. W. Gardiner, *Handbook of stochastic methods for physics, chemistry and natural sciences* (Springer Verlag, Berlin, 2009).

[6] P. Hänggi, P. Talkner, and M. Borkovec, Rev. Mod. Phys. **62**, 251 (1990).

[7] P. D. Ditlevsen, Geophys. Res. Lett. **26**, 1441 (1999).

[8] H. G. E. Hentschel and I. Procaccia, Phys. Rev. A **29**, 1461 (1984).

[9] Z. Pasternak, F. Bartumeus, and F. W. Grasso, J. Phys. A: Math. Gen. **42**, 434010 (2009).

[10] M. Weiss, M. Elsner, F. Kartberg, and T. Nilsson, Biophys J. **87**, 3518 (2004).

[11] I. Bronstein, Y. Israel, E. Kepten, S. Mai, Y. Shav-Tal, E. Barkai, and Y. Garini, Phys. Rev. Lett. **103**, 018102 (2009).

[12] A. Fuliński and P. F. Góra, Phys. Rev. E **64**, 011905 (2001).

[13] A. Janicki and A. Weron, *Simulation and chaotic behavior of α-stable stochastic processes* (Marcel Dekker, New York, 1994).

[14] G. Samorodnitsky and M. S. Taqqu, *Stable non-Gaussian random processes: Stochastic models with infinite variance* (Chapman and Hall, New York, 1994).

[15] K. A. Penson and K. Górska, Phys. Rev. Lett. **105**, 210604 (2010).

[16] K. Górska and K. A. Penson, Phys. Rev. E **83**, 061125 (2011).

[17] C. W. Gardiner, *Handbook of Stochastic Methods for Physics, Chemistry and the Natural Sciences*, Vol. 13 of *Springer Series in Synergetics*, 3rd ed. (Springer-Verlag, Berlin, 2004).

[18] I. Podlubny, *Fractional differential equations* (Academic Press, San Diego, 1999).

[19] V. V. Yanovsky, A. V. Chechkin, D. Schertzer, and A. V. Tur, Physica A **282**, 13 (2000).

[20] S. G. Samko, A. A. Kilbas, and O. I. Marichev, *Fractional integrals and derivatives. Theory and applications.* (Gordon and Breach Science Publishers, Yverdon, 1993).

[21] A. A. Kilbas, H. M. Srivastava, and J. J. Trujillo, *Theory and applications of fractional differential equations, Volume 204 (North-Holland Mathematics Studies)* (Elsevier Science Inc., New York, 2006).

[22] A. Padash, A. V. Chechkin, B. Dybiec, I. Pavlyukevich, B. Shokri, and R. Metzler, J. Phys. A: Math. Theor. **52**, 454004 (2019).

[23] A. Padash, A. V. Chechkin, B. Dybiec, M. Magdziarz, B. Shokri, and R. Metzler, J. Phys. A **53**, 275002 (2020).

[24] A. Janicki, *Numerical and statistical approximation of stochastic differential equations with non-Gaussian measures* (Hugo Steinhaus Centre for Stochastic Methods, Wrocław, 1996).

[25] J. M. Chambers, C. L. Mallows, and B. W. Stuck, J. Am. Stat. Assoc. **71**, 340 (1976).

[26] R. Weron, Statist. Probab. Lett. **28**, 165 (1996).

[27] R. Weron, Research Report HSC Wroclaw University of Technology **1**, 1 (1996).

[28] H. Risken, *The Fokker-Planck equation. Methods of solution and application* (Springer Verlag, Berlin, 19996).

[29] B. Dybiec, A. V. Chechkin, and I. M. Sokolov, J. Stat. Mech. P07008 (2010).

[30] S. I. Denisov, W. Horsthemke, and P. Hänggi, Phys. Rev. E **77**, 061112 (2008).

[31] I. M. Sokolov, B. Dybiec, and W. Ebeling, Phys. Rev. E **83**, 041118 (2011).

[32] S. Zozor and C. Vignat, Phys. Rev. E **84**, 031115 (2011).

[33] A. V. Chechkin, J. Klafter, V. Y. Gonchar, R. Metzler, and L. V. Tanatarov, Chem. Phys. **284**, 233 (2002).

[34] A. V. Chechkin, J. Klafter, V. Y. Gonchar, R. Metzler, and L. V. Tanatarov, Phys. Rev. E **67**, 010102(R) (2003).

[35] A. V. Chechkin, V. Y. Gonchar, J. Klafter, R. Metzler, and L. V. Tanatarov, J. Stat. Phys. **115**, 1505 (2004).

[36] A. V. Chechkin, V. Y. Gonchar, J. Klafter, and R. Metzler, in *Fractals, Diffusion, and Relaxation in Disordered Complex Systems: Advances in Chemical Physics, Part B*, edited by W. T. Coffey and Y. P. Kalmykov (John Wiley & Sons, New York, 2006), Vol. 133, pp. 439–496.

[37] A. V. Chechkin, R. Metzler, J. Klafter, and V. Y. Gonchar, in *Anomalous transport: Foundations and applications*, edited by R. Klages, G. Radons, and I. M. Sokolov (Wiley-VCH, Weinheim, 2008), pp. 129–162.

[38] A. A. Dubkov and B. Spagnolo, Acta Phys. Pol. B **38**, 1745 (2007).

[39] F.-J. Elmer, J. Phys. A: Math.Gen. **30**, 6057 (1997).

[40] E. Sparre Andersen, Math. Scand. **1**, 263 (1953).

[41] E. Sparre Andersen, Math. Scand. **2**, 195 (1954).

[42] R. K. Getoor, Trans. Am. Math. Soc. **101**, 75 (1961).

[43] H. Widom, Trans. Am. Math. Soc. **98**, 430 (1961).

[44] H. Kesten, Illinois J. Math. **5**, 267 (1961).

[45] H. Kesten, Illinois J. Math. **5**, 246 (1961).

[46] A. Zoia, A. Rosso, and M. Kardar, Phys. Rev. E **76**, 021116 (2007).

[47] T. Burkhardt, J. Phys. A: Math. Gen. **26**, L1157 (1993).

[48] T. W. Burkhardt, in *First-Passage Phenomena and Their Applications*, edited by R. Metzler, S. Redner, and G. Oshanin (World Scientific, Singapore, 2014), pp. 21–44.

[49] J. Masoliver and J. M. Porrà, Phys. Rev. Lett. **75**, 189 (1995).

[50] J. Masoliver and J. M. Porrà, Phys. Rev. E **53**, 2243 (1996).

[51] M. Abramowitz and I. A. Stegun, *Handbook of mathematical functions with formulas, graphs, and mathematical tables* (Dover Publications, New York, 1964), Vol. 55.

[52] H. A. Kramers, Physica (Utrecht) **7**, 284 (1940).

[53] S. Arrhenius, Z. Phys. Chem. **4U**, 226 (1889).

[54] P. Imkeller and I. Pavlyukevich, Stoch. Proc. Appl. **116**, 611 (2006).

[55] P. Imkeller and I. Pavlyukevich, J. Phys. A: Math. Gen. **39**, L237 (2006).

[56] P. D. Ditlevsen, Phys. Rev. E **60**, 172 (1999).

[57] B. Dybiec, E. Gudowska-Nowak, and P. Hänggi, Phys. Rev. E **75**, 021109 (2007).

[58] K. Huang, *Statistical mechanics* (John Wiley, New York, 1963).

[59] K. Capała, A. Padash, A. V. Chechkin, B. Shokri, R. Metzler, and B. Dybiec, Chaos **30**, 123103 (2020).

Multimodal stationary states in symmetric single-well potentials driven by Cauchy noise

Karol Capała, Bartłomiej Dybiec

Marian Smoluchowski Institute of Physics, and Mark Kac Center for Complex Systems Research, Jagiellonian University, ul. St. Łojasiewicza 11, 30–348 Kraków, Poland

E-mail: karol@th.if.uj.edu.pl, bartek@th.if.uj.edu.pl

Abstract. Stationary states for a particle moving in a single-well, steeper than parabolic, potential driven by Lévy noise can be bi-modal. Here, we explore in details conditions that are required in order to induce multimodal stationary states having more than two modal values. Phenomenological arguments determining necessary conditions for emergence of stationary states of higher multimodality are provided. Basing on these arguments, appropriate symmetric single-well potentials are constructed. Finally, using numerical methods it is verified that stationary states have anticipated multimodality.

Keywords: stationary states, fractional dynamics, Lévy flights

1. Introduction

A particle immersed into a liquid constantly interacts with other particles of its environment. These collision results in the irregular, observable motion of a test particle, which is called the Brownian motion. The theory of the Brownian motion had been rigorously and independently developed by Einstein [1] and Smoluchowski [2] in series of papers which made fundamental contributions to kinetic theory of matter, theory of fluctuations and nonequilibrium statistical mechanics.

The Brownian motion is an example of a continuous-space and a continuous-time Markov process with independent increments. Brownian motion can be described by the simplest form of the overdamped Langevin equation

$$\dot{x} = \xi(t), \tag{1}$$

where $\xi(t)$ is the Gaussian white noise. In the theory of stochastic processes, the Brownian motion is the Wiener process. In Eq. (1), $\xi(t)$ is the so called noise which is used as efficient way of approximation of not fully known interactions of a test particle with its environment. Increasing number of observations suggest that fluctuations in real systems do not need to follow the Gaussian law. The natural generalization of the Gaussian density is provided by the α-stable density [3, 4] which lead to the so called Lévy flights.

Lévy flights correspond to summation of uncorrelated random steps drawn from a heavy tailed density. Typically it is assumed that tails are of the power-law type. Therefore, Lévy flights extends Brownian motion for which the step increments are Gaussian. A simple scaling argument shows that, unlike Gaussian Wiener process, Lévy flights are characterized by infinite variance, so that the width of the diffusive “packet” must be understood in terms of some fractional moments or the interquartile distance [5]. The infinite variance of free Lévy flights is responsible for peculiar properties of systems driven by Lévy noise, see [6, 7] and below. Therefore, the scenario of Lévy flights should be contrasted with the complementary model of Lévy walks [8], which assures finite and constant propagation velocity.

Theory of Lévy flights has been developed in a series of papers including among others [9–16]. Lévy flights have been studied in various contexts [17] with applications ranging from economy and finance [18] to superdiffusion of micellar systems [19], studies of turbulence [20], description of photons in hot atomic vapors [21] and laser cooling [22, 23]. These studies included not only experimental [24] but also various theoretical aspects [25–28] of Lévy flights.

A test particle might be not only perturbed by the noise but also it can be driven by the deterministic force, e.g. $f(x) = -V'(x)$, which is to be added to the right hand side of Eq. (1). The overdamped Langevin equation

$$\dot{x}(t) = -V'(x) + \xi(t) \tag{2}$$

is a one of fundamental equation in theory of stochastic systems. In Eq. (2), $-V'(x)$ stands for the deterministic force, while $\xi(t)$ denotes, as in Eq. (1), the stochastic term.

In the limit of vanishing noise strength the motion of an overdamped particle becomes deterministic and especially simple. The deterministic force drives a particle along the potential slope, e.g. to a minimum of the potential which is stable. Presence of noise introduces randomization of trajectories. Moreover, it changes stability of minima of the potential. Combined action of a Gaussian white noise and deterministic forces produces stationary states in potential wells which are of the Boltzman Gibbs type. Replacement of the Gaussian driving with Lévy noise significantly alters conditions for existence, properties and shape of stationary states [13, 29–32]. Eq. (2) provides foundations of the Kramers rate theory [33, 34], which can be also generalized to the non-equilibrium, Lévy flight regime [35, 36]. Furthermore, Eq. (2) can be extended for time dependent forces resulting in plenitude of noise-induced effects like stochastic resonance [37], resonant activation [38] and ratcheting effect [39].

In this paper we are analyzing the problem of stationary states in stochastic systems described by an overdamped Langeving equation. The problem we aim to address is whether action of nonequilibrium noises of α-stable type can induce multimodal stationary states in symmetric single-well potentials. Despite the fact that the conclusive answer to this problem is known for a long time, it is still unknown whether it is possible to observe multimodal states characterized by more than two modal values. Within the current manuscript we are filling this gap. In the next section (Sec 2) a model under studies with required theory is presented. Section Results (Sec. 3) provides obtained results proving that for a properly tailored symmetric single-well potentials one can produce tri- and higher modal stationary states. The manuscript is closed with Summary and Conclusions (Sec. 4).

2. Model

We are studying the system described by Eq. (2) in which the Gaussian white noise is replaced by a more general noise of the α-stable type [7, 32, 40]. From the whole class of α-stable noises we concentrate on symmetric ones [3, 4, 6]. α-stable white noise is a formal time derivative of the α-stable process, whose increments are distributed according to an α-stable density, which is uni-modal, heavy-tailed probability density. The characteristic function of the symmetric α-stable variables [3, 4] is given by

$$\varphi(k) = e^{i\sigma^\alpha |k|^\alpha}, \tag{3}$$

where α ($0 < \alpha \leqslant 2$) is the stability index determining the exponent characterizing power-law decay of α-stable densities, which for $\alpha < 2$ is of $|x|^{-(\alpha+1)}$ type. The scale parameter σ controls the distribution width. For $\alpha < 2$, the variance of an α-stable density is infinite, thus the distribution width needs to be understood as the interquantile width. For $\alpha = 2$, the characteristic function (3) reduces to the characteristic function of the normal (Gaussian) density. The case of $\alpha = 1$ corresponds to the Cauchy distribution. Increments of an α-stable process are distributed according to the α-stable density with the characteristic function $\varphi(k) = \exp(i\Delta t\sigma^\alpha|k|^\alpha)$. Therefore, the

Langevin equation (2) can be approximated by [3, 41]

$$x(t+\Delta t) = x(t) - V'(x)\Delta t + \xi_t \Delta t^{1/\alpha}, \tag{4}$$

where ξ_t represents a sequence of independent identically distributed random variables [42–44] following the α-stable density, see Eq. (3).

Complementary to the Langevin equation, the evolution of the probability density is described by the fractional Smoluchowski-Fokker-Planck equation [4, 15, 45]

$$\frac{\partial p(x,t)}{\partial t} = -\frac{\partial}{\partial x} V'(x,t)p(x,t) + \sigma^\alpha \frac{\partial^\alpha p(x,t)}{\partial |x|^\alpha}, \tag{5}$$

where the fractional Riesz-Weil derivative [45, 46] is defined via the Fourier transform $\mathcal{F}_k\left(\frac{\partial^\alpha f(x)}{\partial |x|^\alpha}\right) = -|k|^\alpha \mathcal{F}_k\left(f(x)\right).$

For systems driven by the Gaussian white noise, i.e. the α-stable noise with $\alpha = 2$, stationary states exist for any potential $V(x)$ having the property $V(x) \to \infty$ as $|x| \to \infty$. Moreover, stationary states are of the Boltzmann-Gibbs type, i.e. $\ln p(x) \propto -V(x)$. Systems driven by an α-stable noise display very different properties than their Gaussian white noise-driven counterparts. First of all, for a single-well potential of $|x|^n$ type, the exponent n characterizing the steepness of the potential needs to be large enough in order to produce stationary states [47]. More precisely, the following relation needs to be satisfied

$$n > 2 - \alpha. \tag{6}$$

Furthermore, if a stationary state exists it is not of the Boltzmann-Gibbs type [25].

In analogy with systems driven by Gaussian white noise, for $n = 2$ stationary states for systems driven by α-stable noise reproduce the noise distribution. Therefore, stationary states are given by the rescaled α-stable density with the same stability index α like the driving noise [30]. In addition to $n = 2$, the formulas for the stationary state is known for $V(x) = x^4/4$ driven by the Cauchy noise, i.e. the α-stable noise with $\alpha = 1$. The appropriate formula [29–31] for the stationary density reads

$$p_{\alpha=1}(x) = \frac{1}{\pi\sigma^{1/3}\left[(x/\sigma^{1/3})^4 - (x/\sigma^{1/3})^2 + 1\right]}. \tag{7}$$

The probability density (7) is a bi-modal density. Bi-modality is a general property of stationary states in steeper than parabolic potentials subject to the action of Lévy noises [29, 30]. Consequently, the stationary state produced in a symmetric single-well potential does not reproduce the symmetry of the potential, i.e. it is not uni-modal, see Fig. 1. The transition between uni-modal and bi-modal stationary states takes place at $n = 2$. For $n > 2$ stationary states are bi-modal with the minimum at the origin, while for $2 - \alpha < n < 2$ they are uni-modal with the maximum at the origin. In double-well potentials, stationary states are bi-modal [48, 49] Finally, for an infinite rectangular potential well the stationary state is

$$p(x) = \frac{\Gamma(\alpha)(2L)^{1-\alpha}(L^2 - x^2)^{\alpha/2-1}}{\Gamma^2(\alpha)}, \tag{8}$$

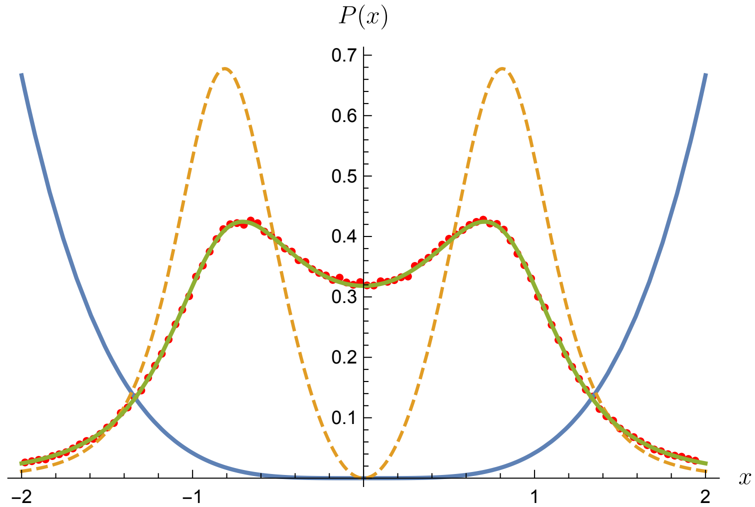

Figure 1. Stationary state for the quartic potential $V(x) = x^4/4$ subject to action of the α-stable driving with α=1 (Cauchy noise) and $\sigma = 1$ (dots), quartic potential (blue solid line), exact solution (7) (green solid line) and the potential curvature (orange dashed line). Simulation parameters: $N = 10^6$, $\Delta t = 10^{-3}$ and $t_{\max} = 100$.

see [50], where $\Gamma(\dots)$ is the Euler-Gamma function. In the special case of $\alpha = 1$, the stationary state, see Eq. (8), is given by the arcsin distribution.

The infinite rectangular potential well with impenetrable boundaries located at $x = \pm L$ can be obtained as $n \to \infty$ limit of the symmetric single-well potential

$$V_n(x) = \frac{(x/L)^{2n}}{2n}, \tag{9}$$

for which stationary states for $\alpha = 1$ are also known [51]. Detailed examination of such a transition allow one to see how stationary states in systems driven by α-stable noise emerges [52]. Additionally, Eq. (7) provides an example that demonstrates the influence of the scale parameter on the shape of stationary states. From Eq. (7), one can conclude that with the increasing σ maxima of probability density (7) shift toward larger absolute values of arguments. This displacement is related to the fact that for the large σ more probability mass is shifted to the tails of the jump length distribution, thus making central part of the distribution less prominent. Analogously, the increase in the exponent characterizing steepness of the potential n, see Eq. (9), moves maxima of the stationary states towards $x = \pm L$. Finally, in the limit of $n = \infty$ maxima are located exactly at boundaries, i.e. $\pm L$, see Eq. (8).

In short, the stationary state is determined by the interplay between random and deterministic forces. The deterministic force is defined by a static potential $V(x)$, while a stochastic force arises due to noise. Since the studied system is overdamped, see Eq. (2), the deterministic force is responsible for sliding down of a particle to the potential minimum. The random force resulting from the noise $\xi(t)$ is the only force which can move a particle away from the minimum of the potential. Therefore, the competition between random excursion and deterministic sliding defines the shape of a stationary state. This mechanism is related to the decomposition of α-stable noises [53–55].

The above mentioned description presents a general mechanism responsible for the shape of stationary states. This mechanism is of very general type and as a such do not provide simple estimates for positions of maxima of stationary states. Therefore, we extend a phenomenological arguments [29, 31] which could provide more information about stationary states, e.g. about positions of modal values.

As a test bench we use the quartic $x^4/4$ potential well perturbed by the Cauchy noise with $\sigma = 1$, for which the stationary state is given by Eq. (7). Fig. 1 presents results of computer simulations (dots), the quartic potential (blue solid line) and the potential curvature (orange dashed line). For a plane curve given by $V(x)$, the curvature is

$$\kappa(x) = \frac{V''(x)}{[1 + V'(x)^2]^{3/2}}. \tag{10}$$

In order to increase clarity of Fig. 1, the curvature $\kappa(x)$ is divided by a constant. From Fig. 1 it is clearly visible that maxima of stationary state are located closely to the maxima of the curvature of $V(x)$, see [29, 31]. For further reference, let us call $\bar{x}_i$ i-th value of x for which curvature $\kappa(x)$ has its local maximum. The significant likelihood of concentrating of probability mass near maxima of curvature comes from the fact that maximum of curvature describes a point where a transition from dominance of almost vertical to flat behaviour of the potential takes place. This is especially well visible for the infinite rectangular potential well because at the point of maximal curvature the potential changes from the horizontal to the vertical (reflecting boundary). Potential slope is directly connected with the change of a particle position, see Eq. (2), while the curvature describes how rapidly movement of the particle changes at a small distance. Therefore, a maximum of the curvature establish a point where a change of a particle position is the most hampered. Please notice, that the conjecture associating maxima of the potential curvature with modal values of stationary states [31] confirm also uni-modal — bi-modal transition at $n = 2$ for single-well potentials of $|x|^n/n$ type.

Due to peculiar properties of systems driven by α-stable noises one can inquire about possibility of producing multimodal stationary states in symmetric single-well potentials. In the following section we show that for properly tailored symmetric single-well potentials it is possible to produce stationary states having more than two modal values.

3. Results

In this section we show numerically that for special types of symmetric single-well potentials it is possible to obtain multimodal stationary states characterized by more than two modal values. In particular, we demonstrate sample symmetric, differentiable, single-well potentials (Sec. 3.1) resulting in three-modal, four-modal and five-modal stationary states. Moreover, we show "glued" symmetric single-well potentials (Sec. 3.2) which are also able to produce multimodal stationary states. All considered potentials are symmetric single-well, i.e. the only one minimum of the potential is located at $x = 0$. Importantly, for $x > 0$ ($x < 0$) potentials are non-decaying (non-decreasing) functions of x with the non-monotonous dependence of the curvature characterized by several maxima.

Sample potentials used in further numerical studies are pre-selected by the curvature condition and then numerically fine-tuned. The requirement of several maxima of the potential curvature is necessary to obtain a multimodal stationary state. Unfortunately, this condition solely could be not sufficient. For instance, maxima of the potential curvature need to be adequately separated. Otherwise, maxima of a stationary state can interfere resulting in smaller number of peaks in the stationary state than the number of maxima in the potential curvature. Therefore, the condition on the number of maxima of the potential curvature needs to be accompanied by additional numerical tests. Exemplary values of the potential parameters, used in further studies, represent sample values of coefficients resulting in pronounced stationary states having required number of modal values.

3.1. Continuous differentiable potentials

Three mods Let us start with the overdamped Langevin equation (2) with the symmetric single-well potential

$$V(x) = x^2 - ax^4 + x^6. \tag{11}$$

The above potential has one minimum located at $x = 0$ and three points in which the curvature has its local maxima. We use numerical methods in order to find stationary states for the system described by Eq. (2).

Numerical results for the potential (11) with $a = 19/11$ together with the potential profile are shown in Fig. 2. As it is visible in Fig. 2, the stationary state has three well visible peaks. One of them is located at the minimum of the potential at $x = 0$ which is also the local maximum of the potential curvature. For small value of x the potential (11) can be approximated by the parabolic part. Therefore, dynamics of a particle at $x \approx 0$ is of the same type like the motion in the parabolic potential, which results in the emergence of the single peak at $x = 0$. Two other peaks appear near to two remaining maxima of curvature of the potential due to action of the deterministic force produced by outer ($|x| > 1$) parts of the potential.

The parameter a in Eq. (11) is adjusted to assure that the potential $V(x)$ is still of a single-well type and the stationary state is tri-modal. For $a = 19/11$ the potential (11) is close of having three minima, since for $a > \sqrt{3}$ the potential has three minima. In the case of $a > \sqrt{3}$, the stationary state is tri-modal. Consequently, $a = \sqrt{3}$ gives the upper bound of the domain of the a parameter. For $a < 0$, the stationary state is unimodal. Therefore, we had to consider $0 < a < \sqrt{3}$. Finally, we have performed additional simulations in order to find the critical value of the a parameter for a transition between tri-modal and unimodal stationary state. From our simulations, we see that the critical

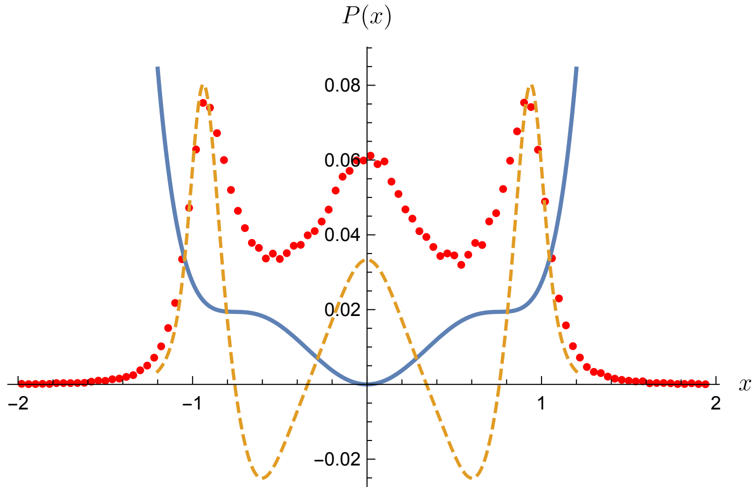

Figure 2. The stationary state for the potential given by Eq. (11) with $a = 19/11$ subject to the α-stable driving with α=1 (Cauchy noise) and $\sigma = 1$ (dots), the potential profile (blue solid line) and the potential curvature (orange dashed line). Simulation parameters: $N = 10^6$, $\Delta t = 10^{-3}$, $t_{\max} = 100$.

value is located between $1.17 < a_c \leq 1.20$. Unfortunately, due to inherent uncertainties of our methodology, it is very hard to provide a better estimate.

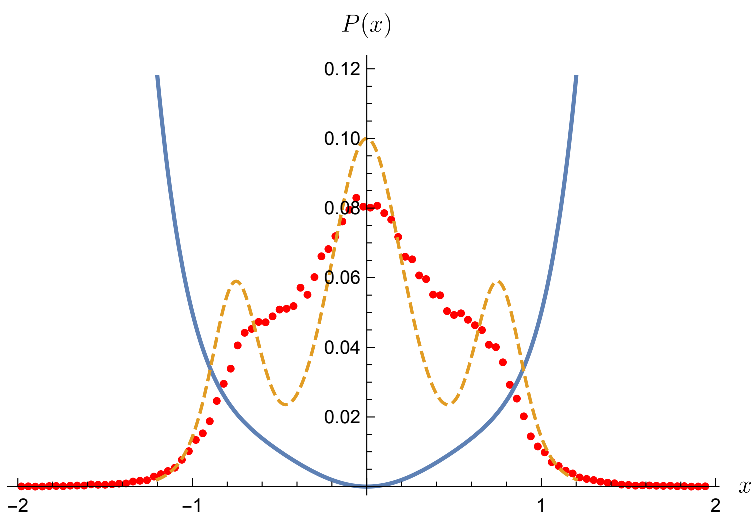

Figure 3. The same as in Fig. 2 for $a = 1$.

Different situations is observed for the potential given by Eq. (11) with $a = 1$, which is smaller than a_c, see Fig. 3. The potential still has one minimum at $x = 0$. The curvature has three maxima: $\bar{x}_0$ and $\bar{x}_{\pm}$. The maximum $\bar{x}_0$ located at $x = 0$ is dominating and remaining points of maximal curvature $\bar{x}_{\pm 1}$ are closer to each other than for $a = 19/11$, see Fig. 2. Relative changes in the curvature are also smaller than for $a = 19/11$. In Fig. 3, there is only one maximum of the stationary density located at the origin because of different curvature profile than in Fig. 2. In other words, maxima of curvature are not distanced (separated) enough to induce tri-modal stationary state. Nevertheless, the influence of curvature is still visible. More precisely, for $x < 0$, in the range where curvature decays from its local maximum $\bar{x}_-$ to its global minimum the stationary density increases slower than in the areas of growing curvature. The very similar effect is observed for $x > 0$, where the decay of the stationary density is slower in the interval where the curvature grows.

Four mods As a sample potential with the single minimum located at $x = 0$ and four maxima of the curvature we use

$$V(x) = \frac{7}{6}x^4 - 2x^6 + x^8. \tag{12}$$

Since the potential (12) has four maxima of the curvature, we are expecting that a stationary state will have four modal values. Indeed, in Fig. 4 four maxima of the stationary density located near points of the maximal curvature are visible. Maxima located at $x \approx \pm 1$ are significantly higher than maxima at $x \approx \pm 0.4$, because the curvature at these points is substantially smaller. In contrast to the potential considered in the previous subsection, the probability density has minimum at $x = 0$ due to minimum of the potential curvature. Alternatively, shape of the stationary density around $x = 0$ can be explained by the analysis of the potential. The potential given by Eq. (12), for small x, behaves like x^4 while the potential given by Eq. (11) like x^2 resulting in the maximum of stationary density in the former case and minimum of stationary denity in the current case.

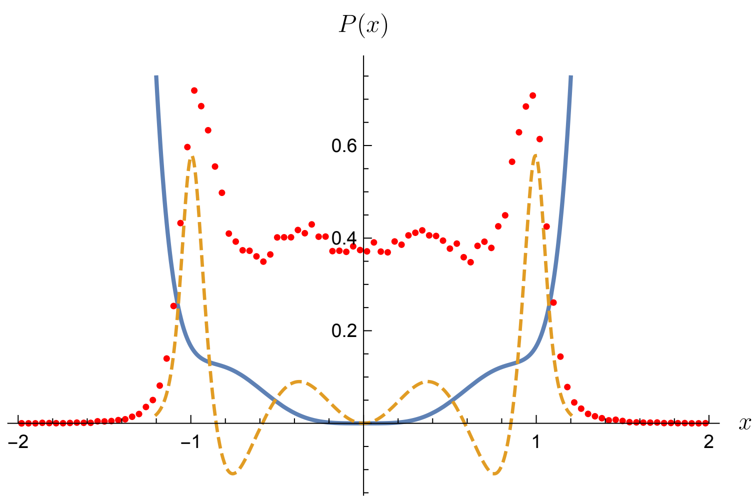

Figure 4. The stationary state for the potential (12) subject to the α-stable driving with α=1 (Cauchy noise) and $\sigma = 1$ (dots), potential profile (blue solid line) and the potential curvature (orange dashed line). Simulation parameters: $N = 9.6 \times 10^4$, $\Delta t = 10^{-6}$, $t_{\max} = 100$.

Five mods In order to produce five modal values in the stationary state we use a potential

$$V(x) = 13.4789x^2 - 24.8828x^4 + 22.6289x^6 \\ - 8.125x^8 + x^{10} \quad (13)$$

having five maxima of the curvature. As it is confirmed by Fig. 5, the stationary state corresponding to the potential (13) has five modal values. Additional Fig. 6 examines in more details the sensitivity of the stationary state to the scale parameter σ, which is ten times larger than in Fig. 5. Increase in the scale parameter decreases the height of the central maximum and spreads outer peaks. The decrease of the central peak in the stationary state is related to the central part of distribution of random pulses. More precisely, for larger values of the scale parameter σ, peaks of α-stable densities become lower and wider transferring effectively a part of the probability mass to tails of distributions. This in turn, can spread outer peaks of stationary densities and increase their height as it can be deducted from comparison of Figs. 5 and 6.

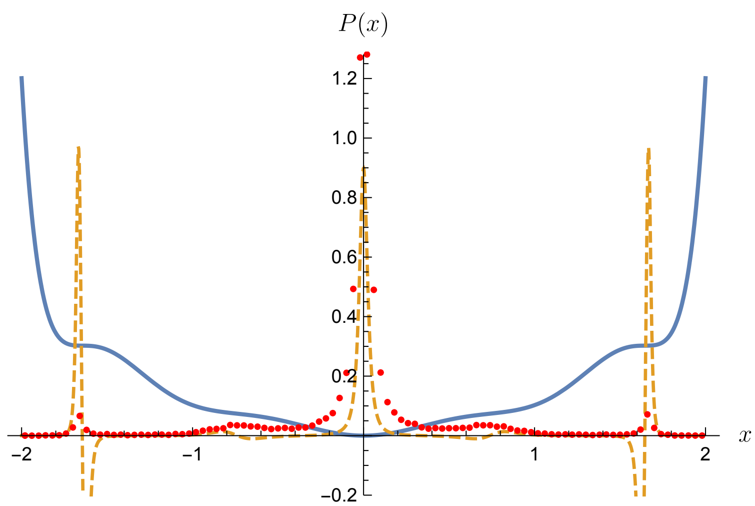

Figure 5. The stationary state for the potential (13) subject to the α-stable driving with α=1 (Cauchy noise) and $\sigma = 1$ (dots), potential profile (blue solid line) and the potential curvature (orange dashed line). Simulation parameters: $N = 9.6 \times 10^4$, $\Delta t = 10^{-6}$, $t_{\max} = 100$.

Next, considered sample potential which allow for the emergence of a five-modal stationary state can be

$$V(x) = 49.0625x^2 - 69.5313x^4 + 43.4414x^6 \\ - 11.125x^8 + x^{10}. \quad (14)$$

Stationary states corresponding to the potential (14) are presented in Figs. 7 and 8. As in the previous case, see Eq. (13), the increase in the scale parameter σ decreases the height of the central peak and makes outer peaks more pronounced. Therefore, for large σ in the stationary state there are five well visible peaks, see Fig. 8.

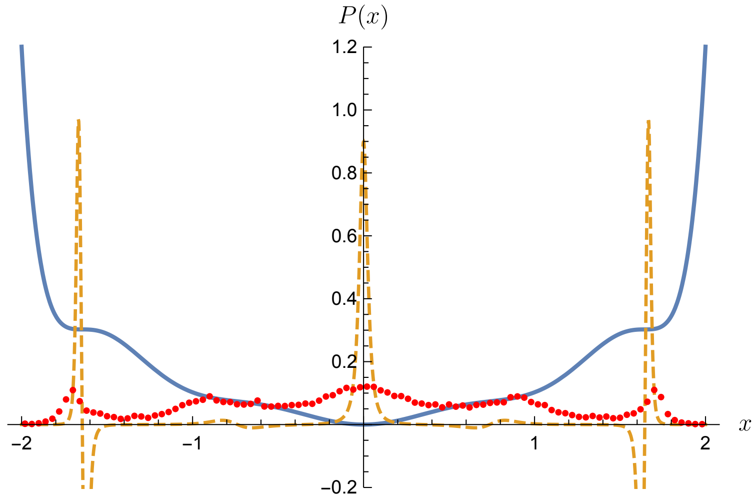

Figure 6. The same as in Fig. 5 for $\sigma = 10$.

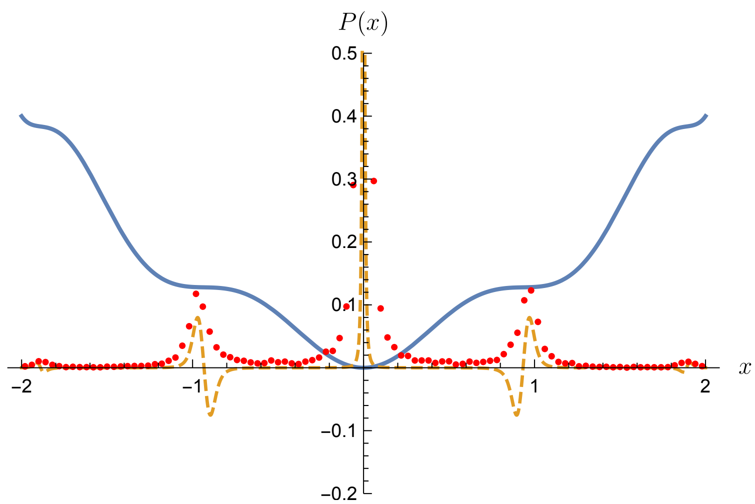

Figure 7. The stationary state for the potential (14) subject to the α-stable driving with α=1 (Cauchy noise) and $\sigma = 1$ (dots), potential profile (blue solid line) and the potential curvature (orange dashed line). Simulation parameters: $N = 9.6 \times 10^4$, $\Delta t = 10^{-6}$, $t_{\max} = 100$.

3.2. "Glued" potentials

Stationary states with more than two modal values can be also produced in continuous non-differentiable "glued" potentials. For instance, let us consider the potential given by

$$V(x) = \begin{cases} \frac{(x+1)^4}{16} + \frac{1}{4} & \text{for} \quad x < 1 \\ \frac{x^4}{4} & \text{for} \quad |x| \leqslant 1 \\ \frac{(x-1)^4}{16} + \frac{1}{4} & \text{for} \quad x > 1 \end{cases} . \tag{15}$$

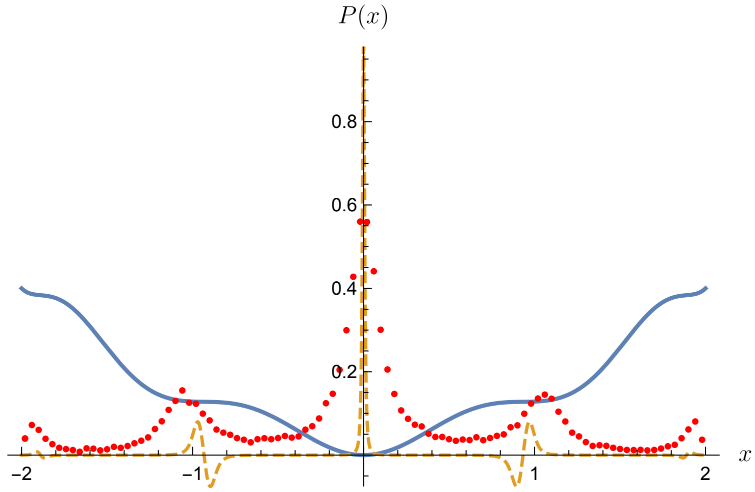

Figure 8. The same as in Fig. 7 for $\sigma = 10$.

The stationary state, along with the potential profile and the potential curvature is depicted in Fig. 9. The potential (15) consist of tailored x^4 parts. For small x, the stationary state is determined by the part of the potential located at $|x| < 1$. This part of the potential is quartic, thus it produces two maxima. Two further maxima, at larger absolute values of arguments, are produced by outer parts of the potential well. On the one hand, one can see the stationary state as an outcome of competition between two parts (inner and outer) of the potential, which are responsible for the emergence of modal values. On the other hand, it is possible to provide alternative explanation based on competition between deterministic and random forces. The inner part of the potential produces two maxima in an analogous way like the $x^4/4$ potential, see Fig. 1. If a particle, due to random force, escapes to a distant point it starts to slide down towards $x = 0$. The time scale associated with the deterministic sliding is infinite making probability mass to concentrate on almost horizontal part of the potential close to $|x| = 1$ giving rise to two outer maxima of the stationary state, see Fig. 9. For a potential given by Eq. (15), replacement of the quartic part at $|x| < 1$ with the parabolic potential destroys inner maxima of the stationary state. The inner part of the stationary density is uni-modal, which is consistent with results for the parabolic potential. Finally, also the phenomenological interpretation based on the potential curvature works. Maxima of the stationary states are located close to maxima of the potential curvature.

The mechanism responsible for emergence of maxima of the stationary state in

Fig. 9 can be further extended. For example, the following potential

$$V(x) = \begin{cases} \frac{1}{4}(x+3)^4 + \frac{3}{4} & \text{for} \quad x < -3 \\ \frac{1}{4}(x+2)^4 + \frac{1}{2} & \text{for} \quad -3 \leqslant x < -2 \\ \frac{1}{4}(x+1)^4 + \frac{1}{4} & \text{for} \quad -2 \leqslant x < -1 \\ \frac{x^4}{4} & \text{for} \quad |x| \leqslant 1 \\ \frac{1}{4}(x-1)^4 + \frac{1}{4} & \text{for} \quad 1 < x \leqslant 2 \\ \frac{1}{4}(x-2)^4 + \frac{1}{2} & \text{for} \quad 2 < x \leqslant 3 \\ \frac{1}{4}(x-3)^4 + \frac{3}{4} & \text{for} \quad x > 3 \end{cases} \tag{16}$$

results in emergence of eight-modal stationary state, see Fig. 10, see Fig. 10. The procedure of tailoring potentials, see Eqs. (15) and (16), can be further continued. Please note, however, that outer maxima are the strongest because they aggregate particles sliding down from the whole outer parts of the potential.

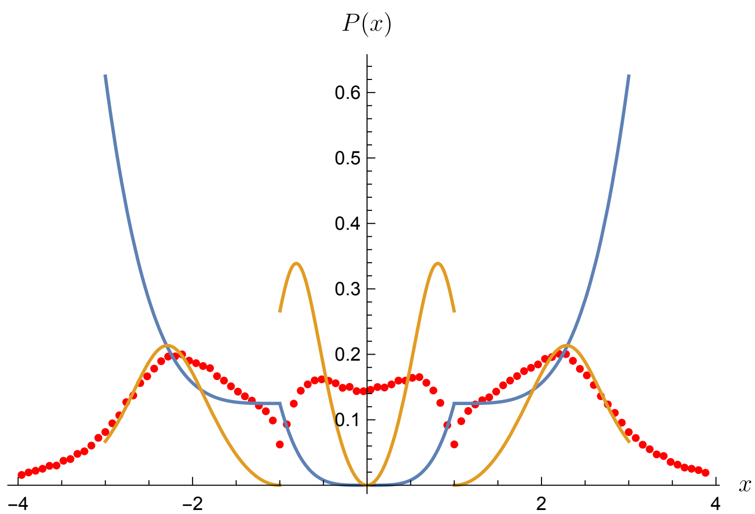

Figure 9. The stationary state for the potential given by (15) subject to the α-stable driving with α=1 (Cauchy noise) and $\sigma = 1$ (dots), the potential profile (blue solid line) and the potential curvature (orange dashed line). Simulation parameters: $N = 10^6$, $\Delta t = 10^{-3}$, $t_{\max} = 100$.

4. Summary and Conclusion

It is well known that stationary states in systems driven by Lévy noise can display intriguing properties [13, 29–32]. Almost twenty years ago it was proved that stationary states of non-harmonic Lévy, e.g. quartic, oscillators can be bi-modal [29]. Nevertheless, so far, it has not been verified if stationary states in symmetric single-well potential can be characterized by more than two modal values. The current manuscript provides conclusive and positive answer to this problem.

We have grounded our considerations on a condition of existence of modal values which attribute maxima of probability density to maxima in the potential curvature

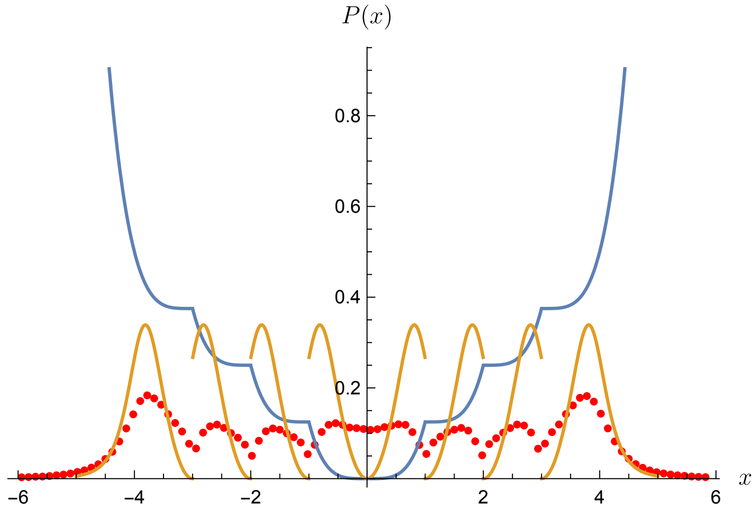

Figure 10. The same as in Fig. 9 for the potential given by Eq. (16).

[31]. In the next step this conjecture has been used to construct symmetric single-well potentials resulting in desired multimodality. Finally, we have numerically investigated properties of stationary states proving that stationary states indeed have anticipated multimodality. This step is necessary because the curvature condition might be not sufficient to acquire anticipated multi-modality. Therefore, the final test and fine-tuning of potential parameters need to be performed manually. All considered potential assured existence of stationary states, because every potential for large $|x|$ is steeper than x^4 which is well above the minimal steepness ensuring existence of stationary states.

Peaks in the stationary state which are located close to the origin are determined by the behaviour of the potential at small x. Therefore, if the dominating part of the potential at $x \approx 0$ is steeper than parabolic the stationary state has a minimum at the origin what is especially well visible for the quartic potential. In contrast, for potentials less steep than parabolic, the stationary state has a global maximum at the origin. In general, modal values of stationary states are located in the vicinity of maxima of the potential curvature. The mechanism of emergence of multimodal stationary states is better visible for "glued" potentials than for continuous differentiable potentials.

Within simulations, we have focused on the Cauchy noise which is a special example of the Lévy noise with the stability index $\alpha = 1$. However, similar considerations can be performed for other allowed values of the stability index. In the limiting case of $\alpha = 2$, the α-stable noise becomes the Gaussian white noise. Therefore, stationary states become of the Boltzmann-Gibbs type and for single-well potentials they are single-modal.

Obtained findings indicate that the stationary state in a single-well potential can be of non-trivial, multimodal type. Therefore, it might be important to asses the role of multi-modal stationary states in noise-induced effects. This problem seems to be especially relevant in the context of averaging over equilibrium initial conditions, sensitivity to initial conditions or the problem of transition over the potential barrier. For the Kramers problem, the issue of placing the boundary which discriminate states [48, 56] might be further complicated due to multi-modality of stationary states.

Acknowledgments

This project was supported by the National Science Center grant (2014/13/B/ST2/02014). Computer simulations have been performed at the Academic Computer Center Cyfronet, AGH University of Science and Technology (Kraków, Poland) under CPU grant "Dyn-Stoch". Fruitful suggestions from Aleksei Chechkin are greatly acknowledged.

References

[1] Einstein A 1905 *Ann. Phys.* **17** 549–560

[2] Von Smoluchowski M 1906 *Ann. Phys.* **21** 756–780

[3] Janicki A and Weron A 1994 *Simulation and chaotic behavior of α-stable stochastic processes* (New York: Marcel Dekker)

[4] Samorodnitsky G and Taqqu M S 1994 *Stable non-Gaussian random processes: Stochastic models with infinite variance* (New York: Chapman and Hall)

[5] Dybiec B, Gudowska-Nowak E and Sokolov I M 2008 *Phys. Rev. E* **78** 011117

[6] Dubkov A A, Spagnolo B and Uchaikin V V 2008 *Int. J. Bifurcation Chaos. Appl. Sci. Eng.* **18** 2649–2672

[7] Metzler R, Chechkin A V, Gonchar V Y and Klafter J 2007 *Chaos Solitons Fractals* **34** 129–142

[8] Zaburdaev V, Denisov S and Klafter J 2015 *Rev. Mod. Phys.* **87** 483

[9] Metzler R and Klafter J 2000 *Phys. Rep.* **339** 1–77

[10] Barkai E 2001 *Phys. Rev. E* **63** 046118–046134

[11] Anh V V and McVinish R 2003 *J. Appl. Math. Stoch. Anal.* **16** 97

[12] Brockmann D and Sokolov I M 2002 *Chem. Phys.* **284** 409

[13] Chechkin A V, Gonchar V Y, Klafter J and Metzler R 2006 Fundamentals of Lévy flight processes *Fractals, Diffusion, and Relaxation in Disordered Complex Systems: Advances in Chemical Physics, Part B* vol 133 ed T Coffey W and P Kalmykov Y (New York: John Wiley & Sons) pp 439–496

[14] Jespersen S, Metzler R and Fogedby H C 1999 *Phys. Rev. E* **59** 2736

[15] Yanovsky V V, Chechkin A V, Schertzer D and Tur A V 2000 *Physica A* **282** 13–34

[16] Schertzer D, Larchevêque M, Duan J, Yanovsky V V and Lovejoy S 2001 *J. Math. Phys.* **42** 200–212

[17] Klages R, Radons G and Sokolov I M 2008 *Anomalous transport: Foundations and applications* (Weinheim: Wiley-VCH)

[18] Bouchaud J P and Georges A 1990 *Phys. Rep.* **195** 127–293

[19] Bouchaud J P, Ott A, Langevin D and Urbach W 1991 *J. de Physique II* **1** 1465–1482

[20] Shlesinger M F, Klafter J and West B J 1986 *Physica A* **140** 212–218

[21] Mercadier M, Guerin W, M Chevrollier M and Kaiser R 2009 *Nat. Phys.* **5** 602–605

[22] Bardou F, Bouchaud J P, Aspect A and Cohen-Tannoudji C 2002 *Lévy statistics and laser cooling* (Cambridge: Cambridge University Press)

[23] Barkai E, Aghion E and Kessler D A 2014 *Phys. Rev. X* **4** 021036–021069

[24] Solomon T H, Weeks E R and Swinney H L 1993 *Phys. Rev. Lett.* **71** 3975–3978

[25] Eliazar I and Klafter J 2003 *J. Stat. Phys.* **111** 739–768

[26] Sokolov I M and Metzler R 2004 *J. Phys. A: Math. Gen.* **37** L609–L615

[27] Garbaczewski P and Stephanovich V 2009 *Phys. Rev. E* **80** 031113

[28] Garbaczewski P 2010 *Physica A* **389** 936–944

[29] Chechkin A V, Klafter J, Gonchar V Y, Metzler R and Tanatarov L V 2002 *Chem. Phys.* **284** 233–251

[30] Chechkin A V, Klafter J, Gonchar V Y, Metzler R and Tanatarov L V 2003 *Phys. Rev. E* **67** 010102(R)

[31] Chechkin A V, Gonchar V Y, Klafter J, Metzler R and Tanatarov L V 2004 *J. Stat. Phys.* **115** 1505–1535

[32] Chechkin A V, Metzler R, Klafter J and Gonchar V Y 2008 Introduction to the theory of Lévy flights *Anomalous transport: Foundations and applications* ed Klages R, Radons G and Sokolov I M (Weinheim: Wiley-VCH) pp 129–162

[33] Kramers H A 1940 *Physica (Utrecht)* **7** 284

[34] Hänggi P, Talkner P and Borkovec M 1990 *Rev. Mod. Phys.* **62** 251

[35] Chechkin A V, Gonchar V Y, Klafter J and Metzler R 2005 *EPL (Europhys. Lett.)* **72** 348–354

[36] Dybiec B, Gudowska-Nowak E and Hänggi P 2007 *Phys. Rev. E* **75** 021109–021116

[37] Gammaitoni L, Hänggi P, Jung P and Marchesoni F 2009 *Eur. Phys. J. B* **69** 1–3

[38] Doering C R and Gadoua J C 1992 *Phys. Rev. Lett.* **69** 2318–2321

[39] Reimann P 2002 *Phys. Rep.* **361** 57–265

[40] Peszat S and Zabczyk J 2007 *Stochastic partial differential equations with Lévy noise: An evolution equation approach* vol 113 (Cambridge: Cambridge University Press)

[41] Janicki A 1996 *Numerical and statistical approximation of stochastic differential equations with non-Gaussian measures* (Wrocław: Hugo Steinhaus Centre for Stochastic Methods)

[42] Chambers J M, Mallows C L and Stuck B W 1976 *J. Amer. Statistical Assoc.* **71** 340–344

[43] Weron A and Weron R 1995 *Lect. Not. Phys.* **457** 379–392

[44] Weron R 1996 *Statist. Probab. Lett.* **28** 165–171

[45] Podlubny I 1999 *Fractional differential equations* (San Diego: Academic Press)

[46] Samko S G, Kilbas A A and Marichev O I 1993 *Fractional integrals and derivatives. Theory and applications.* (Yverdon: Gordon and Breach Science Publishers)

[47] Dybiec B, Chechkin A V and Sokolov I M 2010 *J. Stat. Mech.* P07008–P07024

[48] Dybiec B, Gudowska-Nowak E and Sokolov I M 2007 *Phys. Rev. E* **76** 041122

[49] Sliusarenko O Y, Surkov D A, Gonchar V Y and Chechkin A V 2013 *Eur. Phys. J ST* **216** 133–138

[50] Denisov S I, Horsthemke W and Hänggi P 2008 *Phys. Rev. E* **77** 061112–1–4

[51] Dubkov A A and Spagnolo B 2007 *Acta Phys. Pol. B* **38** 1745–1758

[52] Kharcheva A A, Dubkov A A, Dybiec B, Spagnolo B and Valenti D 2016 *J. Stat. Mech.* P054039–P054051

[53] Imkeller P and Pavlyukevich I 2006 *Stochastic Processes and their Applications* **116** 611–642

[54] Imkeller P and Pavlyukevich I 2006 *J. Phys. A: Math. Gen.* **39** L237–L246

[55] Samorodnitsky G and Grigoriu M 2007 *Theor. Math. Phys.* **150** 332–346

[56] Dybiec B and Gudowska-Nowak E 2007 *Acta Phys. Pol. B* **38** 1759–1773

Stationary states for underdamped anharmonic oscillators driven by Cauchy noise

Karol Capała[1, a)] and Bartłomiej Dybiec[1, b)]
Marian Smoluchowski Institute of Physics, and Mark Kac Center for Complex Systems Research, Jagiellonian University, ul. St. Łojasiewicza 11, 30–348 Kraków, Poland

(Dated: 14 March 2022)

Using numerical methods, we have studied stationary states in the underdamped anharmonic stochastic oscillators driven by Cauchy noise. Shape of stationary states depend both on the potential type and the damping. If the damping is strong enough, for potential wells which in the overdamped regime produce multimodal stationary states, stationary states in the underdamped regime can be multimodal with the same number of modes like in the overdamped regime. For the parabolic potential, the stationary density is always unimodal and it is given by the two dimensional α-stable density. For the mixture of quartic and parabolic single-well potentials the stationary density can be bimodal. Nevertheless, the parabolic addition, which is strong enough, can destroy bimodlity of the stationary state.

PACS numbers: 05.40.Fb, 05.10.Gg, 02.50.-r, 02.50.Ey,

The increasing number of observations shows that fluctuations in complex systems do not need to follow the Gaussian distribution but display power-law behavior. T he non-equilibrium fluctuations can be approximated and modeled by α-stable (Lévy) noise. Properties of dynamical systems driven by Lévy noise are significantly different from their Gaussian white noise driven counterparts. This is especially well visible in noise induced effects but also in stationary states. Here, we study the archetypal models of anharmonic, inertial stochastic oscillators driven by the Lévy noise. Therefore, within the current manuscript we extend understanding of uderdamped, Lévy noise driven systems. We demonstrate that stationary states strongly deviate from the Boltzmann-Gibbs distribution as in single-well potentials multimodal stationary densities can be observed. Moreover, contrary to the Gaussian driving, stationary densities depend on the damping. Finally, we show under which conditions stationary states in singe-well potentials can be multimodal.

I. INTRODUCTION

The overdamped Langevin eqution

$$\dot{x}(t) = -V'(x) + \zeta(t). \tag{1}$$

is the archetypal equation in the theory of stochastic systems. It describes the evolution of the position $x(t)$ of the overdamped, noise driven particle moving in the potential $V(x)$. The potential $V(x)$ produces the deterministic force $f(x) = -V'(x)$, while $\zeta(t)$ stands for the noise, which approximates (random) interactions of the observed particle with its environment. In the simplest realms it is assumed that the noise $\zeta(t)$ is white and Gaussian[1,2]. For such a noise $\langle\zeta(t)\rangle = 0$ and $\langle\zeta(t)\zeta(s)\rangle = \sigma^2\delta(t-s)$.

Numerous extensions of Eq. (1) to time dependent forces $f(x,t)$ account for description of various noise induced effects: stochastic resonance[3], resonant activation[4], ratcheting effect[5–7], to name a few. Eq. (1) also underlines description of stationary states in noisy systems, which constitute the main topic of current research. If $\zeta(t)$ is the Gaussian white noise, a stationary state exists for any potential well such that $V(x) \to \infty$ as $|x| \to \infty$. It is given by the Boltzmann-Gibbs distribution, i.e. $P(x) \propto \exp[-V(x)/\sigma^2]$, see Refs. 1 and 8.

Noise in Eq. (1) does not need to be Gaussian. A natural generalization of the Gaussian white noise is provided by the Lévy noise. α-stable, Lévy type noise is a non-equilibrium noise which is the formal time derivative of the α-stable process $L(t)$, see Ref. 9, whose probability density follow an α-stable density[9,10] with the scale parameter which grows in time. The characteristic function (Fourier transform) $\phi(k) = \langle\exp[ikL(t)]\rangle$ of symmetric Lévy process is given by

$$\phi(k) = \exp\left[-\sigma^\alpha(t)|k|^\alpha\right]. \tag{2}$$

Symmetric α-stable densities are unimodal probability densities with power-law tails. The stability index α ($0 < \alpha \leqslant 2$) describes the tails asymptotic which for $\alpha < 2$ is of $|x|^{-(\alpha+1)}$ type. The scale parameter σ controls the distribution width. For the Lévy motion it grows in time as $\sigma(t) = \sigma_0 t^{1/\alpha}$, where σ_0 is the scale parameter characterizing the strength of Lévy noise $\zeta(t)$. More precisely, increments of the Lévy process $\Delta L = L(t+\Delta t) - L(t)$ are distributed according to the α-stable density with the characteristic function $\exp[\Delta t\sigma_0^\alpha|k|^\alpha]$. For $\alpha < 2$, the variance of an α-stable density is infinite, thus the distribution width can be defined by the interquantile width or fractional moments only[9,11]. For $\alpha = 2$, the Lévy noise is equivalent to the Gaussian white noise. In the most general scenario, not considered here, the Lévy noise can be asymmetric and shifted[9,11]. Non-gaussian, heavy tailed fluctuations have been observed in numerous experimental setups[12–17] and used in description of multiple phenomena[18–20], for a review see Ref. 21. Moreover, in the last two decades theory of systems driven by the Lévy noise has been significantly advanced[22–34].

The problem of stationary states in overdamped systems

[a)]Electronic mail: karol@th.if.uj.edu.pl
[b)]Electronic mail: bartek@th.if.uj.edu.pl

driven by α-stable noises has been studied for the long time. It is well known that stationary states do not exist for all type of potential wells. Moreover, if they exist, they are not of the Boltzmann-Gibbs type[31]. For single-well potentials of $V(x) = |x|^\nu/\nu$ type ($\nu > 0$) stationary states exist for sufficiently large ν. Surprisingly, the limiting ν depends on the stability index α. Stationary states exist for $\nu > 2 - \alpha$, see Ref. 35. For some potential wells exact formulas for stationary states are known. For $\nu = 2$ the stationary state reproduces the noise pulses distribution, i.e. it is given by the α-stable density with the same stability index α[36–38] as the noise $\zeta(t)$. For $\nu > 2$ stationary states, even in single-well potentials, are no longer unimodal[36,37,39]. For $V(x) = x^4/4$ and $\alpha = 1$ (Cauchy noise) the stationary state is given by[27,36,37,40,41]

$$P_{\alpha=1}(x) = \frac{1}{\pi\sigma_0^{1/3}\left[\left(x/\sigma_0^{1/3}\right)^4 - \left(x/\sigma_0^{1/3}\right)^2 + 1\right]}. \quad (3)$$

Probability density given by Eq. (3) has two maxima at $x = \pm\sigma_0^{1/3}/\sqrt{2}$. For more general, polynomial, single-well potentials of x^ν/ν type, with $\nu = 4n$ or $\nu = 4n+2$ (where n is integer and positive), stationary states are also bimodal and given by finite series[42]. For the parabolic addition to the quartic potential

$$V(x) = \frac{x^4}{4} + a\frac{x^2}{2} \quad \text{with} \quad a > 0, \quad (4)$$

there is a critical value of $a_c = 0.794$ such that for $a > a_c$ the stationary state is no-longer bimodal[36,37,40].

For the system described by the Langevin equation (1), one can numerically estimate the time dependent probability density of finding a particle in the vicinity of x at time t under the initial condition $x(t_0) = x_0$ as $P(x,t|x_0,t_0) = \langle\delta(x-x(t))\rangle$. The time evolution of the probability density $P(x,t|x_0,t_0)$ is described by the fractional Smoluchowski-Fokker-Planck equation[11,29,43]

$$\frac{\partial P}{\partial t} = -\frac{\partial}{\partial x}V'(x,t)P + \sigma^\alpha\frac{\partial^\alpha P}{\partial|x|^\alpha}. \quad (5)$$

The fractional operator $\partial^\alpha/\partial|x|^\alpha$ is the fractional Riesz-Weil derivative[43,44] which can be defined via the Fourier transform $\mathcal{F}_k\left(\frac{\partial^\alpha f(x)}{\partial|x|^\alpha}\right) = -|k|^\alpha\mathcal{F}_k\left(f(x)\right).$

Equation (1) is the large damping limit of the full Langevin equation[45,46]

$$\ddot{x}(t) = -\gamma\dot{x}(t) - V'(x) + \zeta(t). \quad (6)$$

Please note that in the case of full dynamics with $\alpha = 2$ the noise strength σ depends on the damping parameter γ, as they are linked by the fluctuation dissipation relation[46,47]. Contrary to the Gaussian case, for $\alpha < 2$, damping and strength of fluctuations are two independent parameters. The time evolution of the full probability density associated with Eq. (6) is described by the fractional Kramers equation. The joint probability density $P = P(x,v,t|x_0,v_0,t_0)$ evolves according to the fractional Kramers equation[46,48]

$$\frac{\partial P}{\partial t} = \left[-v\frac{\partial}{\partial x} + \frac{\partial}{\partial v}\left(\gamma v + V'(x)\right) + \sigma^\alpha\frac{\partial^\alpha}{\partial|v|^\alpha}\right]P. \quad (7)$$

Stationary states for the model described by Eq. (6) and associated with the diffusion equation (7) exist for every value of the stability index α, under the condition that $V(x)$ grows to infinity fast enough. For example, the parabolic potential is sufficient. For $\alpha = 2$ steady states are given by the Boltzmann-Gibbs distribution under the condition that the potential $V(x)$ satisfies the same constraint as in the overdamped case. For $V(x) = x^2/2$, the stationary state is given by the 2D α-stable density[49,50] with the non-trivial, γ-dependent, spectral measure[11].

Within the current manuscript, we extend analysis of underdamped, anharmonic stochastic oscillators driven by Lévy noise. We focus on the Cauchy noise with the noise strength $\sigma_0 = 1$, as it allows for easy comparison of limiting cases. We explore the model in the weak damping limit, and through increasing the damping coefficient, we study how results for overdamped regime are restored. Thanks to this, we extend our understanding of anomalous underdamped setups, which are less studied that overdamped models. Our numerical analysis are included in Section Results (Sec. II). The manuscript is closed with Summary and Conclusions (Sec. III) and accompanied with the Appendix.

II. RESULTS

The system described by the full Langevin eqaution (6) can be studied for any value of the stability index α. For $\alpha = 2$, the α-stable noise is equivalent to the Gaussian white noise. In such a case, for any $V(x)$ such that $V(x) \to \infty$ as $|x| \to \infty$, the stationary state exits and it is given by the Boltzmann-Gibbs distribution

$$P(x,v) \propto \exp\left[-\frac{1}{\sigma^2}\left(\frac{v^2}{2} + V(x)\right)\right]. \quad (8)$$

The damping parameter γ controls the rate of reaching the stationary state, but it does not affect the shape of stationary state. Moreover, in the stationary state, see Eq. (8), despite the functional dependence $\dot{x} = v$, the position and the velocity are statistically independent, because the stationary density factorizes. The very different situation is observed for $\alpha < 2$. Due to presence of damping, the stationary state exist for a potential $V(x)$ such that $V(x) \to \infty$ as $|x| \to \infty$ fast enough. For instance, the parabolic potential is sufficient to produce stationary states. For a fixed potential, the shape of the stationary state depends on the value of γ. Moreover, in the stationary state, velocity and position are no longer statistically independent. This behaviour is especially well visible for the underdamped stochastic harmonic oscillator[49,51], when stationary states are non-elliptical, 2D α-stable densities[11] characterized by non-trivial spectral measures[50].

Exploration of the full dynamics, allow us to verify under which conditions stationary states reproduce steady states

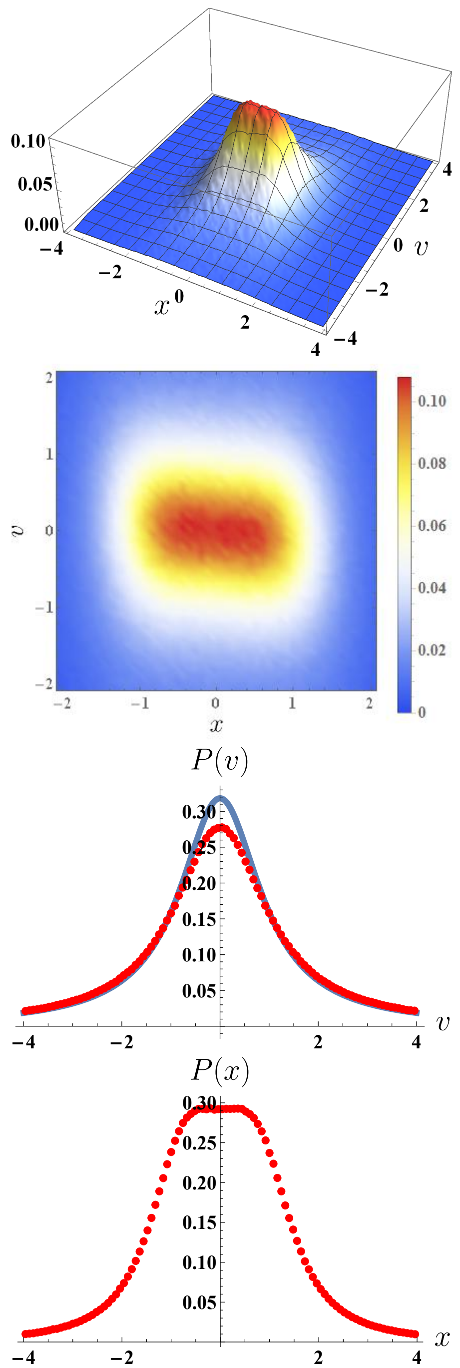

FIG. 1. Stationary probability density $P(x, v)$ as 3D-plot and heat map (top panels), velocity marginal density $P(v)$ (points) with the asymptotic density (A8) (solid line) and the position marginal distribution $P(x)$ (points) with the asymptotic density (3). The damping parameter γ is set to $\gamma = 1$.

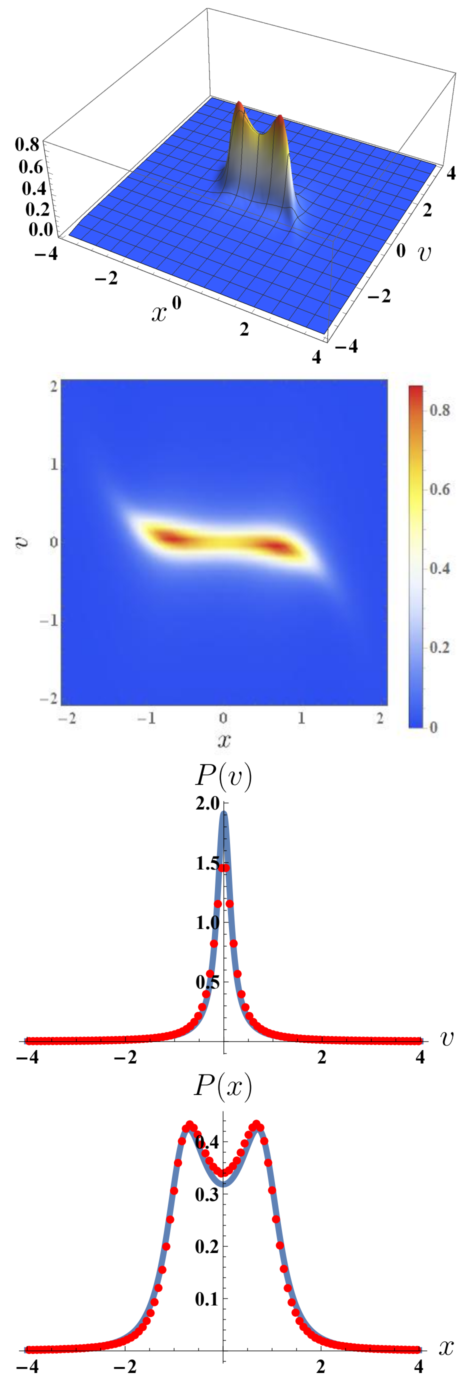

FIG. 2. The same as in Fig. 1 for $\gamma = 6$.

recorded in overdamped systems. We restrict ourselves mainly to $\alpha = 1$, because for the simplest overdamped systems driven by the Cauchy noise exact results are known. Such a special choice simplifies the comparison of numerical results with known asymptotic regimes.

Results presented in this section have been constructed numerically by simulations of the underdamped Langevin equation (9). The part with the α-stable noise, e.g. $\dot{v} = -\gamma v - V'(x) + \zeta(t)$, has been integrated with the stochastic Euler-Maryuama method[9,10]. The positions $x(t)$ have been constructed trajectorywise from $v(t)$ realizations. The Langevin equation (6) has been integrated with the integration time step $\Delta t = 10^{-3}$ and averaged over $N = 10^7$ realizations. From constructed trajectories time dependent and stationary states have been constructed.

The case of $\nu = 2$ was explicitly studied in Refs. 49 and 50, where it was shown that the stationary density is given by the 2D α-stable density. Therefore, we start with the stochastic, underdamped, quartic oscillator ($V(x) = x^4/4$) driven by the Cauchy noise $\zeta(t)$. The Langevin equation, Eq. (6), can be rewritten as

$$\begin{cases} \dot{v}(t) = -\gamma v - x^3 + \zeta(t) \\ \dot{x}(t) = v(t) \end{cases} . \tag{9}$$

One might expect that, analogously like in the overdamped case, the stationary state for Eq. (9) could be bimodal also in the underdamped regime. By exploring dependence of the shape of the stationary state on the damping parameter, we will show that it is not always the case. On the one hand, in the absence of damping ($\gamma = 0$) there is no stationary state for the model described by Eq. (9) because the diffusive packet expands boundlessly. On the other hand, Eq. (9) in the strong damping limit $\gamma \to \infty$ reduces to the well-known problem of the overdamped Cauchy oscillator[36,37]

$$\dot{x}(t) = -x^3 + \zeta(t). \tag{10}$$

As it was mentioned in the introduction, this model has the bimodal stationary state given by Eq. (3). Nevertheless, it is unknown what happens for weak damping (small γ) and how the transition from weak to strong damping is reflected in the shape of stationary densities.

Figure 1 presents the stationary state for the model described by Eq. (9) with $\gamma = 1$. Subsequent panels (from top to bottom) present the 3D surface, 2D heat map and marginal $P(v)$ and $P(x)$ densities. The stationary density is unimodal and it reflects symmetries of the potential. The velocity marginal, $P(v)$, and position marginal, $P(x)$, densities are unimodal as well. Solid lines in bottom panels of Fig. 1 present the limiting velocity distribution, see Eq. (A8), and the stationary state for the overdamped quartic Cauchy oscilator, see Eq. (3). For $\gamma = 1$, limiting marginal densities differ from recorded $P(v)$ and $P(x)$ marginal densities.

For the increasing damping γ, distributions of a velocity become narrower, because the acceleration of the particle becomes hindered. This is confirmed by Eq. (A7), which demonstrates that, with the increasing γ, the scale parameter σ is reduced. At the same time, the impact of rare 'long jumps' in velocity becomes limited. This is reflected in the shape of position marginal distribution, which becomes similar to the solution of the overdamped quartic Cauchy oscillator. The increase in γ leads eventually to appearance of bimodality in $P(x)$ at $\gamma \approx 1.5$. Maxima of the full probability density still are placed at $v = 0$ but $x = 0$ becomes saddle point (maximum in the velocity distribution and local minimum in the position density). Just above $\gamma = 1.5$ maxima are located near $x = 0$ and their height is practically negligible. Nevertheless, the further increase in the damping parameter makes them more pronounced. With increasing γ, maxima moves towards larger $|x|$ and become well separated from the background. Finally, for even larger γ ($\gamma \gg 1.5$) the damping starts to play the dominating role in Eq. (9), and the process becomes practically overdamped. This effect is recorded already for $\gamma = 6$, see Fig. 2. It is well-visible in the velocity marginal distribution, where already for $\gamma = 6$ most of probability mass is concentrated around $v = 0$. At the same time, the position marginal distribution is similar to the solution of the overdamped Cauchy oscillator, which is given by Eq. (3). Consequently, a particle most likely has zero velocity, $v = 0$, and it is most likely localized around $x = \pm 1/\sqrt{2}$ which is the position of the maxima of probability density for the overdamped Cauchy oscillator with $\sigma_0 = 1$. The bend shape of $P(x, v)$ density, see the second from the top panel of Fig. 2, is produced by the deterministic force. For instance, if $x \gg 0$ there is a strong deterministic force towards origin. This negative restoring force is responsible for the large (negative) value of the velocity. Analogously, for $x \ll 0$, the force and the velocity are positive. Moreover, as demonstrated in bottom panels of Fig. 2, for large friction coefficient, i.e. $\gamma = 6$, limiting marginal densities, see Eqs. (A8) and (3), are similar to observed $P(v)$ and $P(x)$ marginal densities.

The emergence of a multimimodal stationary state is an effect of the combined action of all three (deterministic, damping and random) forces which are included in Eq. (9). Noise pulses occasionally give a particle significant velocity, allowing it to move far from the potential minimum. Deterministic force $-x^3$ is the restoring force. It pulls the particle back to the potential minimum, thus, it is responsible for the particle acceleration. The larger distance from the origin, the larger acceleration is. Simultaneously, with the increase in the velocity, the damping increases. Therefore, the damping and the deterministic force counterbalance. If the damping coefficient is large enough, the time needed to deterministically slide to the minimum of the potential becomes infinite. The probability of visiting the origin can be increased due to random pulses. Nevertheless, during the sliding the stochastic force typically displaces the particle further away before it reaches $x = 0$. For sufficient large γ the number of trajectories not reaching $x = 0$ becomes larger than the number of trajectories which visited the potential minimum. This leads to accumulation of the probability mass outside the potential minimum and emergence of two modal values.

The transition between unimodal and bimodal stationary state, induced by the increase in the damping coefficient γ, can be also explained in terms of velocity marginal distribution. Due to "heavy tails" of the velocity distribution, "long jumps" (abrupt changes) in the velocity are observed. Because of huge value of the deterministic force $f(x) = -x^3$ at $|x| \gg 1$, displacements to $|x| > 1$ are produced by tails of the velocity distribution. At the same time, with the increasing γ, the central ($v \approx 0$) part of the velocity distributions becomes narrow, see Eq. (A7). As a consequence, sudden changes in velocity becomes prevailing making the return to the potential minimum unlikely. This in turn produce the transfer of the probability mass outside the vicinity of the potential minimum. In contrast, for small γ, the $P(v)$ distribution is wide, i.e. a lot of the probability mass is located in vicinity of $v \approx 0$. A particle makes a lot of short jumps which are not sufficient to move a particle to distant points. Consequently, observed stationary states are unimodal. Nevertheless, the limit of vanishing damping requires further studies.

The system described by Eq. (9) is characterized by two relaxation times τ_v and τ_x, see Ref. 23. The damping coefficient controls the rate of velocity relaxation which is characterized by the relaxation time $\tau_v \propto 1/\gamma$. At the same time, the relaxation in the x is described by $\tau_x \propto (\gamma L/\sigma)^\alpha$, where L is the typical system size. Situations considered in Figs. 1 and 2 differ not only in shape of stationary states but also in relaxation times. In Fig. 1 the stationary distribution $P(x)$ is reached before $P(v)$ while in Fig. 2 the velocity relaxation is faster than the spatial relaxation. Nevertheless, we leave for the further studies the detailed examination of the issue of velocity and spatial relaxations in uderdamped Langevin dynamics in single-well potentials.

The potential used in Eq. (9) is the special case of more general binomial potential

$$V(x) = \frac{x^4}{4} + a\frac{x^2}{2}. \tag{11}$$

In the overdamped regime, for the potential given by Eq. (11), there exists a critical value $a_c = 0.794$, such that stationary state is unimodal for every $a > a_c$, see Ref. 37. Consequently, the increase in the strength of the parabolic addition to the quartic potential induce bimodal — unimodal transition. In the underdamped regime described by Eq. (6), one can also explore how results with $a = 0$ generalize to $a \neq 0$ case. We expect that for $a > 0$ the critical value of the damping parameter γ for which the probability function becomes bimodal should increase in comparison to the $a = 0$ case, when $\gamma \approx 1.5$. Indeed, bimodality is observed in simulations with a larger γ. For example, for $a = 0.5$ a bimodal stationary state is recorded for $\gamma \approx 4$, see Fig. 3.

A pronounced difference from the $a = 0$ case is visible for the parameter a close to the critical value a_c. For instance, for $a = 0.7$, the full probability density function has two maxima, see top panel of Fig. 4. At the same time, position and velocity marginal densities remain unimodal, even for very large γ, see bottom panel of Fig. 4.

Moreover, for $a < 0$, another counter-intuitive effect is observed. Due to double-well shape of the potential given by Eq. (11) with $a < 0$ one may expect bimodal stationary state. Nevertheless, if the damping coefficient γ is sufficiently small, the probability density seems to be unimodal. Fig. 5 shows results for $a = -0.2$ and $\gamma = 0.5$. For a small value of the damping parameter γ, energy is slowly dissipated and the velocity (because of the damping) slowly changes. Therefore, a particle with a little help from the noise can easily surmount the potential barrier and penetrate neighborhood of both potential minima (unless $a \ll 0$ and $\alpha \lesssim 2$). When a is further reduced, the stationary state becomes clearly bimodal.

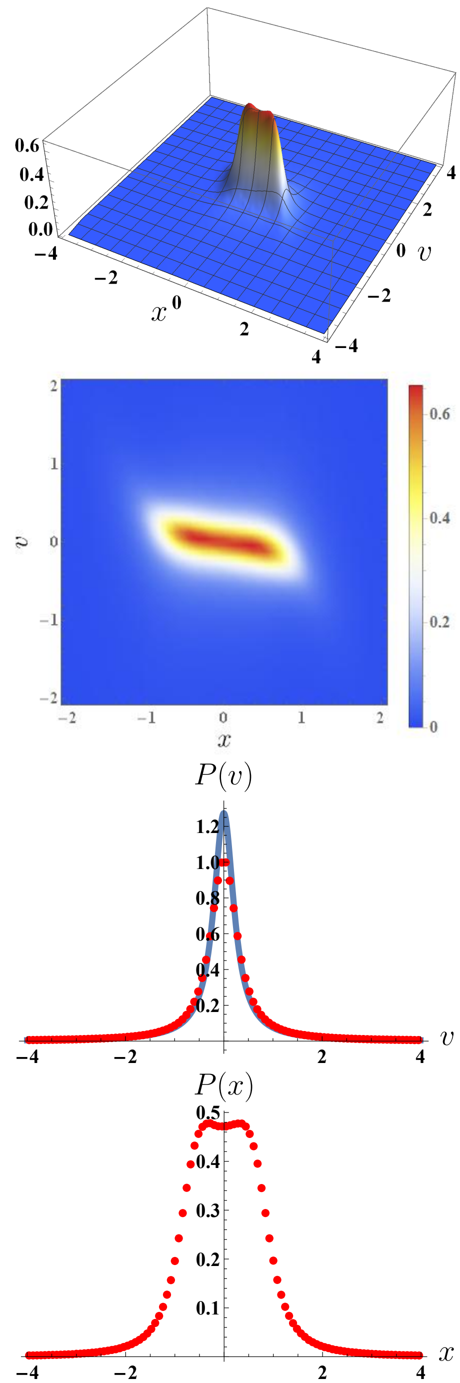

FIG. 3. The stationary state and marginal densities for the potential given by Eq. (11) with $a = 0.5$ and $\gamma = 4$.

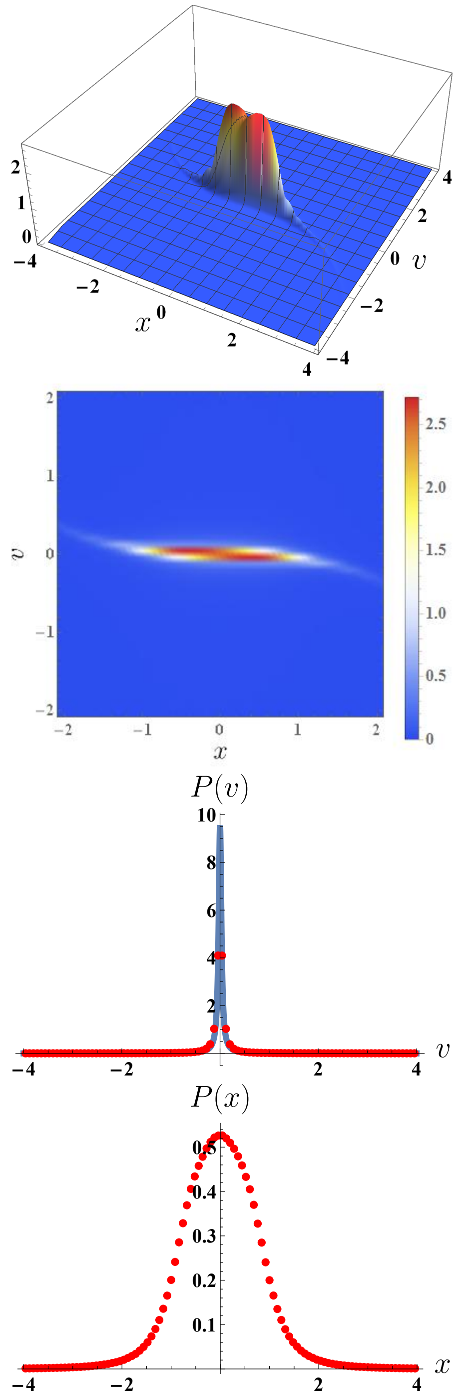

FIG. 4. The same as in Fig. 3 for $a = 0.7$ and $\gamma = 30$.

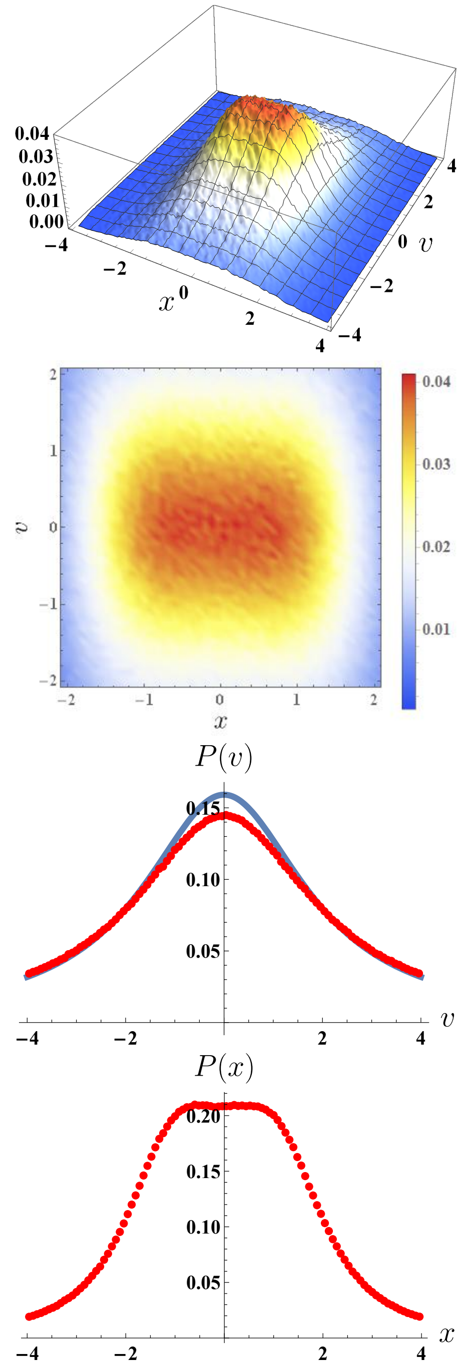

FIG. 5. The same as in Fig. 3 for $a = -0.2$ and $\gamma = 0.5$.

In order to elucidate the role of parameters: a in the potential (11) and the damping γ in the full Langevin equation (6), Fig. 6 presents the phase diagram. Blue region represents bimodal stationary states, while the white region corresponds to unimodal stationary states. For $a < 0.5$, the value of damping coefficient γ for which bimodality appears increases slowly. For $a > 0.5$ the growth of critical damping becomes rapid.

At the same time bimodality of position marginal distribution is not observed. Finally, for $a > a_c = 0.794$, the stationary states are unimodal regardless of the value of the damping parameter.

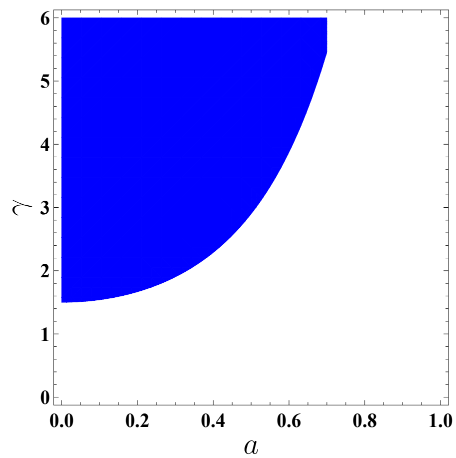

FIG. 6. The phase diagram for $V(x) = x^4/4 + ax^2/2$. The blue region represents values of parameter a and γ for which the full stationary state is bimodal.

In the context of the potential (11), it important to discuss the role of the stability index α in more details. Changes in model properties due to α are milder than due to a. Similarly to the overdamped motion, in the potential given by Eq. (9), see Ref. 36, with the increasing value of α, height of peaks decrease and finally they disappear. At the same time, there is no change in the friction coefficient γ for which transition from unimodal to bimodal stationary state occurs or this change is to small to be visible in presented simulations.

We have also examined single-well polynomial potentials. For instance we have used

$$V(x) = x^6 - \frac{19}{11}x^4 + x^2, \tag{12}$$

which in the overdamped regime results in the trimodal stationary state[39]. For the potential given by Eq. (12) behaviour is very similar as for $V(x) = x^4/4$. For a small value of the damping coefficient γ, stationary states reflect symmetry of the potential. When γ is large enough additional maxima of stationary density appear. The exemplary stationary state for the potential given by Eq. (12) with $\gamma = 2$ is depicted in Fig. 7. With the decreasing γ, local minima of $P(x)$ at $x \approx \pm 0.6$ becomes shallower. Finally, for sufficiently small γ they disappear (results not shown).

Finally, we have explored the motion in the infinite rectangular potential well. In such a case the motion is restricted in space, because the particle is located within the finite interval. During interactions with reflecting walls, the velocity changes its sign. One can expect that, for finite damping, the position marginal density $P(x)$ is uniform while the velocity marginal density $P(v)$ is the same as for a free particle. Such a shape of marginal densities is confirmed by the Kramers equation because the stationary density $P(x, v) = CP(v)$ satisfies Eq. (7). The very different situation is observed in the $\gamma \to \infty$ limit. In such a case the motion becomes overdamped. The particle is characterized by the position only. For $\alpha = 2$, $P(x)$ is uniform, while for $\alpha < 2$ it is u-shaped with modes at reflecting boundaries[52]. Indeed, for finite damping, results of computer simulation show that $P(x, v) = \frac{1}{2L}P(v)$, where $2L$ is the width of the infinite rectangular potential well and $P(v)$ is the same as for the free particle, i.e. it is given by the α-stable density with scale parameter which grows in time.

III. SUMMARY AND CONCLUSIONS

Using numerical methods for the Langevin equation, we have studied stationary states in the underdamped anharmonic stochastic oscillators. Analogously like in the overdamped case, stationary states exist for potential wells which are steep enough. Potential wells which asymptotically grow faster than quadratic are sufficient to produce stationary states. For the parabolic potential, the stationary state exists as well and it is given by the 2D α-stable density. Within these studies, we have used potentials with dominating terms x^4 or x^6, which are well above minimal required steepness. The problem of minimal steepness of the potential which is sufficient to produce stationary states in underdamped stochastic oscillators remains open. We expect that the condition on ν in $V(x) = |x|^\nu/\nu$ should be not weaker than for the overdamped case, i.e. $\nu > 2 - \alpha$.

In order to produce multimodal stationary state, e.g. multimodal position marginal density $P(x)$, system dynamics needs to be close to the overdamped regime, i.e. the marginal density $P(v)$ needs to be narrow. This mean that the damping coefficient γ needs to be large enough. Multimodal stationary states in a single-well potential emerge, when particles are unlikely to be found in the vicinity of the potential minimum. If the motion is close to the overdamped (narrow $P(v)$), analogously like in the overdamped stochastic oscillators, for $\nu > 2$, time required to deterministically slide to $x = 0$ is practically infinite. The sliding is also interrupted by random jumps, which further decrease chances of reaching the minimum of the potential. Therefore, for $\nu > 2$ and γ large enough, stationary states can be multimodal. For large γ, the motion practically becomes overdamped – the velocity marginal density $P(v)$ is characterized by the narrow central part, see Eq. (A7), while it still has power-law tails. In the limit of $\gamma \to \infty$ position marginal densities $P(x)$ reproduce those one of overdamped systems. Appreciable, this equivalence is recorded for finite γ. Therefore, for appropriately selected potentials[39] stationary densities can be characterized by more than two modes. Consequently, it is possible to fine-tune the potential to produce any given number of modes.

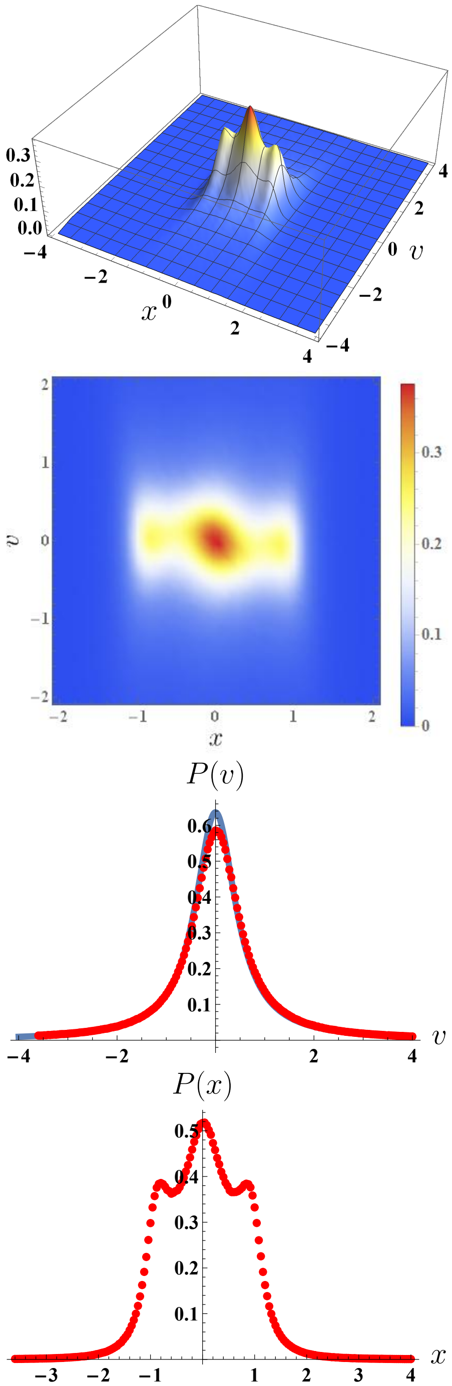

FIG. 7. The stationary state and marginal densities for the potential given by Eq. (12) and $\gamma = 2$.

ACKNOWLEDGEMENT

This project was supported by the National Science Center (Poland) grant 2018/31/N/ST2/00598. This research was supported in part by PLGrid Infrastructure. Fruitful suggestions from Maciej Majka are greatly acknowledged.

Appendix A: Stationary states in the parabolic potential

In the case of the linear friction, the evolution of the velocity is described by the following Langevin equation

$$\frac{dv}{dt} = -\gamma v - V'(x) + \sigma_0 \zeta(t), \tag{A1}$$

where $\zeta(t)$ is the α-stable noise. Disregarding $-V'(x)$ in Eq. (A1) results in the linear Langevin equation which is associated with the following Smoluchowski-Fokker-Planck equation

$$\frac{\partial P(v,t)}{\partial t} = \frac{\partial}{\partial v}\left[\gamma v P(v,t)\right] + \sigma_0^\alpha \frac{\partial^\alpha P(v,t)}{\partial |v|^\alpha}. \tag{A2}$$

The stationary state fulfills

$$0 = \frac{d}{dv}\left[\gamma v P(v,t)\right] + \sigma_0^\alpha \frac{d^\alpha P(v,t)}{d|v|^\alpha}. \tag{A3}$$

Eq. (A3) in the Fourier space reads

$$\gamma k \frac{d\hat{P}(k)}{dk} = -\sigma_0^\alpha |k|^\alpha \hat{P}(k), \tag{A4}$$

where $\hat{P}(k)$ is the Fourier transform $\hat{P}(k) = \int_{-\infty}^{\infty} P(v) e^{ikv} dv$. The characteristic function $\hat{P}(k)$ satisfies

$$\frac{d\hat{P}(k)}{dk} = -\frac{\sigma_0^\alpha}{\gamma} \operatorname{sign}(k) |k|^{\alpha-1} \hat{P}(k). \tag{A5}$$

The solution of Eq. (A5) is given by

$$\hat{P}(k) = \exp\left[-\frac{\sigma_0^\alpha}{\gamma\alpha}|k|^\alpha\right], \tag{A6}$$

which is the characteristic function of the symmetric α-stable distribution, see Eq. (2), with the scale parameter

$$\sigma = \frac{\sigma_0}{(\gamma\alpha)^{1/\alpha}}. \tag{A7}$$

Consequently, with the increasing γ, the stationary distribution becomes narrower. For instance, for the Cauchy noise ($\alpha = 1$), the stationary density is the Cauchy distribution

$$P(v) = \frac{1}{\pi} \frac{\sigma}{\sigma^2 + v^2}. \tag{A8}$$

[1] W. Horsthemke and R. Lefever, *Noise-inducted transitions. Theory and applications in physics, chemistry, and biology* (Springer Verlag, Berlin, 1984).

[2]C. W. Gardiner, *Handbook of Stochastic Methods for Physics, Chemistry and the Natural Sciences*, Vol. 13 of *Springer Series in Synergetics*, 3rd ed. (Springer-Verlag, Berlin, 2004).
[3]L. Gammaitoni, P. Hänggi, P. Jung, and F. Marchesoni, Eur. Phys. J. B **69**, 1 (2009).
[4]C. R. Doering and J. C. Gadoua, Phys. Rev. Lett. **69**, 2318 (1992).
[5]M. O. Magnasco, Phys. Rev. Lett. **71**, 1477 (1993).
[6]P. Reimann, Phys. Rep. **361**, 57 (2002).
[7]Y. Li, Y. Xu, J. Kurths, and X. Yue, Chaos **27**, 103102 (2017).
[8]L. E. Reichl, *A modern course in statistical physics* (John Wiley, New York, 1998).
[9]A. Janicki and A. Weron, *Simulation and chaotic behavior of α-stable stochastic processes* (Marcel Dekker, New York, 1994).
[10]A. Janicki, *Numerical and statistical approximation of stochastic differential equations with non-Gaussian measures* (Hugo Steinhaus Centre for Stochastic Methods, Wrocław, 1996).
[11]G. Samorodnitsky and M. S. Taqqu, *Stable non-Gaussian random processes: Stochastic models with infinite variance* (Chapman and Hall, New York, 1994).
[12]J. P. Bouchaud and A. Georges, Phys. Rep. **195**, 127 (1990).
[13]J. P. Bouchaud, A. Ott, D. Langevin, and W. Urbach, J. Phys. II France **1**, 1465 (1991).
[14]R. Klages, G. Radons, and I. M. Sokolov, *Anomalous transport: Foundations and applications* (Wiley-VCH, Weinheim, 2008).
[15]T. H. Solomon, E. R. Weeks, and H. L. Swinney, Phys. Rev. Lett. **71**, 3975 (1993).
[16]P. Barthelemy, J. Bertolotti, and D. Wiersma, Nature (London) **453**, 495 (2008).
[17]J. L. Cabrera and J. G. Milton, Chaos **14**, 691 (2004).
[18]M. Mercadier, W. Guerin, M. M. Chevrollier, and R. Kaiser, Nat. Phys. **5**, 602 (2009).
[19]F. Bardou, J. P. Bouchaud, A. Aspect, and C. Cohen-Tannoudji, *Lévy statistics and laser cooling* (Cambridge University Press, Cambridge, 2002).
[20]E. Barkai, E. Aghion, and D. A. Kessler, Phys. Rev. X **4**, 021036 (2014).
[21]A. A. Dubkov, B. Spagnolo, and V. V. Uchaikin, Int. J. Bifurcation Chaos. Appl. Sci. Eng. **18**, 2649 (2008).
[22]R. Metzler and J. Klafter, Phys. Rep. **339**, 1 (2000).
[23]A. V. Chechkin, and V. Yu. Gonchar, J. Exp. Theor. Phys. **91**, 635 (2000).
[24]E. Barkai, Phys. Rev. E **63**, 046118 (2001).
[25]V. V. Anh and R. McVinish, J. Appl. Math. Stoch. Anal. **16**, 97 (2003).
[26]D. Brockmann and I. M. Sokolov, Chem. Phys. **284**, 409 (2002).
[27]A. V. Chechkin, V. Y. Gonchar, J. Klafter, and R. Metzler, in *Fractals, Diffusion, and Relaxation in Disordered Complex Systems: Advances in Chemical Physics, Part B*, edited by W. T. Coffey and Y. P. Kalmykov (John Wiley & Sons, New York, 2006), Vol. 133, pp. 439–496.
[28]S. Jespersen, R. Metzler, and H. C. Fogedby, Phys. Rev. E **59**, 2736 (1999).
[29]V. V. Yanovsky, A. V. Chechkin, D. Schertzer, and A. V. Tur, Physica A **282**, 13 (2000).
[30]D. Schertzer, M. Larchevêque, J. Duan, V. V. Yanovsky, and S. Lovejoy, J. Math. Phys. **42**, 200 (2001).
[31]I. Eliazar and J. Klafter, J. Stat. Phys. **111**, 739 (2003).
[32]I. M. Sokolov and R. Metzler, J. Phys. A: Math. Gen. **37**, L609 (2004).
[33]P. Garbaczewski and V. Stephanovich, Phys. Rev. E **80**, 031113 (2009).
[34]P. Garbaczewski, Physica A **389**, 936 (2010).
[35]B. Dybiec, A. V. Chechkin, and I. M. Sokolov, J. Stat. Mech. P07008 (2010).
[36]A. V. Chechkin, J. Klafter, V. Y. Gonchar, R. Metzler, and L. V. Tanatarov, Chem. Phys. **284**, 233 (2002).
[37]A. V. Chechkin, J. Klafter, V. Y. Gonchar, R. Metzler, and L. V. Tanatarov, Phys. Rev. E **67**, 010102(R) (2003).
[38]B. Dybiec, E. Gudowska-Nowak, and I. M. Sokolov, Phys. Rev. E **76**, 041122 (2007).
[39]K. Capała and B. Dybiec, J. Stat. Mech. **2019**, 033206 (2019).
[40]A. V. Chechkin, V. Y. Gonchar, J. Klafter, R. Metzler, and L. V. Tanatarov, J. Stat. Phys. **115**, 1505 (2004).
[41]A. V. Chechkin, R. Metzler, J. Klafter, and V. Y. Gonchar, in *Anomalous transport: Foundations and applications*, edited by R. Klages, G. Radons, and I. M. Sokolov (Wiley-VCH, Weinheim, 2008), pp. 129–162.
[42]A. A. Dubkov and B. Spagnolo, Acta Phys. Pol. B **38**, 1745 (2007).
[43]I. Podlubny, *Fractional differential equations* (Academic Press, San Diego, 1999).
[44]S. G. Samko, A. A. Kilbas, and O. I. Marichev, *Fractional integrals and derivatives. Theory and applications.* (Gordon and Breach Science Publishers, Yverdon, 1993).
[45]G. E. Uhlenbeck and L. S. Ornstein, Phys. Rev. **36**, 823 (1930).
[46]H. Risken, *The Fokker-Planck Equation: Methods of Solution and Applications* (Springer-Verlag, Berlin, 1996).
[47]K. Sekimoto, *Stochastic energetics* (Springer Verlag, Berlin, 2010), Vol. 799.
[48]E. Lutz, Phys. Rev. Lett. **86**, 2208 (2001).
[49]I. M. Sokolov, B. Dybiec, and W. Ebeling, Phys. Rev. E **83**, 041118 (2011).
[50]S. Zozor and C. Vignat, Phys. Rev. E **84**, 031115 (2011).
[51]B. Dybiec, E. Gudowska-Nowak, and I. M. Sokolov, Phys. Rev. E **96**, 042118 (2017).
[52]S. I. Denisov, W. Horsthemke, and P. Hänggi, Phys. Rev. E **77**, 061112 (2008).

Nonlinear friction in underdamped anharmonic stochastic oscillators

Karol Capała,[a] Bartłomiej Dybiec,[b] and Ewa Gudowska-Nowak[c]
Institute of Theoretical Physics and Mark Kac Center for Complex Systems Research, Jagiellonian University, ul. St. Łojasiewicza 11, 30–348 Kraków, Poland

(Dated: 14 March 2022)

Non-equilibrium stationary states of overdamped anharmonic stochastic oscillators driven by Lévy noise are typically multimodal. The very same situation is recorded for an underdamped Lévy noise driven motion in single-well potentials with linear friction. Within current manuscript we relax the assumption that the friction experienced by a particle is linear. Using computer simulations, we study underdamped motions in single-well potentials in the regime of nonlinear friction. We demonstrate that it is relatively easy to observe multimodality in the velocity distribution as it is determined by the friction itself and it is the same as the multimodality in the overdamped case with the analogous deterministic force. Contrary to the velocity marginal density, it is more difficult to induce multimodality in the position. Nevertheless, for a fine-tuned nonlinear friction, the spatial multimodality can be recorded.

PACS numbers: 05.40.Fb, 05.10.Gg, 02.50.-r, 02.50.Ey,

Properties of dynamical systems driven by Lévy noise are very different from their Gaussian white noise driven counterparts. For instance, in the overdamped regime, in order to bound Lévy flights the potential well needs to be steep enough. Surprisingly, for single-well potentials steeper than parabolic non-equilibrium stationary states (NESS) are bimodal. Properties of overdamped systems are better explored than properties of underdamped systems. Therefore, within the current manuscript, we continue studies on the Lévy noise driven dynamics in underdamped systems in the regime of linear and nonlinear friction. Using heuristic arguments and numerical simulations, we explore the role of underlying assumptions and study NESS properties along with conditions for their existence. We demonstrate that, in the underdamped regime, it is easy to induce bimodality in the velocity probability distribution function (PDF), because the phenomenon is determined solely by the form of velocity-dependent friction. Contrary to the multimodality in the velocity, nonlinear friction typically results in unimodal marginal position distributions. Nevertheless, for suitably predefined nonlinear friction, spatially-separated modes in PDF can be generated. Furthermore, superlinear friction is shown to weaken the condition on the steepness of single-well potentials which are capable of bounding underdamped Lévy noise driven motions.

I. INTRODUCTION AND MODEL

Motion of a stochastic particle in the presence of a conservative force, damping and thermal fluctuations is conveniently described by the Langevin equation

$$\ddot{x}(t) = -\gamma\dot{x}(t) - V'(x) + \zeta(t), \tag{1}$$

where γ ($\gamma > 0$) is the damping, $\zeta(t)$ stands for the noise and the unit mass term $m = 1$ is assumed. By attributing thermal origin to the fluctuations of the stochastic force, $\zeta(t)$ can be modeled as Gaussian and white with $\langle\zeta(t)\rangle = 0$ and $\langle\zeta(t)\zeta(s)\rangle = \gamma\sigma^2\delta(t-s)$, as damping γ and strength of fluctuations σ are then connected by a celebrated Einstein's relation[1,2]. Presence of noise randomizes trajectories $(x(t), \dot{x}(t) = v(t))$ making them different even for the same initial conditions. Consequently, an ensemble of particles immersed in a given $(x(0), v(0))$ point starts to diffuse. Erratic trajectories of the ensemble do not allow for the measurement of the particle's velocity, while it is possible to measure the mean-square displacement from the initial position and show that it is growing linearly in time.

The time evolution of the full probability density associated with Eq. (1) is described by the Kramers equation[1]

$$\frac{\partial P}{\partial t} = \left[-v\frac{\partial}{\partial x} + \frac{\partial}{\partial v}\left(\gamma v + V'(x)\right) + \gamma\sigma^2\frac{\partial^2}{\partial v^2}\right]P, \tag{2}$$

where $P = P(x, v, t|x_0, v_0, t_0)$.

Stationary states for the model described by Eq. (1) and associated long-time solutions to the diffusion equation (2) exist for any confining potential $V(x)$ increasing to infinity as $|x| \to \infty$. More importantly, they are given by the equilibrium Boltzmann-Gibbs distribution, thus establishing a relation with thermodynamics:

$$P(x, v) \propto \exp\left[-\frac{1}{\sigma^2}\left(\frac{v^2}{2} + V(x)\right)\right]. \tag{3}$$

The form of the stationary density given by Eq. (3) clearly indicates that velocity and position are statistically independent. Moreover, in the system described by Eq. (1) with the Gaussian white noise, the condition of detailed balance is fulfilled[3,4]. These two, important equilibrium properties are not satisfied under action of Lévy noises[5–9].

Within the current manuscript, using methods of stochastic dynamics, we will be exploring properties of non-equilibrium stationary states (NESS) for models described by the full, underdamped Langevin equation in the regime of nonlinear dissipative force. Models of that type refer to non-equilibrium

[a] Electronic mail: karol@th.if.uj.edu.pl
[b] Electronic mail: bartek@th.if.uj.edu.pl
[c] Electronic mail: ewa.gudowska-nowak@uj.edu.pl

cases where the friction is not a constant but a function of the velocities $\gamma = T(v)$ and the Einstein relation is no longer fulfilled. Interesting applications of models of Brownian motion with nonlinear friction have been addressed in various fields: mechanical devices like microspeakers and vibration isolation systems and energy harvesters[10], self-organized systems exhibiting sustained oscillations[11], description of motion of charged particles in plasma[12] or active Brownian motion models of biological motors[13].

To start with, let us briefly recollect a special limit of Eq. (1) with the strong damping. At strong friction the velocity can be adiabatically eliminated[14] from Eq. (1) resulting in the overdamped Langevin equation

$$\gamma \dot{x}(t) = -V'(x) + \zeta(t). \tag{4}$$

The motion described by Eq. (4) is spatially diffusive and fully characterized by the position only. The time evolution of the probability density $P(x,t|x_0,t_0) = \langle \delta(x - x(t)) \rangle \equiv P$ fulfills the Smoluchowski-Fokker-Planck equation

$$\frac{\partial P}{\partial t} = \frac{1}{\gamma}\frac{\partial}{\partial x}\left[-V'(x) + \sigma^2 \frac{\partial}{\partial x}\right] P, \tag{5}$$

with the stationary solution given again by the Boltzmann-Gibbs form

$$P(x) \propto \exp\left[-\frac{V(x)}{\sigma^2}\right]. \tag{6}$$

In more general realms the noise $\zeta(t)$ does not need to be Gaussian. For example it can be of the Lévy, α-stable type. The symmetric Lévy noise is the formal time derivative of the symmetric α-stable motion $L(t)$, see Ref. 15, whose characteristic function $\phi(k) = \langle \exp[ikL(t)] \rangle$ is

$$\phi(k) = \exp\left[-t\sigma^\alpha |k|^\alpha\right] \tag{7}$$

with the parameter σ scaling the strength of fluctuations. Following this definition $\zeta(t)$ is a symmetric, Markov α-stable noise which turns into a standard Gaussian form for $\alpha = 2$. However, unlike standard Brownian motions for which the mean-square displacement (MSD) grows linearly in time, the dispersion of the position in the Lévy motion (cf. Eq. (4) with $V(x) \equiv 0$) diverges and the width of the resulting asymptotic Lévy (super)-diffusion must be characterized by some fractional moments[16–18] or the interquantile distance. Symmetric α-stable densities are unimodal probability densities which for $\alpha < 2$ exhibit a power-law asymptotics with tails decaying as $|x|^{-(\alpha+1)}$. Moreover, for Lévy noise driven systems, the condition of detailed balance is not satisfied[5,8]

In case of motions described by the Langevin equations and perturbed by a generalized Lévy noise, the associated diffusion equations (2) and (5) become fractional Smoluchowski-Fokker-Planck or Kramers equations[18–20]. In Eq. (2), $\partial^2/\partial v^2$ is then replaced by $\partial^\alpha/\partial|v|^\alpha$, see Ref. 21, while in Eq. (5) $\partial^2/\partial x^2$ is exchanged with $\partial^\alpha/\partial|x|^\alpha$, see Ref. 22 and 23. The Riesz-Weil $\partial^\alpha/\partial|x|^\alpha$ fractional derivative[19,24] is defined via the Fourier transform $\mathcal{F}_k\left(\frac{\partial^\alpha f(x)}{\partial|x|^\alpha}\right) = -|k|^\alpha \mathcal{F}_k\left(f(x)\right)$.

The significant differences in statistical properties of systems driven by non-Gaussian Lévy fluctuations, and in particular divergence of the second moment, imply lack of a simple Einstein's fluctuation-dissipation relation between fluctuations' strength and magnitude of dissipation[8,9,25,26]. Accordingly, in Eqs. (1) and (2), the damping γ and the noise strength σ have to be interpreted as independent parameters. Consequently, for $\alpha < 2$, in Eq. (2) $\gamma\sigma^2\partial^2/\partial v^2 \to \sigma^\alpha\partial^\alpha/\partial|v|^\alpha$, while in Eq. (5) $\sigma^2\partial^2/\partial x^2 \to \sigma^\alpha\partial^\alpha/\partial|x|^\alpha$.

Lévy processes have been massively studied on theoretical and numerical levels[22,23,25,27–31]. Because of significant likelihood of observation of long jumps, Lévy noises and Lévy statistics can be successfully applied to description of catastrophic events like economic crises[32,33], outburst of epidemics[34] or climate changes[35]. The significant number of observations confirms presence of non-Gaussian fluctuations in the variety of complex dynamical systems and experimental setups. Among others, Lévy flights have been recorded in financial time series[36], rotating flows[37], superdiffusion of micellar systems[38], transmission of light in polidispersive materials[39], photon scattering in hot atomic vapors[40], dispersal patterns of humans and animals[41,42], laser cooling[43,44], gaze dynamics[45] and search strategies[46,47].

In the overdamped regime described by Eqs. (4) and (5) and under the action of an harmonic potential $V(x) = x^2/2$, NESS in the presence of additive Lévy noises are given by the rescaled α-stable density with the same stability index α as the noise[25,48–50]. This is a natural consequence of action of the deterministic linear force and the generalized central limit theorem[51]. In a more general potential wells the turnover from unimodal to bimodal non-equilibrium stationary probability densities occurs[52]. As an exemplary case, we refer to Lévy flights in the potential $V(x) = x^4/4$, when the Langevin equation takes the following form

$$\gamma \dot{x}(t) = -x^3(t) + \zeta(t). \tag{8}$$

For the Lévy noise with $\alpha = 1$ (Cauchy noise), the NESS of the system can be readily derived[31,48,49,52,53] and is given by

$$P_{\alpha=1}(x) = \frac{1}{\pi\sigma^{1/3}\left[(x/\sigma^{1/3})^4 - (x/\sigma^{1/3})^2 + 1\right]}. \tag{9}$$

The probability density (9) is the symmetric bimodal distribution with modes at $x = \pm\sigma^{1/3}/\sqrt{2}$ and the power-law asymptotics $P(|x|) \propto |x|^{-4}$. The observed bimodality (9) is related to the general property of the Lévy noise — induced bifurcation in modality of the corresponding PDF for $t \to \infty$, see Refs. 48, 49, and 54. In more general single-well potentials — NESS (their PDFs) can be characterized by more than two modes[55].

The multimodality of NESS in overdamped systems calls to inquire whether PDFs in underdamped regime can be multimodal. As it was shown in earlier works[6,56], for $V(x) = x^2/2$, NESS $P(x,v)$ are given by the 2D α-stable density[17,57], whose marginal densities are unimodal and given by 1D α-stable densities — in an analogy to their Gaussian white noise-driven cases. Contrary to the stationary states in Gaussian white noise driven systems, see Eq. (3), under action of Lévy noises two dimensional non-equilibrium stationary densities $P(x,v)$ do not factorize. Therefore, position and velocity are not statistically independent[6]. In Ref. 6, due to divergence of covariance, the level of dependence was measured by the codifference[17,58]. The nonlinear friction could increase the statistical dependence between position and velocity, as already the combined action of nonlinear friction and Gaussian white noise[59] introduces dependence. Moreover, we expect that in systems with full dynamics, analogously like in overdamped models[5,8], the condition of detailed balance is violated. Nevertheless, these issues (level of dependence and detailed balance) need further verification. In Ref. 60, we have extended studies on underdamped systems under action of Lévy noises and have analyzed properties of non-equilibrium stationary PDFs for anharmonic potentials in the case of linear damping . We have shown that in the system described by Eq. (1), i.e., in the regime of linear friction, the non-equilibrium stationary state can be multimodal under the condition that damping is strong enough. The constraint of the strong damping is related to the fact that for infinite damping ($\gamma \to \infty$) the motion described by Eq. (1) becomes overdamped and the corresponding Lévy noise driven motion in single-well potentials (steeper than parabolic) NESS become at least "bimodal" for long times[55]. In practical realizations though, this bimodality is observed for the finite damping.

The problem of multimodality of NESS, which is posed here, is related to the more general issue of existence of NESS. We can ask the question what is the minimal steepness n of the potential allowing for bounding of underdamped Lévy flights. The problem of the potential steepness is related to the friction. The friction in Eq. (1) is linear. Consequently, the velocity v changes according to

$$\dot{v}(t) = -\gamma v(t) - V'(x) + \zeta(t). \tag{10}$$

In general, steady state for the system described by Eq. (10) is unknown. Nevertheless, some intuitive insight might be gain by considering the motion of a free particle, i.e., the case where deterministic force $-V'(x)$ is omitted. If we disregard the deterministic force $-V'(x)$ in Eq. (10) we get the following equation

$$\dot{v}(t) = -\gamma v(t) + \zeta(t), \tag{11}$$

which can be used to approximate $P(v)$ densities. The quality of such approximation increases with the increase in γ, see Figs. 1 – 2. Under such an approximation, the evolution of the velocity $v(t)$ is described by the same equation like the evolution of the position $x(t)$ in the overdamped dynamics in the parabolic potential, see Eq. (4). Therefore, the steady state density $P(v)$ is given by the α-stable density with the same stability index α like the noise $\zeta(t)$, see Refs. 48–50, and the rescaled scale parameter

$$\sigma = \frac{\sigma_0}{(\gamma\alpha)^{1/\alpha}}, \tag{12}$$

where σ_0 is the scale parameter of the Lévy noise $\zeta(t)$ in Eq. (11). For $\gamma = 0$ there is no stationary velocity distribution, but the velocity is still distributed according to the α-stable density with the scale parameter growing in time as $\sigma(t) = \sigma_0 t^{1/\alpha}$. Consequently, for $\gamma = 0$, there is no stationary state for the underdamped model described by Eq. (10). For $\gamma > 0$, with the linear friction, the $P(v)$ density is very well approximated by the α-stable density. Therefore, for the linear friction, the problem of existence of NESS for the model described by Eq. (1) is equivalent to the problem of existence of NESS for the overdamped motion in $V(x)$, see Eq. (4) and Ref. 61. Consequently, for $n > 2 - \alpha$ non-equilibrium stationary states exist.

In more elaborate situation the friction term $T(v)$ in Eq. (1) does not need to be linear[62–67]. In such a case the Langevin equation (1) generalizes to

$$\left\{ \begin{array}{lcl} \dot{x}(t) &=& v(t) \\ \dot{v}(t) &=& T(v) - V'(x) + \zeta(t) \end{array} \right. . \tag{13}$$

As an example, the dynamical behavior of a mechanical system with dry friction has been described[68] by

$$T(v) = -\gamma\, \mathrm{sign}(v)|v|^{\kappa-1} \quad (\kappa > 0). \tag{14}$$

The linear friction corresponds to $\kappa = 2$. The friction $T(v)$ can be seen as an analog of the deterministic force $-V'(x)$ in the overdamped regime, compare Eq. (4) and the second line of Eq. (13). Consequently, it is possible to find the generalized v-potential. Following this analogy, it is possible to relate the problem of existence of the steady state density $P(v)$ to the problem of existence of NESS in the overdamped dynamics. Therefore, in order to bound velocity, the condition on κ is the same as the condition on n in $V(x) = |x|^n/n$, i.e.,

$$\kappa > 2 - \alpha. \tag{15}$$

Furthermore, for $\kappa > 4-\alpha$, marginal densities $P(v)$ are characterized by the finite variance, see Refs. 48 and 61. Therefore, we can consider the sub-linear friction with κ bounded from below, i.e., $2 - \alpha < \kappa < 2$. In such a case the density $P(v)$ exists and most likely, for $n > 2 - \alpha$, a non-equilibrium stationary state $P(x,v)$ also exists. The regime of super-linear friction, $\kappa > 2$, which is studied within the current manuscrip, is more transparent than the sub-linear case. For $\kappa > 2$, the density $P(v)$ asymptotically behaves as a power-law with lighter tails than noise in Eq. (13). In other words, for $\kappa > 2$, tails of $P(v)$ distribution decay faster than tails of the α-stable density associated with the Lévy noise $\zeta(t)$ in Eq. (1). For example, for $T(v) = -\gamma v^3$ with $\alpha = 1$, asymptotics of $P(v)$ is $P(|v|) \propto |v|^{-4}$, see Eq. (9). Therefore, we can speculate that the minimal exponent in the potential $V(x) = |x|^n/2$ is still bounded from below ($n > 0$) but now it can be smaller than $2 - \alpha$. For instance, for $\kappa = 4$ the variance of $P(v)$ is finite, therefore we expect that $P(x)$ exists for any $n > 0$, what is confirmed by numerical simulations (results not shown).

In the next section (Sec. II) we present results of our analysis of non-equilibrium stationary states (NESS) for anharmonic stochastic oscillators under nonlinear friction. The manuscript is closed with Summary and Conclusions (Sec. III).

II. RESULTS

In what follows, we relax the assumption of linear friction and assume that friction depends nonlinearly on the particle velocity. We start with $T(v) = -\gamma v^3$. Such a system is described by the following Langevin equation

$$\begin{cases} \dot{x}(t) &= v(t) \\ \dot{v}(t) &= -\gamma v^3(t) - x^3(t) + \zeta(t) \end{cases}. \tag{16}$$

Results of simulations depicted in Figs. 1 and 2 are significantly different from results for the linear friction with the same potential $V(x)$ and the same noise, i.e., the Cauchy noise ($\alpha = 1$), see Ref. 60. If one disregards the deterministic $-x^3$ force, the Langevin equation for the velocity evolution becomes similar to the overdamped equation (8) with the position x replaced by the velocity v. Therefore, we could expect that, analogously to the bimodal non-equilibrium stationary density $P(x)$ associated with Eq. (8), the velocity marginal density $P(v)$ becomes also bimodal. This bimodality is also reflected in the shape of the full probability density: In the top panel of Figs. 1 and 2, there are two maxima separated only in the velocity direction. For $\gamma = 1$ (Fig. 1), there is no multimodality in the position marginal PDF. Contrary to the case of linear friction, see Ref. 60, the increase in γ does not induce bimodal steady states in the position marginal distribution even for $\gamma = 6$ (Fig. 2). The change in γ affects only widths of marginal distributions but it does not change its modality tails' asymptotics. When the damping increases, position probability densities $P(x)$ become localized around minimum of the deterministic potential.

Altogether, in contrast to results of former investigations,[60] we observe bounding of velocities induced by nonlinear dissipation, i.e., for $\kappa > 4 - \alpha$, velocity is characterized by the finite variance. Nonlinear friction regularizes the stochastic motion subject to Lévy noise (probability of large velocities decays faster than the tails of the noise distribution) and leads to the form of the marginal stationary density $P(v)$ with non-vanishing most likely (modal) velocities. This observation remains in a strong opposition to unimodal distribution characterizing stationary velocities in a domain of linear friction.

At the same time the position marginal non-equilibrium stationary densities $P(x)$ are very different from their linearly damped counterparts, compare bottom panels of Figs. 1, 2 and especially of Fig. 7 with appropriate densities in the regime of linear friction.[60] For instance, the marginal $P(x)$ density in Fig. 2 is unimodal, while for linear friction with the same potential and under the action of the same noise it is bimodal. Moreover, numerically estimated $P(x)$ are narrower and, most likely, do not display power-law asymptotics, because nonlinear damping, more efficiently cuts off probability of observing large velocities.

In analogy to the Langevin dynamics with linear friction, the lack of bimodality in the position marginal distribution can be better understood in terms of the analysis of the velocity marginal distribution: Even for the large value of the friction parameter γ, the velocity distribution is bimodal. Therefore, occurrence of non-zero velocity is very likely and consequently more trajectories visit $x = 0$ as large velocity helps

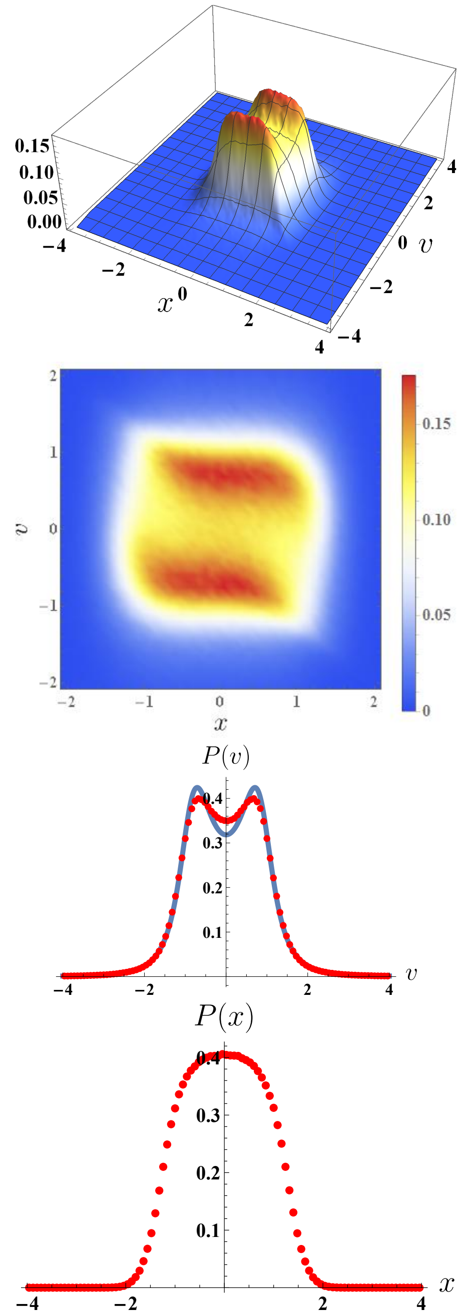

FIG. 1. Non-equilibrium stationary probability density $P(x, v)$ as the 3D-plot and the 2D map (top panels), the velocity non-equilibrium stationary marginal density $P(v)$ (points) with the analytical solution (9) with σ given by Eq. (12) (solid line) and the position non-equilibrium stationary marginal density $P(x)$ (bottom panels). The driving noise is the Cauchy noise, i.e., the Lévy noise with $\alpha = 1$. The damping parameter γ is set to $\gamma = 1$.

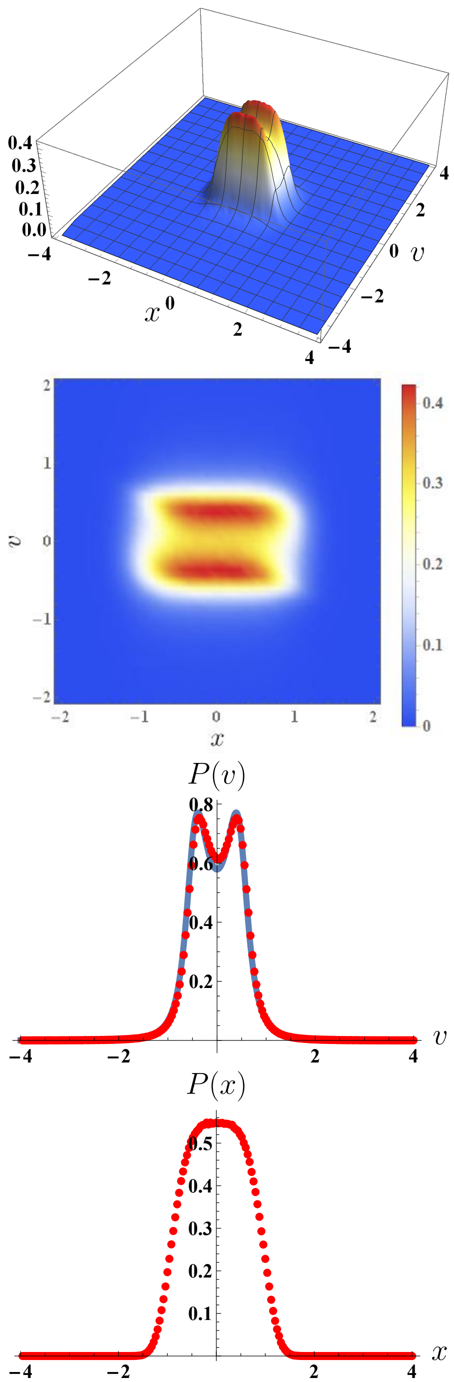

FIG. 2. The same as in Fig. 1 for $\gamma = 6$.

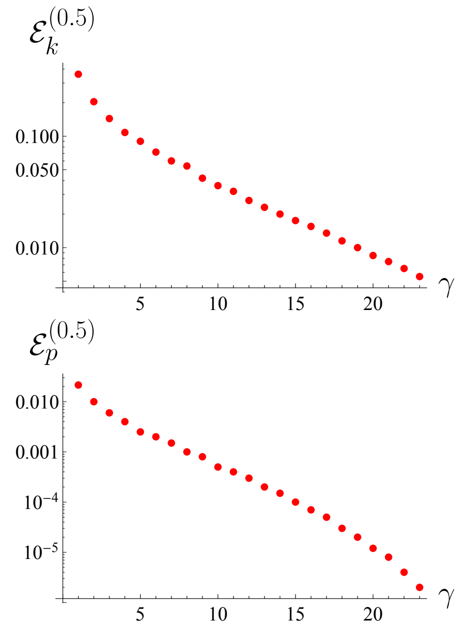

FIG. 3. Median of the kinetic energy $\mathcal{E}_k^{(0.5)}$ (top panel) and potential energy $\mathcal{E}_p^{(0.5)}$ (bottom panel) as a function of friction parameter γ for the system described by Eq. (16).

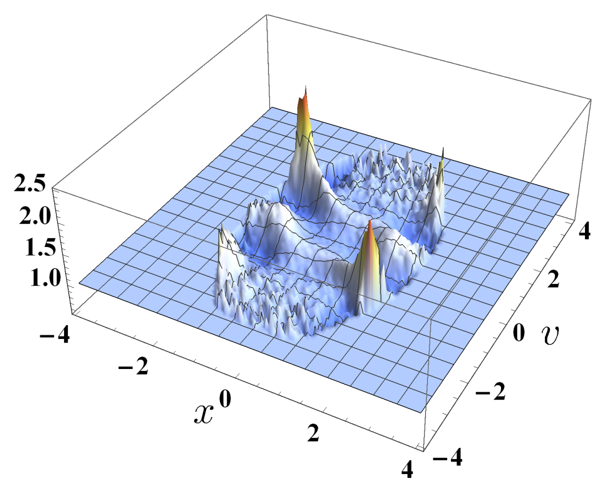

FIG. 4. Ratio $P(x,v)/[P(x)P(v)]$, see Fig. 1, quantifying departure from the corresponding Boltzmann-Gibbs equilibrium stationary states, for which $P(x,v)/[P(x)P(v)] \equiv 1$.

to reach the origin. Therefore, instead of minimum of $P(x)$ at the origin, there is a maximum. In the deterministic dynamics, i.e., for $\zeta(t) \equiv 0$, the nonlinear damping secures observation of long lasting, persistent oscillations in $x(t)$, even at large values of γ. As a result, and contrary to the overdamped case, a trajectory reaches the potential minimum in a finite time. In consequence, the likelihood of returning to initial position before next "long jump" is not negligible. Existence of two modal values in the velocity marginal distribution may

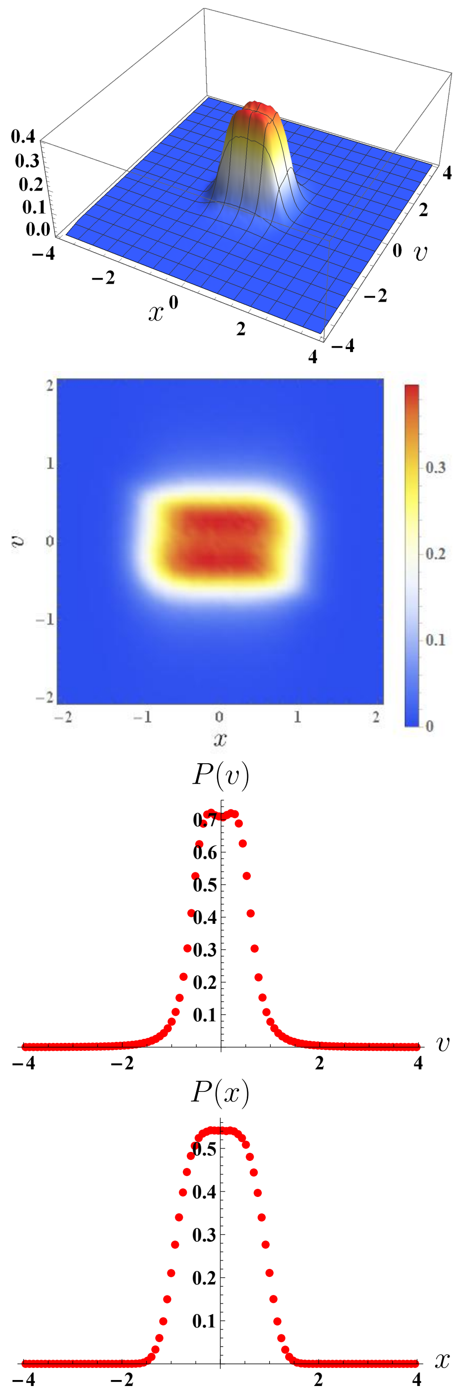

FIG. 5. Non-equilibrium stationary probability density $P(x, v)$ as the 3D-plot and the 2D map (top panels), the velocity non-equilibrium stationary marginal density $P(v)$ and the position non-equilibrium stationary marginal density $P(x)$ (bottom panels). The driving noise is the Cauchy noise, i.e., the Lévy noise with $\alpha = 1$, while the friction term is given by Eq. (17) with $\gamma = 4$ and $a = 0.2$.

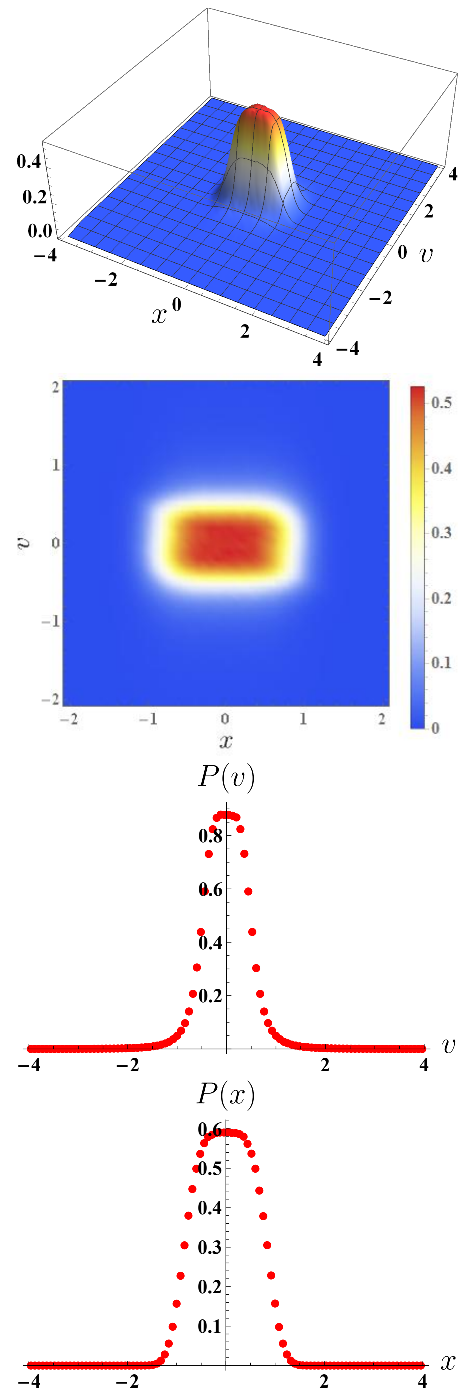

FIG. 6. The same as in Fig. 5 for $\gamma = 6$.

be attributed to these oscillations which occur between noise pulses inducing transition between the modes[69].

The velocity marginal distributions $P(v)$ depicted in Figs. 1 and 2 deviate from the analytical solution (9) with the scale parameter given by Eq. (12), especially in the central part. Eq. (9) is the solution of the Eq. (11), which differs from the second line of Eq. (16) by disregarding the deterministic force, while simulations are performed for the whole dynamics, i.e., the deterministic force $-V'(x)$ is also taken into account. The discrepancy between results of simulations and non-equilibrium stationary density given by Eq. (9) is produced by the deterministic force $-V'(x)$. In the force free case, $-V'(x) \equiv 0$, a perfect agreement is observed. Moreover, with the increasing damping the level of disagreement decreases, see Fig. 1 and 2, because for larger γ the velocity distribution is narrower and, most importantly, it equilibrates faster[20].

Let us further analyze statistical properties of kinetic $\mathcal{E}_k$ and potential $\mathcal{E}_p$ energies of such a system. Analogously to position x and velocity v, also kinetic $\mathcal{E}_k$ and potential $\mathcal{E}_p$ energies are now random variables. Their distributions can be calculated by use of PDFs $P(x, v)$ and suitable transformation of variables. Due to a $|v|^{-4}$ asymptotic of the velocity marginal distribution, see Eq. (16), the mean value of kinetic energy ($\langle \mathcal{E}_k \rangle = \langle v^2 \rangle/2$) exists. Moreover, a very fast decay of tails of the position PDF suggests that also the mean value of the potential energy ($\langle \mathcal{E} \rangle_p = \langle V(x) \rangle$) should exist. As it is demonstrated in figures, velocity and positions distribution are well localized. Nevertheless, it is very difficult to calculate numerically mean values of kinetic and potential energies. Regardless of the integration time step Δt, there is a non-negligible probability of observing very strong noise pulses which are responsible for the occurrence of very large velocities and long displacements resulting in the possibility of reaching distant positions. These extreme events make the numerical calculation of the average energies ill posed. Already a single extreme observation makes averages to explode in an uncontrollable way. Therefore, instead of calculating averages, we have employed medians of kinetic ($\mathcal{E}_k^{(0.5)}$) and potential ($\mathcal{E}_p^{(0.5)}$) energies as they are robust parameters to rare but extreme events (outliers). Fig. 3, please note log-linear scale, presents medians of energy distributions as functions of damping parameter γ for the process described by Eq. (16). Both medians $\mathcal{E}_k^{(0.5)}$ and $\mathcal{E}_p^{(0.5)}$ exponentially decrease with the increasing γ. Note that the median of kinetic energy $\mathcal{E}_k^{(0.5)}$ is about order of magnitude larger then the median of potential energy $\mathcal{E}_p^{(0.5)}$. One may also observe that $\mathcal{E}_p^{(0.5)}$ decays faster that $\mathcal{E}_k^{(0.5)}$. This difference may be deduced from marginal distributions: First, most of the probability mass is located in the $(-1, 1)$ interval, both for position and velocity. Therefore, due to the relation between the velocity v and the kinetic energy ($\mathcal{E}_k = v^2/2$) and the position x and the potential energy ($\mathcal{E}_p = x^4/4$), most of the probability mass for energies is located in the $[0, 1)$ intervals. For the argument from the $[0, 1)$ interval, the function x^4 increases slower than v^2, thus, if the velocity and position marginal distribution were the same, one could expect the lower value of the median of the potential energy than the corresponding median of the kinetic energy. However, both distributions differ significantly. Due to fast-decaying tails of the position marginal distribution, probability mass for the potential energy is concentrated near 0. At the same time, for the kinetic energy, the probability mass is moved towards larger values of v, because of power-law tails and bimodality of the velocity probability density. These differences produce significantly higher value of the median of kinetic energy in comparison to the median of the potential energy.

In Ref. 6 it was demonstrated that the non-equilibrium stationary states for the Lévy harmonic oscillator (under linear friction) are given by the 2D α-stable densities and position and velocity are not statistically independent. The analogous situation is observed for anharmonic Lévy oscillators in the regime of nonlinear friction, which are studied within the current manuscript. In order to prove statistical dependence of x and v we have plotted the ratio of the full non-equilibrium stationary probability density $P(x, y)$ and marginal densities $P(x), P(v)$, i.e., $P(x, y)/[P(x)P(y)]$, see Fig. 4. Close inspection of Fig. 4 clearly indicates that position x and velocity v are not independent and the joint PDF assumes non-Boltzmann form. Despite the fact that for studied anharmonic Lévy oscillators under nonlinear damping variances of x and v exist, the statistical properties of cross-correlation xv cannot be reliably calculated. Therefore, we have limited ourselves to depicting the sample ratio of probability densities leaving the problem of quantifying the dependence between x and v for further studies.

The parabolic addition to the quartic potential destroys the multimodality of overdamped steady states[48,49,52]. Therefore, we check the mixture of cubic and linear friction

$$T(v) = -\gamma(v^3 + av) \quad (a > 0). \tag{17}$$

Analogously to the overdamped setup[48], increase in a above a critical value a_c ($a_c = 0.794$) destroys bimodality in the velocity marginal density $P(v)$. Moreover, for $a > a_c$, not only $P(v)$ but also the full non-equilibrium stationary density $P(x, v)$ becomes unimodal. In contrast, for $0 < a < a_c$, the velocity PDF $P(v)$, as well as the full density $P(x, v)$ are multimodal. At the same time, the marginal position distribution $P(x)$ is unimodal, see Figs. 1 – 2 and 5 – 6, which present results for the Cauchy noise.

Finally, we have examined motion of a Langevin particle under action of the Cauchy noise with the velocity dependent friction term given by a polynomial steeper than cubic. For that purpose we have used the following set of equations

$$\begin{cases} \dot{x}(t) &= v(t) \\ \dot{v}(t) &= -\gamma\left[6v^5 - \frac{76}{11}v^3 + 2v\right] - x^3(t) + \zeta(t) \end{cases} . \tag{18}$$

The friction term was chosen in a such way that, in the absence of $-x^3$ force, the velocity marginal density is trimodal[55]. Such a choice of the friction was primarily motivated by possibility of examination of the probability density behavior for the system in which velocity marginal distribution has both zero and non-zero modal values. Numerical simulations confirm that, even in the presence of a quartic potential $V(x)$, the velocity marginal distribution remains trimodal. Therefore, basing on the marginal velocity distribution, the probability mass or the concentration of particles may be divided into two distinct groups. The first group, with velocities corresponding to the outer maxima ($|v| \gg 0$) of the velocity marginal distribution, behaves very similar like particles described by Eq. (16). They produce two modal values corresponding to these velocities. At the same time, in the spatial domain, those modes produce a single peak at $x = 0$, so that the spatial multimodality for $v \neq 0$ is not observed. The second group of particles includes those ones with the velocity close to zero (represented by the central mode of the velocity marginal distribution). Due to small velocities, dynamics of particles from the second group can be similar to the overdamped motion. For $v \approx 0$, the full probability density $P(x, v)$ has two maxima as $P(x, v \approx 0)$ depends nonmonotonously on x. At the same time, the position marginal distribution $P(x)$ remains unimodal, see Fig. 7, which shows NESS and marginal densities for Eq. (18) with $\gamma = 4$. Fig. 7 demonstrates the strong trimodality in the marginal steady density $P(v)$, which was already discussed above and in Ref. 55. The position marginal distribution $P(x)$ stays unimodal, despite of two modal values of the full probability density with modes at non-zero positions. In total, the model described by Eq. (18) has four modes — two at $v \approx 0$ and two at $v \neq 0$.

The nonlinear friction used in Eq. (18), i.e.,

$$T(v) = -\gamma \left[6v^5 - \frac{76}{11}v^3 + 2v \right]. \tag{19}$$

is a nonmonotonous function of v. Clearly, such a nonlinear friction only dissipate energy, i.e., it does not lead to the active Lévy motion[70,71]. In Ref. 55 it was shown that, in the overdamped system, the deterministic force given by Eq. (19) with v replaced by x produces trimodal non-equilibrium stationary state. In accordance with these findings, for the underdamped motion, the velocity distribution is also trimodal with modes located at the same locations as in the underdamped model. Now, presence of three modes in overdamped systems[55] can be reinterpreted. The most likely values of velocities are those corresponding to the minimal friction. Unfortunately, this simple intuitive explanation is of the qualitative type only, because its prediction on the position of modal values are significantly worse than arguments based on the extremes of the potential curvature[48,52,55].

III. SUMMARY AND CONCLUSIONS

Here we have analyzed numerically stochastic dynamics of underdamped stochastic oscillators subject to velocity-dependent nonlinear damping and additive Lévy white noise.

So far, it is known that non-equilibrium stationary states (NESS) for overdamped anharmonic stochastic oscillators, $V(x) = |x|^n/n$, driven by Lévy noise exist for $n > 2 - \alpha$. More importantly, at $n = 2$, the corresponding non-equilibrium stationary PDFs change from unimodal to bimodal forms. Emergence of bimodal NESS for $n > 2$ can be intuitively explained in the limit of a vanishing noise. In the weak noise limit, for $n > 2$, time of deterministic sliding

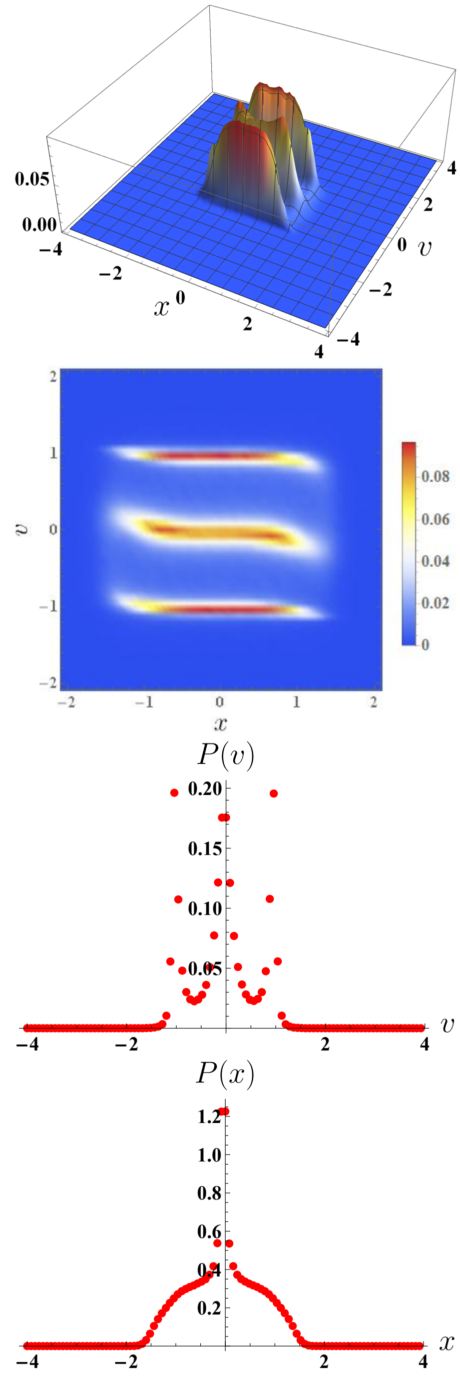

FIG. 7. The non-equilibrium stationary states and marginal densities for $T(v)$ given by Eq. (19) with $\gamma = 4$. The driving noise is the Cauchy noise, i.e., the Lévy noise with $\alpha = 1$.

from $|x| > 0$ to the origin is infinite. The competition between deterministic sliding and escapes induced by noise pulses is responsible for depletion of the probability of finding a particle at $x = 0$. In consequence, $P(x)$ has a local minimum at $x = 0$ and the distribution becomes bimodal. Putting it differently, for overdamped motion in single-well potentials, difficulty in reaching origin is responsible for emergence of bimodal NESS. The very same scenario is observed for underdamped dynamics. However, in this situation, due to non-zero velocity, a trajectory can more easily visit the origin. In consequence, it is harder to observe multimimodal non-equilibrium stationary states in underdamped motions than in the overdamped motions. Moreover, nonlinear friction additionally hampers emergence of multimodal steady states.

Stochastic underdamped systems are characterized by a velocity and a position, which are distributed according to some probability density. If the particle moves in the external potential and this movement is subject to damping, the probability density can asymptotically attain the stationary density. For Lévy noise, this takes place under the condition that nonlinear friction is strong enough and the potential grows sufficiently fast. The problem of multimodality of NESS for the underdamped dynamics is more complex than for the overdamped dynamics, because one can ask about multimodality in the full probability density $P(x, v)$ or in marginal non-equilibrium stationary densities $P(x)$ and $P(v)$.

For underdamped motion in the regime of the nonlinear friction it is easy to record multimodality in the velocity, and consequently in the full density, as this feature is mainly determined by the friction term. At the same time the spatial multimodality is more difficult to be induce. Importantly, in the underdamped system the non-equilibrium stationary $P(v)$ densities, despite action of the additional deterministic $= V'(x)$ force, are practically the same as $P(x)$ densities for analogous overdamped systems, i.e., for overdamped systems with the same deterministic force as friction, i.e., $-V'(x) = T(x)$. For instance, for the linear friction, $P(v)$ densities are of the α-stable type. Nevertheless, some differences between non-equilibrium stationary $P(x)$ in overdamped systems and $P(v)$ in the underdamped system can be produced by the deterministic force $-V'(x)$, which accompanies action of friction in the equation describing time evolution of the velocity.

As the main type of nonlinear friction we have used $T(v) = -\gamma \operatorname{sign}(v)|v|^{\kappa-1}$, which for $\kappa > 2$ is responsible for observation of multimodal velocity marginal densities $P(v)$. Nevertheless, the multimodality in v do not transfer into spatial multimodality of non-equilibrium stationary states. The increase in damping coefficient γ not only influences the modality of NESS but also affects the energy distribution widths, cf. Fig. 3. The width of energy distribution is the decaying function of γ. At the same time, the median of kinetic energy is order of magnitude larger than the median of potential energy, because kinetic energy is quadratic in the velocity while the potential energy is quartic function of the position. Moreover tails of velocity distribution are heavier than tails of position distribution. The addition of a linear component to such a friction form, $T(v) = -\gamma \operatorname{sign}(v)|v|^{\kappa-1} - \gamma a v$, is capable of destroying the velocity multimodality, as can be clearly visible for $\kappa = 4$, cf. Fig. 2 vs. Fig. 6. Eventually, higher order damping, e.g., damping given by Eq. (19), produces trimodal NESS in the velocity with one mode at $v \approx 0$ and two modes at $|v| > 0$. On the one hand, particles with $v \approx 0$ are close to be overdamped and consequently, due to the potential cubic force, $-V'(x) = -x^3$, they follow a bimodal distribution. On the other hand, particles with $|v| > 0$ are distributed according to a unimodal density. The full density $P(x, v)$ has four modal values because for $v = 0$ additional spatial multimodality is produced.

Finally, in the limit of $\gamma \to \infty$, velocity becomes overdamped. Actually, already for finite γ, the motion becomes practically overdamped. Therefore, in the case of linear friction, the non-equilibrium stationary density $P(x)$ approaches the one characterizing overdamped motion in the very same potential. For the nonlinear friction the situation is very different. Due to nonlinearity of the damping, overdamped Langevin equation is not restored in the strong friction limit. Consequently, non-equilibrium stationary state for nonlinear friction is different that the steady state for the overdamped motion in the very same potential.

ACKNOWLEDGEMENT

This project was supported by the National Science Center (Poland) grant 2018/31/N/ST2/00598. This research was supported in part by PLGrid Infrastructure.

DATA AVAILABILITY

The data that support the findings of this study are available from the corresponding author (KC) upon reasonable request.

[1] H. Risken, *The Fokker-Planck Equation: Methods of Solution and Applications* (Springer-Verlag, Berlin, 1996).
[2] K. Sekimoto, *Stochastic energetics* (Springer Verlag, Berlin, 2010), Vol. 799.
[3] L. E. Reichl, *A modern course in statistical physics* (John Wiley, New York, 1998).
[4] K. Huang, *Statistical mechanics* (John Wiley, New York, 1963).
[5] P. Garbaczewski and V. Stephanovich, Phys. Rev. E **84**, 011142 (2011).
[6] I. M. Sokolov, B. Dybiec, and W. Ebeling, Phys. Rev. E **83**, 041118 (2011).
[7] Ł. Kuśmierz, W. Ebeling, I. Sokolov, and E. Gudowska-Nowak, Acta Phys. Pol. B **44**, (2013).
[8] Ł. Kuśmierz, A. Chechkin, E. Gudowska-Nowak, and M. Bier, EPL (Europhys. Lett.) **114**, 60009 (2016).
[9] Ł. Kuśmierz, B. Dybiec, and E. Gudowska-Nowak, Entropy **20**, 658 (2018).
[10] S. Elliott, M. Ghandchi Tehrani, and R. Langley, Phil. Trans. R. Soc. A. **373**, 20140402 (2015).
[11] Y. L. Klimontovich, *Statistical physics of open systems* (Kluwer Academic Publishers, Holland, 1994).
[12] J. Dunkel, W. Ebeling, and S. A. Trigger, Phys. Rev. E **70**, 046406 (2004).
[13] A. Fiasconaro, E. Gudowska-Nowak, and W. Ebeling, J. Stat. Mech. Theor. Exp. P01029 (2009).
[14] C. W. Gardiner, *Handbook of stochastic methods for physics, chemistry and natural sciences* (Springer Verlag, Berlin, 2009).
[15] A. Janicki and A. Weron, Stat. Sci. **9**, 109 (1994).
[16] A. Janicki and A. Weron, *Simulation and chaotic behavior of α-stable stochastic processes* (Marcel Dekker, New York, 1994).
[17] G. Samorodnitsky and M. S. Taqqu, *Stable non-Gaussian random processes: Stochastic models with infinite variance* (Chapman and Hall, New York, 1994).
[18] A. A. Dubkov, B. Spagnolo, and V. V. Uchaikin, Int. J. Bifurcation Chaos. Appl. Sci. Eng. **18**, 2649 (2008).

[19] I. Podlubny, *Fractional differential equations* (Academic Press, San Diego, 1999).
[20] A. V. Chechkin and V. Y. Gonchar, J. Exp. Theor. Phys. **91**, 635 (2000).
[21] E. Lutz, Phys. Rev. Lett. **86**, 2208 (2001).
[22] V. V. Yanovsky, A. V. Chechkin, D. Schertzer, and A. V. Tur, Physica A **282**, 13 (2000).
[23] D. Schertzer *et al.*, J. Math. Phys. **42**, 200 (2001).
[24] S. G. Samko, A. A. Kilbas, and O. I. Marichev, *Fractional integrals and derivatives. Theory and applications.* (Gordon and Breach Science Publishers, Yverdon, 1993).
[25] S. Jespersen, R. Metzler, and H. C. Fogedby, Phys. Rev. E **59**, 2736 (1999).
[26] Ł. Kuśmierz, J. M. Rubi, and E. Gudowska-Nowak, J. Stat. Mech. **2014**, P09002 (2014).
[27] R. Metzler and J. Klafter, Phys. Rep. **339**, 1 (2000).
[28] E. Barkai, Phys. Rev. E **63**, 046118 (2001).
[29] V. V. Anh and R. McVinish, J. Appl. Math. Stoch. Anal. **16**, 97 (2003).
[30] D. Brockmann and I. M. Sokolov, Chem. Phys. **284**, 409 (2002).
[31] A. V. Chechkin, V. Y. Gonchar, J. Klafter, and R. Metzler, in *Fractals, Diffusion, and Relaxation in Disordered Complex Systems: Advances in Chemical Physics, Part B*, edited by W. T. Coffey and Y. P. Kalmykov (John Wiley & Sons, New York, 2006), Vol. 133, pp. 439–496.
[32] *On growth and form: Fractal and non-fractal patterns in physics*, edited by H. E. Stanley and N. Ostrowsky (Springer Verlag, Berlin, 1986).
[33] R. N. Mantegna and H. E. Stanley, *An introduction to econophysics. Correlations and complexity in finance* (Cambridge University Press, Cambridge, 2000).
[34] M. E. J. Newman and G. T. Barkema, *Monte Carlo methods in statistical physics* (Clarendon Press, Oxford, 1999).
[35] P. D. Ditlevsen, Phys. Rev. E **60**, 172 (1999).
[36] J. P. Bouchaud and A. Georges, Phys. Rep. **195**, 127 (1990).
[37] T. H. Solomon, E. R. Weeks, and H. L. Swinney, Physica D **76**, 70 (1994).
[38] J. P. Bouchaud, A. Ott, D. Langevin, and W. Urbach, J. Phys. II France **1**, 1465 (1991).
[39] P. Barthelemy, J. Bertolotti, and D. Wiersma, Nature (London) **453**, 495 (2008).
[40] M. Mercadier, W. Guerin, M. M. Chevrollier, and R. Kaiser, Nat. Phys. **5**, 602 (2009).
[41] D. Brockmann, L. Hufnagel, and T. Geisel, Nature (London) **439**, 462 (2006).
[42] D. W. Sims *et al.*, Nature (London) **451**, 1098 (2008).
[43] F. Bardou, J. P. Bouchaud, A. Aspect, and C. Cohen-Tannoudji, *Lévy statistics and laser cooling* (Cambridge University Press, Cambridge, 2002).
[44] E. Barkai, E. Aghion, and D. A. Kessler, Phys. Rev. X **4**, 021036 (2014).
[45] T. A. Amor *et al.*, Sci. Rep. **6**, 20815 (2016).
[46] M. F. Shlesinger and J. Klafter, in *On growth and form: Fractal and non-fractal patterns in physics*, edited by H. E. Stanley and N. Ostrowsky (Springer Verlag, Berlin, 1986), p. 279. See Ref.[32].
[47] A. M. Reynolds and C. J. Rhodes, Ecology **90**, 877 (2009).
[48] A. V. Chechkin *et al.*, Chem. Phys. **284**, 233 (2002).
[49] A. V. Chechkin *et al.*, Phys. Rev. E **67**, 010102(R) (2003).
[50] B. Dybiec, E. Gudowska-Nowak, and I. M. Sokolov, Phys. Rev. E **76**, 041122 (2007).
[51] W. Feller, *An introduction to probability theory and its applications* (John Wiley, New York, 1968).
[52] A. V. Chechkin *et al.*, J. Stat. Phys. **115**, 1505 (2004).
[53] A. V. Chechkin, R. Metzler, J. Klafter, and V. Y. Gonchar, in *Anomalous transport: Foundations and applications*, edited by R. Klages, G. Radons, and I. M. Sokolov (Wiley-VCH, Weinheim, 2008), pp. 129–162.
[54] A. A. Dubkov and B. Spagnolo, Acta Phys. Pol. B **38**, 1745 (2007).
[55] K. Capała and B. Dybiec, J. Stat. Mech. 033206 (2019).
[56] S. Zozor and C. Vignat, Phys. Rev. E **84**, 031115 (2011).
[57] M. Teuerle, P. Żebrowski, and M. Magdziarz, J. Phys. A: Math. Gen. **45**, 385002 (2012).
[58] A. Wyłomańska, A. Chechkin, J. Gajda, and I. M. Sokolov, Physica A **421**, 412 (2015).
[59] A. Dechant, S. T. Shafier, D. A. Kessler, and E. Barkai, Phys. Rev. E **94**, 022151 (2016).
[60] K. Capała and B. Dybiec, Chaos **29**, 093113 (2019).
[61] B. Dybiec, A. V. Chechkin, and I. M. Sokolov, J. Stat. Mech. P07008 (2010).
[62] J. T. Oden and E. Pires, J. Appl. Mech. **50**, 67 (1983).
[63] E. Pollak and A. M. Berezhkovskii, J. Chem. Phys. **99**, 1344 (1993).
[64] M. Urbakh, J. Klafter, D. Gourdon, and J. Israelachvili, Nature **430**, 525 (2004).
[65] P. Romanczuk *et al.*, Eur. Phys. J. ST **202**, 1 (2012).
[66] B. Lindner, New J. Phys. **9**, 136 (2007).
[67] B. Lindner, New J. Phys. **12**, 063026 (2010).
[68] F.-J. Elmer, J. Phys. A: Math.Gen. **30**, 6057 (1997).
[69] B. Dybiec, K. Capała, A. V. Chechkin, and R. Metzler, J. Phys. A: Mat. Theor. **52**, 015001 (2019).
[70] P. Romanczuk and L. Schimansky-Geier, Phys. Rev. Lett **106**, 230601 (2011).
[71] J. Nötel, I. M. Sokolov, and L. Schimansky-Geier, J. Phys. A: Math. Theor. **50**, 034003 (2016).

Inertial Lévy flights in bounded domains

Karol Capała[a] and Bartłomiej Dybiec[b]
Institute of Theoretical Physics, and Mark Kac Center for Complex Systems Research, Jagiellonian University, ul. St. Łojasiewicza 11, 30–348 Kraków, Poland

(Dated: 14 March 2022)

The escape from a given domain is one of the fundamental problems in statistical physics and the theory of stochastic processes. Here, we explore properties of the escape of an inertial particle driven by Lévy noise from a bounded domain, restricted by two absorbing boundaries. Presence of two absorbing boundaries assures that the escape process can be characterized by the finite mean first passage time. The detailed analysis of escape kinetics shows that properties of the mean first passage time for the integrated Ornstein–Uhlenbeck process driven by Lévy noise are closely related to properties of the integrated Lévy motions which, in turn, are close to properties of the integrated Wiener process. The extensive studies of the mean first passage time were complemented by examination of the escape velocity and energy along with their sensitivity to initial conditions.

PACS numbers: 05.40.Fb, 05.10.Gg, 02.50.-r, 02.50.Ey,

Widely studied, first escape and first arrival processes form the basis of multiple physical phenomena with practical applications. Extensive exploration of the first escape of an inertial particle from bounded domains under the action of symmetric Lévy noises reveals universality, as measured by the mean first passage time, of escape kinetics in equilibrium and non-equilibrium domains. These similarities are due to the continuity of the integrated processes, which partially reduce the significance of the discontinuity of velocity in underdamped systems driven by Lévy noises. However, the study of other escape characteristics like velocity or energy at the moment of first escape shows their high sensitivity to the stability index α as well as a dependence on initial conditions. These studies demonstrate potentially counterintuitive properties of escape kinetics as, for instance, the slowest escape does not need to correspond to the lowest median of the escape energy.

I. INTRODUCTION

Stochastic methods[1,2] are widely used in the description of various systems which are too complicated to treat them exactly, or their dynamics contain an intrinsic random component. The Newton equation plays a fundamental role in classical mechanics. It describes the fully deterministic dynamics, nevertheless it can be easily extended to account for random perturbations. The Newton equation supplemented by the random component is referred to as the Langevin equation[3]. Typically, it is assumed that the noise is white and Gaussian, but multiple non-white or non-Gaussian extensions have been suggested[4,5].

The Langevin equation[3] is studied in two main regimes: the overdamped regime and in the regime of full (underdamped) dynamics. In the overdamped domain, a random walker is fully characterized by its position only, while in the underdamped regime by position and velocity. Therefore, overdamped situations are simpler to analyze than the full dynamics. Nevertheless, already the overdamped Langevin equation can be used to describe and explain various noise-induced effects, like noise-enhanced stability[6–8], resonant activation[9,10] and stochastic resetting[11–13]. These phenomena do not exhaust all noise induced effects[14–16], but they are the most relevant in the context of current research, where we focus on the problems of first escape from bounded domains[17].

In the overdamped regime, under the action of the Gaussian white noise, one can study the free motion, which corresponds to the Wiener process[2], or motion in a force field, e.g., Ornstein–Uhlenbeck process[1]. Escape properties of such random motions in bounded and half-bounded domains are well known and widely studied[18] also in non-equilibrium realms[19]. Contrary to the overdamped motion, on the one hand, the regime of full dynamics is more intuitive, as it incorporates velocity and position. Consequently, some of the everyday intuitions can be easily transferred to provide a qualitative understanding of stochastic dynamics. On the other hand, such processes are more complex to analyze and simulate. Regime of underdamped (full) dynamics can be also referred to as the integrated process[20] or randomly accelerated process[21,22] since typically it is assumed that the noise affects the velocity evolution only while the position is the integral of the velocity. Moreover, in the full regime it is possible to study undamped[21,23–27] and damped motions[28–30]. Randomly accelerated motion of a free particle corresponds to the integrated Wiener process, while the damped motion to the integrated Ornstein–Uhlenbeck process. Action of the additional deterministic force results in the forced motions[31–33].

Escape processes from bounded (interval), and semi-bounded (half-line) domains are very different. In the regime of Markovian diffusion, the escape from a finite interval is characterized by the finite mean first passage time and an exponential distribution of first passage times[34]. At the same time, the escape from a half-line cannot be characterized by the mean first passage time as it diverges. The first pas-

[a]Electronic mail: karol@th.if.uj.edu.pl
[b]Electronic mail: bartek@th.if.uj.edu.pl

sage time density is given by the Lévy–Smirnoff (inverse-Gaussian) distribution[35–39] and it has power-law asymptotics with the exponent $-3/2$. The asymptotics of the first passage time density is universal as the same tail asymptotics is recorded for any symmetric Markovian drivings[37,40–42]. The similar generality is observed for the integrated Ornstein–Uhlenbeck process driven by weak Lévy noise[28]. In the overdamped regime, exit conditions are imposed on the position, as it is only one possibility. In the underdamped regime there are more options, since stopping conditions can be imposed on the position[26,43,44] or on the velocity[27–29].

Here, we study the properties of full (underdamped) dynamics in bounded domains restricted by two absorbing boundaries with the absorption condition imposed on the position. We relax the assumption regarding the noise type, therefore the driving noise can be of the more general α-stable type, containing the white Gaussian noise as a special case[36,45,46]. Consequently, our studies extend the works on the integrated Ornstein–Uhlenbeck process driven by Lévy noise[28] to domains restricted by two absorbing boundaries. Our studies rely on numerical methods, because, to the best of our knowledge, the analytical solution for the MFPT for the integrated Ornstein–Uhlenbeck process driven by the Lévy noise is unknown. Contrary to the underdamped case, in the regime of the overdamepd dynamics analytical results are known not only for symmetric drivings[47] but also for the escape under action of asymmetric Lévy flights[48,49]. The model under study is presented in the next section (Sec. II – Model). Results of computer simulations are provided in Sec. III (Results). The paper is closed with Summary and Conclusions (Sec. IV). Technical information is moved to the Appendices.

II. MODEL

We study the archetypal, underdamped Lévy noise-driven escape of a free particle from the finite interval $[-l,l]$. The Langevin equation[50,51] describing the motion of a single particle reads

$$m\ddot{x}(t) = -\gamma\dot{x}(t) + \sigma\zeta(t), \tag{1}$$

where x is the particle position ($x \in [-l,l]$). $\zeta(t)$ stands for the symmetric α-stable (Lévy type) noise, and σ measures the strength of fluctuations. The Lévy noise is the formal time derivative of the α-stable motion $L(t)$, see Ref. 52, with the characteristic function given by

$$\phi(k) = \langle \exp[ikL(t)] \rangle = \exp\left[-t|k|^{\alpha}\right]. \tag{2}$$

In the Eq (2), α ($0 < \alpha \leqslant 2$) stands for the stability index, which controls the tail asymptotics of α-stable densities[36,45]. For $\alpha < 2$, asymptotic behavior is of the power-law type, with the exponent $-(\alpha+1)$. The case of $\alpha = 2$ corresponds to the Gaussian white noise, i.e., $\langle \zeta(t)\zeta(s) \rangle_{\alpha=2} = \delta(t-s)$. Furthermore, using the transformation

$$\begin{cases} \tilde{x} &= x/l, \\ \tilde{t} &= \gamma t/m \end{cases}, \tag{3}$$

Eq. (1) can be transformed to the dimensionless variables $\tilde{x}$ and $\tilde{t}$. In such variables (after dropping tildes)

$$\ddot{x}(t) = -\dot{x}(t) + \sigma\zeta(t), \tag{4}$$

where the dimensionless fluctuation strength is expressed by dimensional variables as

$$\frac{\sigma m^{1/\alpha}}{l\gamma^{(1+\alpha)/\alpha}},$$

see Appendix A. Consequently, in addition to the stability index α, the only one parameter in Eq. (4) is the dimensionless strength of fluctuations σ. The case of $\gamma = 0$, see Eq. (1), should be treated separately. In the dimensionless units, for the undamped motion ($\gamma = 0$) one gets

$$\ddot{x}(t) = \zeta(t), \tag{5}$$

where

$$\begin{cases} \tilde{x} &= x/l, \\ \tilde{t} &= t/\left[\frac{ml}{\sigma}\right]^{\frac{\alpha}{1+\alpha}} \end{cases}. \tag{6}$$

Consequently, there are no free parameters in the undamped system, see Appendix A.

In dimensionless units, the escape from the $(-l,l)$ interval is transformed into the problem of escape from the $(-1,1)$ interval. The problem of escape is studied in the regime of the full dynamics under the action of linear friction, therefore the particle is characterized by the position x and velocity $v = \dot{x}$. The central quantity of interest is the mean first passage time (MFPT) $\mathcal{T}(x_0,v_0)$

$$\begin{aligned} \mathcal{T}(x_0,v_0) &= \langle t_{\mathrm{fp}}(x_0,v_0) \rangle \\ &= \langle \min\{t>0 : x(0)=x_0 \wedge v(0)=v_0 \wedge |x(t)| \geqslant 1\} \rangle. \end{aligned} \tag{7}$$

The mean first passage time $\mathcal{T}(x_0,v_0)$ is the average of first passage times $t_{\mathrm{fp}}(x_0,v_0)$. The first passage time $t_{\mathrm{fp}}(x_0,v_0)$ is recorded when a particle leaves the domain of motion, i.e., the $(-1,1)$ interval, for the first time. Since the motion is underdamped, the first passage time depends on the full initial condition (x_0,v_0). In the dimensionless units, the motion starts in the $(-1,1)$ interval, i.e., $x_0 \in (-1,1)$, while the velocity can attains any value, i.e., $v(0) \in \mathbb{R}$. The studied model extends examination of the exit time properties of the inertial equilibrium process driven by Gaussian white noise[24,25,53] to the non-equilibrium domain, i.e., to the situation where the driving noise is of the out-of-equilibrium type.

Eq. (4) can be rewritten as a set of two first-order equations

$$\begin{cases} \dot{v}(t) &= -v(t) + \sigma\zeta(t) \\ \dot{x}(t) &= v(t) \end{cases}. \tag{8}$$

The first line of Eq. (8) describes the evolution of the velocity. The velocity equation is the analogue of the overdamped Langevin equation describing the noise-driven motion in the parabolic ($V(x) = x^2/2$) potential[54–56]. Using this analogy, the velocity can attain the stationary distribution given by the α-stable density with the same stability index α[54–56] as the noise $\zeta(t)$. The characteristic function of stationary velocity distribution reads

$$\phi_v(k) = \exp\left[-\frac{\sigma^\alpha}{\alpha}|k|^\alpha\right], \tag{9}$$

which is the characteristic function of the symmetric α-stable distribution, see Eq. (2), with the scale parameter σ'

$$\sigma' = \sigma\alpha^{-1/\alpha}. \tag{10}$$

The asymptotic behavior of $p(v)$ is given by

$$p(v) \sim \sigma^\alpha \frac{\Gamma(\alpha+1)}{\pi} \sin\frac{\pi\alpha}{2} \times \frac{1}{|v|^{\alpha+1}}. \tag{11}$$

The exact shape of the velocity distribution is sensitive to the initial velocity, furthermore it can be affected by the absorption at $x = \pm 1$. The initial velocity shifts the modal value to nonzero locations, while the absorption can efficiently inhibit the achievement of a stationary velocity distribution, making it narrower. Nevertheless, the velocity distribution is of the α-stable type with the same value of the stability index α as the driving noise, because the instantaneous velocity is a linear transformation of α-stable variables. Moreover, the scale parameter characterizing the instantaneous velocity distribution cannot be larger than the scale parameter characterizing the stationary velocity distribution, i.e., $\sigma\alpha^{-1/\alpha}$.

The first line of Eq. (8) shows that v is the the α-stable analog of the Ornstein–Uhlenbeck process[57], i.e., the so-called Lévy-driven Ornstein–Uhlenbeck process[58,59]. Moreover, due to the condition $x(t) = \int^t v(s)ds$, the $x(t)$ is the so-called integrated process, i.e., the integrated Lévy-driven Ornstein–Uhlenbeck process[28]. In the case of $\gamma = 0$, see Eq. (1), $v(t)$ is given by the α-stable process, while $x(t)$ is the integrated α-stable motion. The special case of $\alpha = 2$ corresponds to: the integrated Ornstein–Uhlenbeck process ($\gamma > 0$) or the integrated Wiener process ($\gamma = 0$). Analogously, $\alpha = 1$ gives rise to the integrated Cauchy process ($\gamma = 0$) or the integrated Ornstein–Uhlenbeck–Cauchy process ($\gamma > 0$). The stopping condition, see Eq. (8), is imposed on the particle position. The system described by Eq. (4), is studied as long as $|x| < 1$.

III. RESULTS

The model described by Eq. (4) is studied by means of computer simulations. The velocity part, containing the α-stable noise, is approximated using the Euler-Maruyama scheme[45,60], while the spatial part is constructed trajectory-wise[51]. The MFPTs $\mathcal{T}(x_0, v_0)$ are calculated as the average value of the collected first passage times $t_{\mathrm{fp}}(x_0, v_0)$. Each first passage time $t_{\mathrm{fp}}(x_0, v_0)$ is estimated from a single trajectory $x(t)$ ($x(0) = x_0$ and $v(0) = v_0$), which is simulated as long as $|x(t)| < 1$. The averaging is performed over the ensemble of $N = 10^6$ first passage times obtained from N trajectories constructed with the integration time step $\Delta t = 10^{-3}$.

The main quantity characterizing the escape kinetics is the mean first passage, see Eq. (8). The mean first passage time depends on both the value of the stability index α and the strength of fluctuations σ. Since the motion is restricted to the $(-1, 1)$ interval, the initial position x_0 belongs to $(-1, 1)$. There are no constraints on the initial velocity v_0. It can be directed towards any of the absorbing boundaries.

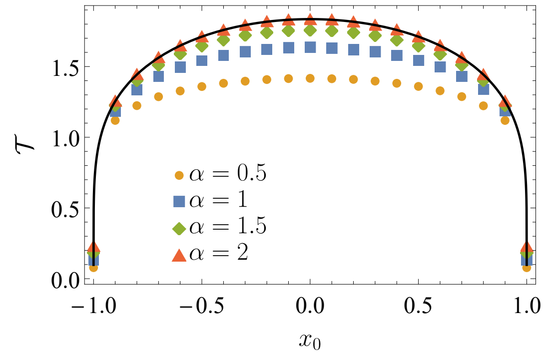

FIG. 1. The mean first passage time (MFPT) $\mathcal{T}(x_0, 0)$ for integrated α-stable motions. Various points correspond to various values of the stability index α ($\alpha \in \{0.5, 1, 1.5, 2\}$) from the lowest to highest MFPT respectively. Solid lines show the theoretical formula for $\alpha = 2$ (integrated Wiener process), see Eq. (13).

We start our analysis with the undamped motion, i.e., with the integrated α-stable motion (Sec. III A), which for $\alpha = 2$ corresponds to the integrated Wiener process. Next, we switch to the problem of inertial damped motion, i.e., the integrated Ornstein–Uhlenbeck process driven by Lévy noise (Sec. III B).

A. Integrated α-stable motion

The integrated α-stable motion corresponds to $\gamma = 0$ in Eq. (1). In dimensionless units, see Appendix A, it is described by the following Langevin equation

$$\ddot{x}(t) = \zeta(t). \tag{12}$$

Eq. (12) with $\alpha = 2$ describes the integrated Wiener process. More precisely, $\zeta_{\alpha=2}(t) = \sqrt{2}\xi(t)$ (where $\xi(t)$ stands for the standard Gaussian white noise) as the α-stable density with $\alpha = 2$ is the normal distribution with the standard deviation $\sqrt{2}$. Such a process has been studied in Refs. 24 and 25, where the exact, up to quadrature, formula for the MFPT with any allowed value of x_0 and v_0 has been derived. The general formula[24,25] significantly simplifies for $v_0 = 0$, see Eq. (B3). After transformation of the $[0, l]$ setup[24,25] to the $[-l, l]$ and passing to dimensionless variables, see Appendix A, the formula for the MFPT with $v_0 = 0$ reads

$$\mathcal{T}(x,0) = \frac{2}{3^{1/6}\Gamma(7/3)} \left[\frac{1+x}{2}\right]^{1/6} \left[\frac{1-x}{2}\right]^{1/6} \times \left\{ {}_2F\left(1, -\frac{1}{3}; \frac{7}{6}; \frac{1+x}{2}\right) + {}_2F\left(1, -\frac{1}{3}; \frac{7}{6}; \frac{1-x}{2}\right) \right\}, \tag{13}$$

where ${}_2F(a, b; c; x)$ is the Gauss hypergeometric function[61]. For more details see Appendix B.

Fig. 1 shows dependence of the mean first passage time on x_0 for various values of the stability index α ($\alpha \in \{0,5,1,1.5,2\}$ – from bottom to the top) with the fixed initial velocity v_0, i..e, $v_0 = 0$. The solid line depicts the MFPT for $\alpha = 2$ given by Eq. (13). With the decreasing value of the stability index α (in dimensionless variables) the MFPT decreases, i.e., the escape on average becomes faster. Nevertheless, the qualitative dependence of the MFPT on x_0 with various values of α is similar. In dimensional units, the order of MFPT curves is sensitive to the system parameters.

B. Integrated Ornstein–Uhlenbeck Lévy-driven process

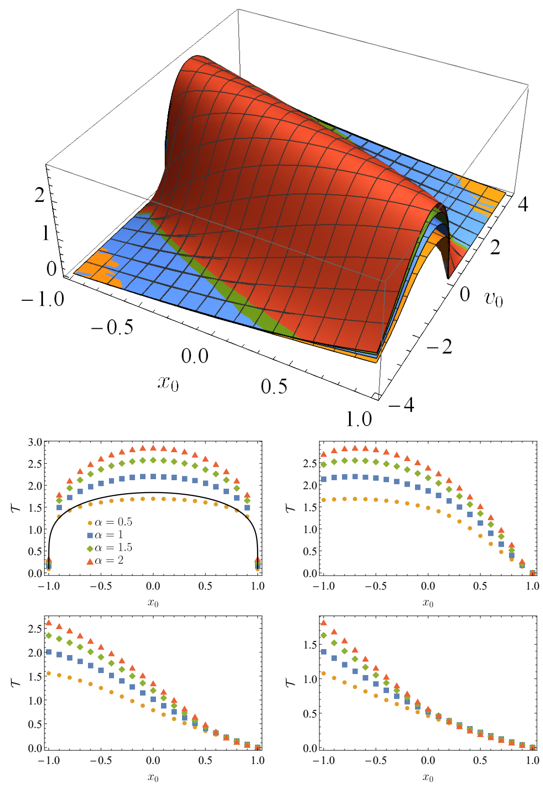

FIG. 2. The MFPT $\mathcal{T}(x_0, v_0)$ as a function of the initial condition (x_0, v_0) for various values of the stability index α ($\alpha \in \{0.5, 1, 1.5, 2\}$) from the lowest to highest MFPT respectively. Bottom part shows cross-sections for $v_0 = 0$ (top left), $v_0 = 1$ (top right), $v_0 = 2$ (bottom left) and $v_0 = 3$ (bottom right). The scale parameter σ is set to $\sigma = 1$.

Fig. 2 depicts the MFPT for the damped motion described by Eq. (4) as the function of the initial condition (x_0, v_0) for representative values of the stability index α ($\alpha \in \{0.5, 1, 1.5, 2\}$ from bottom to top). Moreover, the bottom panel of Fig. 2 shows cross-sections corresponding to various initial velocities: $v_0 = 0$ (top left), $v_0 = 1$ (top right), $v_0 = 2$ (bottom left) and $v_0 = 3$ (bottom right). Additionally the cross-section for $v_0 = 0$ is accompanied by the exact curve showing MFPT for the integrated Wiener process, see Eq. (13). Analogously, like for the integrated α-stable motion, the MFPT surfaces are symmetric with respect to exchange (x_0, v_0) with $(-x_0, -v_0)$, i.e.,

$$\mathcal{T}(x_0, v_0) = \mathcal{T}(-x_0, -v_0). \tag{14}$$

The relation given by Eq. (14) arises due to symmetry of the experimental setup and system dynamics. From Fig. 2, especially from cross-sections, it is clearly visible that the MFPT is sensitive to the exact value of the stability index α. For $\sigma = 1$, decrease in the value of the stability index α facilitates the escape kinetics. For $v_0 = 0$ MFPT curves are symmetric along $x_0 = 0$, moreover quantitative dependence of MFPT on x_0 with $v_0 = 0$ is the same as for the integrated Wiener process with $v_0 = 0$. The initial (positive) velocity significantly accelerates the escape process for positive x_0 and slows down escapes with negative x_0.

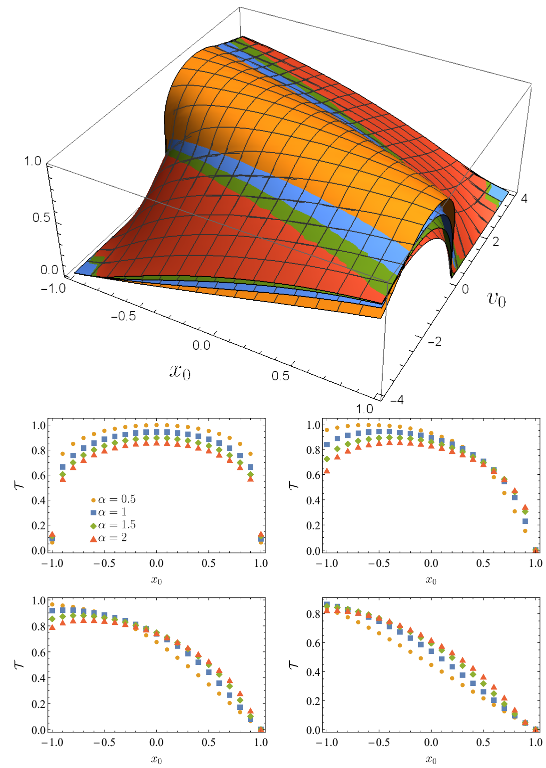

FIG. 3. The same as in Fig. 2 for $\sigma = 4$.

Fig. 3 presents dependence of the MFPT on the initial conditions for the noise strength $\sigma = 4$, which is significantly larger than the one considered in Fig. 2. The change in σ not only facilitates escape in comparison to $\sigma = 1$, but changes the order of surfaces in the 3D plot and curves in cross-sections. For $\sigma = 4$, with $v_0 = 0$, the fastest escape is recorded for Gaussian noise ($\alpha = 2$). Moreover, contrary to smaller σ (e.g., $\sigma = 1$), this time MFPT is decreasing function of α. Subsequent Fig. 4 demonstrates that for the fixed value of the stability index α, alterations in the scale parameter can produce well visible changes in the mean first passage time, especially for not too large initial velocities.

The subsequent Fig. 4 explores the sensitivity of the mean first passage time to the strength of fluctuations under the action of the Cauchy noise (α-stable noise with $\alpha = 1$). Due to the property given by Eq. (14), Fig. 4 shows results for $v_0 > 0$ only. The highest sensitivity to the fluctuation strength is recorded, when a particle starts its motion far from the boundary which is crossed during the escape from the domain of motion, see Fig. 5. With the increasing $|v_0|$ the level of sensitivity decreases. Finally, for very large v_0 results with various scale parameters σ are indistinguishable.

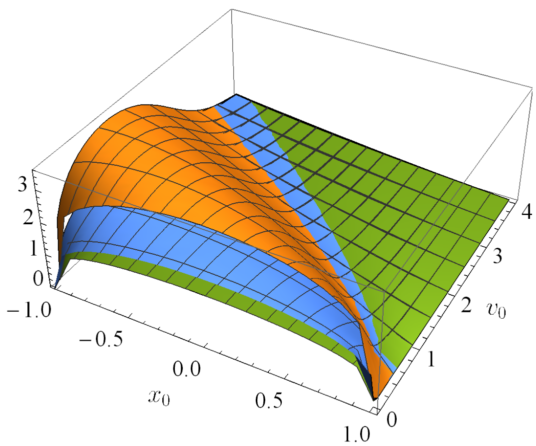

FIG. 4. The MFPT as a function of the initial condition (x_0, v_0) for the fixed value of the stability index $\alpha = 1$ (Cauchy noise) and various strengths of fluctuations σ ($\sigma \in \{0.5, 1, 2\}$ (orange, blue, green).

The particle escaping from the $(-1, 1)$ interval can exit via the left or right boundary. The tendency to exit via a particular boundary can be quantified by the splitting probability π_R. For instance, π_R measures the fraction of escapes via the right boundary. At the same time, the fraction of escapes via the left boundary can be calculated as $\pi_L = 1 - \pi_R$. The dependence of the splitting probability π_R on the initial condition (x_0, v_0) is depicted in Fig. 5. The top panel shows the results for the Cauchy ($\alpha = 1$) noise, while the bottom one for the Gaussian ($\alpha = 2$) noise. Positive initial velocity favors escape via the right boundary. This tendency is especially visible for the initial positions near the right boundary. The change in the value of the stability index α from $\alpha = 1$ (top panel) to $\alpha = 2$ (bottom panel) does not change the qualitative dependence of the splitting probability on the initial condition. Only small quantitative changes are visible in the situation when a motion starts near the boundary with the initial velocity pointing to the more distant boundary.

The stopping condition is imposed on the particle position $x(t)$, see Eq. (8), which is continuous as the integral of the velocity. Due to the continuity of trajectories, every trajectory hits the absorbing boundary. Therefore, the last hitting point

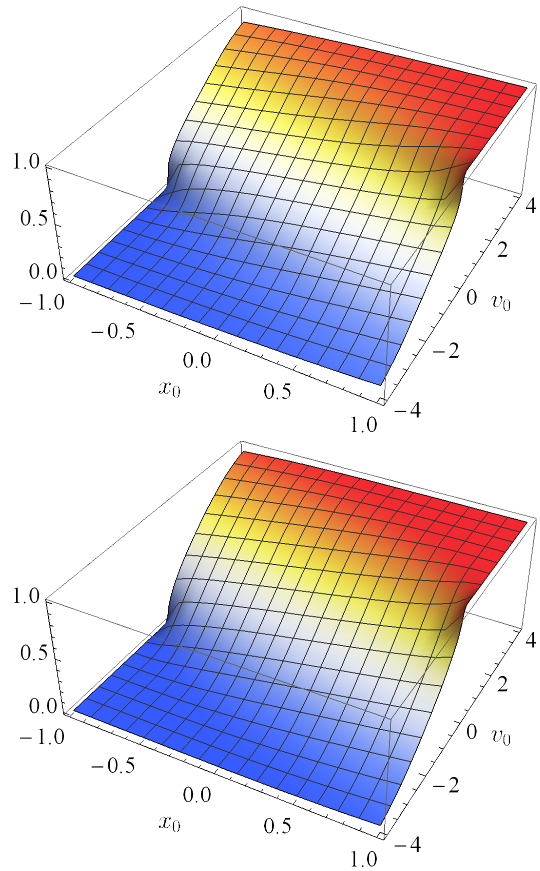

FIG. 5. The probability π_R that the particle escapes from the finite interval $(-1, 1)$ through the right boundary, i.e., $x = 1$, as a function of the initial condition (x_0, v_0) for the fixed value of the stability index $\alpha = 1$ (Cauchy noise – top panel) and $\alpha = 2$ (Gaussian noise – bottom panel). The scale parameter σ is set to $\sigma = 1$.

density is given by $\pi_R \delta(x - 1) + (1 - \pi_R)\delta(1 - x)$, where π_R is the probability to escape through the right boundary. Nevertheless, the escape is not only characterized by the splitting probability, see Fig. 5, but also by the exit velocity, i.e., the instantaneous velocity at the moment of the first escape. The distribution of the exit velocities is determined by the instantaneous velocity distribution, which is given by the symmetric α-stable density, and the initial condition (x_0, v_0). The initial condition is capable of introducing asymmetry to the exit velocity distribution. For $x_0 = 0$ with $v_0 = 0$, the distribution of exit velocities is symmetric.

Fig. 6 presents the median ($v_{0.5}$) of exit velocities as a function of the initial condition (x_0, v_0). Various surfaces in the top panel of Fig. 6 correspond to various values of the stability index α ($\alpha \in \{0.5, 1, 1.5, 2\}$). α-stable distributions with such values of stability indices are very different. Nevertheless, the medians of the exit velocities are quite similar, which is further corroborated by cross-sections depicted in the bottom panel of Fig. 6. Unexpectedly, for some values of the initial velocity, e.g., $v_0 = 1$, there is a local minimum of the median ($v_{0.5}$) of the exit velocity, see bottom row of Fig. 6. As it is visible from the splitting probability, see Fig. 5, cross sections in Fig. 6 correspond to the situations when the first escape takes place via both absorbing boundaries. The level of competition is sensitive both to the initial position and the initial velocity as they determine which part of the velocity distribution is responsible for the final jump. If a particle is close to the boundary it can (most likely) leave the domain of motion with a small velocity through the closest boundary or it can escape via the distant boundary with a large velocity with the opposite sign. The chances of escaping via the more distant boundary are decreasing with the increasing α making local minima of $v_{0.5}$ shallower and shifted to larger x_0, see bottom left panel of Fig. 6.

In order to further explore properties of exit velocity, we have calculated the ratio of interquantile widths

$$\mathcal{R} = \frac{v_{0.5} - v_{0.1}}{v_{0.9} - v_{0.5}}, \tag{15}$$

where $v_{\dots}$ indicates quantiles of a given order q ($0 < q < 1$) of the exit velocity, e.g., $v_q(t)$ is defined by

$$q = \int_{-\infty}^{v_q(t)} p(v;t)dv. \tag{16}$$

In the above equation, $p(v;t)$ stands for exit velocity distribution. The ratio defined by Eq. (15) measures the fraction of widths of intervals containing 40% of the exit velocities above ($v_{0.9} - v_{0.5}$) and below ($v_{0.5} - v_{0.1}$) the median ($v_{0.5}$). Its value reflects the symmetry of the exit velocity distribution: for $\mathcal{R} = 1$, the intervals' widths in the numerator and the denominator are the same. If $\mathcal{R} < 1$ the exit velocity density is skewed to the right, while for $\mathcal{R} > 1$ to the left. Fig. 7 depicts the interquantile width ratios, which show that the width ratio $\mathcal{R}$ is sensitive to the exact value of the stability index α. For $\alpha = 0.5$ the ratio of interquantile widths is practically equal to 1, as with decreasing α exit velocities become more symmetric. Finally, in the limit of $\alpha \to 0$, the ratio $\mathcal{R}$ is equal to 1, because the escape events become position independent. In the opposite limit of $\alpha \to 2$, the escape process strongly depends on the initial position, because it is easier to escape via the closest boundary. Fig. 6 and 7 present results for $v_0 > 0$ because results for $v_0 < 0$ can be obtained by symmetry. For instance, quantiles of order q ($0 < q < 1$) are connected with quantiles of order $1-q$ by the relation $v_q(x_0, v_0) = -v_{1-q}(-x_0, -v_0)$ from which implies that $\mathcal{R}(-x_0, -v_0) = 1/\mathcal{R}(x_0, v_0)$.

From analysis of Fig. 7, supported by the examination of the splitting probability (Fig. 5) and median of the exit velocity (Fig. 6), it can be deduced that there are two mechanisms which can produce $\mathcal{R} \approx 1$. One, the most intuitive, is related to the symmetry of the exit velocity. This mechanism is observed for $v_{0.5} = 0$, where the instantaneous velocity distribution is symmetric and approximately half of escapes are via the left (right) boundary with negative (positive) velocities. Such a behavior is the strongest for $x_0 \approx 0$ and $v_0 \approx 0$, and the decrease in α widens the domain where $\mathcal{R} \approx 1$. The other mechanism is related to the initial velocity. For large $|v_0|$ the mean first passage time is small and it is mainly determined by the initial velocity, which determines the time dependence of the median of the velocity distribution. The nonzero median of the velocity distribution forces the median of the position distribution to move towards one of the absorbing boundaries. This in turn facilitates the escape. Moreover, the escape time is so short that the width (as measured by the interquantile width) of the velocity distribution is small and median quite large that escapes are performed over one of the boundaries determined by the initial condition. In overall, the median of exit velocity is significant and, simultaneously, the exit velocities follow narrow, symmetric along the median, density making $\mathcal{R}$ again close to 1. In other regions, where escapes are performed via both absorbing boundaries, we can see the competition between escapes to the left and to the right.

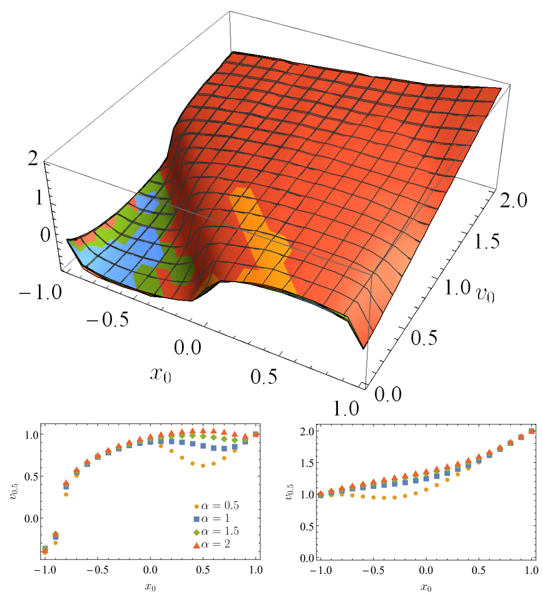

FIG. 6. Medians of the exit velocity $v_{0.5}$ as a function of the initial condition (x_0, v_0) for various values of the stability index α ($\alpha \in \{0.5, 1, 1.5, 2\}$ (orange, blue, green, red)) (top panel) and cross-sections for $v_0 = 1$ (bottom left) and $v_0 = 2$ (bottom right). The scale parameter σ is set to $\sigma = 1$.

Finally, to further study the properties of escape kinetics, we have inspected energies at the moment of boundary crossing. Fig. 8 shows median of the energy distributions along with sample cross-sections. One may think that the slowest escapes (largest MFPTs) correspond to the lowest median of the escape energy. However, it is not the case. For the initial conditions (x_0, v_0) corresponding to longest escape time, there is a local maximum (hump) in the median of the escape energy. Such a maximum originates due to slow escapes. More precisely, a particle spends a lot of time within the interval. During that time a chance for an abrupt change in the velocity increases and the particle is likely to leave the domain of motion with a large velocity (and energy). Height of the hump

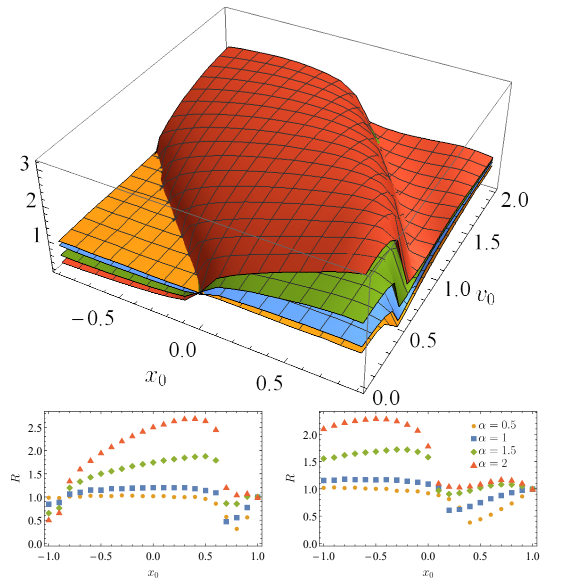

FIG. 7. Interquantile widths ratios $\mathcal{R} = (v_{0.5} - v_{0.1})/(v_{0.9} - v_{0.5})$ for $\alpha \in \{0.5, 1, 1.5, 2\}$ (top panel) and cross-sections for $v_0 = 1$ (bottom left) and $v_0 = 2$ (bottom right). The scale parameter σ is set to $\sigma = 1$.

in the median of energy is very sensitive to the stability index α and decays rapidly with its decreasing value, therefore, in the top panel of the Fig. 8, maximum is well visible only for $\alpha = 0.5$. In general, for a fixed initial condition located within the hump, the median of the exit energy decays with the decreasing value of the stability index α. Consequently, the smallest α curve is the predominant one. After removing results corresponding to $\alpha = 0.5$ the hump with $\alpha = 1.0$ starts to prevail. Nevertheless, the qualitative dependence of the median of the exit energy is quite similar. The biggest qualitative differences start to appear when α approaches 2.

Interestingly, the well-defined hump in the median of energy distribution is placed within a gutter. The trough rises upwards with increasing modulus of the initial velocity. Therefore, starting from the top of the hump, with the increasing (decreasing) initial velocity median decreases, attains minimum value and finally it starts to increase. This indicates that the increase in the value of the initial velocity v_0 does not always lead to the larger escape energy. As it is clearly visible in Fig. 8, escapes with largest initial velocities, see Fig. 2, are performed with the largest energies. Moreover, the medians of the escape energy in this case are insensitive to the stability index α and, therefore, they are indistinguishable in the plot. It suggests that escapes energies for large v_0 are mainly controlled by the initial condition.

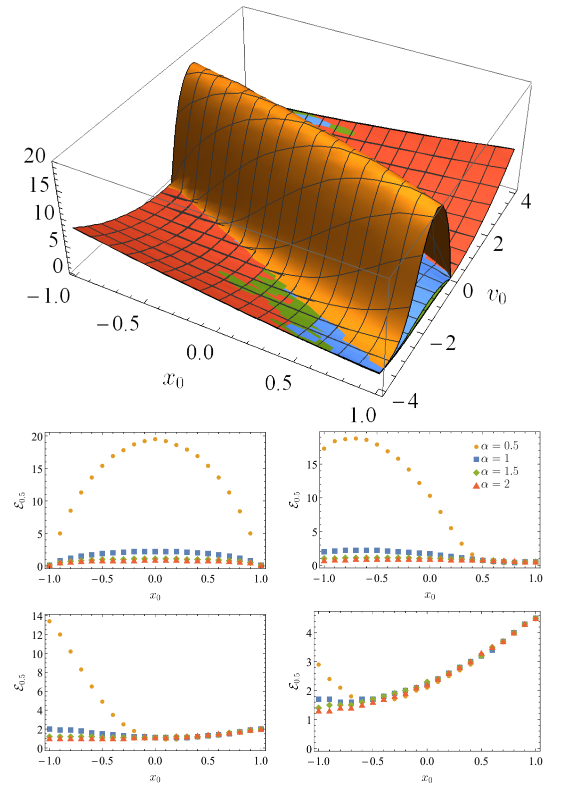

FIG. 8. Median of exit energy $\mathcal{E}_{0.5}$ as a function of the initial condition (x_0, v_0) for various values of the stability index α ($\alpha \in \{0.5, 1, 1.5, 2\}$ (orange, blue, green, red)). Bottom part shows cross-sections for $v_0 = 0$ (top left), $v_0 = 1$ (top right), $v_0 = 2$ (bottom left) and $v_0 = 3$ (bottom right). The scale parameter σ is set to $\sigma = 1$.

IV. SUMMARY AND CONCLUSIONS

In the weak noise limit of the integrated Ornstein–Uhlenbeck process driven by Lévy noise, the distribution of first passage times from the half-line attains the universal form[28], which is independent of the driving noise type. This is related to the general properties of escape kinetics from the half-line under symmetric Markovian drivings. Such escapes are characterized by first passage time densities with the universal power-law asymptotics predicted by the Sparre Andersen scaling[37,40–42]. Due to the heavy tail of the first passage time density, the first passage density has a power-law asymptotic with the exponent $-3/2$. The escape from the half-line cannot be characterized by the mean first passage time as this quantity diverges.

Using numerical methods, we have studied the properties of underdamped Lévy noise-driven escape from finite intervals restricted by two absorbing boundaries. For such a process, contrary to the escape from the half-line, the exit time distributions have exponential asymptotics making the mean first passage time well defined characteristics. Detailed examination of the integrated Lévy-driven Ornstein–Uhlenbeck process indicates that the mean first passage time displays limited sensitivity to the exact value of the stability index α. Therefore, despite very different velocity distributions, the qualitative system properties are very close to the properties of the integrated Wiener process. Nevertheless, the increase in the scale parameter (the only significant parameter besides α) can differentiate results corresponding to various values of the stability index α. The symmetry of the domain of motion and system dynamics is responsible for additional symmetries of the mean first passage times with respect to the initial conditions.

The extensive analysis of the mean first passage time was supplemented by examination of the escape velocities and energies along with their sensitivity to the initial conditions. On the one hand, for the Lévy-driven Ornstein–Uhlenbeck process, medians of the escape velocity are weakly sensitive to the stability index α. On the other hand, analysis of the asymmetry of the escape velocity distributions show a high level of sensitivity to the stability index. In particular, distributions change from almost always symmetric (small α) to possibly strongly dependent on the initial condition ($\alpha \lesssim 2$). Putting it differently, for large α, depending on the initial condition, the escape velocity distribution can be symmetric or not. For example, for the same initial position, the escape velocity distribution can be asymmetric (small initial velocity) and symmetric (large initial velocity). In contrast to velocities, the studies of escape energies manifest significant sensitivity of the medians to the value of the stability index α, especially for small initial velocities. Finally, the median of the escape energy can decrease with the increasing value of initial velocity.

Appendix A: Dimensionless units

The dimensional Langevin equation

$$m\ddot{x}(t) = -\gamma\dot{x}(t) + \sigma\zeta(t), \tag{A1}$$

can be transformed to dimensionless units $\tilde{x}$ and $\tilde{t}$ by rescaling the space variable x and time t

$$\begin{cases} \tilde{x} = \frac{x}{x_0} \\ \tilde{t} = \frac{x}{t_0} \end{cases}. \tag{A2}$$

The noise term is a formal time derivative of the α-stable motion, which is a $1/\alpha$ self-similar process. Therefore, it transforms as

$$\begin{aligned} \sigma\zeta(t) &= \sigma\frac{dL(t)}{dt} = \sigma\frac{d}{dt}L(t_0\tilde{t}) = \sigma\frac{d}{dt}t_0^{\frac{1}{\alpha}}L(\tilde{t}) \qquad \text{(A3)} \\ &= \sigma t_0^{\frac{1}{\alpha}}\frac{d}{dt}L(\tilde{t}) = \sigma t_0^{\frac{1}{\alpha}}\frac{d\tilde{t}}{dt}\frac{d}{d\tilde{t}}L(\tilde{t}) \\ &= \sigma t_0^{\frac{1}{\alpha}-1}\zeta(\tilde{t}). \end{aligned}$$

At the same time standard derivatives account the following forms

$$m\frac{d^2x(t)}{d^2t} = m\frac{x_0}{t_0^2}\frac{d^2\tilde{x}}{d\tilde{t}^2} \tag{A4}$$

and

$$\gamma\frac{dx(t)}{dt} = \gamma\frac{x_0}{t_0}\frac{d\tilde{x}}{d\tilde{t}}. \tag{A5}$$

After substituting in Eq. (A1) one gets

$$m\frac{x_0}{t_0^2}\frac{d^2\tilde{x}}{d\tilde{t}^2} = -\gamma\frac{x_0}{t_0}\frac{d\tilde{x}}{d\tilde{t}} + \sigma t_0^{\frac{1}{\alpha}-1}\zeta(\tilde{t}). \tag{A6}$$

Dividing both sides by $m\frac{x_0}{t_0^2}$ and dropping tildes result in

$$\frac{d^2x}{dt^2} = -\gamma\frac{t_0}{m}\frac{dx}{dt} + \frac{\sigma t_0^{1+\frac{1}{\alpha}}}{mx_0}\zeta(t). \tag{A7}$$

Since we are interested in the exploration of escape from $[-l, l]$ interval we set x_0 to l, thus $\tilde{x} = \frac{x}{l}$. Consequently, in the dimensionless units, we are studying escape from the $(-1, 1)$ interval. For $\gamma > 0$, setting $\gamma\frac{t_0}{m}$ to 1 one gets $t_0 = \frac{m}{\gamma}$ and

$$\tilde{t} = \frac{\gamma}{m}t. \tag{A8}$$

Moreover, for $\gamma > 0$ one finds the rescaled $\tilde{\sigma}$

$$\tilde{\sigma} = \frac{\sigma t_0^{1+\frac{1}{\alpha}}}{mx_0} = \frac{\sigma m^{\frac{1}{\alpha}}}{l\gamma^{1+\frac{1}{\alpha}}}. \tag{A9}$$

The case of $\gamma = 0$ needs to be considered separately. We still use $\tilde{x} = \frac{x}{l}$, while the time transformation is found from the condition

$$\frac{\sigma t_0^{1+\frac{1}{\alpha}}}{mx_0} = 1 \tag{A10}$$

resulting in

$$t_0 = \left[\frac{mx_0}{\sigma}\right]^{\frac{\alpha}{1+\alpha}} = \left[\frac{ml}{\sigma}\right]^{\frac{\alpha}{1+\alpha}}. \tag{A11}$$

In summary, in the dimensionless units, for $\gamma > 0$, one has

$$\ddot{x}(t) = -\dot{x}(t) + \sigma\zeta(t), \tag{A12}$$

while for $\gamma = 0$

$$\ddot{x}(t) = \zeta(t). \tag{A13}$$

For the sake of simplicity, in the above equations, the tildes have been dropped out. The motion is continued as long as $|x| < 1$. Therefore, the damped motion is characterized by the dimensionless σ only, while in the undamped case there are no free parameters.

The α-stable density with $\alpha = 2$ reduces to the normal (Gaussian) distribution with the standard deviation $\sqrt{2}$. Therefore, special care is required if one wants to compare results for α-stable driving with $\alpha = 2$ to results derived under action of the Gaussian white noise. The factor $\sqrt{2}$, see Eq. (A11), needs to be accounted for.

Appendix B: Integrated Brownian motion (random acceleration process)

In Refs. 24 and 25 the problem of escape of the integrated Wiener (random acceleration process[22]) process from $[0, l]$ has been studied. For

$$\ddot{x}(t) = \xi(t), \tag{B1}$$

with $\langle\xi(t)\xi(s)\rangle = D\delta(t-s)$ the closed (up to quadrature) formula for the MFPT has been derived. In the case of $v_0 = 0$ the general formula simplifies to

$$\mathcal{T}(x,0) = \frac{4^{1/6}}{3^{1/6}\Gamma(7/3)}\left[\frac{2l^2}{D}\right]^{1/3}\left[\frac{x}{l}\right]^{1/6}\left[1-\frac{x}{l}\right]^{1/6} \times \left\{{}_2F\left(1,-\frac{1}{3};\frac{7}{6};\frac{x}{l}\right)+{}_2F\left(1,-\frac{1}{3};\frac{7}{6};1-\frac{x}{l}\right)\right\}, \tag{B2}$$

where ${}_2F\,(a,b;c;x)$ is the Gauss hypergeometric function[61].

The formula (B2) can be transformed to the setup used in the main text by rescaling the interval width, i.e., $l \to 2l$, and exchanging $x \to l + x$ and $D \to 2\sigma^2$ (because α-stable density with $\alpha = 2$ is the normal distribution with the variance equal to 2) resulting in

$$\mathcal{T}(x,0) = \frac{4^{1/6}}{3^{1/6}\Gamma(7/3)}\left[\frac{4l^2}{\sigma^2}\right]^{1/3}\left[\frac{l+x}{2l}\right]^{1/6}\left[\frac{l-x}{2l}\right]^{1/6} \times \left\{{}_2F\left(1,-\frac{1}{3};\frac{7}{6};\frac{l+x}{2l}\right)+{}_2F\left(1,-\frac{1}{3};\frac{7}{6};\frac{l-x}{2l}\right)\right\}. \tag{B3}$$

Eq. (B3) gives the formula for the MFPT with $v_0 = 0$ in the dimensional units corresponding to the setup studied in the main text (escape from $[-l,l]$ under action of α-stable noise). Eq. (B3) can be transformed to dimensionless units by identifying x/l with dimensionless position and dividing the whole formula by t_0 given by Eq. (A11) with $m = 1$, i.e., $t_0 = (l/\sigma)^{2/3}$ since in[24,25] particle mass is set to unity, see Eq. (B1). All these operations are equivalent to setting $\sigma = 1$ and $l = 1$ in Eq. (B3). Such a substitution is consistent with the dimensionless Langevin equation, which for the integrated α-stable motion does not have any free parameters.

ACKNOWLEDGEMENTS

This research was supported in part by PLGrid Infrastructure and by the National Science Center (Poland) grant 2018/31/N/ST2/00598.

DATA AVAILABILITY

The data that support the findings of this study are available from the corresponding author (KC) upon reasonable request.

REFERENCES

[1] W. Horsthemke and R. Lefever, *Noise-inducted transitions. Theory and applications in physics, chemistry, and biology* (Springer Verlag, Berlin, 1984).
[2] C. W. Gardiner, *Handbook of stochastic methods for physics, chemistry and natural sciences* (Springer Verlag, Berlin, 2009).
[3] W. T. Coffey and Y. P. Kalmykov, *The Langevin equation: With applications to stochastic problems in Physics, Chemistry and Electrical Engineering* (World Scientific, Singapore, 2012).
[4] J. Klafter, A. Blumen, and M. F. Shlesinger, Phys. Rev. A **35**, 3081 (1987).
[5] J. Klafter, M. F. Shlesinger, and G. Zumofen, Phys. Today **49**, 33 (1996).
[6] N. V. Agudov and B. Spagnolo, Phys. Rev. E **64**, 035102 (2001).
[7] A. A. Dubkov, N. V. Agudov, and B. Spagnolo, Phys. Rev. E **69**, 061103 (2004).
[8] D. Valenti, L. Magazzù, P. Caldara, and B. Spagnolo, Phys. Rev. B **91**, 235412 (2015).
[9] M. H. Devoret, J. M. Martinis, D. Esteve, and J. Clarke, Phys. Rev. Lett. **53**, 1260 (1984).
[10] C. R. Doering and J. C. Gadoua, Phys. Rev. Lett. **69**, 2318 (1992).
[11] M. R. Evans and S. N. Majumdar, Phys Rev. Lett. **106**, 160601 (2011).
[12] M. R. Evans and S. N. Majumdar, J. Phys. A: Math. Theor. **44**, 435001 (2011).
[13] M. R. Evans, S. N. Majumdar, and G. Schehr, J. Phys. A: Math. Theor. **53**, 193001 (2020).
[14] R. D. Astumian and F. Moss, Chaos **8**, 533 (1998).
[15] P. Reimann, Phys. Rep. **361**, 57 (2002).
[16] L. Gammaitoni, P. Hänggi, P. Jung, and F. Marchesoni, Eur. Phys. J. B **69**, 1 (2009).
[17] O. Benichou, M. Coppey, M. Moreau, P. H. Suet, and R. Voituriez, EPL (Europhys. Lett.) **70**, 42 (2005).
[18] A. N. Borodin and P. Salminen, *Handbook of Brownian motion: facts and formulae* (Birkhäuser, Bassel, 2002).
[19] V. V. Palyulin, G. Blackburn, M. A. Lomholt, N. W. Watkins, R. Metzler, R. Klages, and A. V. Chechkin, New J. Phys. **21**, 103028 (2019).
[20] O. E. Barndorff-Nielsen and N. Shephard, Scand. J. Stat. **30**, 277 (2003).
[21] D. J. Bicout and T. W. Burkhardt, J. Phys. A: Math. Gen. **33**, 6835 (2000).
[22] T. W. Burkhardt, in *First-Passage Phenomena and Their Applications*, edited by R. Metzler, G. Oshanin, and S. Redner (World Scientific Publishing, 2014) pp. 21–44.
[23] M. Goldman, Ann. Math. Stat. **6**, 2150 (1971).
[24] J. Masoliver and J. M. Porrà, Phys. Rev. E **53**, 2243 (1996).
[25] J. Masoliver and J. M. Porrà, Phys. Rev. Lett. **75**, 189 (1995).
[26] M. Lefebvre, SIAM J. Appl. Math. **49**, 1514 (1989).
[27] C. H. Hesse, Int. J. Stoch. Anal. **2005**, 237 (2005).
[28] R. Hintze and I. Pavlyukevich, Bernoulli **20**, 265 (2014).
[29] C. Hesse, Stoch. Models **7**, 447 (1991).
[30] M. Magdziarz, Physica A **387**, 123 (2008).
[31] T. Srokowski, Phys. Rev. E **85**, 021118 (2012).
[32] Z.-W. Bai and M. Hu, Physica A **479**, 91 (2017).
[33] K. Capała and B. Dybiec, Phys. Rev. E **102**, 052123 (2020).
[34] B. Dybiec, E. Gudowska-Nowak, E. Barkai, and A. A. Dubkov, Phys. Rev. E **95**, 052102 (2017).
[35] S. Redner, *A guide to first passage time processes* (Cambridge University Press, Cambridge, 2001).
[36] G. Samorodnitsky and M. S. Taqqu, *Stable non-Gaussian random processes: Stochastic models with infinite variance* (Chapman and Hall, New York, 1994).
[37] A. V. Chechkin, R. Metzler, V. Y. Gonchar, J. Klafter, and L. V. Tanatarov, J. Phys. A: Math. Gen. **36**, L537 (2003).
[38] T. Koren, M. A. Lomholt, A. V. Chechkin, J. Klafter, and R. Metzler, Phys. Rev. Lett. **99**, 160602 (2007).
[39] T. Koren, A. V. Chechkin, and J. Klafter, Physica A **379**, 10 (2007).
[40] E. Sparre Andersen, Math. Scand. **2**, 195 (1954).
[41] E. Sparre Andersen, Math. Scand. **1**, 263 (1953).
[42] B. Dybiec, E. Gudowska-Nowak, and A. V. Chechkin, J. Phys. A: Math. Theor. **49**, 504001 (2016).
[43] M. Lefebvre, Stoch. Proc. Appl. **32**, 281 (1989).
[44] P. Duck, T. Marshall, and E. Watson, J. Phys. A: Math. Gen. **19**, 3545 (1986).
[45] A. Janicki, *Numerical and statistical approximation of stochastic differential equations with non-Gaussian measures* (Hugo Steinhaus Centre for Stochastic Methods, Wrocław, 1996).
[46] A. A. Dubkov, B. Spagnolo, and V. V. Uchaikin, Int. J. Bifurcation Chaos. Appl. Sci. Eng. **18**, 2649 (2008).
[47] R. K. Getoor, Trans. Am. Math. Soc. **101**, 75 (1961).
[48] A. Padash, A. V. Chechkin, B. Dybiec, I. Pavlyukevich, B. Shokri, and R. Metzler, J. Phys. A: Math. Theor. **52**, 454004 (2019).
[49] A. Padash, A. V. Chechkin, B. Dybiec, M. Magdziarz, B. Shokri, and R. Metzler, J. Phys. A: Math. Theor. **53**, 275002 (2020).
[50] G. E. Uhlenbeck and L. S. Ornstein, Phys. Rev. **36**, 823 (1930).

[51] H. Risken, in *The Fokker-Planck Equation: Methods of Solution and Applications* (Springer-Verlag, Berlin, 1996).
[52] A. Janicki and A. Weron, Stat. Sci. **9**, 109 (1994).
[53] J. M. Porrà, J. Masoliver, and K. Lindenberg, Phys. Rev. E **50**, 1985 (1994).
[54] A. V. Chechkin, J. Klafter, V. Y. Gonchar, R. Metzler, and L. V. Tanatarov, Chem. Phys. **284**, 233 (2002).
[55] A. V. Chechkin, J. Klafter, V. Y. Gonchar, R. Metzler, and L. V. Tanatarov, Phys. Rev. E **67**, 010102(R) (2003).
[56] B. Dybiec, E. Gudowska-Nowak, and I. M. Sokolov, Phys. Rev. E **76**, 041122 (2007).
[57] N. G. van Kampen, *Stochastic processes in physics and chemistry* (North–Holland, Amsterdam, 1981).
[58] P. Garbaczewski and R. Olkiewicz, J. Math. Phys. **41**, 6843 (2000).
[59] I. Eliazar and J. Klafter, J. Stat. Phys. **119**, 165 (2005).
[60] A. Janicki and A. Weron, *Simulation and chaotic behavior of α-stable stochastic processes* (Marcel Dekker, New York, 1994).
[61] M. Abramowitz and I. A. Stegun, *Handbook of mathematical functions with formulas, graphs, and mathematical tables*, Vol. 55 (Dover Publications, New York, 1964).

Peculiarities of escape kinetics in the presence of athermal noises

Karol Capała,[1, a)] Bartłomiej Dybiec,[1, b)] and Ewa Gudowska-Nowak[1, c)]
Marian Smoluchowski Institute of Physics, and Mark Kac Center for Complex Systems Research, Jagiellonian University, ul. St. Łojasiewicza 11, 30–348 Kraków, Poland

(Dated: 14 March 2022)

Stochastic evolution of various dynamic systems and reaction networks is commonly described in terms of noise assisted escape of an overdamped particle from a potential well, as devised by the paradigmatic Langevin equation in which additive Gaussian stochastic force reproduces effects of thermal fluctuations from the reservoir. When implemented for systems close to equilibrium, the approach correctly explains emergence of Boltzmann distribution for the ensemble of trajectories generated by Langevin equation and relates intensity of the noise strength to the mobility. This scenario can be further generalized to include effects of non-Gaussian, burst-like forcing modeled by Lévy noise. In this case however, the pulsatile additive noise cannot be treated as the internal (thermal), since the relation between the strength of the friction and variance of the noise is violated. Heavy tails of Lévy noise distributions not only facilitate escape kinetics, but more importantly, change the escape protocol by altering final stationary state to a non-Boltzmann, non-equilibrium form. As a result, contrary to the kinetics induced by a Gaussian white noise, escape rates in environments with Lévy noise are determined not by the barrier height, but instead, by the barrier width. We further discuss consequences of simultaneous action of thermal and Lévy noises on statistics of passage times and population of reactants in double-well potentials.

PACS numbers: 05.40.Fb, 05.10.Gg, 02.50.-r, 02.50.Ey,

Noise induced escape over a static potential barrier is the scenario underlying various fluctuations induced effects. Numerous research explored Gaussian noise and Lévy noise driven kinetics in double-well potential wells. These two kinetics fundamentally differs, as they correspond to the continuous (Gaussian) and discontinuous (Lévy) trajectories which in turn are responsible for very different escape protocols. Here, we study the archetypal models of overdamped, stochastic dynamics in double-well potentials driven by a single Lévy noise or a mixture of Lévy and Gaussian noises. Therefore, within the current studies, we extend understanding of escape processes over a static potential barrier. We explore the role of underlying assumptions by comparing results of numerical simulations with asymptotic scaling predicted by various approximations. We show how the escape protocol is affected by abnormally long jumps (outliers) and what is the role of the central part of the jump length distribution. We demonstrate that for the combined action of Gaussian and Lévy noise sources various asymptotic regimes can be obtained.

I. INTRODUCTION

Non-Gaussian Lévy noises and Lévy statistics are frequently objects of studies in the context of extreme, catastrophic events like economic crises[1,2], outburst of epidemics[3] or millennial climate changes[4]. The increasing number of observations indicates presence of non-Gaussian fluctuations in the variety of complex dynamical systems ranging from financial time series[5] and recordings of turbulent behavior[6], superdiffusion of micellar systems[7] and transmission of light in polidispersive materials[8], to photon scattering in hot atomic vapors[9], anomalous diffusion in laser cooling[10,11], gaze dynamics[12] and memory retrieval in humans[13]. As a natural generalization of the Brownian motion, the Lévy process is characterized by uncorrelated jumps sampled from the heavy-tailed, stable distribution of lengths and has been extensively studied in a large number of theoretical and numerical considerations[14–21]. Contrary to the Wiener process – a mathematical abstract of the Brownian motion – trajectories in the Lévy motion are discontinuous, thus representative for pulsatile, irregular flickering. Whereas a prominent feature of the Brownian motion is a linear growth of the variance of the position with time – this growth becomes faster (superlinear) for Lévy motion. Also, unlike equilibrium noise which refers to the jump sizes distributed according to the Gaussian statistics of finite variance, its nonequilibrium counterpart, the Lévy (non-Gaussian) noise, describes the processes with large outliers and has diverging variance.

Importantly, Lévy motions (called otherwise Lévy flights (LF)) have been shown to break detailed balance and microscopic reversibility[22,23]. Lack of detailed balance for the Langevin dynamics with Lévy flights has important thermodynamic consequences: In static, periodic potentials with broken spatial symmetry solely action of the Lévy noise induces the directed transport[24]. The key element of the ratcheting effect[25,26] is the acceleration of the escape process into the direction of the steeper slope of the potential. This acceleration of the transport over the narrower potential barrier plays an important role in the Lévy noise driven Kramers problem[4]. In the weak noise limit, escape from the potential well induced by Lévy noise is always faster[27] than the analogous process induced by the Gaussian white noise and the most probable

[a)]Electronic mail: karol@th.if.uj.edu.pl
[b)]Electronic mail: bartek@th.if.uj.edu.pl
[c)]Electronic mail: ewa.gudowska-nowak@uj.edu.pl

escape path is executed via a single long jump. This causes the mean first passage time (MFPT) to depend dominantly on the barrier width δ, i.e. $T \propto \delta^\alpha$ instead of barrier height ΔE, i.e. $T \propto \exp(\beta \Delta E)$, typical for the Kramers kinetics in the presence of thermal (Gaussian) noise. A similar, fully tractable analytically, solution to the first passage time problem is observed for escapes from bounded domains under the action of Lévy flights[28–32].

In line with Kramers approach the kinetic mechanism of a chemical reaction is described by means of a diffusion process along an internal coordinate x whose stationary states before and after the reaction correspond to the minima of a double-well potential $V(x)$ located at x_1 and x_2 and separated by an energy barrier[33], see Fig. 1. Assuming local equilibrium in the internal space allows one to formulate the Gibbs equation and identify the diffusion currents in terms of kinetic equations balancing the reactant and product concentrations[34]. Furthermore, derivation of rate constants for forward and reverse reactions gives the ratio (the equilibrium constant)

$$k_+/k_- = \exp[\beta(V(x_1) - V(x_2))] \tag{1}$$

which in the ideal case depends only on system's temperature via the Boltzmann coefficient β.

Within the paper we discuss escape from the potential wells induced/affected by Lévy noises and analyze departure from equilibrium kinetics as expressed by the above equilibrium constant. Asymptotic properties of systems driven by Lévy noise can be studied by the known Lévy-Itô decomposition[35,36] of Lévy flights in terms of the sum of a Poisson compound process and a Gaussian white noise. Consequently, anomalous long jumps, which determine escape kinetics over the barriers, are represented by the Poissonian component of the noise.

The paper starts with an introduction of a generic model system described by a Langevin equation (Section II), followed by presentation of simulations' details. Results derived for various double-well potentials are discussed in Section III. In the same Section asymptotic properties of escape kinetics affected by the combined action of the Lévy and Gaussian noises are analyzed. The paper concludes with a summary (Section IV) referring to main results and potential research areas.

II. MODEL

The barrier-crossing is modeled in terms of spatially diffusive (overdamped) motion of a particle subject to the deterministic force field $f(x) = -V'(x)$ and a fluctuating force $\xi(t)$ describing interactions of the system with its environment:

$$\frac{dx}{dt} = -\frac{dV(x)}{dx} + \sigma\xi(t). \tag{2}$$

Here σ is a parameter measuring intensity of fluctuations which equals $\sigma = \sqrt{2/\beta}$ for the motion of a Brownian particle in the strong friction limit.

We further assume that fluctuating force $\xi(t)$ is not Gaussian but instead, can be represented as a formal time derivative of the symmetric α-stable motion[37] $L(t)$, whose characteristic function $\phi(k) = \langle \exp[ikL(t)] \rangle$ attains the form

$$\phi(k) = \exp\left(-t\sigma^\alpha |k|^\alpha\right). \tag{3}$$

The stochastic process $\{X(t), t \geqslant 0\}$ described by Eq. (2) has increments

$$\begin{aligned} \Delta x &= x(t + \Delta t) - x(t) \\ &= -V'(x(t))\Delta t + \Delta t^{1/\alpha} \sigma \xi_t, \end{aligned} \tag{4}$$

where ξ_t represents a sequence of independent, identically distributed random variables[38–40] following the symmetric α-stable density[41,42] with the unity scale parameter. The scale parameter σ becomes an independent, external parameter. For a clarity of the presentation, the scale parameter σ in Eqs. (2) and (4) is extracted from the noise definition, see Eq. (3).

Main properties of the escape kinetics can be drawn from the analysis of Eq. (4): For a motion in a piecewise-linear potential starting in the left potential minimum, see Fig. 1, the Euler approximation (4) reduces to

$$\Delta x = -\frac{\Delta E_1}{\delta_1}\Delta t + \Delta t^{1/\alpha}\sigma\xi_t, \tag{5}$$

where $\Delta E_1 = E_b - E_1$ is the depth of the left potential well. Without loss of generality, we can assume that $E_b = 0$, see top panel of Fig. 1. The transition between potential wells includes the surmounting of the potential barrier, while the sliding along the potential slope is expected to be instantaneous. Accordingly, the transition from the left to the right minimum of the potential is recorded for trajectories for which

$$\Delta x \geqslant \delta_1, \tag{6}$$

where δ_1 is the distance from the left minimum of the potential to the barrier top. From the discretization scheme (4) and Eq. (6) one gets the following condition

$$-\frac{\Delta E_1}{\delta_1}\Delta t + \Delta t^{1/\alpha}\sigma\xi \geqslant \delta_1, \tag{7}$$

which results in

$$\xi \geqslant \xi_1 = \frac{1}{\sigma \Delta t^{1/\alpha - 1}}\left[\frac{\delta_1}{\Delta t} + \frac{\Delta E_1}{\delta_1}\right]. \tag{8}$$

For the symmetric α-stable density, the probability of observing a jump larger than ξ_1 is

$$P(\xi \geqslant \xi_1) \propto \xi_1^{-\alpha}. \tag{9}$$

Consequently, from Eq. (8) one obtains

$$P\left(\xi \geqslant \xi_1\right) \propto \left(\frac{\delta_1}{\Delta t} + \frac{\Delta E_1}{\delta_1}\right)^{-\alpha}. \tag{10}$$

Analogously, for backward passages

$$P\left(\xi \geqslant \xi_2\right) \propto \left(\frac{\delta_2}{\Delta t} + \frac{\Delta E_2}{\delta_2}\right)^{-\alpha}. \tag{11}$$

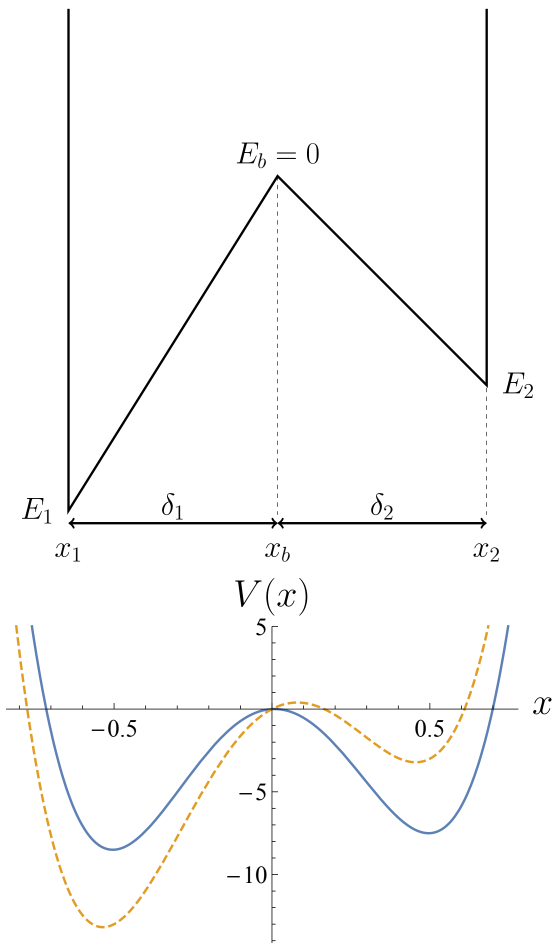

FIG. 1. Piecewise-linear, double-well potential (top panel) and the continuous double-well potential (bottom panel) used in the study. The continuous potential $V(x) = 128x^4 - 64x^2 + ax$, is given by Eq. (21) with the parameter a controlling the potential asymmetry. Here, the solid line corresponds to $a = 1$ and the dashed line to $a = 10$.

Eqs. (10) and (11) define escape (transition) rates k_{12}, k_{21} from the left/right potential wells:

$$\left(\frac{\delta_2 + \frac{\Delta E_2}{\delta_2}\Delta t}{\delta_1 + \frac{\Delta E_1}{\delta_1}\Delta t}\right)^{\alpha} \propto \frac{k_{12}}{k_{21}} \tag{12}$$

For a typical chemical reaction scheme between reactants (R) and products (P), $R \rightleftharpoons P$, the ratio k_{12}/k_{21} can be related at equilibrium to the mass action law and the equilibrium concentration of species[43]

$$\frac{k_{12}}{k_{21}} = \frac{P_2}{P_1}. \tag{13}$$

Here P_1 and P_2 are (equilibrium, steady state) probabilities of finding the system in either (left/right) potential wells. The probability $P_1(t)$ that the system is in the left state is given by

$$P_1(t) = \int_{-\infty}^{x_b} p(x,t)dx, \tag{14}$$

where $p(x,t)$ is a time dependent probability density of finding a particle at time t in the vicinity of x, and x_b is the point separating left and right states. Analogously, the formula for $P_2(t)$ reads

$$P_2(t) = \int_{x_b}^{\infty} p(x,t)dx = 1 - P_1(t). \tag{15}$$

If stationary P_1 and P_2 exist, they are obtained from the above integrals in the $t \to \infty$ limit with $p(x,t)$ replaced by the stationary density $p(x)$.

For a fixed potential barrier Eq. (12) reduces, in the $\Delta t \to 0$ limit, to the situation considered in[4,35,36]

$$\frac{P_2}{P_1} = \frac{k_{12}}{k_{21}} \propto \left(\frac{\delta_2}{\delta_1}\right)^{\alpha}. \tag{16}$$

At the same time, for fixed Δt and a high barrier ($\Delta E \gg 1/\Delta t$) one may obtain[44]

$$\frac{P_2}{P_1} = \frac{k_{12}}{k_{21}} \propto \left(\frac{\Delta E_2}{\Delta E_1}\right)^{\alpha}. \tag{17}$$

The scalings predicted by Eqs. (16) and (17) should be contrasted with the Gaussian white noise limit, in which the ratio of Kramers rates[33,45] leads to

$$\frac{P_2}{P_1} = \frac{k_{12}}{k_{21}} \propto \exp\left[\frac{E_2 - E_1}{\sigma^2}\right]. \tag{18}$$

Within the stochastic description of chemical kinetics, the transition rates can be conveniently defined in terms of inverse of the mean first passage time (MFPT), e.g. $k_{12} = T_{12}^{-1}$ where

$$\begin{aligned} T_{12} &= \langle \tau \rangle \\ &= \langle \min\{\tau : x(0) = x_1 = -\delta_1 \text{ and } x(\tau) \geqslant x_b\} \rangle. \end{aligned} \tag{19}$$

For Gaussian noise ($\alpha = 2$) entering Eq. (2) the MFPT can be calculated exactly[46] and reads

$$\begin{aligned} T(x_0 \to x_b) = \frac{1}{\sigma^2} \int_{x_0}^{x_b} dz \exp\left[V(z)/\sigma^2\right] \\ \times \int_{-\infty}^{z} dy \exp\left[-V(y)/\sigma^2\right], \end{aligned} \tag{20}$$

while for $\alpha < 2$ one needs to rely either on stochastic simulations and scaling analysis[47,48] or on a numerical solution of the corresponding fractional diffusion equation.

For the purpose of further analysis we define quotients $\mathcal{P} = P_2/P_1$ and $\mathcal{T} = T(x_1)/T(x_2) = k_{12}/k_{21}$, where in the last expression indices refer to the location of the left/right minimum of the potential. In order to consider Lévy fluctuations embedded in confining (steep) potentials securing existence of variances of stationary states, we analyze motion in a piecewise-linear (cf. Fig. 1) and in a continuous double-well potential

$$V(x) = 128x^4 - 64x^2 + ax. \tag{21}$$

In the latter form of $V(x)$ the parameter a controls the potential asymmetry, depths of minima and their location. The coefficients of the polynomial terms have been chosen to secure that recrossing events are rare, for which the potential wells have to be deep enough and the barrier region sufficiently narrow[61]. Otherwise, especially for Gaussian white noise, discrimination between states is less apparent. It should be stressed that both forms of potentials are sufficient to restrain the trajectories of Lévy flights from infinite escapes[49–52] by introducing impermeable boundaries and (or) deep wells confining the motion.

III. RESULTS

Results included in following subsections have been constructed numerically by methods of stochastic dynamics. Eq. (2) was integrated by the Euler-Maryuama method, see Eq. (4), with the time step of integration $\Delta t = 10^{-5}$ and averaged over 10^4 – 10^5 repetitions. We start with the study of properties of anomalous kinetics in piecewise-linear and continuous potentials driven by a single Lévy noise only (Sec. III A). Next, we focus on the combined action of Gaussian white noise and Lévy noise (Sec. III B). Finally, in order to further explore role of combined action of two noise sources we confront results of Lévy noise-driven kinetics with the problem of escape from a finite interval (Sec. III C).

A. Escape induced by Lévy noise

Figure 1 presents a sample piecewise-linear (top panel) and a continuous (bottom panel) double-well potentials. For convenience we choose a potential with maximum at $x_b = 0$ and the maximal value $E_b = 0$. For such a potential we can easily control the ratio of widths δ_2/δ_1 and depths of potential wells. The potential depicted in the top panel of Fig. 1 gives the full flexibility and allows verification of various hypothesis regarding stochastic dynamics. The continuous double-well potentials given by Eq. (21) with $a = 1$ (blue solid line) and $a = 10$ (orange dashed line) are depicted in the bottom panel of Fig. 1. For $a = 1$, the depths of potential wells are $\Delta E_1 \approx 8.5$, $\Delta E_2 \approx 7.5$ and the ratio of locations of minima $\delta_2/\delta_1 \approx 0.98$. Analogously, for $a = 10$, we have $\Delta E_1 \approx 13.2$, $\Delta E_2 \approx 3.2$ and $\delta_2/\delta_1 \approx 0.85$. Piecewise-linear and continuous setups differs mainly with respect to the relative depth of potential wells and shape of the potential for $x < x_1$ and $x > x_2$ due to the way of restricting the domain of motion, compare top versus bottom panel of Fig. 1 and Eq. (21).

Results of numerical simulations with various parameters characterizing the piecewise-linear double-well potential, see Fig. 1, are depicted in top and middle panels of Fig. 2. These results are compared and confronted with appropriate asymptotic formulas, see Eqs. (16), (17) and the full formula (12). Finally, findings for the piecewise-linear potential are also confronted with results for the continuous potential with $a = 1$, see bottom panel of Fig 2.

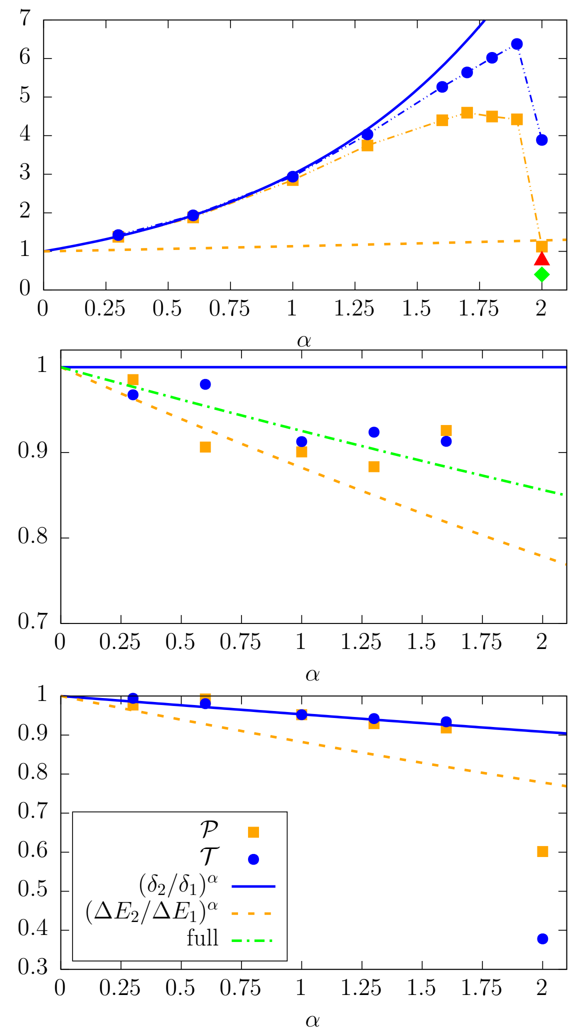

FIG. 2. Symbols represent the ratios $\mathcal{P}$ of occupation probabilities (■) and $\mathcal{T}$ of transition rates (•). Results of simulations are displayed with points while lines show various theoretical scalings discussed in the text: "full" (green dot-dashed, see Eq. (12)), "width ratio" (blue solid, see Eq. (16)) and "depth ratio" (orange dashed, see Eq. (17)). Subsequent panels correspond to various setups: piecewise-linear potential with $\Delta E_1 = 8.5$, $\Delta E_2 = 7.5$, $x_1 = 0.25$ and $x_2 = 0.75$ (top panel), piecewise-linear potential with $\Delta E_1 = 85000$, $\Delta E_2 = 75000$, $x_1 = 0.7$ and $x_2 = 0.7$ (middle) and the continuous potential (21) with $a = 1$ (bottom). The red triangle (▲) and the green rhombus (◆) in the top panel depict analytical evaluation of $\mathcal{P}$, $\mathcal{T}$, respectively, derived with the stationary $p(x)$ for the Gaussian ($\alpha = 2$) noise.

Top panel of Fig. 2 presents results for $\Delta E_1 = 8.5$, $\Delta E_2 =$

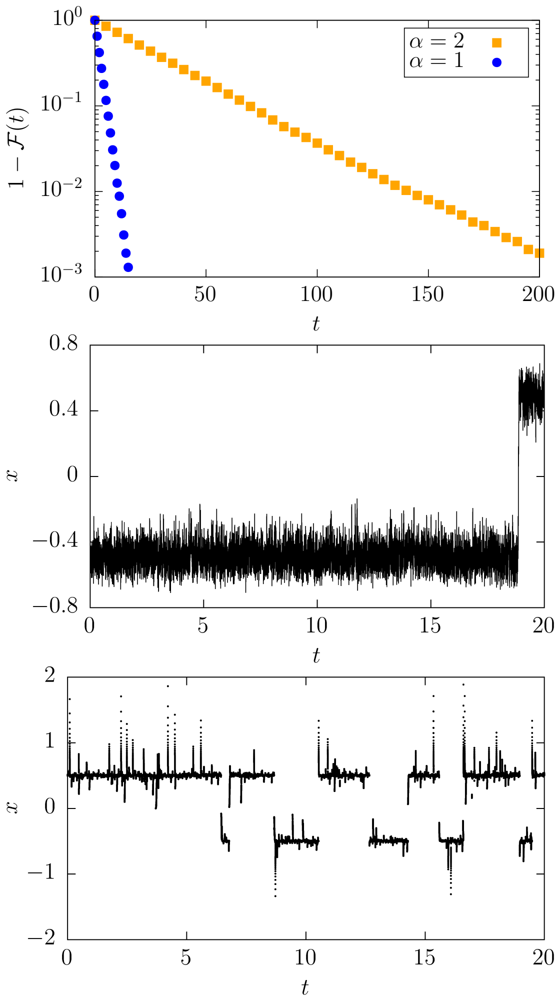

FIG. 3. Survival probability, i.e. complementary cumulative density of first passage times (top panel) and exemplary trajectories for $\alpha = 2$ (middle panel) and $\alpha = 1$ (bottom panel) for a continuous potential (21) with $a = 1$. The trajectory for $\alpha = 1$ has been plotted with symbols, in order to emphasise its discontinuity.

7.5, $x_1 = 0.25$ and $x_2 = 0.75$. Orange dots depict the ratio ($\mathcal{P} = P_2/P_1$) of occupation probabilities whereas blue dots represent the ratio ($\mathcal{T} = T(x_1)/T(x_2) = k_{12}/k_{21}$) of transition rates. The blue solid line shows the "width ratio" $(\delta_2/\delta_1)^\alpha$ predicted by Eq. (16), while the orange dashed line depicts the "depth ratio" $(\Delta E_1/\Delta E_2)^\alpha$ given by Eq. (17). For small values of the stability index α, blue dots and orange squares coincide, while for $\alpha \geqslant 1.3$ they start to differ. The scaling predicted by Eq. (16) is confirmed by numerical simulations with $\alpha < 1.3$. In the top panel of Fig. 2 there are two additional points. There is a red triangle corresponding to the analytically calculated value of MFPTs for $\alpha = 2$. Moreover, using the stationary $p(x) \propto \exp(-V(x)/\sigma^2)$ representative for this case we can evaluate P_1 and P_2 from Eqs. (14) and (15).

The green symbol (rhombus) in the top panel of Fig. 2 indicates ratio $\mathcal{T}$ calculated from Eq. (20). The ratios of reaction rates, calculated by use of exact formulas valid for $\alpha = 2$, significantly differ from the prediction of "width ratio" given by Eq. (16), but they are close to the "depth ratio" scaling predicted by Eq. (17), see the red triangle and the green rhombus in the top panel of Fig. 2.

Relations given by Eqs. (12) and the ratio $\mathcal{P}$ hold only when transitions between potential wells are performed in a single long jump[4,53]. This condition is well satisfied in the limit of vanishing noise intensity for deep potential wells, when the particle is driven by the Lévy noise with the small value of the stability index α. Contrary to small α, for α large enough the central part of a noise distribution plays an increasingly important role, as for growing α more probability mass is located around $x = 0$. If a slope of the potential barrier is not steep enough, multiple-step re-crossings of the barrier become more frequent[54]. Therefore, not only Eq. (13) does not hold but also transitions from a shallower potential well become more probable.

The middle panel of Fig. 2 presents results for a deep potential well. In contrast to the top panel of Fig. 2, there is an additional green dot-dashed line corresponding to the full formula given by Eq. (12). For a very deep potential well, the α dependence predicted by Eq. (12) is the closest to the results of stochastic simulations. It indicates existence of the regime where effects of the barrier width and barrier height contribute to the evaluated rate. This regime corresponds to a finite discretization time step Δt fulfilling the additional constraint

$$\delta \sim \Delta E \Delta t. \tag{22}$$

Otherwise, in the limit of $\Delta t \to 0$, the "width ratio" scaling predicted by Eq. (16) is visible.

The bottom panel of Fig. 2 presents results for the potential (21) with $a = 1$ along with two lines corresponding to limiting scaling given by Eqs. (16) (blue solid line) and (17) (orange dashed line). For $a = 1$ with $\alpha < 2$, numerical results obtained by use of the "in-well" population method or the MFPT ($\mathcal{P}$ versus $\mathcal{T}$) are coherent. Furthermore, for $\alpha < 2$, calculated ratios are very close to the "width ratio" prediction of Eq. (16). Note, that despite the approximation (16) is valid in the limit of vanishing noise[4,27,35] it seems to work very well also for finite noise strength σ[47,48].

The escape process is Markovian and characterized by finite MFPT, consequently first passage time distributions are exponential[61]. This characteristics can be observed by analysis of the survival probabilities depicted in Fig. 3. Top panel of Fig. 3 presents sample survival probabilities (the probability that a particle remains within the initial potential well up to time t) under Cauchy ($\alpha = 1$) and Gaussian ($\alpha = 2$) drivings for escape events over the continuous potential given by Eq. (21) with $a = 1$. Inspection of trajectories reveals difference in escape scenario induced by Gaussian and Cauchy noises. Trajectories under action of the Gaussian noise are continuous and a particle surmounts the potential barrier in a series of subsequent jumps. For the Cauchy driving, the trajectory is discontinuous and escape is typically performed in a single long jump. Moreover, for $\alpha = 1$, a particle can make distant excursions to outer points. Replacement of the continuous potential with the piece-wise liner, see top panel of Fig. 1, bounds the motion to the finite interval restricted by minima of the potential.

B. Additive thermal and Lévy noise

The scaling of the ratio of escape rates, see Eqs. (12) and (16) is derived using the asymptotic properties of α-stable densities. Such a derivation disregard the central part of the random force distribution. The central part of the jump length distribution control short jumps which are responsible for penetration of the potential barrier[4]. Therefore, in the current subsection, we assume that the particle is driven by two stochastic forces[55–58], so that the Langevin equation assumes the form

$$\frac{dx}{dt} = -V'(x) + \sigma\xi(t) + \eta(t). \tag{23}$$

As in Eq. (2), $\xi(t)$ stands for the Lévy noise whereas the additional, independent term $\eta(t)$ is assumed to be the Gaussian white noise, describing thermal fluctuations in the system. In such a setup the Gaussian white noise can be considered as the internal noise, while the Lévy noise is the external fluctuating force. Putting it differently, parameters of the Gaussian noise are defined (with help of fluctuation dissipation theorem) by internal parameters, while parameters of the Lévy noise are externally controlled[58,59]. For the sake of clarity, from now on we assume that the intensity of the Gaussian fluctuations stays fixed, i.e. it is set to unity. The scale parameter σ describes then the strength of the external Lévy noise with respect to the intensity of thermal fluctuations. As the reference case for the study of a combined action of two independent noise sources, we use the continuous potential of Sec. III A, see Eq. (21) and bottom panel of Fig. 1. Therefore, we use the same potential as in the bottom panel of Fig. 2, i.e. the potential given by Eq. (21) with $a = 1$ or $a = 10$. Please note, that the model studied in bottom panel of Fig. 2 corresponds to Eq. (23) with $\eta(t) \equiv 0$ and $a = 1$.

First, we verify how the combined action of two noises changes properties of trajectories. Fig. 4 presents a sample trajectory for a particle moving in a potential (21) with $a = 1$ driven by simultaneous action of Cauchy and Gaussian noise. In contrast to pure Cauchy driving, see bottom panel of Fig. 3, trajectory explores more vicinity of potential's minima. Moreover, due to Gaussian component of the stochastic driving a particle is more likely to visit neighborhood of the potential barrier. Nevertheless, majority of escape event is still performed in a single long jump, but now the last visited point before escape from a potential well is typically closer to the boundary than for pure Cauchy driving.

Comparison of bottom panel of Fig. 2 and top panel of Fig. 5 reveals that incorporation of the additional Gaussian noise source significantly weakens the agreement between the prediction of "width ratio" given by Eq. (16) and results of computer simulations. The presence of the Gaussian noise changes the escape scenario by increasing chances of an escape in a sequence of jumps[60]. Consequently, due to the increased width of the central part of the jump length distribution, the role played by the tails of Lévy distribution is depleted, what in turn results in stronger deviations from the "width ratio" predicted by Eq. (16). These deviations are amplified for all values of the stability index α, except the special case of $\alpha = 2$. For $\alpha = 2$, the Lévy noise is equivalent to the Gaussian white noise. Therefore, the presence of two Gaussian noise sources facilitate escape kinetics as they can be combined in the single Gaussian white noise with the increased width. The increased width of the resultant Gaussian white noise, with help of fluctuation dissipation theorem, can be attributed to the increase in the system temperature. Please, note that the situation is more subtle for the underdamped models, which are not studied here. For the potential given by Eq. (21) with $a = 1$, the scaling predicted by Eq. (16) is very similar to the ratio given by Eq. (18).

In the middle panel of Fig. 5, the scale parameter σ is reduced to $\sigma = 0.1$. For lower σ the central part of the jump length distribution, amplified due to presence of the Gaussian white noise, is even more prominent. In the middle panel of Fig. 5, deviations between the weak noise theory, see Eq. (16) and the actual scaling are amplified. In order to assure that the increased disagreement is due to presence of the Gaussian component we have performed additional simulations with $\sigma = 0.1$ and $\eta \equiv 0$. For $\sigma = 0.1$ and $\eta \equiv 0$, we obtained results which are quantitatively indistinguishable from those one included in the bottom panel of Fig. 2. This effect indicates that the increased disagreement in the middle panel of Fig. 5 is produced by the action of the Gaussian, thermal white noise. Moreover, it demonstrates that the approximation given by Eq. (16), which is derived in the $\sigma \to 0$ limit, works pretty well for finite σ, see bottom panel of Fig. 2.

The bottom panel of Fig. 5 examines the model for $\sigma = 10$. The agreement between results of computer simulations and Eq. (16) seems to be restored. Unfortunately, this agreement is a coincidence due to the potential shape and the combined action of two very different effects. First of all, tails of the jump length distribution leads to the scaling predicted by Eq. (16). Nevertheless, due to a large value of the scale parameter σ, also the central part of the jump length distribution becomes non-negligible. The influence of the central part of the jump length distribution on the escape kinetics can be quantified by the MFPT for a system driven by a Gaussian noise with some effective[4] σ_{eff}. Due to the shape of the potential, more precisely almost symmetric location of potential's minima, both scalings (16) and (18) give similar approximations for the ratio of reaction rates.

To eliminate this accidental agreement, the potential (21) with $a = 10$ was used. Now minima of the potential have depth of $\Delta E_1 \approx 13.2$ and $\Delta E_2 \approx 3.2$ and their locations are not as symmetric as for $a = 1$, see bottom panel of Fig. 1. As it is clearly visible in Fig. 6, the results of computer simulations with $a = 10$ and $\sigma = 1$ differ from Eq. (16). The pronounced disagreement is produced by the Gaussian white noise component, which increases likelihood of continuous (instead of single jump) transition over the potential barrier. Furthermore, for $a = 10$, the right potential well is shallow, what further increases deviations from the scaling given by

Eq. (16). In the middle panel of Fig. 6 the scale parameter σ is increased to $\sigma = 10$. Paradoxically, the disagreement between the asymptotic scaling and results of computer simulations, due to a presence of the Gaussian white noise, is further amplified by the Lévy noise. More precisely, for $\sigma = 10$, the assumption of a weak noise, which is crucial for asymptotics predicted by Eq. (16), does not hold, even without the Gaussian white noise.

The agreement between results of computer simulations and the asymptotic scaling (16) can be reintroduced by disregarding the Gaussian white noise source, i.e. by setting $\eta(t) \equiv 0$ as in the bottom panel of Fig. 6. For instance, for $a = 10$ with $\sigma = 1$ the agreement is significant (results not shown). At the same time for the increased $\sigma = 10$ the accordance is observed for $\alpha < 1$, see bottom panel of Fig. 6. For $\alpha > 1$ with $\sigma = 10$ the central part of the Lévy distribution is too wide to make the single jump escape scenario dominating what in turn introduces violations of Eq. (16).

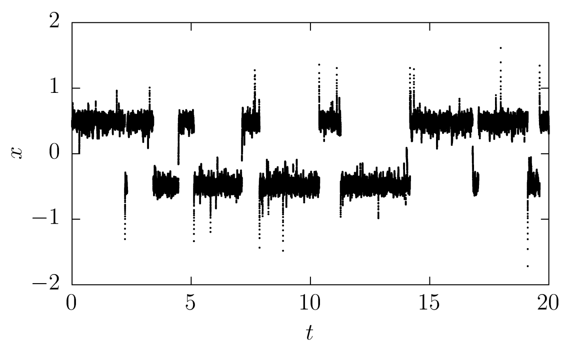

FIG. 4. Sample trajectory for a particle moving in the continuous double-well potential (21) with $a = 1$ driven by simultaneous action of Cauchy ($\alpha = 1$) and Gaussian ($\alpha = 2$) noises.

From the examination of the escape kinetics driven by the combined action of two independent Lévy and Gaussian noise sources we can deduct following scenarios resulting in the violation of "width ratio" given by Eq. (16): (i) addition of the Gaussian white noise source, (ii) increasing of the scale parameter in the Lévy noise and (iii) decreasing depth of potential wells. The scenarios (i) and (ii) are related, because both of them increase the width of the central part of the jump length distribution which is responsible for the penetration of the potential barrier, see Ref. 4. Consequently, elimination of the Gaussian noise, under the condition that σ is small enough, reintroduces the scaling given by Eq. (16), see Fig. 2 and bottom panel of Fig. 6. Nevertheless, due to finite σ, when $\alpha \to 2$ even in Fig. 2 and bottom panel of Fig. 6 violations of Eq. (16) are visible. These violations can be decreased by the reducing the scale parameter σ. Finally, the scenario (iii) breaks the two state approximation as "in-well" densities become wide.

In the Ref. 61, we have studied the model of escape kinetics induced by general α-stable noises in a symmetric double-well potential given by Eq. (21) with $a = 0$. In particular, for a particle starting in one of the potential wells we have calculated the ratio $\mathcal{R} = T_{w-w}/T_{w-b}$ of mean first pas-

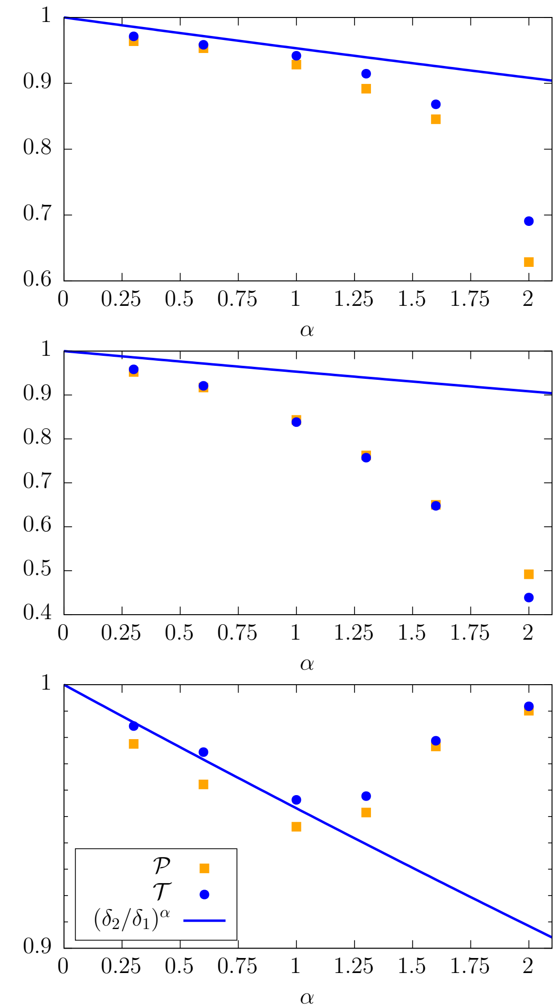

FIG. 5. Symbols represent the ratios $\mathcal{P}$ of occupation probabilities (■) and $\mathcal{T}$ of transition rates (•) for the continuous double-well potential (21) with $a = 1$. Solid lines show the theoretical "width ratio" scaling (blue solid, see Eq. (16)). Subsequent panels correspond to various values of the σ parameter scaling the strength of Lévy noise: $\sigma = 1$ (top panel), $\sigma = 0.1$ (middle panel) and $\sigma = 10$ (bottom panel). The legend is included in the bottom panel.

sage times for well-bottom-to-well-bottom T_{w-w} and well-bottom-to-barrier-top T_{w-b} escape scenarios. For the Gaussian white noise such a ratio is equal to two, i.e. $\mathcal{R} = 2$, see 45. Action of the Lévy noise breaks this property of escape kinetics in double-well potentials — the ratio of MFPTs becomes smaller than two. Addition of the Gaussian white noise (with the scale parameter set to unity) to the model considered in Ref. 61 increases the value of the ratio of mean first passage times approximately by 10%. The ratio has increased because the additional Gaussian white noise increased the role played by the central part of the jump length distribution. Nevertheless, the ratio $\mathcal{R}$ is still smaller than two, see Fig. 7. For more

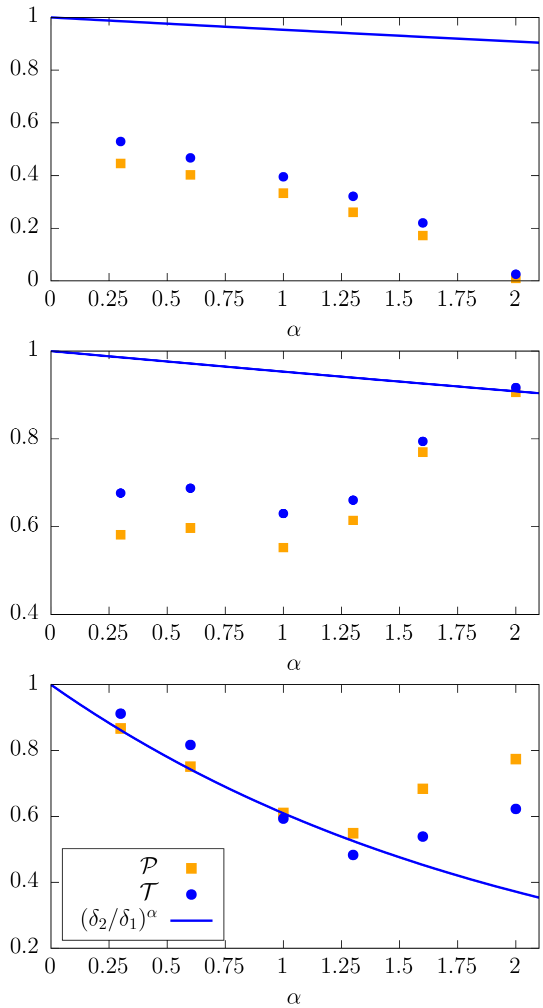

FIG. 6. The same as in Fig. 5 for $a = 10$ with $\sigma = 1$ (top panel), $\sigma = 10$ (middle panel) and $\sigma = 10$ with $\eta(t) \equiv 0$ (bottom panel). The legend is included in the bottom panel.

details see Ref. 61.

C. Escape from finite intervals

From the examination of the escape kinetics induced by a mixture of noises it can be deducted that addition of thermal noise changes the escape kinetics. Presence of the additional thermal noise changes the escape protocol from a single long jump scenario to a sequence of shorter jumps controlled by the central part of the jump length distribution. In order to elucidate this issue in more details, we switch to the archetypal model of escape from the finite interval $[-L, L]$. Initially a particle is located in the middle of the interval, i.e. $x(0) = 0$, and the motion is continued until $|x| < L$. The exact formula

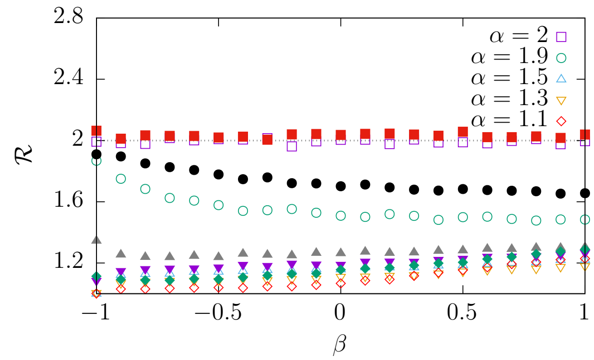

FIG. 7. Ratio $\mathcal{R}$ of mean first passage times for well-bottom-to-well-bottom T_{w-w} and well-bottom-to-barrier-top T_{w-b} for the Lévy noise (empty points) and mixture of Gaussian and Lévy noises (full symbols) for the symmetric double-well potential given by Eq. (21) with $a = 0$. For more details see Ref. 61.

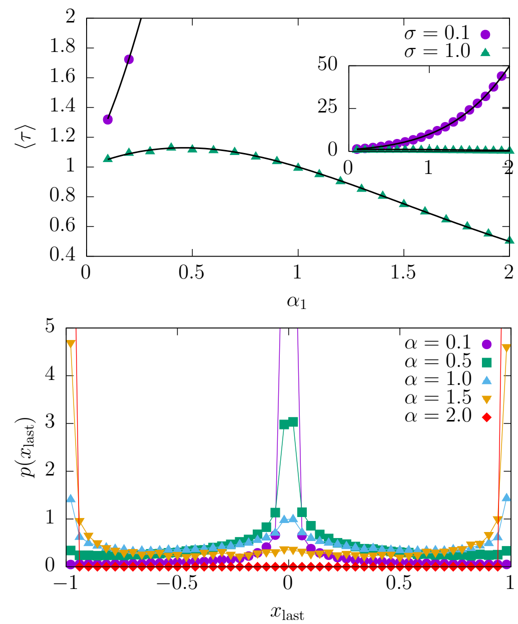

FIG. 8. Mean first passage time $\langle\tau\rangle$ for the escape from the finite interval $[-1, 1]$ (top panel) and the last hitting point density $p(x_{\mathrm{last}})$ for $\sigma = 0.1$ (bottom panel). Solid lines in the top panel correspond to the exact, theoretical formula, see Eq. (20). Other parameters: initial condition $x(0) = 0$, time step of integration $\Delta t = 10^{-4}$ and number of repetitions $N = 10^5$.

for the MFPT reads

$$\langle\tau\rangle = \frac{1}{\Gamma(1+\alpha)} \frac{L^\alpha}{\sigma^\alpha}, \tag{24}$$

see Refs. 28–32. Furthermore, the intuitive argumentation supporting Eq. (24) is included in the Appendix A. In addition to the MFPT, we studied the last hitting point densities $p(x_{\mathrm{last}})$, where x_{last} is the last point visited before leaving the $[-1, 1]$ interval. Top panel of Fig. 8 presents MFPT as a function of the stability index α for $L = 1$ with $\sigma = 1$ and $\sigma = 0.1$. Results of computer simulations nicely follow theoretical curve given by Eq. (24) with $L = 1$. Results for $\sigma = 1$ are presented in the main plot, while for $\sigma = 0.1$ in the inset, as values of MFPT for $\sigma = 0.1$ are significantly larger than for $\sigma = 1$. For $\sigma = 0.1$ escape kinetics slows down with the increase of the stability index α because $(L/\sigma)^\alpha = (1/0.1)^\alpha = 10^\alpha$ is a growing function of the stability index α, see Eq. (24).

The bottom panel of Fig. 8 shows the last hitting point density for $\sigma = 0.1$. The $p(x_{\mathrm{last}})$ distribution for $\sigma = 1.0$ is practically the same as for $\sigma = 0.1$, therefore we show the distribution for $\sigma = 0.1$ only. For processes with continuous trajectories $x_{\mathrm{last}} = \pm L$ because the escape is performed by approaching of one of the absorbing boundaries. The very different situation is observed for Lévy flights, which have discontinuous trajectories. The most probable x_{last} is the origin, as $x(0) = 0$, but with the increasing α, maxima at the borders emerge. The escape from the vicinity of the initial position can be dominating, but the escape itself is it not immediate. For example, for $\alpha = 0.5$, on average the escape occurred after approx 10^4 jumps since $\Delta t = 10^{-4}$. Initial short jumps (controlled by the central part of the jump length distribution) resulted in the spreading of the last visited point around the initial condition. Bottom panel of Fig. 8 confirms that, for small values of the stability index α ($\alpha < 1$), the escape from the vicinity of the initial position is the most probable. The different situation is observed for $\alpha > 1$ when the random walker is very likely to approach absorbing boundaries.

In the next step, using the model of Lévy noise induced escape, we study the differences between escape protocols for single noise and mixture of noises induced escape. We use mixture of two Lévy noises characterized by stability indices α_1 and α_2 with $\sigma_1 = \sigma_2 = 1$ or $\sigma_1 = 1,\ \sigma_2 = 0.1$. Mixture of two independent Lévy noises can be replaced by a single Lévy noise if only they are characterized by the same stability index α. For $\alpha_1 = \alpha_2$, the sum of two independent identically distributed α-stable random variables is distributed according to the α-stable density with the same α and the scale parameter

$$\sigma = [\sigma_1^\alpha + \sigma_2^\alpha]^{1/\alpha}, \tag{25}$$

Therefore, using Eq. (24) with σ given by Eq. (25) it is possible to calculate the exact value of the MFPT.

Figure 9 presents results for escape driven by two noises. Subsequent columns correspond to different values of scale parameters: $\sigma_1 = \sigma_2 = 1$ (left column) and $\sigma_1 = 1,\ \sigma_2 = 0.1$ (right column). Top panel presents MFPT as function of stability indices α_1 and α_2. Second from the top panel show sample cross-section of the MFPT surface. For $\alpha_1 = \alpha_2$ results of computer simulations (points) nicely follow exact results (solid lines), see Eqs. (24) and (25). Finally, bottom panels depict last hitting point densities $p(x_{\mathrm{last}})$ with $\alpha_1 = 0.5$ and $\alpha_1 = 1.5$. For $\sigma_1 = \sigma_2$, the MFPT surface is symmetric with respect to the interchange of α_1 and α_2, otherwise it is not symmetric along the diagonal. For $\sigma_2 = 0.1$, the escape is slower because the width of the jump length distribution is reduced in comparison to $\sigma_2 = 1$, compare left and right panels of Fig. 9.

Examination of the last hitting point density shows that addition of the second noise can modify the escape scenario. For example, for $\alpha = 0.5$, the most probable is escape from the vicinity of the initial position, see bottom panel of Fig. 8. The bottom panel of Fig. 8 should be contrasted with the second from the bottom panel of Fig. 9 which present last hitting point densities for $\alpha_1 = 0.5$. First of all, addition of the thermal noise (Lévy noise with $\alpha = 2$), produce peaks at boundaries both for $\sigma_2 = 1$ and $\sigma_2 = 0.1$, although for $\sigma_2 = 0.1$ their height is lower. For $\sigma_2 = 1$ already addition of Lévy noise with $\alpha > 1$ produces modes at boundaries, while for $\sigma_2 = 0.1$ the first noise significantly weakens the action of the second one.

Bottom panels of Fig. 9 presents last hitting point densities $p(x_{\mathrm{last}})$ for a free particle in finite interval, while the model studied in Secs. III A and III B correspond to the motion in double-well potentials. Nevertheless, already examination of the free motion is very instructive. It clearly shows that trajectories become more continuous-like with addition of the second noise with a larger value of the stability index α. Contrary to the free motion, in the case of external force, emergence of peaks at boundaries will be weakened because there is an external, deterministic, force pushing particles back to the potential minimum. Moreover, due to the outer part of the potential, on the outer side of minima particles experience the restoring force pushing them back to minima of the potential. This in turn increases the fraction of escape events from the potential minima, i.e. it amplifies $p(x_{\mathrm{last}})$ at $x_{\mathrm{last}} \approx x_1$ and $x_{\mathrm{last}} \approx x_2$.

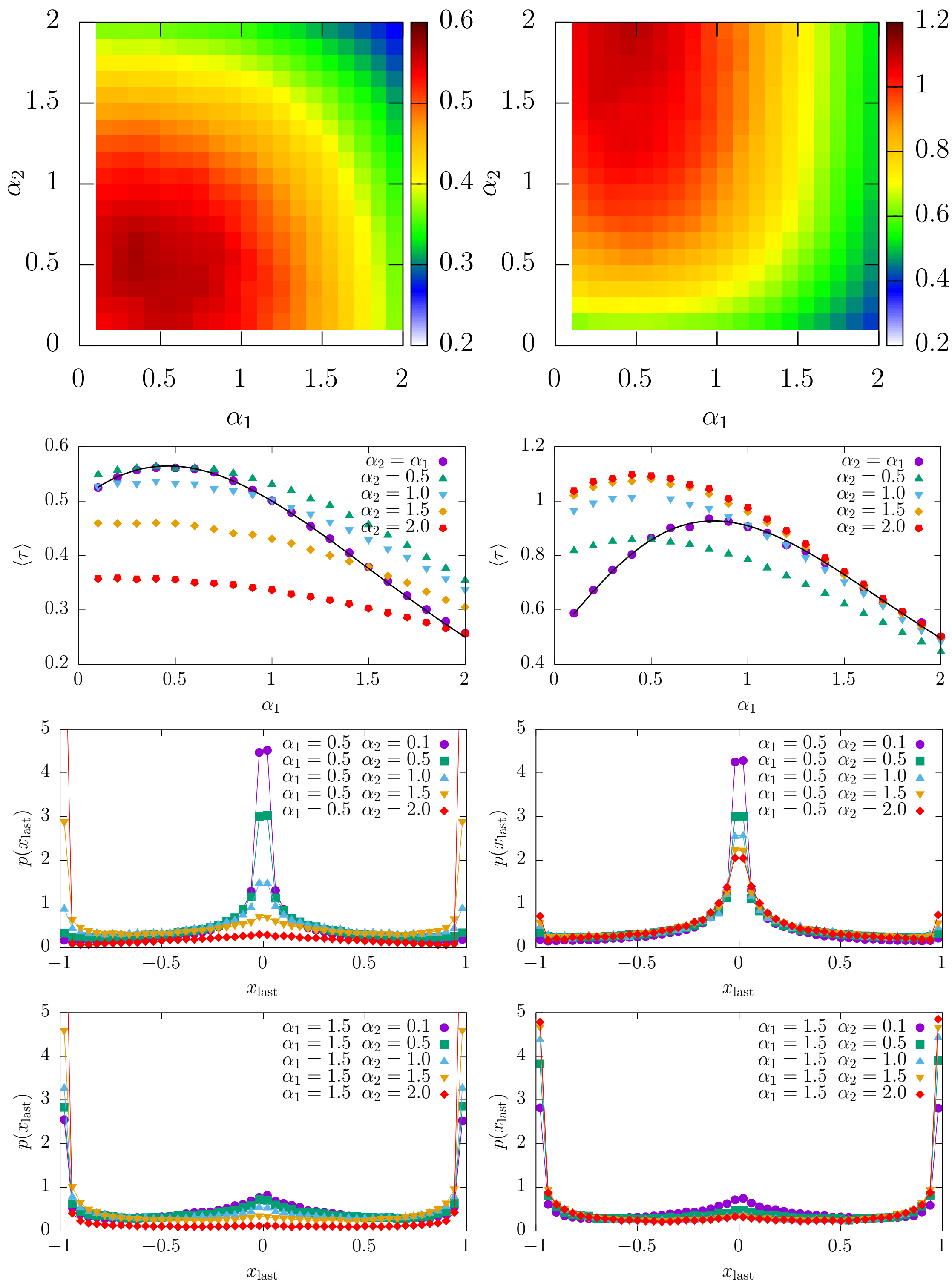

FIG. 9. Mean first passage time $\langle\tau\rangle$ for the escape from the finite interval $[-1, 1]$ (top panel), cross-section of the MFPT(α_1, α_2) surface (second from the top panel), and the last hitting point densities $p(x_{\mathrm{last}})$ (bottom panels). Solid lines in the second from the top panel correspond to the exact, theoretical formula, see Eq. (24). Other parameters: initial condition $x(0) = 0$, time step of integration $\Delta t = 10^{-4}$ and number of repetitions $N = 10^5$. Columns correspond to various values of the scale parameters: $\sigma_1 = \sigma_2 = 1$ (left column) and $\sigma_1 = 1,\ \sigma_2 = 0.1$ (right column).

IV. SUMMARY AND CONCLUSIONS

The noise induced escape over a potential barrier is an archetypal process modeling many phenomena. In particular, it is a key element of the Kramers theory of chemical kinetics. According to the Kramers theory, the reaction rate depends primarily on the relative height ΔE of the potential barrier separating states, $k \propto \exp(-\beta \Delta E)$, and decreases with the increasing barrier height. Such a dependence of the reaction rate is typical for systems driven by thermal fluctuations represented in the form of the Gaussian white noise. The escape scenarios driven by non-Gaussian Lévy noises differ significantly from those induced by thermal fluctuations, in the sense that for weak noises the escape events are performed in single long jumps. Consequently, the reaction rate is not sensitive to the barrier height but to the barrier width, i.e. $k \propto \delta^{-\alpha}$. Despite the fact that this approximation is derived in the weak noise limit, it also works pretty well for finite noise strengths. In a combined action of Lévy and Gaussian noises one observes competition between Lévy noise induced long jumps and contributions of short-length displacements secured by Gaussian part of fluctuations. As a result, trajectories surmounting the potential start to penetrate the barrier and the escape rate becomes sensitive to the barrier height. The very same behavior is observed for the noise induced escape from finite intervals where addition of noise with lighter tails increases probability of approaching absorbing boundaries because the likelihood of approaching absorbing boundaries is controlled by the central part of the jump length distribution which is amplified by the additional noise source.

Divergent moments of Lévy statistics and Lévy motion seem to stay in conflict with energetic and thermodynamics of the stochastic differential equation of the Langevin type[23,44,57,58]. Yet, accumulating evidence shows that Markovian Lévy flights (LFs) with distribution of jumps emerging from the generalized version of the central limit theorem are well suited representations of complex phenomena, to name just a few recent applications of LFs in description of mental searches[62], analysis of free neutron output in a fusion experiment with a deuteron plasma[56], investigations of gene-regulatory networks[63] or examination of self-regulatory motion of insects[64].

Long displacements of walkers in fractional dynamics on networks have been shown to improve efficiency to reach any node of the network by inducing small world properties[66], independently of the network structure. This observation is crucial in developing algorithms for optimization based on Lévy flights techniques. A similar statement can be drawn from the data analysis of option markets which indicate that dispersal of asset prices in actively traded markets is influenced by Lévy flights or tempered Lévy flights[1,67]. Also here, the LFs driven Langevin equation seems to be a proper model of studies, despite infinite variance of fluctuations. The environments powered by Lévy noise can be natural sources of epicatalytic reactions[44]: whereas in a common catalysis the establishment of equilibrium is speed up by lowering the barrier between two states, in epicatalysis the effect can be achieved by altering the steady state distribution alike to our analysis in Section II. Since also description of various critical phenomena requires non-local interactions in space (and time) – it seems plausible to further carefully explore pros and cons of using LF models in realistic applications.

ACKNOWLEDGMENTS

This project was supported by the National Science Center (Poland) grant 2018/31/N/ST2/00598. This research was supported in part by PL-Grid Infrastructure. Computer simulations have been performed at the Academic Computer Center Cyfronet, AGH University of Science and Technology (Kraków, Poland) under CPU grant DynStoch.

Appendix A: Mean escape time

The two state approximation along with the assumption that escape is performed via the single long jump can be used to calculate the mean first passage time of a free particle from a bounded domain. For the system described by the Eq. (2) the escape takes place under the condition

$$\sigma \xi \Delta t^{1/\alpha} \geqslant \delta \tag{A1}$$

leading to

$$\xi \geqslant \xi_0 = \frac{\delta}{\sigma} \Delta t^{-1/\alpha}. \tag{A2}$$

For the α stable density the probability of performing jump longer than ξ_0 is $p = P(\xi \geqslant \xi_0) = \xi_0^{-\alpha}$. Therefore, we obtain the estimation

$$p = P(\xi \geqslant \xi_0) = \frac{\delta^{-\alpha}}{\sigma^{-\alpha}} \Delta t. \tag{A3}$$

In order to calculate the mean first passage time, it is necessary to calculate the average number of jumps needed to escape for the first time. The number of jumps k required to escape for the first time follows the geometric distribution

$$p_k = (1-p)^{k-1} p, \tag{A4}$$

because the escape is performed after $(k-1)$ unsuccessful trails. The mean number of jumps is

$$\langle k \rangle = \sum_{k=1}^{\infty} p_k k = \frac{1}{p}. \tag{A5}$$

Since, jumps are performed every Δt the MFPT $\langle \tau \rangle$ is

$$\langle \tau \rangle = \Delta t \langle k \rangle = \frac{\Delta t}{p} = \frac{\delta^{\alpha}}{\sigma^{\alpha}}. \tag{A6}$$

Alternatively, Eq. (A6) can be derived by investigating scaling of $\langle x^2 \rangle$ with the increasing number of jumps, see Refs. 5 and 65. Formula (20) resembles the general formula for the

MFPT[28–32] for a particle starting in the middle of the interval of half-width δ subject to the action of Lévy noise

$$\langle\tau\rangle = \frac{\delta^\alpha}{\Gamma(1+\alpha)\sigma^\alpha}. \tag{A7}$$

The considerations leading to Eq. (20) do not take into account the process of surmounting the potential barrier. Consequently, the escape from the potential well should be not faster than the constructed estimate, see Eqs. (A6) and (A7).

REFERENCES

[1] *On growth and form: Fractal and non-fractal patterns in physics*, edited by H. E. Stanley and N. Ostrowsky (Springer Verlag, Berlin, 1986).
[2] R. N. Mantegna and H. E. Stanley, *An introduction to econophysics. Correlations and complexity in finance* (Cambridge University Press, Cambridge, 2000).
[3] M. E. J. Newman and G. T. Barkema, *Monte Carlo methods in statistical physics* (Clarendon Press, Oxford, 1999).
[4] P. D. Ditlevsen, Phys. Rev. E **60**, 172 (1999).
[5] J. P. Bouchaud and A. Georges, Phys. Rep. **195**, 127 (1990).
[6] M. F. Shlesinger, J. Klafter, and B. J. West, Physica A **140**, 212 (1986).
[7] J. P. Bouchaud, A. Ott, D. Langevin, and W. Urbach, J. Phys. II France **1**, 1465 (1991).
[8] P. Barthelemy, J. Bertolotti, and D. Wiersma, Nature (London) **453**, 495 (2008).
[9] M. Mercadier, W. Guerin, M. M. Chevrollier, and R. Kaiser, Nat. Phys. **5**, 602 (2009).
[10] F. Bardou, J. P. Bouchaud, A. Aspect, and C. Cohen-Tannoudji, *Lévy statistics and laser cooling* (Cambridge University Press, Cambridge, 2002).
[11] E. Barkai, E. Aghion, and D. A. Kessler, Phys. Rev. X **4**, 021036 (2014).
[12] T. A. Amor, S. D. S. Reis, D. Campos, H. J. Herrmann, and J. S. Andrade, Sci. Rep. **6**, 20815 (2016).
[13] A. M. Reynolds and M. A. Frye, PLoS One **2**, e354. (2007).
[14] R. Metzler and J. Klafter, Phys. Rep. **339**, 1 (2000).
[15] E. Barkai, Phys. Rev. E **63**, 046118 (2001).
[16] V. V. Anh and R. McVinish, J. Appl. Math. Stoch. Anal. **16**, 97 (2003).
[17] D. Brockmann and I. M. Sokolov, Chem. Phys. **284**, 409 (2002).
[18] A. V. Chechkin, V. Y. Gonchar, J. Klafter, and R. Metzler, in *Fractals, Diffusion, and Relaxation in Disordered Complex Systems: Advances in Chemical Physics, Part B*, edited by W. T. Coffey and Y. P. Kalmykov (John Wiley & Sons, New York, 2006), Vol. 133, pp. 439–496.
[19] S. Jespersen, R. Metzler, and H. C. Fogedby, Phys. Rev. E **59**, 2736 (1999).
[20] V. V. Yanovsky, A. V. Chechkin, D. Schertzer, and A. V. Tur, Physica A **282**, 13 (2000).
[21] D. Schertzer, M. Larchevêque, J. Duan, V. V. Yanovsky, and S. Lovejoy, J. Math. Phys. **42**, 200 (2001).
[22] P. Garbaczewski and V. Stephanovich, Phys. Rev. E **84**, 011142 (2011).
[23] Ł. Kuśmierz, A. Chechkin, E. Gudowska-Nowak, and M. Bier, EPL (Europhysics Letters) **114**, 60009 (2016).
[24] B. Dybiec, E. Gudowska-Nowak, and I. M. Sokolov, Phys. Rev. E **78**, 011117 (2008).
[25] M. O. Magnasco, Phys. Rev. Lett. **71**, 1477 (1993).
[26] P. Reimann, Phys. Rep. **361**, 57 (2002).
[27] P. Imkeller, I. Pavlyukevich, and T. Wetzel, Eur. Phys. J. ST **191**, 211 (2010).
[28] R. M. Blumenthal, R. K. Getoor, and D. B. Ray, Trans. Am. Math. Soc. **99**, 540 (1961).
[29] R. K. Getoor, Trans. Am. Math. Soc. **101**, 75 (1961).
[30] M. Kac and H. Pollard, Canadian J. Math. **2**, 375 (1950).
[31] H. Widom, Trans. Am. Math. Soc. **98**, 430 (1961).
[32] H. Kesten, Illinois J. Math. **5**, 267 (1961).
[33] H. A. Kramers, Physica (Utrecht) **7**, 284 (1940).
[34] I. Pagonabarraga, A. Pérez-Madrid, and J. M. Rubi, Physica A **237**, 205 (1997).
[35] P. Imkeller and I. Pavlyukevich, Stochastic Processes and their Applications **116**, 611 (2006).
[36] P. Imkeller and I. Pavlyukevich, J. Phys. A: Math. Gen. **39**, L237 (2006).
[37] A. Janicki and A. Weron, Stat. Sci. **9**, 109 (1994).
[38] J. M. Chambers, C. L. Mallows, and B. W. Stuck, J. Amer. Statistical Assoc. **71**, 340 (1976).
[39] A. Weron and R. Weron, Lect. Not. Phys. **457**, 379 (1995).
[40] R. Weron, Statist. Probab. Lett. **28**, 165 (1996).
[41] A. Janicki and A. Weron, *Simulation and chaotic behavior of α-stable stochastic processes* (Marcel Dekker, New York, 1994).
[42] A. Janicki, *Numerical and statistical approximation of stochastic differential equations with non-Gaussian measures* (Hugo Steinhaus Centre for Stochastic Methods, Wrocław, 1996).
[43] D. T. Gillespie, Am. J. Phys. **64**, 225 (1996).
[44] M. Bier, Phys. Rev. E **97**, 022113 (2018).
[45] P. Hänggi, P. Talkner, and M. Borkovec, Rev. Mod. Phys. **62**, 251 (1990).
[46] C. W. Gardiner, *Handbook of stochastic methods for physics, chemistry and natural sciences* (Springer Verlag, Berlin, 2009).
[47] A. V. Chechkin, O. Y. Sliusarenko, R. Metzler, and J. Klafter, Phys. Rev. E **75**, 041101 (2007).
[48] A. V. Chechkin, V. Y. Gonchar, J. Klafter, and R. Metzler, EPL (Europhys. Lett.) **72**, 348 (2005).
[49] A. V. Chechkin, J. Klafter, V. Y. Gonchar, R. Metzler, and L. V. Tanatarov, Chem. Phys. **284**, 233 (2002).
[50] A. V. Chechkin, J. Klafter, V. Y. Gonchar, R. Metzler, and L. V. Tanatarov, Phys. Rev. E **67**, 010102(R) (2003).
[51] A. V. Chechkin, V. Y. Gonchar, J. Klafter, R. Metzler, and L. V. Tanatarov, J. Stat. Phys. **115**, 1505 (2004).
[52] B. Dybiec, A. V. Chechkin, and I. M. Sokolov, J. Stat. Mech. P07008 (2010).
[53] A. Vezzani, E. Barkai, and R. Burioni, arXiv preprint arXiv:1804.02932 (2018).
[54] M. Cieśla, K. Capała, and B. Dybiec, Phys. Rev. E **99**, 052118 (2019).
[55] W. Ebeling and M. Y. Romanovsky, Contri. Plas. Phys. **49**, 477 (2009).
[56] W. Ebeling, M. Y. Romanovsky, I. Sokolov, and I. Valuev, Eur. Phys. J. ST **187**, 157 (2010).
[57] Ł. Kuśmierz, B. Dybiec, and E. Gudowska-Nowak, Entropy **20**, 658 (2018).
[58] Ł. Kuśmierz, J. M. Rubi, and E. Gudowska-Nowak, J. Stat. Mech **2014**, P09002 (2014).
[59] K. Kanazawa, T. G. Sano, T. Sagawa, and H. Hayakawa, Phys. Rev. Lett. **114**, 090601 (2015).
[60] M. Bier and R. D. Astumian, Phys. Lett. A **247**, 385 (1998).
[61] B. Dybiec, E. Gudowska-Nowak, and P. Hänggi, Phys. Rev. E **75**, 021109 (2007).
[62] A. Baronchelli and F. Radicchi, Chaos, Solitons & Fractals **56**, 101 (2013).
[63] X. Chen, F. Wu, J. Duan, J. Kurths, and X. Lie, Appl. Math. Comp. **348**, 425 (2019).
[64] J. Noetel, V. L. S. Freitas, E. E. N. Macau, and L. Schimansky-Geier, Chaos: An Interdisciplinary Journal of Nonlinear Science **28**, 106302 (2018).
[65] K. Szczepaniec and B. Dybiec, J. Stat. Mech. P06031 (2015).
[66] A.P. Riascos, and J.L. Mateos, Phys. Rev. E **90**, 032801 (2014).
[67] A. Karlova, P. Hagan, Wilmott **2016** doi=10.1002/wilm.10536 (2016).

Underdamped, anomalous kinetics in double-well potentials

Karol Capała[1, *] and Bartłomiej Dybiec[1, †]
[1] *Institute of Theoretical Physics, and Mark Kac Center for Complex Systems Research, Jagiellonian University, ul. St. Łojasiewicza 11, 30–348 Kraków, Poland*
(Dated: March 14, 2022)

The noise driven motion in a bistable potential acts as the archetypal model of various physical phenomena. Here, we contrast properties of the overdamped escape dynamics with the full (underdamped) dynamics. In the weak noise limit, for the overdamped particle driven by a non-equilibrium, α-stable noise the ratio of forward and backward transition rates depends only on the width of a potential barrier separating both minima. Using analytical and numerical methods, we show that in the regime of full dynamics, contrary to the overdamped case, the ratio of transition rates depends both on widths and heights of the potential barrier separating minima of the double-well potential. The derived analytical formula for the ratio of transition rates is corroborated by extensive numerical simulations. Results of numerical simulations especially well follow the analytical predictions in the weak noise limit when the most probable escape scenario is via a single, strong, noise-kick, which is sufficient to induce a quasi-deterministic transition over the potential barrier. Such an escape trajectory can be analyzed in terms of the instantaneous velocity, which is fully characterized by its density function which is of the same type as the probability density underlying the noise distribution.

PACS numbers: 05.40.Fb, 05.10.Gg, 02.50.-r, 02.50.Ey,

I. INTRODUCTION

A noise induced escape of a particle is one of archetypal problems in stochastic dynamics. It underlines various noise driven effects. Among others, it was studied by H. A. Kramers in the case of the Gaussian white noise (GWN) in overdamped (large viscosity) and underdamped (small viscosity) regimes [1]. In these cases, the "velocity of chemical reactions" (reaction rate) depends only on the height of the barrier separating reactants. Moreover, in the overdamped regime, the obtained formula for the reaction rate can be interpreted as the Arrhenius equation [2]. Therefore, the stochastic motion in the double-well potential can be used as an effective model of chemical reactions. Since then, the noise induced escape of a particle was intensively studied in the overdamped [3, 4] and underdamped [4–7] regimes as well as in quantum setups [8–10].

The Gaussian white noise is a very special representative of the more general family of α-stable white noises. Except the Gaussian white noise, α-stable noises have the so-called "heavy tails", i.e., they allow for occurrence of extreme events with a significantly larger probability than the Gaussian distribution. For instance, noise induced displacements under Lévy noises with $0 < \alpha < 2$ follow the power-law distribution with the exponent $-(\alpha+1)$. Consequently, for $\alpha < 2$, only fractional moments of order ν which is smaller than α exist [11, 12], i.e. $\langle |x|^\nu \rangle < \infty$. Power-law, heavy-tails of α-stable densities are responsible not only for divergence of moments, but also for discontinuity of paths of processes driven by Lévy noises [13]. In particular, in the overdamped and underdamped regime, position or velocity, respectively, is discontinuous. Finiteness of higher order moments can be reintroduced by the so called truncated (tempered) Lévy flights [14–20].

Heavy-tailed, Lévy type fluctuations, similarly to the equilibrium, thermal GWN noise, leads to many surprising noise-induced phenomena like ratcheting effect [21–23], stochastic resonance [24] or resonant activation [25]. Non-Gaussian, heavy-tailed fluctuations have been observed in plenitude of experimental setups ranging from disordered media [26], biological systems [27], rotating flows [28], optical systems and materials [29, 30], physiological applications [31], financial time series [32–34], dispersal patterns of humans and animals [35, 36], laser cooling [37] to gaze dynamics [38] and search strategies [39, 40]. They are studied both experimentally [28, 38, 41] and theoretically [42–47] including the problem of fluctuation-dissipation relations in non-equilibrium systems [48–52]. Consequently, despite some nonphysical features of Lévy flights, e.g., infinite propagation velocity, due to their well-known mathematical properties, e.g., self similarity, infinite divisibility and generalized central limit theorem, α-stable noises are widely applied in various models displaying anomalous fluctuations or describing anomalous diffusion. One may also consider their more physical counterparts, namely Lévy walks [53], for which "long jumps" are performed with finite velocity. Despite this difference, such systems can still exhibit some similar phenomena to Lévy flights [54, 55].

One might expect that α-stable noise can significantly change properties of escape kinetics in overdamped systems. Indeed, contrary to the Gaussian white noise driving, for which the rate of reaction rates depends only on the depth of the potential well [1], under α-stable noise the ratio of transition rates is sensitive to the width of the potential barrier [56–59]. In the weak noise limit, i.e., when the noise intensity tends to 0, the dependence of the ratio of transition rates solely on the width of the potential barrier can be demonstrated [57, 58]. This relation holds also for finite noise intensity, as long as noise intensity is much smaller that the depth

* karol@th.if.uj.edu.pl
† bartek@th.if.uj.edu.pl

of the potential well [60], however the combined action of the Lévy noise and the Gaussian noise might reintroduce the sensitivity of the ratio of transition rates to the barrier height [61].

In the regime of full dynamics, a particle is characterized both by the velocity and the position. Depending on the noise type, the velocity can be discontinuous, e.g., for Lévy noises with $\alpha < 2$. At the same time, the position is continuous, which might change properties of the same models in comparison to their overdamped counterparts. In this manuscript, we extend the discussion on the underdamped kinetics driven by Lévy noises in double-well potentials. In the next section (Sec. II Model) we derive the relation between transition rates in the weak noise limit given by Eq. (10), which is the main result of this manuscript. In the Sec. III (Results) we present extensive comparisons between the derived approximate formula obtained in Sec. II and results of numerical simulations. The manuscript is closed with Summary and Conclusions (Sec. IV).

II. MODEL

The Langevin equation [62] provides description of a particle motion in a noisy environment. In the underdamped regime, the Langevin equation takes the following form

$$m\ddot{x}(t) = -\gamma\dot{x}(t) - V'(x) + \sigma\zeta(t), \tag{1}$$

where $-V'(x)$ is the deterministic force acting on a particle, while $\zeta(t)$ stands for the noise (random force), which approximates interactions of the test particle with its environment. The scale parameter σ ($\sigma > 0$) controls the strength of fluctuations. In Eq. (1), x has the dimension of length, t of time, $[V(x)] = [\text{energy}]$. Remaining parameters have following units: $[\gamma] = \text{mass}/\text{time}$, $[\sigma] = \text{length} \times \text{mass}/(\text{time})^{1+\frac{1}{\alpha}}$ and $[\zeta] = \text{time}^{\frac{1}{\alpha}-1}$. We assume that the noise $\zeta(t)$ is of white, α-stable, Lévy type, i.e., it generalizes the Gaussian white noise [11, 12]. Contrary to the case of $\alpha = 2$, when σ and γ are related by the Sutherland-Einstein-Smoluchowski formula [63–65], in the non-equilibrium regime, i.e., for $\alpha < 2$, σ and γ are two independent parameters. Moreover, we restrict ourselves to symmetric α-stable noise only, which is the formal time derivative of the symmetric α-stable motion $L(t)$, see [13], whose characteristic function is given by

$$\phi(k) = \langle \exp[ikL(t)] \rangle = \exp\left[-t|k|^{\alpha}\right]. \tag{2}$$

The stability index α ($0 < \alpha \leqslant 2$) controls the noise asymptotics. Importantly, for $\alpha = 2$, the α-stable noise transforms into the standard Gaussian white noise [11, 12]. Increments of the symmetric α-stable motion $L(t)$, i.e., $\Delta L = L(t+\Delta t) - L(t)$, are independent and identically distributed according to a symmetric α-stable density with the characteristic function given by Eq. (2) with t replaced by Δt. Symmetric α-stable densities are unimodal probability densities which for $\alpha < 2$ exhibit a power-law asymptotics with tails decaying as $|\zeta|^{-(\alpha+1)}$, see [11, 12]. Consequently, for $\alpha < 2$, all moments of order greater than α, e.g., variance, diverge.

Equation (1) can be rewritten as the set of two first order equations

$$\begin{cases} m\dot{v}(t) = -\gamma v(t) - V'(x) + \sigma\zeta(t) \\ \dot{x}(t) = v(t) \end{cases}. \tag{3}$$

The deterministic force $-V'(x)$ is produced by the fixed, double-well, potential $V(x)$, with two minima located at x_1 and x_2 ($V(x_1) = E_1$ and $V(x_2) = E_2$) and a single local maximum at x_b ($x_1 < x_b < x_2$ and $V(x_b) = E_b$), see Fig. 1. Without the loss of generality it can be assumed that $x_b = 0$ and $V(x_b) = 0$. Furthermore, we assume that both, the potential barrier separating potential minima and outer (large $|x|$) parts of the potential are steep enough to assure that the particle position is limited to the neighborhood of potential minima.

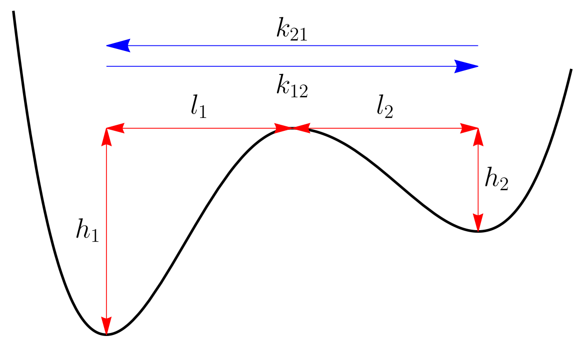

FIG. 1. Schematic sketch of the potential, see Eq. (16), used in numerical studies of noise induced escape kinetics.

Using Eq. (3), we study the problem of noise induced escape over the static potential barrier, with the special attention to the weak noise limit. Under the weak noise approximation, the Lévy noise can be effectively decomposed into the Wiener part (small, bounded jumps) and the compound Poisson process (spikes) [57, 58]. More precisely, the Lévy-Khintchine formula [66] shows that a Lévy process $L(t)$ is built by three independent components: a linear drift (deterministic motion), a Brownian motion and a Lévy jump process. Furthermore, in [57, 58], it has been shown that for the small σ it is possible to introduce a threshold $\delta(\sigma)$ such that all subthreshold pulses are considered as background, while suprathreshold pulses build spikes. The small jumps part makes infinitely many jumps on any time interval of positive length, but the absolute value of these jumps is bounded. In [57, 58], it has been proved that, for appropriately chosen $\delta(\sigma)$, the variance of the background (small jumps) part vanishes in the limit of $\sigma \to 0$. Consequently, between the two subsequent large spikes, the particle is subjected only to a background noise, which, for small σ, is so weak that the motion of a particle is almost deterministic. Moreover, time lags between the two subsequent spikes are so large that the particle practically reaches the bottom of the potential well (underdamped dynamics) or velocity drops almost to zero (full dynamics). Therefore, in the weak noise limit, the only scenario capable of inducing the escape is when a strong enough spike "kicks" the particle. Importantly, the weak noise regime is recorded already for finite, although small, values of the scale parameter σ. The exact value of the σ for which agreement with predictions corresponding to $\sigma \to 0$ is recorded depends on the setup under study. The detailed discussion of the decomposition procedure can be found in Refs. [57, Sec. 2], [58, Sec. 3] or [67, Sec. 3.1]. In overall, the bounded jump component part is responsible for short displacements, while the Poisson part controls long jumps. For the Lévy noise, characterized by the stability index α ($0 < \alpha < 2$), the probability of recording an event ξ larger than ζ is given by

$$P(\xi > \zeta) \sim \zeta^{-\alpha}. \tag{4}$$

In the weak noise limit, the protocol of escaping over the potential barrier is based on a single long "jump" in the velocity, which in a single, strong "kick", gives the particle kinetic energy sufficient to overpass the potential barrier deterministically. More precisely, we assume that initially a particle has velocity v_0, and it is located in the ith minimum of the potential. From this point, it moves deterministically to the top of the potential barrier. During the motion to the top of the barrier, it loses some of its energy due to the friction. Moreover, it is perturbed by the small jumps component, which typically is weak enough not to suppress the transition over the potential barrier. If we disregard the friction, the minimal velocity, which is sufficient to produce the transition from the ith minimum to the barrier top, reads

$$\frac{mv^2}{2} \geqslant E_b - E_i = \Delta E_i. \tag{5}$$

During the motion the energy is dissipated by friction, therefore, the minimal initial velocity v_0 needs to be larger

$$v_0 = v + \frac{\gamma}{m}\int_{t_0}^{t_0+\delta t} v(t)dt, \tag{6}$$

where δt ($\delta t \gg 0$) is the time necessary to reach the top of the potential barrier. The integration over time gives the distance between the initial position x_i and the potential barrier x_b, i.e., l_i. Consequently, the initial velocity reads

$$v_0 = v + \frac{\gamma}{m} l_i. \tag{7}$$

Combining Eqs. (5) and (7), we get the following estimate for the minimal initial velocity v_0

$$v_0 = \sqrt{\frac{2\Delta E_i}{m}} + \frac{\gamma}{m} l_i. \tag{8}$$

Equation (1) describes the full (underdamped) dynamics in the regime of linear damping. For a free particle under linear friction, the velocity is distributed according to the α-stable density with the same stability index α as the noise, see Refs. [68–70] and Appendix A. The deterministic force $-V'(x)$, see the first line of Eq. (3), affects the shape of the stationary velocity distribution. For the weak noise, i.e., small σ, the majority of particles are localized in the vicinity of potential minima, where the deterministic force is small and can be neglected. Consequently, in the weak noise limit, we can assume that the velocity is distributed according to the α-stable density, while for the larger σ it can be approximated by the α-stable density. Please note, that such a situation corresponds to the diverging mean energy $\langle E \rangle$, because α-stable densities with $\alpha < 2$ are characterized by the diverging variance. The divergence of mean energy does not affect our considerations, because we calculate the probability of recording a minimal instantaneous energy. The condition on the minimal instantaneous energy can be transformed into the equivalent condition on the instantaneous velocity, see Eq. (9), which is easier to utilize, due to known asymptotic behavior of α-stable densities, see Eq. (4) and (A9). As the first approximation, we assume that the large initial velocity is directed towards the potential barrier. If the potential barrier is narrow, and outer parts of the potential are steep, the particle is unlikely to explore positions placed beyond minima, i.e., $|x| \gg |x_i|$. Consequently, the large velocity is most likely to be directed towards the potential barrier. As it will be shown later, the transition initiated by the abrupt velocity towards the potential barrier is the most probable and the approximation based on this assumption, see Eq. (10), works very well. If the velocity is not large enough, the particle could be reversed prior to reaching the top of the potential barrier. On the one hand, transitions over the potential barrier are produced by extreme velocities, which are ruled by the tail of the velocity distribution. On the other hand, a particle during its motion to the barrier top is subject to damping and to continuous small perturbations, controlled by the central part of the α-stable density, i.e., the Gaussian like part. Employing Eq. (4), we find the probability that the velocity larger than the minimal value v_0 is recorded

$$P(v > v_0) \sim \left(\sqrt{\frac{2\Delta E_i}{m}} + \frac{\gamma}{m} l_i\right)^{-\alpha}. \tag{9}$$

If the initial position of the particle is in the ith minimum, i.e., $x(t_0) = x_i$, the probability given by Eq. (9) is equal to the transition rate k_{ij}. Therefore the ratio, κ, of forward, k_{12}, and backward, k_{21}, transition reads

$$\kappa = \frac{k_{12}}{k_{21}} = \left(\frac{\sqrt{2\Delta E_2} + \gamma\sqrt{m} l_2}{\sqrt{2\Delta E_1} + \gamma\sqrt{m} l_1}\right)^{\alpha}. \tag{10}$$

The derivation of Eq. (10), assumes that the particle is wandering around a minimum of the potential and waiting for the extreme velocity larger than v_0, see Eq. (8). If the particle velocity is larger than v_0, it can overpass the potential barrier practically in the deterministic manner. For $\gamma \to \infty$, Eq. (10) reduces to the well-known overdamped limit, where the ratio of transition rates depends only on the ratio of distances between potential minima and the barrier top [56–58], i.e.,

$$\kappa = \frac{k_{12}}{k_{21}} = \left(\frac{l_2}{l_1}\right)^{\alpha}. \tag{11}$$

For weak enough noise (small σ), transition rates and their ratio can be calculated using the relationship with the mean first passage times (MFPT), see [3]. For the particle starting in the left minimum x_1 of the potential the MFPT, T_{12}, is defined as

$$T_{12} = \langle \tau \rangle = \langle \min\{\tau : x(0) = -l_1 \ \wedge \ x(\tau) \geqslant 0\} \rangle. \quad (12)$$

Therefore, the forward transition rate, k_{12}, is given by

$$k_{12} = \frac{1}{T_{12}}. \quad (13)$$

Definitions of the MFPT from the right potential well, T_{21}, and the backward transition rate, k_{21}, are analogous to the definition of T_{12} and k_{12}. Finally, from numerically estimated MFPTs the ratio of transition rates can be calculated

$$\kappa = \frac{k_{12}}{k_{21}} = \frac{T_{21}}{T_{12}}. \quad (14)$$

The mean first passage times T_{12} and T_{21} can be obtained using numerical simulations of the Langevin equation, which can be rewritten in the discretized form

$$\begin{cases} v_{i+1} = v_i - \left[(\gamma v_i + V'(x_i))\Delta t + \sigma\, (\Delta t)^{1/\alpha}\, \zeta_i \right] /m \\ x_{i+1} = x_i + v_{i+1}\Delta t \end{cases}, \quad (15)$$

where ζ_i is the sequence of independent and identically distributed α-stable random variables and Δt is the integration times step, which is significantly smaller than the transition time, i.e., $\Delta t \ll \delta t$. The velocity part, containing the α-stable noise, is approximated using the Euler-Maruyama scheme [12, 71], while the spatial part is constructed trajectory-wise. In order to estimate the required MFPT T_{12} (T_{21}) trajectories $x(t)$ are generated using the approximation (15), with the initial condition $x(0) = -l_1$ ($x(0) = l_2$) and $v(0) = 0$, as long as $x(t) < x_b$ ($x(t) > x_b$). From the ensemble of first passage times, the mean first passage times and their ratios are calculated. Within computer simulations, it is assumed that the particle mass is set to $m = 1$.

The approximation given by Eq. (10) suggests that the ratio of escape rates depends both on depths of potential wells and distances between minima and the maximum of the potential. Therefore, we use such a potential which allows easy control of its depths and distances between minima and the maximum

$$V(x) = \begin{cases} 4h_1 \left[\frac{x^4}{4l_1^4} - \frac{x^2}{2l_1^2} \right] & x < 0 \\ 4h_2 \left[\frac{x^4}{4l_2^4} - \frac{x^2}{2l_2^2} \right] & x \geqslant 0 \end{cases}. \quad (16)$$

Parameters h_1 and h_2 control depths of the left and right minimum respectively, while l_1 and l_2 represent distances between the potential maximum and the corresponding minimum. The top of the potential barrier is located at $x_b = 0$. The potential given by Eq. (16) is schematically depicted in Fig. 1.

Numerical results were obtained by use of the discretized version of the Langevin equation, see Eq. (15). Simulations were performed mainly with the integration time step $\Delta t = 10^{-3}$, which is significantly smaller than the transition time δt. Nevertheless, some of them were repeated with the smaller integration time step, i.e., $\Delta t = 10^{-4}$. Such an integration time step was sufficient to ensure stability of the Euler-Maruyama method. Final results were averaged over $N = 10^5 - 10^6$ realizations. For simplicity, we have assumed $m = 1$ and $\gamma = 1$ (except situations when it is varied). Remaining parameters: l_1, l_2, h_1, h_2 and σ varied among simulations. Their exact values are provided within the text and figures' captions.

III. RESULTS

We start our studies with the inspection of trajectories of the process generated by Eq. (1) under Cauchy ($\alpha = 1$) noise, see Fig. 2. The top panel shows results for $\gamma = 1$, while in the bottom panel the damping is set to $\gamma = 5$. Since the motion is perturbed by the α-stable noise, the velocity $v(t)$ is discontinuous, while the position $x(t)$, $x(t) = \int v(t)dt$, is continuous. First of all, with the increasing damping, the particle motion becomes more restricted, i.e., the particle is most likely to be found in the vicinity of one of the potential wells because position fluctuates less. At the same time, the particle loses its velocity and energy faster, what is manifested by faster decay and lower amplitude of velocity oscillations in the bottom panel. Inspection of trajectories confirms that, in order to overpass the potential barrier, the instantaneous velocity needs to be large enough and, interestingly, it can be directed both towards the top of the potential barrier (bottom panel) or outwards (top panel). Horizontal lines in Fig. 2 depict minimal values of velocities towards the potential barrier, see Eq. (8), which are sufficient to induce a transition over the potential barrier. Due to the potential asymmetry, minimal forward (from the left to the right) and backward (from the right to the left) velocities are different. Moreover, because of the damping, the minimal velocity in the direction of the boundary is smaller than the minimal velocity in the opposite direction.

The top panel of Fig. 2 shows the situation when the initial large velocity is pointing in the opposite direction than the potential barrier. After a strong noise pulse at $t \approx 7$, a particle initially moves to the right. It gets to the reversal point, in which the velocity drops to zero and the motion is reversed. The particle returns to the right minimum of the potential, where it has the negative velocity equal to the minimal backward velocity. Consequently, it continues its motion towards the potential barrier, which is successfully overpassed. After passing the potential barrier, due to the deterministic force, the particle accelerates. In the bottom panel of Fig. 2 the initial velocity after a strong pulse at $t \approx 2.5$ is equal to the minimal backward velocity and it is directed towards the potential barrier. Consequently, the particle can successfully pass from the right to the left minimum of the potential. Moreover, during the sliding from the barrier top to the left minimum of the potential, the velocity is perturbed a couple of times, e.g., at $t \approx 2.72$, $t \approx 2.82$ and $t \approx 3.1$ discontinuities in $v(t)$ are visible. Fig. 2 clearly confirms that the assumption of the "single-jump" escape is fully legitimate.

Figure 3 compares numerically calculated ratio of transi-

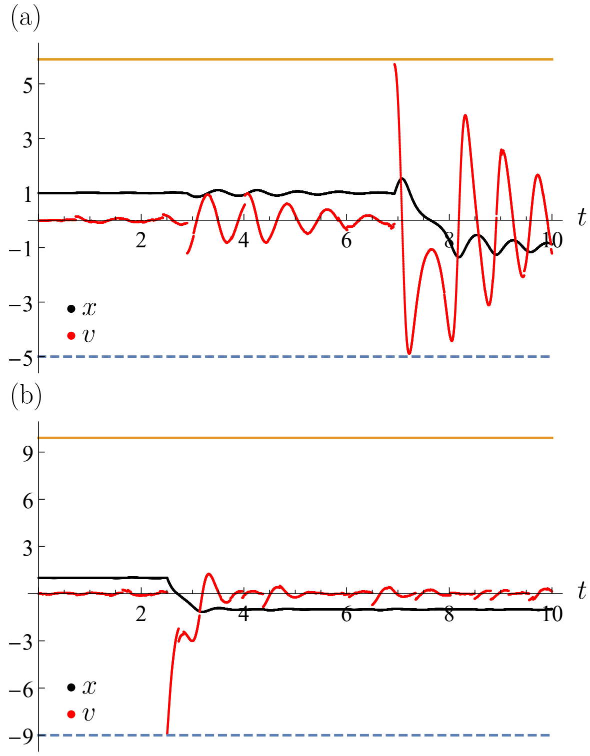

FIG. 2. Sample trajectories of the particle moving in the potential (16) with $l_1 = l_2 = 1$, $h_1 = 12$ and $h_2 = 8$. The stability index α is equal to $\alpha = 1$ and the damping coefficient γ is set to $\gamma = 1$ (top panel — (a)) and $\gamma = 5$ (bottom panel — (b)). Horizontal lines show minimal velocities for forward (solid orange) and backward (dashed blue) transitions which are given by Eq. (8). More details in the text.

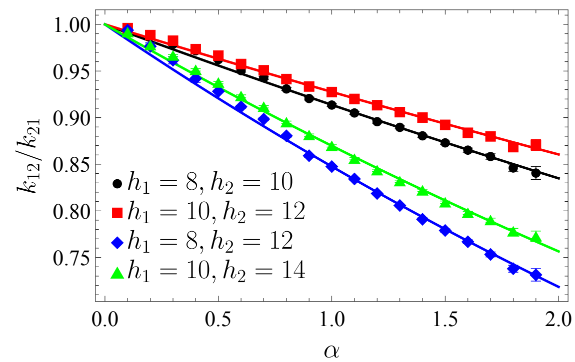

FIG. 3. Ratio $\kappa(\alpha)$ of transition rates from minima of the potential (16) to the barrier top as a function of the stability index α. Various points correspond to numerical results for different depths of potential wells, i.e., different values of h_1 and h_2, while lines plot the scaling given by Eq. (10). Simulation parameters $l_1 = 1$, and $l_2 = 1$, $\gamma = 1$ and $\sigma = 0.2$.

tion rates (points) with predictions of Eq. (10) (lines) as a function of the stability index α. It corresponds to fixed distances between minima and the maximum of the potential ($l_1 = 1 = l_2 = 1$) and various potential depths (h_1 and h_2). Parameters h_1 and h_2, characterizing depths of potential wells, were chosen in such a way that both are of the same order, and their values are significantly larger than the scale parameter $\sigma = 0.2$, i.e., $h_1 \gg 0.2$ and $h_2 \gg 0.2$. Such a choice of parameters ensures that weak noise approximation can be employed. Fig. 3 clearly shows that the ratio of transition rates depends on depths of both potential wells. For $\alpha > 1$, there is a perfect agreement between results of simulations and the formula (10). For small values of the stability index α ($\alpha < 1$), there are some discrepancies. More precisely, the numerically estimated ratio of transition rates is slightly larger than the expected scaling given by Eq. (10).

Lack of the full agreement between predictions of Eq. (10) and numerical results, for small α, post the question about validity of all undertaken assumptions used to derive Eq. (10). First of all, the potential (16) is not completely impenetrable at large $|x|$. A random walker can explore outer parts of the potential corresponding to $x < -l_1$ or $x > l_2$. This could indicate why the lack of full agreement is recorded for small α, for which the central part of the velocity distribution is narrower, and its tails are heavier. For the large enough velocity directing outwards of the barrier top, a particle may explore the outer part of the potential and still overpass the potential barrier, see the top panel of Fig. 2. To verify the role of exploration of outer parts of the potential, the potential (16) was modified by the addition of reflecting boundaries in (i) minima of the potential, i.e., at $-l_1$ and l_2, or (ii) at the same distance from the potential minima as the potential barrier i.e., at $-2l_1$ and $2l_2$. The first option improves the agreement for small α, see red squares in Fig. 4. At the same time, it destroys the agreement for $\alpha \to 2$. In the scenario (ii), ratios of transition rates are indistinguishable (results not shown) from results obtained in the unrestricted dynamics, see Fig. 3. This is in accordance with the observed dependence of $x(t)$, see Fig. 2, which is restricted to $|x(t)| < 2$.

Placing reflecting boundaries in minima of the potential confirms that, indeed, the differences for small α between the scaling given by Eq. (10) and numerical simulations in Fig. 3 come from particles having the velocity directed outwards from the potential barrier. Probability of recording an initial velocity pointing outward the potential barrier which is sufficient to induce a successful transition over the potential barrier can be calculated in the similar manner as in Eq. (9), but this time a particle moves along a different (longer) path. We can assume that the particle reverses its motion at $|x| = 2l_i$, i.e., at $-2l_1$ or $2l_2$, because as it was demonstrated in the scenario (ii) introduction of reflecting boundaries placed at $-2l_1$ and $2l_2$ produced the same results as unrestricted dynamics, see Fig. 2. Therefore, the trajectory length is $3l_i$ and Eq. (8) is replaced by

$$P(v > v_0) \sim \left(\sqrt{\frac{2\Delta E_i}{m}} + 3\frac{\gamma}{m} l_i \right)^{-\alpha}. \tag{17}$$

Finally, taking into account that the initial velocity can be di-

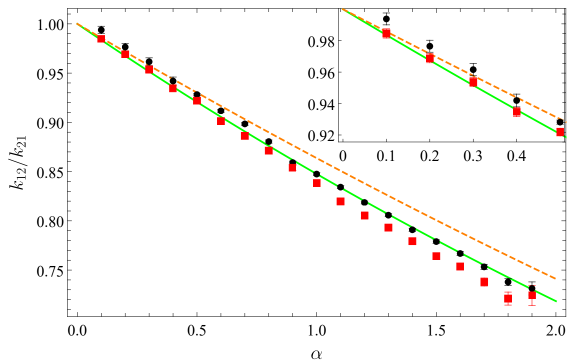

FIG. 4. The same as in Fig. 3, i.e., $\kappa(\alpha)$, for various space restrictions. Black dots (•) represent unrestricted motion, while red squares (■) correspond to the motion restricted by reflecting boundaries placed in the minima of the potential. Lines present scallings given by Eq. (10) (solid green line) and Eq. (18) (dashed orange line). Simulations parameters $h_1 = 8$, $h_2 = 12$, $l_1 = 1$, $l_2 = 1$, $\gamma = 1$ and $\sigma = 0.2$.

rected towards or outwards the potential barrier, from Eqs. (9) and (17), the ratio of transition rates reads

$$\kappa = \frac{\left(\sqrt{2\Delta E_1} + \gamma l_1\right)^{-\alpha} + \left(\sqrt{2\Delta E_1} + 3\gamma l_1\right)^{-\alpha}}{\left(\sqrt{2\Delta E_2} + \gamma l_2\right)^{-\alpha} + \left(\sqrt{2\Delta E_2} + 3\gamma l_2\right)^{-\alpha}}. \quad (18)$$

Fig. 4 compares scalings given by Eq. (10) and Eq. (18) with results of numerical simulations for the unrestricted (black dots) and the restricted space (red squares), i.e., the interval $[-l_1, l_2]$. For $\alpha > 1$ agreement between simulations in the unrestricted space (black dots) and Eq. (10) is clearly visible, as it was already presented in Fig. 3 and discussed within this section. For small α, one might observe, that results of numerical simulations are closer to predictions of Eq. (18) than to the scaling given by Eq. (10), corroborating that, indeed, a part of trajectories explores outer ($|x| > |l_i|$) parts of the space. This effect is further confirmed by the restricted motion with $\alpha < 0.5$ which, up to numerical precision, follow the prediction of Eq. (10). Therefore, results obtained for the dynamics in the unrestricted space (black dots) interpolates between scalings given by Eq. (18) (small α, see the inset of Fig. 4) and Eq. (10) (large α, see the main plot in Fig. 4) with some points, corresponding to intermediate α, laying between these two curves. As already mentioned, results of simulations with reflecting boundaries placed in minima of the potential (red squares) follow scaling given by Eq. (10) for small α only. Contrary to $\alpha < 1$, for $\alpha > 1$, the introduction of the reflecting boundaries destroys the agreement with the theoretical scaling. The disagreement stems from two effects: (i) with increasing α spikes become weaker and more frequent and (ii) bounded fluctuations play a larger role. Consequently, a particle is most likely to be found not in the potential minimum but closer to the barrier. This in turn effectively reduces the width and the height of the potential barrier.

Formula (10) indicates that the ratio of transition rates depends both on the barrier heights and distances between minima and the maximum of the potential. So far we have explored the validity of Eq. (10) for various heights of the potential barrier. Now, we study the correctness of the scaling predicted by Eq. (10) on changes in the distance between minima and the maximum of the potential. Fig. 5 shows ratios of transition rates for various widths l_1 and l_2 with fixed depths $h_1 = 8$, $h_2 = 12$ and $\sigma = 0.2$. In general, results of computer simulations qualitatively follow the scaling given by Eq. (10). Nevertheless, quantitative deviations are especially well visible in situations when $l_1/l_2 \gg 1$, e.g., $l_1/l_2 = 2$ or $l_1/l_2 = 3$.

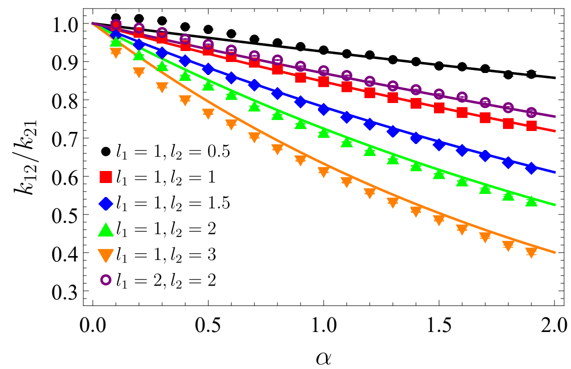

FIG. 5. The same as in Fig. 3, i.e., $\kappa(\alpha)$, for various distances between potential minima and the maximum. Simulation parameters $h_1 = 8$, $h_2 = 12$, $\gamma = 1$ and $\sigma = 0.2$.

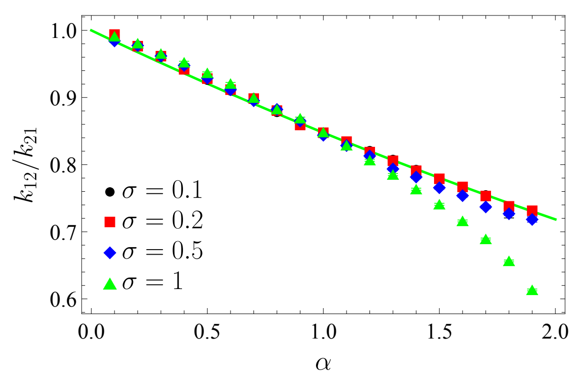

FIG. 6. The same as in Fig. 3, i.e., $\kappa(\alpha)$, for various values of the scale parameter. Simulation parameters $h_1 = 8$, $h_2 = 12$, $l_1 = 1$, $l_2 = 1$ and $\gamma = 1$.

The ratio of transition rates, see Eq. (10), was derived in the weak noise ($\sigma \to 0$) limit. Nevertheless, computer simulations have confirmed the validity of Eq. (10) for small but finite values of the scale parameter σ. Therefore, we have checked if results obtained under the weak noise approximation holds for larger σ, and how the ratio of transition rates behaves in this case. Fig. 6 presents ratios of transition rates for various values of the scale parameter σ. For $\alpha < 1$ results for all used values of σ follow the scaling given by Eq. (10). The situation changes for $\alpha > 1$, because the agreement between results of computer simulations and Eq. (10) is recorded only for small values of σ, e.g., $\sigma = 0.1$ and $\sigma = 0.2$. Results for $\sigma = 0.5$ are still very close to the scaling given by Eq. (10), however, one may observe that the ratio of transition rates is slightly smaller than the weak noise prediction. This deviation amplifies with the increasing σ, and for $\sigma = 1$ results diverge quickly from the weak noise scaling. The amplification of deviations is very similar to the behavior in the overdamped regime [61] and can be attributed to the violation of the weak noise approximation, i.e., for large σ, transitions occur not only via a single change in the velocity, but also due to a series of smaller "kicks". Consequently, Eq. (9) cannot be straight forward applied.

Finally, we estimate numerically the ratio of transition rates for the increasing damping strength. In the limit of $\gamma \to \infty$, Eq. (3) correctly reduces to the overdamped Langevin equation, for which the ratio of transition rates is given by Eq. (11). Therefore, from Eq. (10) one might expect a smooth, steady transition to the ratio of transition rates for the overdamped limit, i.e., to Eq. (11). As it is clearly visible from Fig. 7, the transition is not smooth. With the increasing γ, the ratio of transition rates increases. For small values of the friction parameter γ, simulation results reproduce predictions of Eq. (10), but with the increasing γ results of simulations deviate from the prediction given by Eq. (10). In particular, for $\gamma = 5$, numerically estimated ratios of transition rates follow predictions of Eq. (10) with $\gamma = 10$ almost precisely. For $\gamma = 10$, with $\alpha < 0.75$, the ratio of transition rates reached the overdamped limit. Simultaneously, for $\alpha > 0.75$, $\kappa(\alpha)$ significantly deviates both from the underdamped and overdamped scalings. In overall, this indicates that the overdamped limit is reached already for a finite damping, but the critical value of γ depends on the stability index α. In particular, for small α the overdamped limit is reached faster. Otherwise for γ smaller than critical, results are sensitive not only to the stability index α but also to the damping strengths, see Fig. 7.

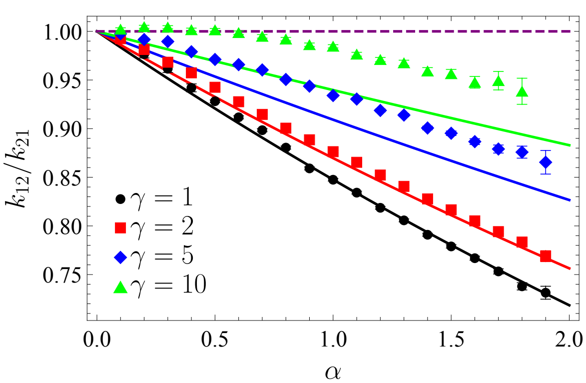

FIG. 7. The same as in Fig. 3, i.e., $\kappa(\alpha)$, for various values of the friction coefficient γ. Simulation parameters $h_1 = 8$, $h_2 = 12$, $l_1 = 1$, $l_2 = 1$ and $\sigma = 0.2$. The purple dashed line corresponds to overdamped scaling given by Eq. (11).

IV. SUMMARY AND CONCLUSIONS

The escape of a particle from the potential well is possible due to action of the noise. The escape protocol is sensitive both to the noise type (Gaussian versus Lévy) and dynamic type (overdamped versus underdamped). In the overdamped regime a particle is fully characterized by the position. The particle can jump over the potential barrier or surmount it. Therefore, during the escape from the potential well a particle is either waiting for the strong enough noise pulse (Lévy) or for a sequence of small kicks (Gaussian driving). In the underdamped regime, the particle needs to harvest energy which is sufficient to overpass the potential barrier. Analogously like in the underdamped regime, the particle steadily accumulates energy (Gaussian noise) or it waits for the abrupt jump in the velocity (Lévy driving).

The most significant difference between Lévy noise and Gaussian noise induced escape is recorded in the overdamped case. Lévy process with $\alpha < 2$ has discontinuous trajectories, while paths of the Brownian motion are continuous. In the weak noise limit, under α-stable noise, the ratio of reaction rates depends on the barrier widths, because the particle waits for the jump which is long enough as it is the main escape protocol. Consequently, the escape time is insensitive to the barrier height. The escape under Gaussian white noise follows a completely different scenario. The particle escapes via a sequence of short jumps, therefore the transition rate is sensitive to the barrier height.

The underdamped regime is very different from the overdamped regime, because in the underdamped regime the trajectory $x(t)$ is continuous both under Lévy and Gaussian drivings. The escaping particle needs to harvest sufficient energy to pass over the potential barrier. Therefore, the ratio of the escape rates is sensitive to the barrier height, also in the weak noise limit, both under Gaussian and Lévy drivings, as the barrier height defines the amount of energy which needs to be accumulated. Various regimes (overdamped and underdamped) and various drivings (Gaussian and Lévy) are compared in Tab. I.

	Gaussian	Lévy
overdamped	ratio of transition rates depends on difference of the potential well depths	ratio of transition rates depends on ratio of the potential well widths
underdamped	ratio of transition rates depends on the potential barrier heights	ratio of transition rates depends on the potential barriers heights and widths

TABLE I. The compilation of information on dependence of the ratio of transition rates in double-well potentials for various escape scenarios (Gaussian driving vs Lévy driving) and various regimes (overdamped vs underdamped).

In the weak noise limit, under action of Lévy noise a particle typically escapes due to a single rapid change in the velocity. Using asymptotic properties of α-stable densities, we have derived the formula for the ratio of escape rates, see Eq. (10), which is the main result of current research. It shows that the ratio of the escape rates depends both on the barrier widths and heights, but the sensitivity to the barrier width is larger. In the limit of the large friction the derived formula correctly reduces to the result already known for the overdamped dynamics, i.e., the ratio of transition rates depends on the width of the potential barrier only [56]. The obtained formula works very well under the assumption that the studied process, more precisely its spatial part, can be approximated as the two state process. Consequently, the potential barrier separating minima and outer parts of the potential needs to be steep enough. Deviations from the derived formula are especially visible when a particle position is not restricted to the vicinity of the potential minima. It happens when the restoring force is not large enough, or noise cannot be considered as weak.

ACKNOWLEDGEMENTS

This research was supported in part by PLGrid Infrastructure and by the National Science Center (Poland) grant 2018/31/N/ST2/00598.

Appendix A: Velocity distribution

In the regime of full dynamics, under linear friction, the velocity evolves according to

$$\frac{dv}{dt} = -\gamma v - V'(x) + \sigma\zeta(t), \tag{A1}$$

see Eq. (3). If we omit the deterministic force $-V'(x)$ in Eq. (A1), the Langevin equation is associated with the following velocity-fractional Smoluchowski-Fokker-Planck equation

$$\frac{\partial P(v,t)}{\partial t} = \frac{\partial}{\partial v}\left[\gamma v P(v,t)\right] + \sigma^\alpha \frac{\partial^\alpha P(v,t)}{\partial |v|^\alpha}. \tag{A2}$$

In the stationary state one has

$$0 = \frac{d}{dv}\left[\gamma v P(v)\right] + \sigma^\alpha \frac{d^\alpha P(v)}{d|v|^\alpha}. \tag{A3}$$

In the Fourier space Eq. (A3) reads

$$\gamma k \frac{d\hat{P}(k)}{dk} = -\sigma^\alpha |k|^\alpha \hat{P}(k), \tag{A4}$$

where $\hat{P}(k)$ is the Fourier transform $\hat{P}(k) = \int_{-\infty}^{\infty} P(v) e^{ikv} dv$. The characteristic function $\hat{P}(k)$ of the stationary distribution $P(v)$ satisfies

$$\frac{d\hat{P}(k)}{dk} = -\frac{\sigma^\alpha}{\gamma}\,\mathrm{sign}(k)|k|^{\alpha-1}\hat{P}(k). \tag{A5}$$

The solution of Eq. (A5) is given by

$$\hat{P}(k) = \exp\left[-\frac{\sigma^\alpha}{\gamma\alpha}|k|^\alpha\right], \tag{A6}$$

which is the characteristic function of the symmetric α-stable distribution, see Eq. (2), with the scale parameter σ'

$$\sigma' = \frac{\sigma}{(\gamma\alpha)^{1/\alpha}}. \tag{A7}$$

With the increasing γ, the stationary distribution becomes narrower. For instance, for the Cauchy noise ($\alpha = 1$), the stationary density is the Cauchy distribution

$$P(v) = \frac{1}{\pi}\frac{\sigma'}{(\sigma')^2 + v^2}. \tag{A8}$$

In more general cases, the asymptotic behavior of $P(v)$ is given by

$$P(v) \sim \sigma^\alpha \frac{\Gamma(\alpha+1)}{\pi} \sin\frac{\pi\alpha}{2} \times \frac{1}{|v|^{\alpha+1}}. \tag{A9}$$

Eq. (4) implies from Eq. (A9).

[1] H. A. Kramers, Physica (Utrecht) **7**, 284 (1940).
[2] S. Arrhenius, Z. Phys. Chem **4U**, 226 (1889).
[3] P. Hänggi, P. Talkner, and M. Borkovec, Rev. Mod. Phys. **62**, 251 (1990).
[4] V. I. Mel'nikov, Phys. Rep. **209**, 1 (1991).
[5] V. I. Mel'nikov and S. V. Meshkov, J. Chem. Phys. **85**, 1018 (1986).
[6] V. A. Shneidman, Phys. Rev. E **56**, 5257 (1997).
[7] V. Barcilon, J. App. Math. **56**, 446 (1996).
[8] I. Rips and J. Jortner, in *Tunneling*, edited by J. Jortner and B. Pullman (Springer Netherlands, Dordrecht, 1986) pp. 213–226.
[9] I. Rips and E. Pollak, Phys. Rev. A **41**, 5366 (1990).
[10] M. Topaler and N. Makri, J. Chem. Phys. **101**, 7500 (1994).
[11] G. Samorodnitsky and M. S. Taqqu, *Stable non-Gaussian random processes: Stochastic models with infinite variance* (Chapman and Hall, New York, 1994).
[12] A. Janicki, *Numerical and statistical approximation of stochastic differential equations with non-Gaussian measures* (Hugo Steinhaus Centre for Stochastic Methods, Wrocław, 1996).
[13] A. Janicki and A. Weron, Stat. Sci. **9**, 109 (1994).

[14] I. M. Sokolov, A. V. Chechkin, and J. Klafter, Physica A **336**, 245 (2004).
[15] J. Rosinski, Stoch. Proc. Appl. **117**, 677 (2007).
[16] R. N. Mantegna and H. E. Stanley, Phys. Rev. Lett. **73**, 2946 (1994).
[17] M. F. Shlesinger, Phys. Rev. Lett. **74**, 4959 (1995).
[18] I. Koponen, Phys. Rev. E **52**, 1197 (1995).
[19] H. Nakao, Phys. Lett. A **266**, 282 (2000).
[20] U. Küchler and S. Tappe, Stoch. Proc. Appl. **123**, 4256 (2013).
[21] M. O. Magnasco, Phys. Rev. Lett. **71**, 1477 (1993).
[22] P. Reimann, Phys. Rep. **361**, 57 (2002).
[23] Y. Li, Y. Xu, J. Kurths, and X. Yue, Chaos **27**, 103102 (2017).
[24] L. Gammaitoni, P. Hänggi, P. Jung, and F. Marchesoni, Eur. Phys. J. B **69**, 1 (2009).
[25] C. R. Doering and J. C. Gadoua, Phys. Rev. Lett. **69**, 2318 (1992).
[26] J. P. Bouchaud and A. Georges, Phys. Rep. **195**, 127 (1990).
[27] J. P. Bouchaud, A. Ott, D. Langevin, and W. Urbach, J. Phys. II France **1**, 1465 (1991).
[28] T. H. Solomon, E. R. Weeks, and H. L. Swinney, Phys. Rev. Lett. **71**, 3975 (1993).
[29] P. Barthelemy, J. Bertolotti, and D. Wiersma, Nature (London) **453**, 495 (2008).
[30] M. Mercadier, W. Guerin, M. M. Chevrollier, and R. Kaiser, Nat. Phys. **5**, 602 (2009).
[31] J. L. Cabrera and J. G. Milton, Chaos **14**, 691 (2004).
[32] J. Laherrère and D. Sornette, Eur. Phys. J. B **2**, 525 (1998).
[33] R. N. Mantegna and H. E. Stanley, *An introduction to econophysics. Correlations and complexity in finance* (Cambridge University Press, Cambridge, 2000).
[34] S. C. Lera and D. Sornette, Phys. Rev. E **97**, 012150 (2018).
[35] D. Brockmann, L. Hufnagel, and T. Geisel, Nature (London) **439**, 462 (2006).
[36] D. W. Sims, E. J. Southall, N. E. Humphries, G. C. Hays, C. J. A. Bradshaw, J. W. Pitchford, A. James, M. Z. Ahmed, A. S. Brierley, M. A. Hindell, D. Morritt, M. K. Musyl, D. Righton, E. L. C. Shepard, V. J. Wearmouth, R. P. Wilson, M. J. Witt, and J. D. Metcalfe, Nature (London) **451**, 1098 (2008).
[37] E. Barkai, E. Aghion, and D. A. Kessler, Phys. Rev. X **4**, 021036 (2014).
[38] T. A. Amor, S. D. S. Reis, D. Campos, H. J. Herrmann, and J. S. Andrade, Sci. Rep. **6**, 20815 (2016).
[39] M. F. Shlesinger and J. Klafter, in *On growth and form: Fractal and non-fractal patterns in physics*, edited by H. E. Stanley and N. Ostrowsky (Springer Verlag, Berlin, 1986) p. 279.
[40] A. M. Reynolds and C. J. Rhodes, Ecology **90**, 877 (2009).
[41] T. H. Solomon, E. R. Weeks, and H. L. Swinney, Physica D **76**, 70 (1994).
[42] R. Metzler and J. Klafter, Phys. Rep. **339**, 1 (2000).
[43] E. Barkai, Phys. Rev. E **63**, 046118 (2001).
[44] A. V. Chechkin, V. Y. Gonchar, J. Klafter, and R. Metzler, in *Fractals, Diffusion, and Relaxation in Disordered Complex Systems: Advances in Chemical Physics, Part B*, Vol. 133, edited by W. T. Coffey and Y. P. Kalmykov (John Wiley & Sons, New York, 2006) pp. 439–496.
[45] S. Jespersen, R. Metzler, and H. C. Fogedby, Phys. Rev. E **59**, 2736 (1999).
[46] R. Klages, G. Radons, and I. M. Sokolov, *Anomalous transport: Foundations and applications* (Wiley-VCH, Weinheim, 2008).
[47] A. A. Dubkov, B. Spagnolo, and V. V. Uchaikin, Int. J. Bifurcation Chaos. Appl. Sci. Eng. **18**, 2649 (2008).
[48] H. Touchette and E. G. D. Cohen, Phys. Rev. E **80**, 011114 (2009).
[49] H. Touchette and E. G. D. Cohen, Phys. Rev. E **76**, 020101 (2007).
[50] A. V. Chechkin and R. Klages, J. Stat. Mech. **2009**, L03002 (2009).
[51] B. Dybiec, J. M. R. Parrondo, and E. Gudowska-Nowak, EPL (Europhys. Lett.) **98**, 50006 (2012).
[52] Ł. Kuśmierz, J. M. Rubi, and E. Gudowska-Nowak, J. Stat. Mech **2014**, P09002 (2014).
[53] V. Zaburdaev, S. Denisov, and J. Klafter, Rev. Mod. Phys. **87**, 483 (2015).
[54] P. Xu, T. Zhou, R. Metzler, and W. Deng, Phys. Rev. E **101** (2020).
[55] X. Wang, Y. Chen, and W. Deng, Phys. Rev. E **101**, 042105 (2020).
[56] P. D. Ditlevsen, Phys. Rev. E **60**, 172 (1999).
[57] P. Imkeller and I. Pavlyukevich, Stoch. Proc. Appl. **116**, 611 (2006).
[58] P. Imkeller and I. Pavlyukevich, J. Phys. A: Math. Gen. **39**, L237 (2006).
[59] M. Bier, Phys. Rev. E **97**, 022113 (2018).
[60] A. V. Chechkin, V. Y. Gonchar, J. Klafter, and R. Metzler, EPL (Europhys. Lett.) **72**, 348 (2005).
[61] K. Capała, B. Dybiec, and E. Gudowska-Nowak, Chaos **30**, 013127 (2020).
[62] C. W. Gardiner, *Handbook of stochastic methods for physics, chemistry and natural sciences* (Springer Verlag, Berlin, 2009).
[63] W. Sutherland, Philos. Mag. **9**, 781 (1905).
[64] A. Einstein, Ann. Phys. **17**, 549 (1905).
[65] M. Von Smoluchowski, Ann. Phys. **21**, 756 (1906).
[66] V. M. Zolotarev, *One-dimensional stable distributions* (American Mathematical Soc., Providence, 1986).
[67] I. Pavlyukevich, B. Dybiec, A. V. Chechkin, and I. M. Sokolov, Eur. Phys. J ST **191**, 223 (2010).
[68] A. V. Chechkin, J. Klafter, V. Y. Gonchar, R. Metzler, and L. V. Tanatarov, Chem. Phys. **284**, 233 (2002).
[69] A. V. Chechkin, J. Klafter, V. Y. Gonchar, R. Metzler, and L. V. Tanatarov, Phys. Rev. E **67**, 010102(R) (2003).
[70] B. Dybiec, E. Gudowska-Nowak, and I. M. Sokolov, Phys. Rev. E **76**, 041122 (2007).
[71] A. Janicki and A. Weron, *Simulation and chaotic behavior of α-stable stochastic processes* (Marcel Dekker, New York, 1994).